DEVELOPMENT OF IMPROVED BURNABLE POISONS FOR COMMERCIAL NUCLEAR POWER REACTORS

Final Report on NERI Project Number 99-0074

M. L. Grossbeck, Department of Nuclear Engineering
The University of Tennessee

J.-P. A. Renier, Nuclear Science and Technology Division
Oak Ridge National Laboratory

Tim Bigelow, Theragenics Corporation

September 2003

Prepared by the
UNIVERSITY OF TENNESSEE
for the
OAK RIDGE NATIONAL LABORATORY
under contract M9SF990074
and the
U.S. DEPARTMENT OF ENERGY
under contract DE-AC05-00OR22725

CONTENTS

ACKNOWLEDGMENTS

This work was supported by the U.S. Department of Energy, NERI Project Number IWO MSF 99-0074. The isotope separation was supported in part by Theragenics Corporation under contract with Oak Ridge National Laboratory.

DEVELOPMENT OF IMPROVED BURNABLE POISONS FOR COMMERCIAL NUCLEAR POWER REACTORS

EXECUTIVE SUMMARY

Burnable poisons are used in all modern nuclear reactors to permit higher loading of fuel without the necessity of an overly large control rod system. This not only permits a longer core life but can also be used to level the power distribution such that power is produced throughout much of the core rather than mostly in a small region where control rods have been removed. Commercial nuclear reactors commonly use B4C in separate non-fueled rods and more recently, zirconium boride coatings on the fuel pellets or gadolinium oxide mixed with the fuel. Although the advantages are great, there are problems with using these materials. Boron, which is an effective neutron absorber, transmutes to lithium and helium upon absorption of a neutron. Helium is insoluble and is eventually released to the interior of the fuel rod, where it produces an internal pressure. When sufficiently high, this pressure stress could cause separation of the cladding from the fuel, causing overly high centerline temperatures. Gadolinium has several very strongly absorbing isotopes, but not all have large cross sections and thus result in residual burnable poison reactivity worth at the end of the fuel life. Even if the amount of this residual absorber is small and the penalty in operation small, the cost of this penalty, even if only several days, can be very high.

This investigation had three objectives: In Phase I the performance of single isotope burnable poisons was studied to select candidate burnable poisons; in Phase II isotopes of three prime candidate elements were separated by the plasma separation process; in Phase III candidate burnable poisons were incorporated into fuel cladding to determine if any detrimental effects existed.

In Phase I candidate burnable poisons were studied to determine the residual negative reactivity left over at the end of the fuel cycle. Since the behavior of burnable poisons can be strongly influenced by their configuration, four forms for the absorbers were studied: homogeneously mixed with the fuel, mixed with only the outer one-third of the fuel pellet, coated on the perimeter of the fuel pellets, and alloyed with the cladding. In addition, the numbers of fuel rods containing burnable poison were chosen as 8, 16, 64, and 104. Other configurations were chosen for a few special cases. An enrichment of 4.5 wt % ^{235}U was chosen for most cases for study in order to achieve a 4-year fuel cycle. A standard pressurized water reactor fuel core was chosen for the study, and state-of-the-art neutronic reactor core computer codes were used for analysis. Power distribution, fuel burnup, reactivity due to burnable poisons and other fission products, spectrum shift, core reactivity, moderator void coefficients, as well as other parameters were calculated as a function of time and fuel burnup.

The results not only showed advantages of separation of burnable poison isotopes but revealed benefits to be achieved by careful selection of the configuration of even naturally occurring elements used as burnable poisons. The savings in terms of additional days of operation is shown in Figure 1, here the savings is plotted for each of six favorable isotopes in the four

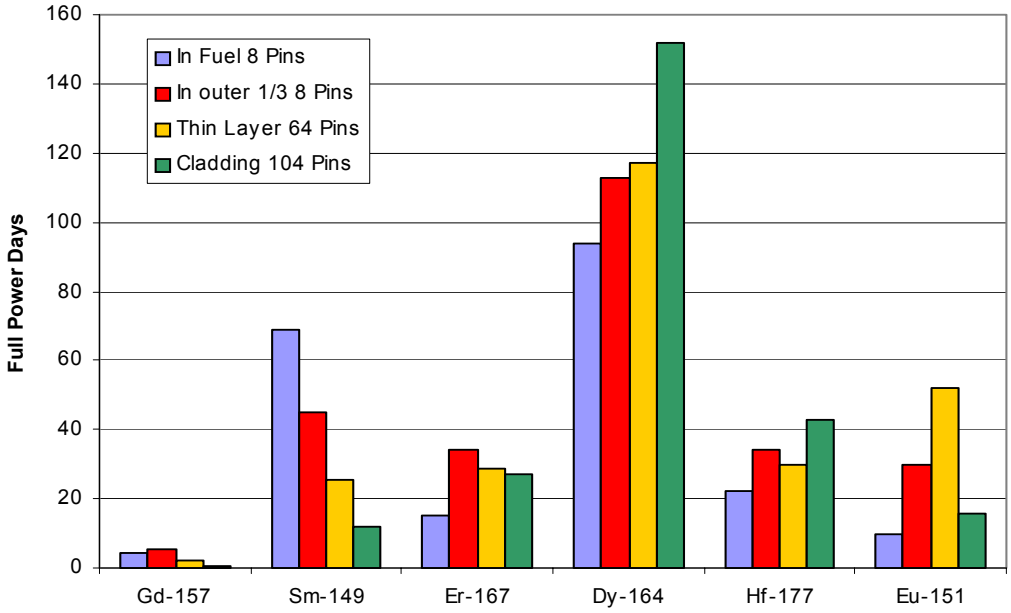

Figure 1 Savings in full power days at the end of a four-year fuel cycle achieved by using the single isotopes specified rather than naturally occurring elements.

configurations. The benefit of isotope separation is most dramatic for dysprosium, but even the time savings in the case of gadolinium is several days. For a modern nuclear plant, one day's worth of electricity is worth about one million dollars, so the resulting savings of only a few days is considerable. It is also apparent that the amount of savings depends upon the configuration of the burnable poison. The savings in cycle length is not the only factor that must be considered.

The following primary factors must all be considered in the choice of a burnable poison:
1. Rate of burnout
2. Initial negative reactivity worth
3. Available volume for burnable poison loading
4. Effect of burnable poison on the moderator void coefficient of reactivity
5. Cost of the burnable poison material
6. Compatibility of the burnable poison with the fuel or cladding

The rate of burnout of the burnable poison is perhaps the most important factor. A burnable poison that burns away in the first month of operation is not useful even if it burns so completely that its presence is not detectable at the end of the fuel cycle. Gadolinium can be distributed such that over 99% is burned in the first 120 days, but this is not ideal if a long fuel cycle is desired.

Figures 2 and 3 illustrate the time dependence of six elements for the case of the burnable poison distributed in the outer one-third of the fuel for naturally occurring elements and single isotopes,

respectively. In this configuration Gd might be used for a 1-year fuel cycle but not for a 4-year cycle. There is a big advantage to using ^{149}Sm over natural samarium, but the time dependence is not favorable in this configuration. However, ^{167}Er burns at an approximately linear rate over 4 years, and there is a significant advantage of separating out ^{167}Er, of which only 1% remains at the end of 4 years. Although the benefit is not as great, ^{164}Dy also demonstrates favorable performance.

Six isotopes were identified as having sufficiently favorable performance to merit study of the efficiency and cost of isotope separation and compatibility with the fuel and cladding. They are ^{157}Gd, ^{149}Sm, ^{167}Er, ^{164}Dy, ^{177}Hf, and ^{151}Eu. Even the lowest savings of isotope separation is on the

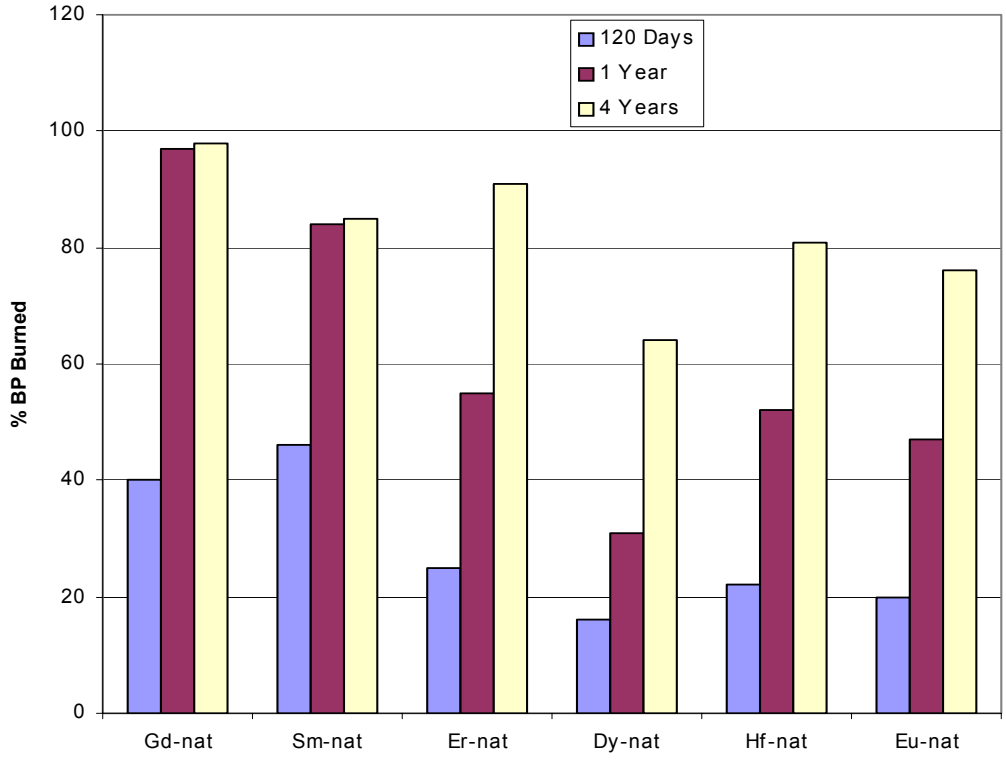

Figure 2 Percentage of burnable poison burned at the end of 120 days, 1 year, and 4 years for naturally occurring elements mixed in the outer third of the fuel rod volume. Eight fuel rods contain burnable poison.

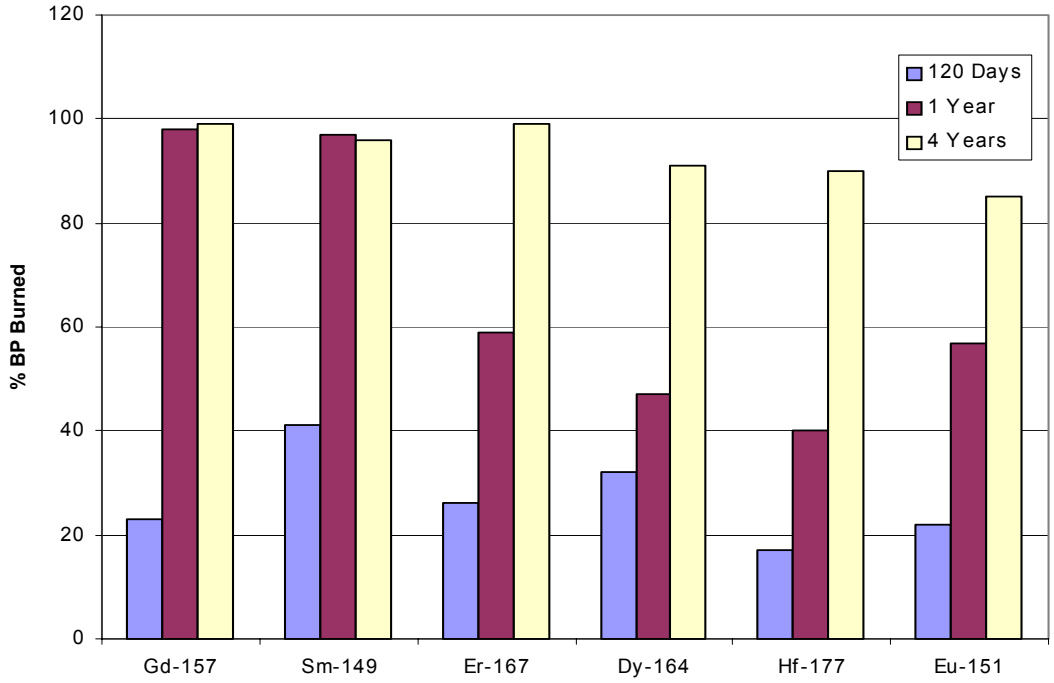

Figure 3 Percentage of burnable poison burned at the end of 120 days, 1 year, and 4 years for single isotopes mixed in the outer third of the fuel rod volume. Eight fuel rods contain burnable poison.

order of several million dollars over the term of one fuel cycle. For the case of dysprosium, the savings is predicted to be on the order of $30 million. It was this large potential savings that prompted the investigation.

Although six isotopes were identified as candidates for separation, not all could be separated because of cost and handling difficulties. Samarium was not selected because of its reactivity and its low boiling point, europium and hafnium were not selected because of their less favorable nuclear properties. Gadolinium-157, dysprosium-164, and erbium-167 were separated following major technical difficulties in target fabrication, which were overcome. Gadolinium-157 was separated to a level of 32% from a natural abundance of 15.7%, ^{164}Dy was separated to a level of 63% from a natural abundance of 28.2%, and ^{167}Er was separated to a level of 33% from a natural abundance of 23%. What is perhaps more important than the actual level of separation is the level of the undesirable isotopes. Considering the total isotopic distribution and evaluating the effect on fuel life, it was estimated that the ^{157}Gd material would save 0.5 days at the end of a four year fuel cycle as opposed to 6.3 for the case of pure ^{157}Gd. For the case of ^{164}Dy, a savings of 37 days would be achieved using the separated material as opposed to 64 days for pure ^{164}Dy. For ^{167}Er, a savings of 6 days would be achieved as opposed to 32 days for pure ^{167}Er.

However, considering the present state of the art with plasma separation, the costs of separation exceed the savings achieved by using the separated isotopes by a factor of 10 to 100. This situation could change as larger PSP machines are built to separate isotopes that cannot be separated by other means. A reduction in costs by a factor of ten is estimated by increasing the magnetic field strength from 2 Tesla to 6 Tesla in the PSP machine. Other separation methods might also be explored in the future. It is possible that different methods would be used for different burnable poisons.

The four burnable poison configurations were considered in terms of incorporating rare earths into the oxide fuel and fuel cladding. It was found that mixing rare earth oxides into oxide fuel had already been studied in detail. The most significant effect of incorporating the rare earth oxides was a reduction in thermal conductivity. This has been studied in detail and is well understood quantitatively. Using radial zoning is also developed, although not without some difficulties. Incorporation of rare earth metals into metallic fuel cladding has been suggested, but no details on how it was done or the results were available. For this reason, the Phase III part of the study focused on alloying rare earth metals in zirconium and Zircaloy-4.

Alloys were prepared by doping zirconium with gadolinium, dysprosium, and erbium to the highest levels calculated to be relevant for burnable poison application. The primary concern with doping metals with elements of far different chemical and structural properties is that the dopant element will migrate to grain boundaries and embrittle the alloy. The alloys were bend tested for ductility and found to remain ductile despite the rare earth content. Ziracaloy-4 was then doped with similar levels of each of the previously used rare earth elements and then cold rolled into sheet, using intermediate anneals. It was found that all alloys were able to withstand 50% reduction of area with only the expected edge cracking.

The conclusion to be drawn from the study is that it is not cost effective at the present time to separate ^{157}Gd gadolinium for commercial reactors. However, dysprosium and erbium can both be used for long-range fuel cycles. In this case, it may be reasonable to separate isotopes because of the fuel cycle savings of weeks through their use. As the PSP process, or another process yet to be investigated for rare earth isotope separation, becomes more efficient, the use of separated isotope burnable poisons may become cost effective. A weakness in the burnable poison production process is the throughput of the PSP process. However, a higher field magnet in the PSP device, such as the suggested 6 Tesla magnet discussed in this report, could produce isotopes a factor of ten less in cost. As Generation IV reactors come on line, a large market for separated Dy and Er could made construction of more and larger separation plants possible. Despite the present cost situation, this study has shown the path for future extended use of burnable poisons in various configurations and has identified new configurations to be used in reactor designs.

INTRODUCTION

A reactor core containing fresh fuel must have excess reactivity to compensate for fuel depletion, production of fission product poisons, and temperature effects that introduce negative reactivity. Control rods can be designed to compensate for this high beginning-of-life (BOL) excess reactivity, but this leads to the requirement of inserting the regulating control rods deeper into the core and/or inserting rods with higher control rod reactivity worths. This leads to the existence of large nonuniform power distributions throughout much of the core life. In pressurized water reactors (PWRs), a soluble boron compound is added to the coolant to compensate for excess reactivity; its concentration is reduced as the fuel is depleted. However, large concentrations of the soluble boron compound lead to an unacceptable reduction in the negative moderator void coefficient of reactivity (MVC). The amount of soluble boron that can be dissolved in the reactor coolant is limited due to the requirement that the MVC must remain negative over the fuel cycle. Too much boron, typically greater than 1,300 ppm at full power, will make the MVC positive.

In order to avoid power peaking in the fuel at full power, the regulating control rods can be inserted only a small distance into the core. In order to compensate for the excess reactivity introduced by freshly loaded fuel and to increase fuel loading and enrichment to extend the fuel-cycle length, burnable poisons (BPs) such as B_4C, ZrB_2, Gd_2O_3, Er_2O_3 and other absorbing materials can be incorporated in the fuel rods or can be located in separate non-fueled pins. The methods of choice in most PWRs are B_4C in separate non-fueled rods and, more recently, a thin coating of ZrB_2 surrounding the fuel pellets of a number of fuel rods, or Gd_2O_3 and Er_2O_3 dispersed inside the fuel pellets of selected fuel rods. In boiling water reactors (BWRs) the method of choice is the incorporation of Gd_2O_3 homogeneously mixed in the fuel pellets of a number of fuel rods.

In the proposed use of the Canadian Deuterium Uranium (CANDU) reactor for burning weapons grade plutonium as a mixed oxide (MOX), depleted uranium is used as the matrix material throughout the fuel bundle (ref 1). In the central fuel rod and in the next ring of fuel rods, Dy burnable poison is mixed with the depleted uranium of those fuel rods not containing plutonium. This increases the amount of plutonium required to achieve a given burnup (and thus increases the Pu disposition rate), reduces the local peak power after refueling, and reduces the local positive moderator void coefficient in the middle of the fuel bundle. As a result, the Dy makes the overall bundle MVC more negative.

As the fuel burns, so does the absorber. Ideally, when the fuel is depleted toward the end-of-life (EOL) of the fuel, so would the combined negative reactivity worth of the burnable poison and its daughters. A BP with a high absorption cross section would be very effective in small concentrations at BOL but would deplete rapidly unless its daughters have a high absorption cross section. A poison with too low an absorption cross section would be present in too high a concentration at EOL of the fuel, thus shortening the fuel life. In a lumped configuration, a shelf-shielding effect can be achieved so that a slower depletion rate of the BP takes place. This can be achieved by incorporating the total required BP inside fewer fuel rods or using a higher concentration of the poison. One way that the depletion rate can be accelerated is by

incorporating the poison over a smaller radial volume of the pellets (pellet zoning). The configuration of the BP is limited only by the creativity of the designer. In some cases, self-shielding is achieved on a microscopic scale by precipitation of an absorber-rich phase from a fuel-BP mixture (ref 2). In the present study, alloying the BP with the cladding is suggested, a new configuration, which offers several advantages. The details of self-shielding have been worked out by Radkowsky as part of the U.S. Naval Reactors Program, and the techniques have been in use for many years (ref 3).

The two most commonly used BPs throughout the world are boron and gadolinium (ref 4). Both homogeneous and lumped configurations have been used. Gadolinium has been used in BWRs for many years (ref 5) and has more recently been used in PWRs (ref 6,7) and VVERs (VVER is the Russian acronym for a water-cooled, water-moderated atomic reactor). The gadolinium is dispersed homogeneously throughout the fuel pellets of a number of fuel rods. Another configuration is application of a thin coating of ZrB_2 to the perimeter of the fuel pellets (ref 6).

The use of natural gadolinium as a burnable poison, as well as less commonly used absorber materials, suffers from a disadvantage in that it has seven naturally occurring isotopes, several of which have low effective absorption cross sections. These would be present in too high concentrations at EOL of the fuel. The situation is complicated by the fact that some of the burnable poison isotopes transmute or decay into other highly neutron-absorbing isotopes. The result is that the burnable poison isotopes and their daughters do not completely burn up. Some residual reactivity remains at EOL of the fuel, thus shortening the useful life of the fuel. To correct this problem either more fuel must be initially loaded or the initial fissile enrichment must be increased to compensate for this negative reactivity burden.

In the case of boron used as a burnable poison, only ^{10}B has a significant absorption (n,α) cross section, and ^{10}B does not transmute into highly absorbing isotopes (ref 8). Of more concern, however, is the production of helium by the reaction

$$^{10}B + n \rightarrow {}^{4}He + {}^{7}Li$$

The helium increases the internal pressure of the fuel rods, and at a sufficiently high burnup, the combination of fission product gases and helium from boron transmutation can attain a pressure higher than the reactor coolant pressure. When this occurs, the cladding can creep away from the fuel, producing a gap that impedes heat transfer. This results in higher fuel temperatures, and in some cases, fuel melting can occur. The increase in internal pressure can be reduced by spreading the boron burnable absorber over more fuel rods, thus reducing the boron loading in each of the fuel rods containing the poison. This, however, increases cost and increases the burnup rate of the boron.

It can be concluded that all burnable poisons in use suffer from disadvantages that limit the level of initial fissile loading and the level of fuel burnup. One solution to the problem might be to use other absorbers, but the number of useful neutron-absorbing elements is small. However, if isotopes were separated so that only the isotopes with desirable neutron absorption cross sections were used, and the isotopes that result in residual negative reactivity burdens were removed, the disadvantages would vanish.

An example of a candidate for isotope separation is samarium, which has six stable isotopes. Separation of ^{149}Sm, which constitutes 13.8% of natural samarium, would provide a high-cross section absorber that burns to a much more weakly absorbing isotope. Gadolinium has several stable isotopes, many of which are strong absorbers, but ^{157}Gd (15.8% natural isotopic abundance) has a very high thermal-absorption cross section, and it transmutes to ^{158}Gd, which has a thermal absorption cross section of only a few barns. Separation of this particular isotope has also been suggested by Hove and Spetz, whose calculations have shown significantly reduced residual negative reactivity (ref 9). Erbium presents a similar situation; ^{167}Er (22.9% natural isotopic abundance) has a 660-barn thermal-capture cross section, producing ^{168}Er with a two-barn thermal cross section. Dysprosium has eight stable isotopes, several of which are strong absorbers. Neutron capture in several of those would lead to another strong absorber, thus resulting in a substantial residual negative reactivity burden at EOL of the fuel. ^{164}Dy (28.1% natural isotopic abundance) with a 2,650-barn thermal absorption cross section transmutes to ^{165}Dy, which then decays to ^{165}Ho with a half-life of 2.3 hours. ^{165}Ho has a 65-barn capture cross section. This can transmute to ^{166}Ho, which has a large thermal cross section.

A major disadvantage to using separated isotopes in the past has been the high cost of separation. As an example, using magnetic separation by a calutron, ^{157}Gd is estimated to cost about $1000 per gram (ref 10). At this rate, the burnable poison loading for a typical BWR would cost more than the fuel. However, newer isotope separation processes are now available that are less expensive. For example, the plasma separation process (PSP), which is used in this investigation, is estimated to cost about a factor of ten less than the calutron process.

In this study, three isotopes were selected for trial separation, ^{157}Gd, ^{164}Dy, and ^{167}Er, using the PSP method. The PSP requires the feed material to be in the form of a metallic target. This has an advantage over some other techniques such as gas centrifuge and gaseous diffusion which require the feed material to be in the form of a gas, which is not possible with some elements. The product material is also in the form of a metal, but it is often necessary to chemically dissolve the material to remove it from the collector plates and reduce it to metallic form or calcine it to an oxide.

The form of a burnable poison can be varied in many ways, limited only by imagination. Spreading the material out into thin layers or spreading it among many rods will increase the burnout rate. Placing the burnable poison in lumps will provide self shielding and slow the burnout rate. In this study, burnable poisons were evaluated in four configurations: homogeniously mixed with oxide fuel, placed in an outer zone of each fuel pellet, coated on the periphery of the fuel pellets, and alloying a metallic burnable poison with the cladding. All locations have advantages. For a long-lived fuel cycle, more than one configuration might prove to be optimum. The method of alloying the burnable poison with the cladding received particular attention because it is a new method which uses metallurgical technology rather than the technology of ceramic powder processing. It has the added advantage that burnable poisons will burn faster and more completely in the cladding not only because of the thin layer but because they are in a higher thermal flux than exists in the fuel. The concern over embrittlement of the cladding by the addition of another element was dismissed by tests that showed that

zircaloy-4 doped with Gd, Dy, and Er could be rolled to 50% reduction of area.

METHOD OF CALCULATION

The first phase of this investigation involved detailed calculations of burnable poison performance in a typical PWR core. This investigation was used to study the effect of burnable poisons in several configurations and, most important, to select the candidate isotopes for actual separation. In the first phase of this study, emphasis was placed on the neutronics performance studies of the use of different burnable poisons in PWRs. Although the results of this phase of the project are summarized in this report, details have been reported in ref. 11. To reduce the scope and extent of the studies in this project, we will concentrate on one standard reactor design. In particular, we will use the standard Westinghouse 17 × 17 fuel assembly design, containing 264 fuel rods, 24 guide tubes (water holes) and one instrument tube. The Zircaloy-4 clad fuel rods contain UO_2-fuel pellets with a density of approximately 95% of theoretical density. When a burnable poison oxide was homogeneously mixed with the pellet, a density of 95% of the theoretical density of the combined UO_2 - burnable poison compound was used. The active fuel height was assumed to be 3.66 m (144 in.). A uniform axial fuel enrichment was used. The fuel rod pitch was 12.6 mm (0.495 in.), the clad outside diameter 9.53 mm (0.375 in.), the clad inside diameter 8.36 mm (0.329 in.), the diametrical gap (cold) 0.17 mm (0.0065 in.), and the pellet outside diameter (cold) 8.192 mm (0.3225 in.). Each fuel rod contained a plenum in the top region of several inches in height to collect fission-product gases and to reduce the buildup of the internal fuel rod pressure during fuel burnup. The plenum is pre-pressurized with argon gas to avoid densification of the fuel pellets.

The initial fuel enrichment was set at 4.5 wt % ^{235}U in order to use a fuel lifetime of 4 years at full power. Several additional studies were made for initial fuel enrichments of 6.0 wt %, together with a 5-year-long fuel lifetime at full power. This enabled us to investigate whether the residual negative reactivity worth of the burnable poisons could be further reduced with longer fuel lifetimes and thus higher burnups. The reactor core contained 193 fuel assemblies, and the rated reactor core power that was used in this study was 3,400 MWth. The average power per fuel assembly was thus 17.6 MWth.

Four different types of burnable poison rods were investigated:

1. A homogeneous mixture of the burnable poison as an oxide inside the fuel pellets of a limited number of fuel rods.
2. A homogeneous mixture of the burnable poison inside the outer one-third volume of the fuel pellets. During this study it was found that because of self-shielding effects inside the pellets that contain burnable poisons, the required amount of burnable poisons to achieve a given initial negative reactivity was smaller than for the case where the poisons were mixed over the entire volume of the pellet. As a consequence, the residual negative reactivity worth at EOL of the fuel was smaller for the case of BP in a one-third outer volume than for the cases where the BP was homogeneously mixed over the entire pellet. However, the initial rate of depletion of the burnable absorbers was higher. Although it would make the fuel fabrication process more complex, prototype zoned fuel pellets are being made on a laboratory scale at the present time.

3. An oxide burnable poison coating on the surface of the pellets in a limited number of fuel rods. This is similar to the technique, recently in use in several PWRs, of using a thin ZrB_2 coating on the outer radial surface of the pellets. The use of burnable poisons such as Gd_2O_3, Sm_2O_3, and others with natural isotopic abundances, might require too thick a pellet coating, which might impede heat transfer. The use of enriched burnable poisons requires a much thinner coating to achieve a given initial negative reactivity worth.
4. A homogeneous mixture of the burnable poison in the form of a metal alloyed with the Zircaloy cladding of a number of fuel rods. The use of burnable poisons with natural isotopic abundances would require a significantly higher concentration in the clad than would single isotopes. In some cases, this level of a rare earth would exceed the solubility limit and would precipitate as a second phase, which could harden the metal and reduce its ductility. Even for the cases where the burnable poison remains in solid solution, in sufficiently high concentrations, it could harden and embrittle the clad. The use of enriched burnable poisons would require a much smaller concentration to achieve a given initial negative reactivity. This increases the probability of finding a burnable poison that does not degrade the integrity of the cladding. This issue was addressed in the final phase of the project. The use of burnable absorbers inside the cladding also changes the chemistry and compatibility issue to one of cladding rather than fuel. The results of the neutronics performance studies show that the introduction of enriched burnable poisons into the clad of selected fuel rods is indeed very promising.

The layout of a standard Westinghouse 17 × 17 fuel assembly design is shown in Figure 4.

	1	2	3	4	5	6	7	8	9	10	11	12	13	14	15	16	17
1	F	F	F	F	F	F	F	F	F	F	F	F	F	F	F	F	F
2	F	F	F	F	F	F	F	F	F	F	F	F	F	F	F	F	F
3	F	F	F	F	F	O	F	F	O	F	F	O	F	F	F	F	F
4	F	F	F	O	F	F	F	F	F	F	F	F	F	O	F	F	F
5	F	F	F	F	F	F	F	F	F	F	F	F	F	F	F	F	F
6	F	F	O	F	F	O	F	F	O	F	F	O	F	F	O	F	F
7	F	F	F	F	F	F	F	F	F	F	F	F	F	F	F	F	F
8	F	F	F	F	F	F	F	F	F	F	F	F	F	F	F	F	F
9	F	F	O	F	F	O	F	F	I	F	F	O	F	F	O	F	F
10	F	F	F	F	F	F	F	F	F	F	F	F	F	F	F	F	F
11	F	F	F	F	F	F	F	F	F	F	F	F	F	F	F	F	F
12	F	F	O	F	F	O	F	F	O	F	F	O	F	F	O	F	F
13	F	F	F	F	F	F	F	F	F	F	F	F	F	F	F	F	F
14	F	F	F	O	F	F	F	F	F	F	F	F	F	O	F	F	F
15	F	F	F	F	F	O	F	F	O	F	F	O	F	F	F	F	F
16	F	F	F	F	F	F	F	F	F	F	F	F	F	F	F	F	F
17	F	F	F	F	F	F	F	F	F	F	F	F	F	F	F	F	F

F: Fuel rod
O: Guide tube
I: Instrument tube

Figure 4. Diagram showing the model of a standard 17 × 17 fuel assembly

A fuel assembly contains 264 fuel rods, 24 guide tubes (water holes), and one instrument tube. In normal PWR operation, non-fueled rods containing B_4C pellets are inserted inside a number of guide tubes of fresh fuel assemblies to compensate for the excess initial reactivity at BOL of the fresh fuel. Depending upon the location of the fuel assemblies in the reactor core, the standard burnable absorber pin configurations can contain 4, 8, 12, 16, 20, or 24 non-fueled burnable poison rods per fuel assembly. Layouts of standard fuel assemblies with 8 and 16 non-fueled burnable poison rods are shown in Figures 5 and 6, respectively.

	1	2	3	4	5	6	7	8	9	10	11	12	13	14	15	16	17
1	F	F	F	F	F	F	F	F	F	F	F	F	F	F	F	F	F
2	F	F	F	F	F	F	F	F	F	F	F	F	F	F	F	F	F
3	F	F	F	F	F	O	F	F	O	F	F	O	F	F	F	F	F
4	F	F	F	(O)	F	F	F	F	F	F	F	F	F	(O)	F	F	F
5	F	F	F	F	F	F	F	F	F	F	F	F	F	F	F	F	F
6	F	F	O	F	F	O	F	F	(O)	F	F	O	F	F	O	F	F
7	F	F	F	F	F	F	F	F	F	F	F	F	F	F	F	F	F
8	F	F	F	F	F	F	F	F	F	F	F	F	F	F	F	F	F
9	F	F	O	F	F	(O)	F	F	I	F	F	(O)	F	F	O	F	F
10	F	F	F	F	F	F	F	F	F	F	F	F	F	F	F	F	F
11	F	F	F	F	F	F	F	F	F	F	F	F	F	F	F	F	F
12	F	F	O	F	F	O	F	F	(O)	F	F	O	F	F	O	F	F
13	F	F	F	F	F	F	F	F	F	F	F	F	F	F	F	F	F
14	F	F	F	(O)	F	F	F	F	F	F	F	F	F	(O)	F	F	F
15	F	F	F	F	F	O	F	F	O	F	F	O	F	F	F	F	F
16	F	F	F	F	F	F	F	F	F	F	F	F	F	F	F	F	F
17	F	F	F	F	F	F	F	F	F	F	F	F	F	F	F	F	F

F: Fuel rod
O: Guide tube
I: Instrument tube
(O) Non-fueled burnable poison rod

Figure 5. Diagram showing the model of a standard 17 × 17 fuel assembly layout with eight non-fueled burnable poison rods.

```
    1  2  3  4  5  6  7  8  9 10 11 12 13 14 15 16 17

 1  F  F  F  F  F  F  F  F  F  F  F  F  F  F  F  F  F
 2  F  F  F  F  F  F  F  F  F  F  F  F  F  F  F  F  F
 3  F  F  F  F  F (O) F  F  O  F  F (O) F  F  F  F  F
 4  F  F  F (O) F  F  F  F  F  F  F  F  F (O) F  F  F
 5  F  F  F  F  F  F  F  F  F  F  F  F  F  F  F  F  F
 6  F  F (O) F  F  O  F  F (O) F  F  O  F  F (O) F  F
 7  F  F  F  F  F  F  F  F  F  F  F  F  F  F  F  F  F
 8  F  F  F  F  F  F  F  F  F  F  F  F  F  F  F  F  F
 9  F  F  O  F  F (O) F  F  I  F  F (O) F  F  O  F  F
10  F  F  F  F  F  F  F  F  F  F  F  F  F  F  F  F  F
11  F  F  F  F  F  F  F  F  F  F  F  F  F  F  F  F  F
12  F  F (O) F  F  O  F  F (O) F  F  O  F  F (O) F  F
13  F  F  F  F  F  F  F  F  F  F  F  F  F  F  F  F  F
14  F  F  F (O) F  F  F  F  F  F  F  F  F (O) F  F  F
15  F  F  F  F  F (O) F  F  O  F  F (O) F  F  F  F  F
16  F  F  F  F  F  F  F  F  F  F  F  F  F  F  F  F  F
17  F  F  F  F  F  F  F  F  F  F  F  F  F  F  F  F  F
```

F: Fuel rod
O: Guide tube
I: Instrument tube
(O): Non-fueled burnable poison rod

Figure 6. Diagram showing the model of a standard 17 × 17 fuel assembly layout with 16 non-fueled burnable poison rods.

In the present analyses of the advanced burnable poisons, no burnable absorber rods were inserted inside the guide tubes of the fuel assemblies. The guide tubes were left open for control-rod motion, or they were left open filled with the water coolant. The burnable poisons were placed only inside fuel rods. These are usually referred to as integral fuel burnable absorbers (IFBAs). Four different checkerboard fuel assembly models containing IFBA rods were used in this study. They contained 8, 16, 64, or 104 fuel rods with burnable absorbers. The layouts and the locations of the IFBA rods are shown in Figures 7 and 8. In the configuration with 104 IFBA rods, the fuel rods surrounding the water holes are replaced with IFBA rods to reduce power peaking. In this configuration each water hole is surrounded by seven or eight IFBA rods. During the early phases of the research, several cases containing 16 IFBA rods were explored that contained two or four extra IFBA rods. These are reported as cases containing 18 or 20 IFBA rods. Note that the presence of water holes in a fuel assembly promotes localized inner-assembly power density peaks caused by the increase in moderation. To reduce the localized power peaks, the IFBA rods are preferentially placed around the water holes. Note: The layouts displayed are non-design, nonproprietary layouts, not actual ones.

	1	2	3	4	5	6	7	8	9	10	11	12	13	14	15	16	17
1	F	F	F	F	F	F	F	F	F	F	F	F	F	F	F	F	F
2	F	F	F	F	F	F	F	F	F	F	F	F	F	F	F	F	F
3	F	F	F	F	F	O	F	F	O	F	F	O	F	F	F	F	F
4	F	F	F	O	F	F	F	F	(*)	F	F	F	F	O	F	F	F
5	F	F	F	F	(*)	F	F	F	F	F	F	F	(*)	F	F	F	F
6	F	F	O	F	F	O	F	F	O	F	F	O	F	F	O	F	F
7	F	F	F	F	F	F	F	F	F	F	F	F	F	F	F	F	F
8	F	F	F	F	F	F	F	F	F	F	F	F	F	F	F	F	F
9	F	F	O	(*)	F	O	F	F	I	F	F	O	F	(*)	O	F	F
10	F	F	F	F	F	F	F	F	F	F	F	F	F	F	F	F	F
11	F	F	F	F	F	F	F	F	F	F	F	F	F	F	F	F	F
12	F	F	O	F	F	O	F	F	O	F	F	O	F	F	O	F	F
13	F	F	F	F	(*)	F	F	F	F	F	F	F	(*)	F	F	F	F
14	F	F	F	O	F	F	F	F	(*)	F	F	F	F	O	F	F	F
15	F	F	F	F	F	O	F	F	O	F	F	O	F	F	F	F	F
16	F	F	F	F	F	F	F	F	F	F	F	F	F	F	F	F	F
17	F	F	F	F	F	F	F	F	F	F	F	F	F	F	F	F	F

F: Fuel rod
O: Guide tube
I: Instrument tube
(*): Fuel rod with burnable absorber (IFBA)

Figure 7. Diagram showing the model of a standard 17 × 17 fuel assembly layout with eight integral fuel burnable absorbers (IFBAs).

	1	2	3	4	5	6	7	8	9	10	11	12	13	14	15	16	17
1	F	F	F	F	F	F	F	F	F	F	F	F	F	F	F	F	F
2	F	F	F	F	F	F	F	F	F	F	F	F	F	F	F	F	F
3	F	F	F	F	F	O	(*)	F	O	F	(*)	O	F	F	F	F	F
4	F	F	F	O	F	F	F	F	F	F	F	F	F	O	F	F	F
5	F	F	F	F	(*)	F	F	F	F	F	F	F	(*)	F	F	F	F
6	F	F	O	F	F	O	F	F	O	F	F	O	F	F	O	F	F
7	F	F	(*)	F	F	F	F	F	F	F	F	F	F	F	(*)	F	F
8	F	F	F	F	F	F	F	(*)	F	(*)	F	F	F	F	F	F	F
9	F	F	O	F	F	O	F	F	I	F	F	O	F	F	O	F	F
10	F	F	F	F	F	F	F	(*)	F	(*)	F	F	F	F	F	F	F
11	F	F	(*)	F	F	F	F	F	F	F	F	F	F	F	(*)	F	F
12	F	F	O	F	F	O	F	F	O	F	F	O	F	F	O	F	F
13	F	F	F	F	(*)	F	F	F	F	F	F	F	(*)	F	F	F	F
14	F	F	F	O	F	F	F	F	F	F	F	F	F	O	F	F	F
15	F	F	F	F	F	O	(*)	F	O	F	(*)	O	F	F	F	F	F
16	F	F	F	F	F	F	F	F	F	F	F	F	F	F	F	F	F
17	F	F	F	F	F	F	F	F	F	F	F	F	F	F	F	F	F

F: Fuel rod
O: Guide tube
I: Instrument tube
(*): Fuel rod with burnable absorber

Figure 8. Diagram showing the model of a standard 17 × 17 fuel assembly layout with 16 integral fuel burnable absorbers (IFBAs).

REACTOR NEUTRONICS CALCULATIONS

Detailed neutronics calculations were performed using state-of-the-art computer codes such as the TALLY-MCNP4C-ORIGEN2.5 (ref 12) Monte Carlo sequence. Following initial calculations using HELIOS (ref 13,14), we switched to the three-dimensional TALLY-MCNP4C-ORIGEN2.5 sequence of computer codes (hereafter called the GP-TALLY code) because the cross sections for some of the isotopes of interest were unavailable. The generation of pointwise cross sections of the burnable poison isotopes of interest can be performed with the NJOY code (ref 15). This provided more flexibility in investigating the neutronic performance of different burnable poison isotopes. In addition, full three-dimensional models of the fuel assemblies and reactor core could be set up.

The MCNP4C code (ref 16) is a general-purpose Monte Carlo N-Particle code that can be used for neutron, photon, electron, or coupled neutron/photon/electron transport, including the capability to calculate eigenvalues for critical systems. The MCNP4C code can treat any arbitrary three-dimensional geometry configuration bounded by first- and second-degree surfaces. Pointwise cross sections for different reaction types, such as (n,fission), (n,γ), (n,2n), (n,3n), (n,p), (n,α) and others, derived from particular cross-section evaluations such as ENDF/B-VI, are available or can be generated with the NJOY code (ref 15). The thermal scattering S(α,β) data as a function of temperature are available for water and other moderators of interest.

The ORIGEN2.5 code is an advanced and updated version of ORIGEN2.1 (ref 12,17). The ORIGEN code is widely used in calculations of the depletion, buildup, and decay of materials during neutron irradiation. It uses the matrix exponential method for burnup and decay. It uses spectrum-weighted one-group cross sections for a variety of neutron reaction types such as (n,fission), (n,γ), (n,2n), (n,3n), (n,p), (n,α) and others. Using different neutron spectra for each of the different regions in the fuel, the burnable poison, and fuel assemblies, region-dependent spectrum-weighted cross sections were used during depletion. The different isotopes in ORIGEN are subdivided into three distinct groups: activation, actinides, and fission products. In order to differentiate the depletion, transmutation, and reactivity worths of the burnable absorbers such as samarium, gadolinium, erbium, and others from the fission products, all the burnable poison isotopes and their decay daughters were placed into the activation products group.

In the burnable absorber performance studies, each of the fuel and burnable-absorber regions was individually modeled. The depletion of the fuel and burnable poison isotopes was individually followed for each of the different regions of each fuel rod as a function of burnup time. The reactivity worths of the poisons and their daughters were also determined as a function of time. The fuel pellets of the rods containing burnable poison were radially subdivided into three or six equal volume regions. This enabled us to follow the self-shielding effects and depletion in the fuel pellets of each fuel rod due to the presence of the burnable poison isotopes. Typically 27 depletion time points for each full-power-year (FPY) were used. However, in the first year, additional depletion steps were used to better track the larger depletion rates of the burnable poisons at BOL. In most cases a fuel lifetime of 4 years at full power was used. Several additional studies were made for longer fuel lifetimes (5 years at full power). At BOL of the fuel, four small depletion time steps of 6 hours each were taken in order to account for equilibrium xenon. The time steps were chosen such

that, by doubling the total number of time steps (each time was further subdivided into two equal parts), the change in the residual reactivity worth fraction was less than 2%. Because of the massive amounts of data that were generated at each depletion time step, and in order to reduce the size of the burnup-dependent data files, only the data for every nine time points were kept to make tables and figures for this report. While typically 27 depletion time points were used for each FPY, only the data for 3 points were kept per FPY. The GP-TALLY code keeps track of approximately 1,100 individual nuclides for each depletion zone at each depletion time step.

The TALLY module can be considered as a driver, a pre-processor, and a post-processor for the MCNP4C and ORIGEN2.5 modules. It sets up all the necessary inputs to the MCNP4C code that are used for the calculations of the eigenvalue, neutron fluxes, and neutron reaction rates. TALLY also updates all the number densities in the inputs to the MCNP4C and ORIGEN2.5 modules at each burnup time step and for each depletion zone. Typically, the TALLY module sets up the necessary MCNP4C "tally" input for each depletion zone and for approximately 200 individual isotopes. This includes all the actinides and all the important fission products. In addition, TALLY sets up the tally input for each of the burnable poison isotopes and their daughters in each of the burnable absorber regions.

The MCNP4C calculated fluxes and spectrum-weighted one-group reaction rates for each of the different fuel and burnable absorber zones are placed into a "tally" data file. This file is then read by the TALLY module. Using the fission rates and their associated power densities and volumes, the TALLY module then normalizes the fluxes to achieve a "user requested" reactor or fuel assembly power, which can be changed at each depletion time step. The neutron fluxes and reaction rates for each isotope and for each depletion zone are then used by TALLY to calculate the region-dependent (n,fission), (n,γ), (n,p), (n,2n), (n,3n), (n,α) neutron spectrum-weighted cross sections. If available, the (n,γ) neutron spectrum-weighted cross section into the metastable state of the daughter nuclide was also calculated in TALLY for use in ORIGEN2.5. If needed, TALLY recalculates the spectrum-weighted fission product yields for each of the actinides and for each of the fuel regions. The different one-group weighted cross sections for six reaction types are then used by the TALLY module to set up the ORIGEN cross-section libraries and the inputs for a multitude of different ORIGEN2.5 runs, including isotope concentrations (approximately 1,600 isotopes for each depletion zone). After depletion and/or decay, the ORIGEN2.5 code generates updated isotope concentrations for the fuel and burnable absorbers for each of the depletion zones. These are then used by TALLY to update the MCNP4C input of the isotope concentrations. For a fuel assembly with 264 fuel rods, 104 of them containing burnable poisons and a radial subdivision of the fuel into three radial depletion zones, and if fuel assembly material symmetry can be taken into account, a total of approximately 150 depletion zones (each containing more than 200 isotopes) are followed per fuel assembly for each axial zone. Thus at each depletion time step, typically a total of 150 ORIGEN2.5 runs were performed for each axial zone. Assuming six different reaction types for each isotope, TALLY typically sets up the input for approximately $150 \times 200 \times 6 = 180{,}000$ different tallies. Because of the limitation on the number of individual tallies that can be set up in one input deck to the MCNP4C code, the input for all the requested tallies is placed within one major neutron tally, into which the sub-tallies for each depletion zone, each isotope, and each reaction type are staged. This TALLY-MCNP4C-ORIGEN2.5 procedure is then repeated for each of the different

depletion time steps. Although TALLY has the capability to set up the necessary inputs for photon tallies, this option was not used in the neutronics performance studies of the burnable absorbers. The photon option was previously implemented in ^{238}Pu production studies, in which the effect of the (γ,n) reactions in generating parasitic ^{236}Pu was investigated.

It was found that the calculation of 180,000 sub-tallies increased the MCNP4C computer times substantially. In some cases the eigenvalue calculations required central processing unit (CPU) times that were an order of magnitude greater than the CPU times for the same MCNP case but with no tallies. To circumvent this major disadvantage, a new feature was added to the TALLY code. At each depletion time step, TALLY accessed the point-wise cross sections for each of the different isotopes and depletion zones in the model. A unified energy structure was then set up that included all the point-wise energy points, including all the energies that describe the cross sections and each of the resonances for the different reaction types of interest. Typically, a unified neutron energy grid contained approximately 15,000 energy points. The TALLY code then added to the MCNP input a neutron flux tally input containing these 15,000 energy groups. The MCNP4C CPU requirements with this very fine neutron group tally was only slightly higher than the CPU requirements for the MCNP4C cases with no tallies. After completion of an MCNP4C eigenvalue calculation, the TALLY code accessed the MCNP4C tally file, and each of the MCNP4C cross-section files that were used in the MCNP4C problem. TALLY then generated spectrum-weighted one-group cross sections for each reaction type, each isotope, and each depletion zone. This feature also enabled us to determine the reactivity worths of each of the burnable absorber isotopes and their daughters.

In this study, we have not analyzed the change in the control rod worth due to the presence of burnable poisons. The loading of burnable poisons result in a shift of the maxwellian spectrum to higher energies, which might change the effective absorption cross section of control rods. In addition, if the control rod worth depends to a considerable extent upon resonance absorption, then the worths might also change with the loading of burnable absorbers.
We strictly performed assembly lattice calculations. The reactor core was filled with the same fuel assemblies, and fuel assembly reshuffling in the reactor core was not performed. An average soluble boron content of 550 ppm was used. The density of the coolant at power was 0.7795 g/cm^3. Typically, the number of source particles per generation was 3,000 to 25,000, and the number of generations was 250 to 500. The statistical standard deviation (STD) for k_{eff} was approximately 0.1% (at one sigma confidence level). The STD for the weighted cross sections was approximately 1 to 3%.

The MVCs were calculated by decreasing the water coolant density by 10%. The one-sigma STDs of the eigenvalues were better than 0.03%. The MVCs were determined using two different approaches. In the first approach, the "generation" eigenvalues were followed for the MCNP4C run containing the nominal water density at full-power conditions and 2,200 psia, and in the second MCNP4C run the "generation" eigenvalues were followed for the same MCNP4C case, but with a water density reduction of 10%. In the second approach, the "perturbation" option in MCNP4C was used, in which the water density was reduced by 10%. The MCNP4C option with first- and second-order perturbation was used. The differences between the two approaches were usually small and within one STD.

NEUTRONICS PERFORMANCE RESULTS FOR ZrB_2

In the cases where boron is used as a burnable poison in fuel rods, only the isotope ^{10}B has a significant absorption (n,α) cross section, and ^{10}B does not transmute into high absorbing isotopes. Of more concern, however, is the production of helium via the ^{10}B (n,α) ^{7}Li reaction. The production of helium gas increases the internal pressure of the fuel rods. It is this disadvantage that provides part of the incentive for this project. The methods of choice in most PWRs are the use of B_4C in separate non-fueled rods, and more recently, the use of a thin coating of ZrB_2 surrounding the radial surface of the fuel pellets in a number of fuel rods.

Neutronic performance calculations for ZrB_2 burnable absorber were done as part of this project so they could be used for comparison with the proposed burnable absorbers. A summary of the results for ZrB_2 is shown in Table 1. Note that the dimensions and concentrations for ZrB_2 are non-design values, since the actual values used in commercial reactors are proprietary. The table displays the initial reactivity worth of the burnable absorber for the entire reactor core. The table also displays the residual reactivity worth fraction of the burnable poison at EOL of the fuel. The fraction is defined as the ratio of the negative reactivity worth of the burnable absorber isotopes and their daughters after 4 years at full power, to the initial negative reactivity worth of the burnable poison at EOL of the fuel.

For a fuel assembly with 104 IFBA rods and 30 wt % ^{10}B-enriched boron, the residual reactivity ratio is 2.404×10^{-4}. The initial reactivity worth ($\delta k_{eff}/k_{eff}$) of the ZrB_2 was -1.279×10^{-1}. The residual reactivity worth is mostly due to the zirconium in the ZrB_2 compound. This residual reactivity worth ratio is very small, and thus negligible.

Table 1 also shows the effect of using the same ZrB_2 coating over a smaller number of IFBA rods, but the residual reactivity ratios are similar even though the initial reactivities are smaller. However, if there is a requirement of having the same total initial reactivity worth spread over a smaller number of rods, then the ratio becomes larger, since the poison rods would have been more self-shielded, and the burnout rate would thus have been smaller. The use of natural boron increases the residual reactivity ratio only very slightly (3.29×10^{-4} vs 2.40×10^{-4}). Note that the residual reactivity ratios are very small for all the cases that use ZrB_2 as BP. Further details of the calculations and the results are given in the Phase I Report for this project, (ref 11).

Table 1. Boron Burnable Poison in a ZrB2 Coating between the UO2 Fuel Pellet and the Zr-4 Cladding of Selected Fuel Rods - Summary Results

Initial BP Isotope	Enrich-ment BP (wt%B10)	Thickness BP Layer (mils)	Initial Density BP ZrB2 Fraction	Initial Fuel Enrich-ment (wt%U235)	Number Fuel Rods with BP (per Fuel Assembly)	BP Mass (per Fuel Assembly) (gram-B10)	Initial BP Reactivity Worth for Reactor Core -dkeff/keff)	Reactivity Ratio 120 FPD vs.BOL BP-tot per B(BOL)	Reactivity Ratio 1 FPY vs. BOL BP-tot per B(BOL)	Reactivity Ratios 4 FPY vs. BOL ZrB2-tot per B(BOL)	He3+He4 per B(BOL)	Zr(ZrB2) per B(BOL)	BP Penalty at 4 FPY (FPD)	He4 Production at 4 FPY (gram)	MVC at BOL dkeff per -10% water density change (STD)
B-none					0	0.0	0.0	0.0	0.0	0.0	0.0	0.0	0.0	0.0	-1.66-3 (2.7-4)
B-nat	19.8	1.5	0.25	4.5	104	2.034+0	9.340-2	4.777-1 (52.2%)	1.045-1 (89.6%)	3.288-4	3.135-9	3.137-4	0.15	9.552+0	-1.44-3 (4.3-4)
B-010	30.0	1.5	0.25	4.5	08	2.364+0	1.099-2	4.925-1 (50.8%)	1.119-1 (88.8%)	2.162-4	6.408-9	2.007-4	0.01	2.334+0	-1.27-3 (2.9-4)
B-010	30.0	1.5	0.25	4.5	18	5.318+0	2.410-2	4.978-1 (50.2%)	1.152-1 (88.5%)	2.243-4	4.409-9	2.070-4	0.03	3.517+0	
B-010	30.0	1.5	0.25	4.5	64	1.891+1	8.344-2	4.942-1 (50.6%)	1.117-1 (88.8%)	2.289-4	3.265-9	2.148-4	0.08	8.974+0	-1.51-3 (7.5-4)
B-010	30.0	2.0	0.25	4.5	64	2.517+1	1.056-1	5.109-1 (48.9%)	1.218-1 (87.8%)	2.428-4	3.296-9	2.276-4	0.14	1.148+1	-2.01-3 (3.5-4)
B-010	30.0	1.5	0.25	4.5	104	3.073+1	1.280-1	5.020-1 (49.8%)	1.191-1 (88.1%)	2.404-4	3.235-9	2.251-1	0.11	1.372+1	-1.50-3 (3.7-4)

NEUTRONICS PERFORMANCE RESULTS FOR GADOLINIUM

The method of choice for adding burnable poisons in most PWRs is through the use of B_4C in separate non-fueled rods, and more recently, the through the application of a thin coating of ZrB_2 surrounding the fuel pellets, or the homogeneous dispersal of Gd_2O_3 or Er_2O_3 inside the fuel pellets of selected fuel rods (ref 6,7). In BWRs the method of choice is the incorporation of Gd_2O_3 homogeneously mixed in the UO_2 pellets of a number of fuel rods.

In this section, we will investigate the potential benefits of using enriched gadolinium as a burnable absorber in PWRs. Four different configurations of the gadolinium burnable poison were investigated.

1. A homogeneous mixture of the burnable poison as an oxide [gadolinia (Gd_2O_3)] inside the fuel pellets of a limited number of fuel rods. A summary of the results is given in Table 5.

2. A homogeneous mixture of the burnable poison gadolinia inside the outer one-third volume of the fuel pellets. A summary of the results is given in Table 6. This configuration of the BP was used to show the effect of zoning the burnable poisons on the burnout times.

3. A coating of the burnable poison gadolinia on the surface of the fuel pellets, similar to the ZrB_2 coatings. A summary of the results is given in Table 7.

4. A homogeneous mixture of the burnable poison gadolinium in the form of a metal alloyed with the Zircaloy cladding of a number of fuel rods. A summary of the results is given in Table 8.

Further details and graphs are given in ref. 11. In all the neutronics calculations presented in this section, a theoretical density of 7.41 g/cm^3 was used for gadolinia (Gd_2O_3), and 7.95 g/cm^3 for metallic gadolinium. A theoretical density of 10.97 g/cm^3 was used for UO_2. The actual density fraction of the fuel pellets and of the burnable poison pellets was 95% of theoretical density.

The half-lives, natural isotopic abundances, and burnup chains related to the depletion and transmutation of gadolinium are given below. Note that the adjacent bands of isotopes such as the Dy isotopes (decay from Tb isotopes) and Sm isotopes (decay from Eu isotopes) are not shown. Also, the isomeric states of certain isotopes are not shown. However, the generation of these daughters was taken into account in the BP depletion and decay calculations.

Half-life					110y	180y	stable	72.3d	6.9d	
					^{157}Tb	^{158}Tb	^{159}Tb	^{160}Tb	^{161}Tb	^{162}Tb
							β-		β-	
Nat. Abund.	0.20%	241.6d	2.2%	14.8%	20.5%	15.7%	24.8%	18.5h	21.9%	3.66m
	^{152}Gd	^{153}Gd	^{154}Gd	^{155}Gd	^{156}Gd	^{157}Gd	^{158}Gd	^{159}Gd	^{160}Gd	^{161}Gd
		EC				β-				
Half-life	stable	13.5y	stable	8.6y	4.75y	15.2d	15.2h			
	^{151}Eu	^{152}Eu	^{153}Eu	^{154}Eu	^{155}Eu	^{156}Eu	^{157}Eu			

Table 5. Gd2O3 Burnable Poison Integrally mixed with the UO2 Fuel Pellets of Selected Fuel Rods - Summary Results.

Initial BP Isotope	Initial Loading BP (wt%Gd2O3 in UO2)	Initial Fuel Enrich-ment (wt%U235)	Number Fuel Rods with BP (per Fuel Assembly)	BP Mass (per Fuel Assembly) (gram)	Initial BP Reactivity Worth for Reactor Core (-dkeff/keff)	Reactivity Ratio 120 FPD vs.BOL BP-tot per Gd(BOL)	Reactivity Ratio 1 FPY vs.BOL BP-tot per Gd(BOL)	Reactivity Ratios 4 FPY vs. BOL Gd-tot per Gd(BOL)	Eu-tot per Gd(BOL)	Tb-tot per Gd(BOL)	BP-totat per Gd(BOL)	BP Penalty at 4 FPY (FPD)	MVC at BOL dkeff per -10% water density change (STD)
Gd-nat	2.0	4.5	08	2.876+2	5.101-2	5.147-1 (49.2%)	2.618-2 (98.8%)	1.300-2	1.318-4	1.600-3	1.472-2	3.3	-1.62-3 (2.8-4)
Gd-nat	4.0	4.5	08	5.697+2	5.844-2	6.957-1 (31.8%)	2.072-1 (81.2%)	2.127-2	2.273-4	2.444-3	2.395-2	5.3	-2.06-3 (2.7-4)
Gd-nat	8.0	4.5	08	1.118+3	6.626-2	7.942-1 (21.4%)	4.806-1 (53.9%)	3.276-2	3.894-4	3.648-3	3.680-2	10.4	-2.67-3 (2.7-4)
Gd-nat	0.5	4.5	16	1.448+2	6.852-2	6.210-2 (94.3%)	7.577-3 (99.8%)	5.101-3	4.955-5	6.541-4	5.805-3	1.5	
Gd-nat	1.0	4.5	16	2.890+2	8.237-2	2.517-1 (75.6%)	1.237-2 (99.7%)	8.379-3	8.243-5	1.039-3	9.500-3	3.2	
Gd-nat	2.0	4.5	16	5.752+2	9.733-2	5.220-1 (48.5%)	2.913-2 (98.6%)	1.349-2	1.378-4	1.620-3	1.525-2	6.4	-9.6-4 (2.7-4)
Gd-nat	4.0	4.5	16	1.140+3	1.104-1	7.057-1 (30.2%)	2.134-1 (80.7%)	2.218-2	2.422-4	2.634-3	2.505-2	11.3	-2.63-3 (2.6-4)
Gd-nat	8.0	4.5	16	2.237+3	1.246-1	8.028-1 (20.5%)	4.778-1 (54.3%)	3.443-2	4.178-4	3.922-3	3.877-2	20.1	-2.49-3 (2.7-4)
Gd-nat	4.0	4.5	20	1.424+3	1.341-1	6.989-1 (30.9%)	2.141-1 (80.6%)	2.237-2	2.469-4	2.706-3	2.532-2	15.6	
Gd-nat	0.1	4.5	64	1.161+2	1.182-1	8.159-3 (99.5%)	3.838-3 (99.9%)	2.598-3	2.498-5	3.539-4	2.977-3	1.3	+2.21-3 (3.4-4)
Gd-nat	0.2	4.5	64	2.321+2	1.700-1	1.357-2 (99.0%)	5.061-3 (99.9%)	3.353-3	3.277-5	4.276-4	3.813-3	2.5	+3.41-3 (3.2-4)
Gd-nat	0.5	4.5	64	5.793+2	2.285-1	6.675-2 (94.0%)	9.011-3 (99.8%)	6.153-3	6.089-5	7.821-4	6.996-3	6.1	+4.41-3 (2.8-4)
Gd-155	1.0	4.5	08	1.442+2	4.889-2	6.637-1 (34.0%)	1.105-1 (90.0%)	1.200-2	3.609-8	1.121-4	1.210-2	2.5	-1.48-3 (2.8-4)
Gd-155	2.0	4.5	08	2.870+2	5.812-2	7.754-1 (22.9%)	3.884-1 (62.3%)	1.760-2	5.935-8	1.527-4	1.775-2	4.75	-2.68-3 (2.6-4)
Gd-155	4.0	4.5	08	5.686+2	6.858-2	8.237-1 (18.1%)	5.865-1 (42.4%)	2.427-2	9.734-8	1.946-4	2.447-2	7.0	-3.66-3 (2.7-4)
Gd-155	1.0	4.5	16	2.884+2	9.292-2	3.748-1 (63.3%)	1.109-1 (90.1%)	1.256-2	3.706-8	1.183-4	1.268-2	5.3	-1.65-3 (3.3-4)
Gd-155	2.0	4.5	16	5.740+2	1.095-1	7.717-1 (23.3%)	3.954-1 (61.6%)	1.871-2	6.170-8	1.629-4	1.887-2	8.6	-2.61-3 (3.1-4)
Gd-155	2.0	4.5	20	7.175+2	1.326-1	7.733-1 (23.1%)	4.036-1 (60.9%)	1.983-2	6.468-8	1.738-4	2.000-2	10.0	
Gd-157	1.0	4.5	08	1.444+2	5.738-2	7.048-1 (29.7%)	1.425-1 (86,1%)	2.953-3	4.585-9	1.582-3	4.534-3	1.1	-1.53-3 (2.8-4)
Gd-157	2.0	4.5	08	2.875+2	6.309-2	8.042-1 (19.7%)	4.149-1 (59.0%)	5.043-3	6.175-9	2.556-3	7.600-3	1.7	-2.28-3 (2.7-4)
Gd-157	4.0	4.5	08	5.696+2	6.963-2	8.290-1 (17.3%)	6.281-1 (37.6%)	7.625-3	9.895-9	3.769-3	1.139-2	3.5	-2.89-3 (2.6-4)
Gd-157	0.1	4.5	16	2.901+1	6.847-2	1.256-3 (100.0%)	8.877-4(100.0%)	5.599-4	2.105-9	3.058-4	8.657-4	0.25	
Gd-157	0.2	4.5	16	5.800+1	8.174-2	7.513-2 (92.6%)	1.507-3(100.0%)	9.335-4	2.085-9	5.064-4	1.440-3	0.5	
Gd-157	0.5	4.5	16	1.448+2	9.799-2	3.543-1 (64.7%)	2.164-3(100.0%)	1.404-3	1.905-9	7.463-4	2.150-3	0.8	-1.00-3 (2.7-4)
Gd-157	1.0	4.5	16	2.889+2	1.075-1	7.075-1 (29.4%)	1.472-1 (85.7%)	3.386-3	3.495-9	1.670-3	5.056-3	2.3	-1.34-3 (2.5-4)
Gd-157	2.0	4.5	16	5.750+2	1.178-1	8.054-1 (19.6%)	4.220-1 (58.3%)	5.494-3	5.776-9	2.696-3	8.190-3	3.9	-2.58-3 (2.7-4)
Gd-157	4.0	4.5	16	1.139+3	1.295-1	8.486-1 (15.3%)	6.297-1 (37.5%)	8.303-3	9.675-9	4.005-3	1.231-2	6.2	-3.53-3 (2.6-4)
Gd-157	1.0	4.5	20	3.611+2	1.312-1	7.142-1 (28.7%)	1.184-1 (88.6%)	3.440-3	3.580-9	1.752-3	5.191-3	2.7	
Gd-157	0.05	4.5	64	5.804+1	1.868-1	6.857-4(100.0%)	6.558-4(100.0%)	4.217-4	9.180-10	2.305-4	6.522-4	0.5	+4.30-3 (3.1-4)
Gd-157	0.1	4.5	64	1.161+2	2.287-1	1.276-3(100.0%)	1.075-3(100.0%)	6.710-4	9.600-10	3.693-4	1.040-3	1.0	+4.47-3 (2.8-4)

Table 6. Gd2O3 Burnable Poison Integrally mixed with the Outer One Third Part of the UO2 Fuel Pellets of Selected Fuel Rods - Summary Results.

Initial BP Isotope	Initial Loading BP (wt%Gd2O3 in UO2)	Initial Fuel Enrich-ment (wt%U235)	Number Fuel Rods with BP (per Fuel Assembly)	BP Mass (per Fuel Assembly) (gram)	Initial BP Reactivity Worth for Reactor Core (-dkeff/keff)	Reactivity Ratio 120 FPD vs.BOL BP-tot per Gd(BOL)	Reactivity Ratio 1 FPY vs.BOL BP-tot per Gd(BOL)	Reactivity Ratios 4 FPY vs. BOL Gd-tot per Gd(BOL)	Eu-tot per Gd(BOL)	Tb-tot per Gd(BOL)	BP-tot per Gd(BOL)	BP Penalty at 4 FPY (FPD)	MVC at BOL dkeff per -10% water density change (STD)
Gd-nat	4.0	4.5	08	1.899+2	4.752-2	3.174-1 (69.0%)	1.430-2 (99.7%)	9.503-3	9.992-5	1.187-3	1.079-2	2.1	
Gd-nat	8.0	4.5	08	3.728+2	5.458-2	6.022-1 (40.5%)	3.233-2 (98.5%)	1.526-1	1.666-4	1.879-3	1.731-2	4.0	
Gd-nat	12.0	4.5	08	5.490+2	5.900-2	7.060-1 (30.1%)	1.082-1 (91.3%)	2.022-2	2.304-4	2.426-3	2.287-2	5.5	

Gd-nat	2.0	4.5	16	1.917+2	7.575-2	1.004-1 (90.6%)	8.869-3 (99.8%)	6.010-3	6.260-5	7.653-4	6.838-3	2.3	
Gd-nat	4.0	4.5	16	3.798+2	8.955-2	3.213-1 (68.7%)	1.511-2 (99.6%)	9.986-3	1.034-4	1.252-3	1.134-2	3.9	-1.28-3 (2.8-4)
Gd-nat	8.0	4.5	16	7.456+2	1.028-1	6.098-1 (39.8%)	3.432-2 (98.4%)	1.624-2	1.757-4	1.963-3	1.838-2	7.9	-1.36-3 (2.6-4)
Gd-nat	12.0	4.5	16	1.098+3	1.109-1	7.161-1 (29.1%)	1.134-1 (90.8%)	2.102-2	2.427-4	2.578-3	2.384-2	10.5	-1.78-3 (2.6-4)
Gd-nat	4.0	4.5	18	4.273+2	1.007-1	3.234-1 (68.5%)	1.491-2 (99.7%)	1.029-2	1.039-4	1.252-3	1.164-2	4.5	
Gd-nat	1.0	4.5	64	3.853+2	2.063-1	2.535-2 (98.0%)	7.208-3 (99.8%)	4.723-3	4.687-5	5.885-4	5.358-3	5.0	
Gd-155	4.0	4.5	08	1.895+2	5.344-2	7.235-1 (28.0%)	1.448-1 (86.7%)	1.334-2	4.300-8	1.300-4	1.347-2	2.8	
Gd-155	1.0	4.5	16	9.613+1	6.820-2	3.062-1 (69.8%)	8.724-3 (99.8%)	6.249-3	1.790-8	6.330-5	6.313-3	1.8	
Gd-155	2.0	4.5	16	1.913+2	8.409-2	5.767-1 (42.8%)	1.739-2 (99.3%)	9.896-3	2.728-8	9.712-5	9.993-3	3.5	-1.01-3 (2.6-4)
Gd-155	4.0	4.5	16	3.791+2	1.014-1	7.306-1 (27.3%)	1.513-1 (86.1%)	1.434-2	4.409-8	1.367-4	1.447-2	6.3	-1.66-3 (2.6-4)
Gd-155	8.0	4.5	16	7.441+2	1.172-1	8.085-1 (19.6%)	5.117-1 (50.0%)	2.083-2	7.470-8	1.912-4	2.102-2	9.4	-2.67-3 (2.5-4)
Gd-155	2.0	4.5	18	2.153+2	9.387-2	5.751-1 (42.9%)	1.584-2 (99.4%)	9.804-3	2.788-8	9.764-5	9.901-3	3.8	
Gd-155	1.0	4.5	64	3.845+2	2.283-1	3.190-1 (68.6%)	1.032-2 (99.7%)	7.468-3	2.016-8	7.963-5	7.548-3	7.2	
Gd-157	4.0	4.5	08	1.899+2	6.076-2	7.703-1 (23.1%)	2.216-2 (98.3%)	3.781-3	4.921-9	1.917-3	5.698-3	1.3	
Gd-157	0.2	4.5	16	1.933+1	6.151-2	6.950-4(100.0%)	6.687-4(100.0%)	4.452-4	2.215-9	2.327-4	6.779-4	0.2	-1.02-3 (2.8-4)
Gd-157	0.5	4.5	16	4.826+1	8.017-2	4.573-3 (99.7%)	1.293-3(100.0%)	7.762-4	1.992-9	4.406-4	1.217-3	0.4	
Gd-157	1.0	4.5	16	9.629+1	9.198-2	2.037-1 (79.8%)	2.118-3(100.0%)	1.304-3	2.239-9	7.393-4	2.043-3	0.7	-1.18-3 (2.8-4)
Gd-157	2.0	4.5	16	1.917+2	1.033-1	6.244-1 (37.7%)	3.794-3(100.0%)	2.394-3	3.025-9	1.252-3	3.646-3	1.6	-1.64-3 (2.7-4)
Gd-157	4.0	4.5	16	3.797+2	1.132-1	7.717-1 (23.9%)	3.265-2 (97.3%)	3.806-3	4.280-9	2.068-3	5.874-3	2.7	-1.78-3 (2.5-4)
Gd-157	0.5	4.5	64	1.931+2	2.594-1	3.689-1 (63.2%)	1.549-3(100.0%)	1.019-3	1.154-9	5.440-4	1.563-3	1.5	

Table 7. Gd2O3 Burnable Poison coating between the UO2 Fuel Pellets and the Zr-4 Cladding of Selected Fuel Rods - Summary Results.

Initial BP Isotope	Thickness BP Layer (mills)	Initial Density Fraction BP Gd2O3	Initial Fuel Enrich-ment (wt%U235)	Number Fuel Rods with BP (per Fuel Assembly)	BP Mass (per Fuel Assembly) (gram)	Initial BP Reactivity Worth for Reactor Core (-dkeff/keff)	Reactivity Ratio 120 FPD vs.BOL BP-tot per Gd(BOL)	Reactivity Ratio 1 FPY vs.BOL BP-tot per Gd(BOL)	Reactivity Ratios 4 FPY vs. BOL Gd-tot per Gd(BOL)	Eu-tot per Gd(BOL)	Tb-tot per Gd(BOL)	BP-tot per Gd(BOL)	BP Penalty at 4 FPY (FPD)	MVC at BOL dkeff per -10% water density change (STD)
Gd-nat	4.0	1.00	4.5	08	4.709+2	5.690-2	6.794-1 (32.7%)	6.434-2 (95.5%)	1.774-2	2.209-4	2.155-3	2.011-2	4.6	
Gd-nat	1.0	1.00	4.5	16	2.376+2	8.035-2	1.536-1 (85.3%)	1.022-2 (99.8%)	7.052-3	7.878-5	8.995-4	8.031-3	2.7	-9.20-4 (2.7-4)
Gd-nat	2.0	1.00	4.5	16	4.738+2	9.371-2	4.214-1 (58.7%)	1.807-2 (99.6%)	1.205-2	1.348-4	1.454-3	1.364-2	5.6	-1.00-3 (2.8-4)
Gd-nat	4.0	1.00	4.5	16	9.418+2	1.075-1	6.793-1 (32.8%)	6.955-2 (95.1%)	1.904-2	2.330-4	2.298-3	2.157-2	10.1	-2.05-3 (2.6-4)
Gd-nat	8.0	1.00	4.5	16	1.860+3	1.221-1	7.900-1 (21.7%)	3.883-1 (63.3%)	2.979-2	4.046-4	3.463-3	3.366-2	17.7	-2.92-3 (2.5-4)
Gd-nat	0.2	1.00	4.5	64	1.906+2	1.552-1	1.028-2 (99.3%)	4.711-3(100.0%)	3.065-3	3.326-5	3.964-4	3.494-3	2.3	+3.15-3 (3.3-4)
Gd-nat	0.5	1.00	4.5	64	4.760+2	2.203-1	4.187-2 (96.4%)	7.764-3 (99.8%)	5.482-3	5.933-5	6.816-4	6.223-3	6.1	+4.65-3 (2.7-4)
Gd-nat	1.0	1.00	4.5	64	9.505+2	2.607-1	1.653-1 (84.3%)	1.292-2 (99.7%)	8.892-3	9.987-5	1.114-3	1.011-2	11.1	+4.42-3 (2.7-4)
Gd-nat	0.5	0.10	4.5	104	7.435+1	1.053-1	4.377-3 (99.8%)	2.771-3(100.0%)	1.873-3	1.991-5	2.387-4	2.132-3	0.9	
Gd-155	4.0	1.00	4.5	08	4.700+2	6.621-2	8.126-1 (19.2%)	5.705-1 (44.0%)	2.276-2	8.709-8	1.942-4	2.296-2	6.5	
Gd-155	1.0	1.00	4.5	16	2.372+2	8.882-2	6.373-1 (36.7%)	2.906-2 (97.1%)	1.052-2	3.210-8	1.079-4	1.063-2	4.0	-1.50-3 (2.8-4)
Gd-155	2.0	1.00	4.5	16	4.729+2	1.057-1	7.623-1 (24.2%)	2.901-1 (72.2%)	1.663-2	5.362-8	1.560-4	1.678-2	7.1	-2.23-3 (2.8-4)
Gd-155	4.0	1.00	4.5	16	9.400+2	1.233-1	8.270-1 (17.7%)	5.752-1 (43.6%)	2.442-2	8.875-8	2.019-4	2.462-2	12.4	-2.90-3 (2.6-4)
Gd-155	2.0	1.00	4.5	18	5.320+2	1.176-1	7.595-1 (24.5%)	2.861-1 (72.7%)	1.718-2	5.299-8	1.526-4	1.732-2	7.9	
Gd-155	4.0	1.00	4.5	18	1.058+3	1.364-1	8.235-1 (18.1%)	5.809-1 (43.0%)	2.463-2	9.323-8	2.060-4	2.483-2	14.0	
Gd-155	0.2	1.00	4.5	64	1.902+2	1.743-1	2.743-1 (72.9%)	6.854-3 (99.8%)	5.051-3	1.324-8	5.378-5	5.105-3	4.2	+2.91-3 (3.0-4)
Gd-155	0.5	1.00	4.5	64										+3.54-3 (2.7-4)
Gd-155	0.5	0.10	4.5	104	7.720+1	1.222-1	2.034-2 (98.3%)	4.129-3(100.0%)	2.872-3	8.193-9	3.254-5	2.904-3	1.4	
Gd-155	1.0	0.10	4.5	104	1.542+2	1.821-1	4.739-2 (95.6%)	5.441-3 (99.8%)	3.826-3	1.067-8	4.258-5	3.868-3	2.1	
Gd-157	4.0	1.00	4.5	08	4.708+2	6.742-2	8.445-1 (15.7%)	6.421-1 (36.2%)	7.217-3	8.615-9	3.452-3	1.067-2	2.7	
Gd-157	0.5	1.00	4.5	16	1.190+2	9.541-2	3.547-1 (65.6%)	2.447-3(100.0%)	1.665-3	2.410-9	8.779-4	2.543-3	0.9	
Gd-157	1.0	1.00	4.5	16	2.376+2	1.062-1	6.942-1 (30.7%)	4.207-3(100.0%)	2.747-3	3.137-9	1.452-3	4.200-3	1.9	-1.35-3 (2.7-4)
Gd-157	2.0	1.00	4.5	16	4.737+2	1.168-1	7.969-1 (20.5%)	2.065-1 (79.9%)	4.493-3	4.797-9	2.389-3	6.872-3	3.2	-2.04-3 (2.4-4)
Gd-157	1.0	1.00	4.5	18	2.673+2	1.173-1	6.957-1 (30.6%)	4.189-3(100.0%)	2.738-3	3.041-9	1.468-3	4.205-3	2.3	
Gd-157	2.0	1.00	4.5	18	5.329+2	1.286-1	8.004-1 (20.1%)	2.170-1 (78.9%)	4.602-3	4.584-9	2.409-3	7.011-3	3.5	
Gd-157	0.2	0.10	4.5	64	1.905+1	1.121-1	3.808-4(100.0%)	3.684-4(100.0%)	2.325-4	1.202-9	1.300-4	3.625-4	0.2	+1.92-3 (3.6-4)
Gd-157	0.5	0.10	4.5	64	4.759+1	1.752-1	5.818-4(100.0%)	5.872-4(100.0%)	3.623-4	9.052-10	2.095-4	5.718-4	0.4	+3.89-3 (3.0-4)
Gd-157	1.0	0.10	4.5	64	9.503+1	2.215-1	9.686-4(100.0%)	9.298-4(100.0%)	5.749-4	8.998-10	3.225-4	8.974-4	0.6	+4.29-3 (2.9-4)
Gd-157	0.1	1.00	4.5	64	9.529+1	2.187-1	9.631-4(100.0%)	9.449-4(100.0%)	6.121-4	9.218-10	3.267-4	9.388-4	0.8	
Gd-157	0.2	0.10	4.5	104	3.096+1	1.636-1	4.292-4(100.0%)	4.112-4(100.0%)	2.573-4	8.930-10	1.451-4	4.024-4	0.3	
Gd-157	0.5	0.10	4.5	104	7.733+1	2.430-1	6.880-4(100.0%)	7.156-4(100.0%)	4.476-4	7.822-10	2.436-4	6.912-4	1.0	

Table 8. Gd Burnable Poison Integrally mixed with the Zr-4 Cladding of Selected Fuel Rods - Summary Results.

Initial BP Isotope	Initial loading BP (wt%Gd in Zr-4)	Initial Fuel Enrich-ment (wt%U235)	Number Fuel Rods with BP (per Fuel Assembly)	BP Mass (per Fuel Assembly) (gram)	Initial BP Reactivity Worth for Reactor Core (-dkeff/keff)	Reactivity Ratio 120 FPD vs.BOL BP-tot per Gd(BOL)	Reactivity Ratio 1 FPY vs.BOL BP-tot per Gd(BOL)	Reactivity Ratios 4 FPY vs. BOL Gd-tot per Gd(BOL)	Eu-tot per Gd(BOL)	Tb-tot per Gd(BOL)	BP-tot per Gd(BOL)	BP Penalty at 4 FPY (FPD)	MVC at BOL dkeff per -10% water density change (STD)
Gd-nat	1.0	4.5	16	5.753+1	5.172-2	9.340-3 (99.4%)	4.126-3(100.0%)	2.857-3	3.097-5	3.278-4	3.216-3	0.70	-1.08-3 (2.9-4)
Gd-nat	2.0	4.5	16	1.153+2	6.921-2	2.783-2 (97.7%)	6.120-3(100.0%)	4.269-3	4.884-5	5.106-4	4.828-3	1.35	-6.9-3 (2.8-4)
Gd-nat	4.0	4.5	16	2.314+2	8.611-2	1.227-1 (87.7%)	9.647-3 (99.8%)	6.570-3	7.318-5	7.469-4	7.387-3	2.8	-1.16-3 (2.6-4)
Gd-nat	8.0	4.5	16	4.665+2	1.010-1	3.719-1 (63.6%)	1.675-2 (99.6%)	1.113-2	1.269-4	1.238-3	1.250-2	5.0	-1.77-4 (2.7-4)
Gd-nat	0.20	4.5	104	7.467+1	1.103-1	3.773-3 (99.8%)	2.655-3(100.0%)	1.758-3	1.912-5	2.091-4	1.986-3	0.80	+1.79-3 (4.2-4)
Gd-155	1.0	4.5	16	5.753+1	5.778-2	1.251-1 (87.9%)	6.419-3 (99.8%)	4.536-3	1.328-8	4.390-5	4.580-3	1.0	-1.08-3 (2.8-4)
Gd-155	2.0	4.5	16	1.153+2	7.646-2	3.483-1 (65.6%)	9.236-3 (99.8%)	6.651-3	1.884-8	6.331-5	6.714-3	2.0	-9.3-4 (2.7-4)
Gd-155	4.0	4.5	16	2.314+2	9.502-2	5.994-1 (40.5%)	2.054-2 (99.0%)	1.022-2	2.890-8	9.310-5	1.032-2	3.9	-1.10-3 (2.7-4)
Gd-155	8.0	4.5	16	4.665+2	1.134-1	7.408-1 (26.4%)	2.258-1 (78.7%)	1.619-2	4.850-8	1.371-4	1.632-2	8.1	-2.02-3 (2.7-4)
Gd-155	0.05	4.5	104	1.866+1	4.391-2	7.161-3 (99.5%)	2.795-3(100.0%)	2.024-3	7.472-9	2.055-5	2.045-3	0.35	
Gd-155	0.20	4.5	104	7.468+1	1.269-1	1.509-2 (98.8%)	3.839-3(100.0%)	2.771-3	7.700-9	2.834-5	2.800-3	1.55	
Gd-157	1.0	4.5	08	2.877+1	4.710-2	6.485-3 (99.5%)	1.250-3(100.0%)	8.286-4	3.059-9	4.226-4	1.251-3	0.25	
Gd-157	2.0	4.5	08	5.764+1	5.462-2	2.615-1 (74.0%)	2.249-3(100.0%)	1.430-3	3.084-9	6.868-4	2.116-3	0.47	
Gd-157	0.20	4.5	16	1.149+1	5.270-2	4.681-4(100.0%)	4.805-4(100.0%)	3.012-4	2.431-9	1.524-4	4.545-4	0.10	
Gd-157	0.50	4.5	16	2.874+1	7.460-2	8.145-4(100.0%)	8.402-4(100.0%)	5.351-4	1.911-9	2.618-4	7.969-4	0.26	
Gd-157	1.0	4.5	16	5.753+1	8.959-2	7.855-3 (99.3%)	1.411-3(100.0%)	8.703-4	1.881-9	4.357-4	1.306-3	0.45	-1.21-3 (2.7-4)
Gd-157	2.0	4.5	16	1.153+2	1.025-1	2.734-1 (72.8%)	2.227-3(100.0%)	1.494-3	2.146-9	7.248-4	2.219-3	0.90	-1.25-3 (2.5-4)
Gd-157	4.0	4.5	16										-1.85-3 (2.6-4)
Gd-157	0.05	4.5	104	1.866+1	1.303-1	3.221-4(100.0%)	3.111-4(100.0%)	2.005-4	1.044-9	1.023-4	3.028-4	0.23	+2.84-3 (9.7-4)
Gd-157	0.10	4.5	104	3.733+1	1.892-1	4.339-4(100.0%)	4.295-4(100.0%)	2.772-4	8.052-10	1.400-4	4.173-4	0.35	+4.40-3 (8.2-4)

The capture cross sections for the gadolinium isotopes are given in ref. 11. The ^{155}Gd and ^{157}Gd stable isotopes of gadolinium exhibit very large neutron capture cross sections. The natural isotopic abundances are 14.8% for ^{155}Gd and 15.7% for ^{157}Gd. Other stable isotopes of gadolinium exhibit small capture cross sections. In the use of gadolinium with natural isotopic abundances as a burnable absorber, their presence will cause a residual negative reactivity worth at EOL of the fuel. The removal of these stable isotopes by enriching gadolinium in ^{155}Gd or ^{157}Gd, will thus reduce the residual negative reactivity worths. In addition, in order to achieve a given initial negative reactivity worth and for a given number of IFBA rods, the percentage of gadolinium enriched in ^{155}Gd or ^{157}Gd that has to be mixed in the UO_2 fuel, coating or cladding will be much smaller. Because of the very large thermal neutron capture cross section of ^{155}Gd and especially of ^{157}Gd, a larger self-shielding effect of the poison can be achieved with the same weight percent of gadolinia in the fuel. If the weight percent of gadolinia in the UO_2 pellets is limited due to material considerations, then the use of enriched gadolinium could lead to longer burnout times of the burnable poisons.

Note that the ^{158}Gd (n,γ) ^{159}Gd reaction produces ^{159}Gd with a half-life of 18.5 days, which then decays into ^{159}Tb. The neutron capture cross section of ^{159}Tb is approximately 23 barns at 0.0253 eV and that ^{159}Tb exhibits large resonances in the epithermal energy region [resonance integral (RI) 420 barns]. For the same initial reactivity worth of the BP, the relative residual reactivity worth at EOL due to ^{159}Tb will thus be larger for ^{157}Gd than for natural Gd or ^{155}Gd.

Table 5 displays the results of using Gd_2O_3 mixed homogeneously with the fuel pellets of a number of fuel rods. For three different cases containing 16 IFBA rods per fuel assembly and having a similar initial reactivity worth of the burnable poison (1.10×10^{-1} for natural Gd and 4 wt % Gd_2O_3, 1.095×10^{-1} for ^{155}Gd and 2 wt % Gd_2O_3, 1.075×10^{-1} for ^{157}Gd and 1.0 wt % Gd_2O_3), the residual reactivity worth fraction was 2.51×10^{-2} for natural Gd, 1.89×10^{-2} for ^{155}Gd and 5.06×10^{-3} for ^{157}Gd. The use of ^{155}Gd gave a slight improvement over natural Gd, and the use of ^{157}Gd gave an improvement by a factor of approximately five. The residual reactivity worth of the BP at EOL of the fuel can be given as an equivalent penalty in FPDs of operation of the reactor: 11.3 FPD for the natural Gd case, 8.6 FPDs for the ^{155}Gd case, and 2.3 FPDs for the ^{157}Gd case. Note also that for these cases (which have a similar initial reactivity worth of the burnable poison), the use of ^{157}Gd decreased the required mass of gadolinia by a factor of four. The residual negative reactivity worth due to the buildup of Tb in the BP is 10% of the total for natural Gd, 1% for ^{155}Gd, and 30% for ^{157}Gd. The residual worth due to the buildup of Eu isotopes is zero for the ^{155}Gd and ^{157}Gd burnable poison cases and less than 1% for the natural Gd case.

Note that for each case, all the BP isotopes and their daughters (which are not present in the initial loading of the BP) have been added as traces to the BP with a number density of 1.0×10^{-15} instead of zero. This is to avoid problems with the calculations at the beginning of cycle (BOC) with the MCNP4C code and to avoid computer exception errors (division by zero) when calculating spectrum-weighted cross sections in the GP-TALLY code.

Figure 9 shows the reactivity worths for a representative case that has 16 IFBA rods per fuel assembly and 4.0 wt% gadolinia homogeneously with the fuel. The worths displayed are for a reactor core containing 193 fuel assemblies at a total power level of 3,400 MWth. Values of the fuel

assembly lattice k_{inf} with and without BP are also shown. Note that during the calculations with the GP-TALLY code, nine depletion time steps were taken between each of the symbols displayed. The figure exhibits several interesting features. For example, the case with 16 IFBA rods whose fuel pellets contain 4.0 wt % Gd_2O_3 with natural Gd exhibits several interesting effects. The reactivity worth of the burnable poison isotope ^{157}Gd decreases rapidly with depletion time and reaches a nearly constant value at approximately 600 FPDs [approximately 22 gigawatt days per metric ton of uranium (GWD/MTU) burnup]. The reactivity worth of ^{156}Gd increases slightly with depletion time, due the production of ^{156}Gd through the ^{155}Gd (n,γ) ^{156}Gd reaction, and it reaches a nearly equilibrium value. Since the neutron capture cross section of ^{157}Gd is much greater than that of ^{156}Gd, the capture reaction rate (and thus the reactivity worth) of ^{157}Gd reaches a secular equilibrium with the capture reaction rate of ^{156}Gd. After most of the original ^{157}Gd nuclei have burned out, ^{157}Gd nuclei are produced through the ^{156}Gd (n,γ) ^{157}Gd reaction. Since the neutron capture cross section of ^{157}Gd is much larger than that of ^{156}Gd, these ^{157}Gd nuclei will burn away at a much higher rate than the ^{156}Gd nuclei, essentially immediately after they were created. This effect is similar to the secular equilibrium effect in the decay of a parent isotope that has a very long half-life, together with its daughter, which has a very short half-life. In the case of ^{156}Gd/^{157}Gd we reach a secular equilibrium between a parent isotope that has a small neutron capture cross section (^{156}Gd), together with its daughter, which has a very large cross section (^{157}Gd). Another secular equilibrium of the reactivity worths is reached between the burnable poison isotopes ^{154}Gd (small absorption cross section) and ^{155}Gd (large absorption cross section).

Another interesting effect is the increase of the reactivity worth of ^{155}Gd as a function of depletion time at the beginning of the fuel cycle, even though the mass of ^{155}Gd decreases (see BP masses in figure 23). This can be explained as follows: The natural isotopic abundances for ^{155}Gd and ^{157}Gd are similar (14.8% vs 15.7%). However, the neutron capture cross section of ^{157}Gd is much larger than the capture cross section of ^{155}Gd. Due to the higher cross section of ^{157}Gd, the total mass of ^{157}Gd decreases faster with depletion time than the mass of ^{155}Gd. The faster reduction of the amount of ^{157}Gd will make the neutron spectrum softer and thus the spectrum-weighted capture cross section of ^{155}Gd will increase even though the mass of ^{155}Gd decreases. However, after approximately 100 days (approximately 4 GWD/MTU burnup), a sufficient amount of ^{155}Gd has been burned out that the reactivity worth of the ^{155}Gd starts to decrease.

The use of 0.5 wt % Gd_2O_3 fully enriched with ^{157}Gd gives an initial reactivity worth of the BP of 9.800×10^{-2} (see Table 5). Doubling the content to 1.0 wt % Gd_2O_3 with ^{157}Gd increases only slightly the initial reactivity worth to 1.075×10^{-1}, an increase of 9.5%. Increasing the content to 2 wt % Gd_2O_3 increases the initial worth to 0.118, an increase of only 12%. The large neutron capture cross section of ^{157}Gd makes the IFBA pellets virtually “black,” and adding more BP only slightly changes the initial reactivity worth of the BP. In Table 5 we also have displayed the relative BP reactivity ratios at 120 FPD and 1 FPY. The burnout times of the BP for the 1.0 wt % loading are substantially

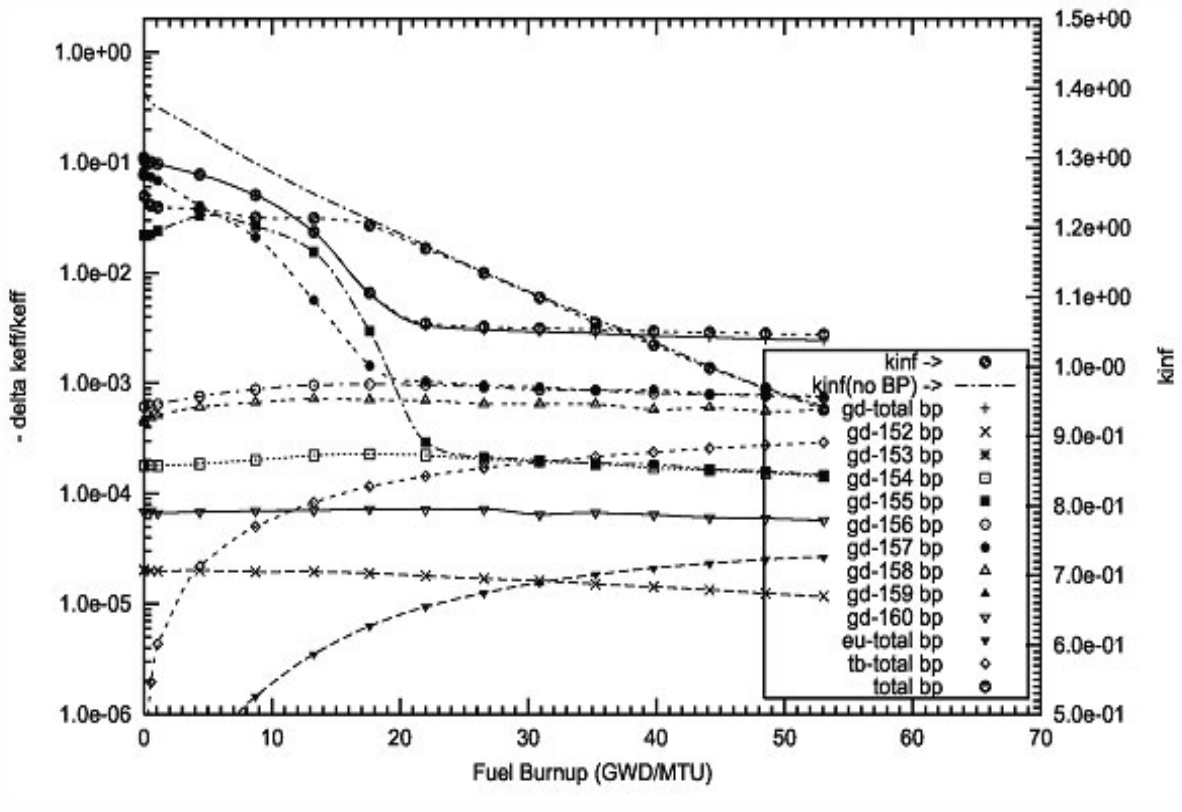

Figure 9 Negative reactivity of BP for Gd-nat and transmutation daughters as a function of fuel life for 17x17 fuel assemblies with 16 poison rods, 4.0 wt.% Gd_2O_3 poison homogeneously mixed in the UO_2 pellets. Reactor power, 3400 MWth, 193 fuel assemblies, initial enrichment, 4.5 wt% ^{235}U

longer than for the 0.5 wt % loading. The burnout rates of the BP can be controlled with the loading and thus with the "blackness" of the BP. Note however that the residual negative reactivity worth at 4 FPY increases from 2.150×10^{-3} to 5.055×10^{-3}. Comparison of the total worth of the burnable poison for the 0.5 wt %, 1.0 wt %, and 2.0 wt % Gd_2O_3 loadings clearly show that the burnout times are much longer for the 1.0 wt % loading than for the 0.5 wt % loading, and even longer for the 2.0 wt % loading.

Comparison of the cases containing 64 IFBA rods with the cases containing 16 or 8 IFBA rods clearly show that, for a given initial reactivity worth, the burnout rates are much greater for 64 IFBA rods than for 16 or 8 IFBA rods. This is clearly due to the self-shielding effect of the neutrons inside the IFBA pellets. The residual BP reactivity worths are smaller for the 64 IFBA cases.

The MVCs were calculated by decreasing the water coolant density by 10%. The one-sigma STDs of the fuel assembly lattice k_{inf} were better than 0.03%. Note that for all the cases containing 8 and 16 IFBA rods, the MVCs remain negative. For the cases with 64 IFBA rods, the MVC becomes

positive for the lattices containing identical standard 17 × 17 fuel assemblies with the same BP loadings. Calculations of the MVC were not performed for checkerboard loadings of fuel assemblies containing 64 IFBA rods in selected reactor core locations, or for fuel assemblies with different fuel-to-water ratios.

Figure 10 displays the initial reactivity worths of the BP as a function the equivalent penalty (given in FPDs of reactor operation) for several configurations containing 16 IFBA rods. The FPD penalty is directly related to the residual negative reactivity worth of the BPs and their daughters at EOL of the fuel. The trend for the four different forms of the BPs are very similar. Note also the clear advantage of using gadolinium enriched in ^{157}Gd over gadolinium with natural isotopic abundances. Figure 11 displays the initial reactivity worths vs FPD penalty for fuel assembly configurations containing 64 IFBA rods. For the cases where the BP is mixed uniformly with the cladding of a number of fuel rods, the required loading using natural gadolinium might be too high (e.g., 8 wt %). In order to achieve a given initial reactivity worth of the BP, the use of gadolinium enriched in ^{157}Gd substantially reduces the required loading in the cladding.

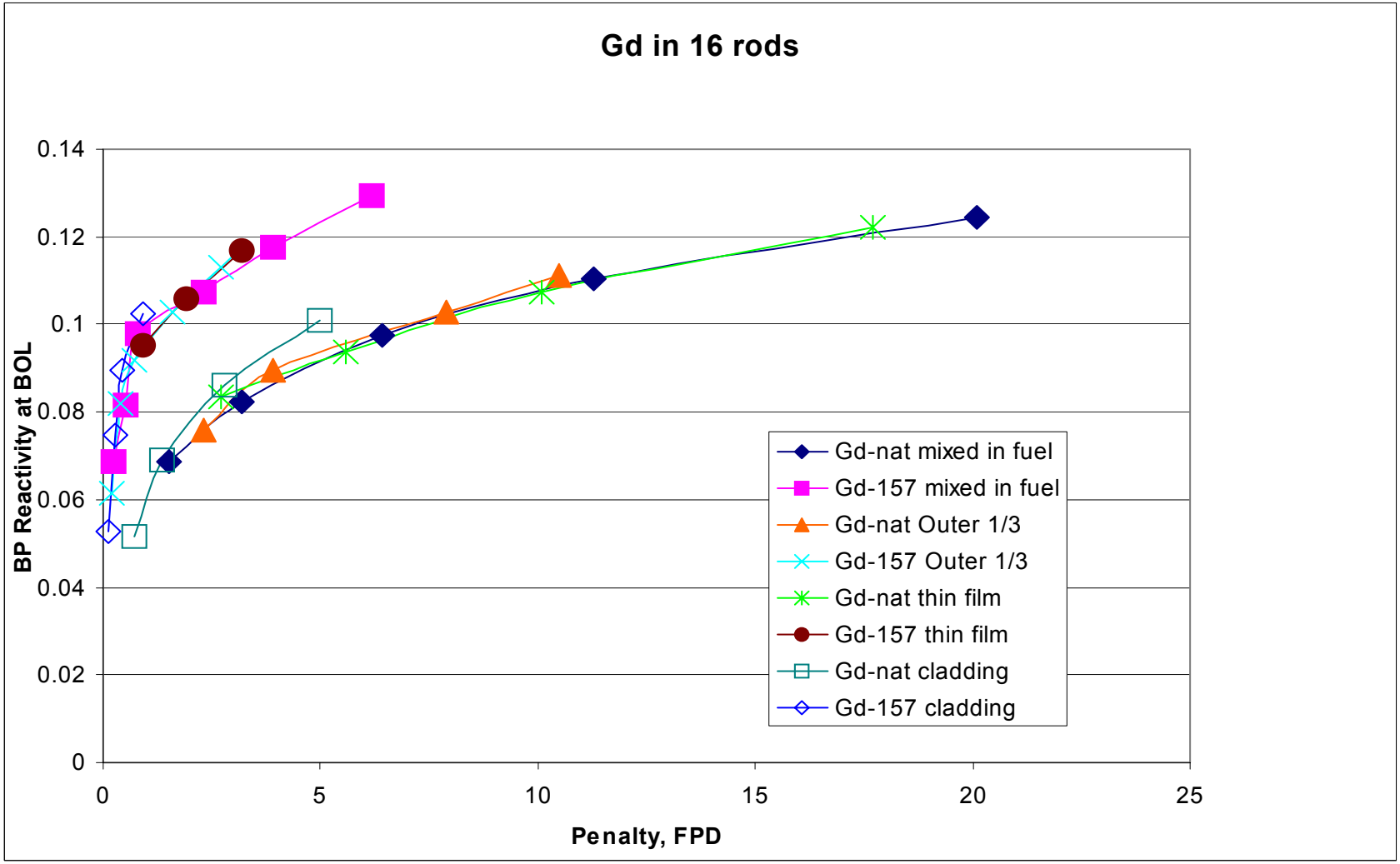

Figure 10 Burnable poison initial reactivity worth as a function of FPD Penalty -- Gd in 16 IFBA rods

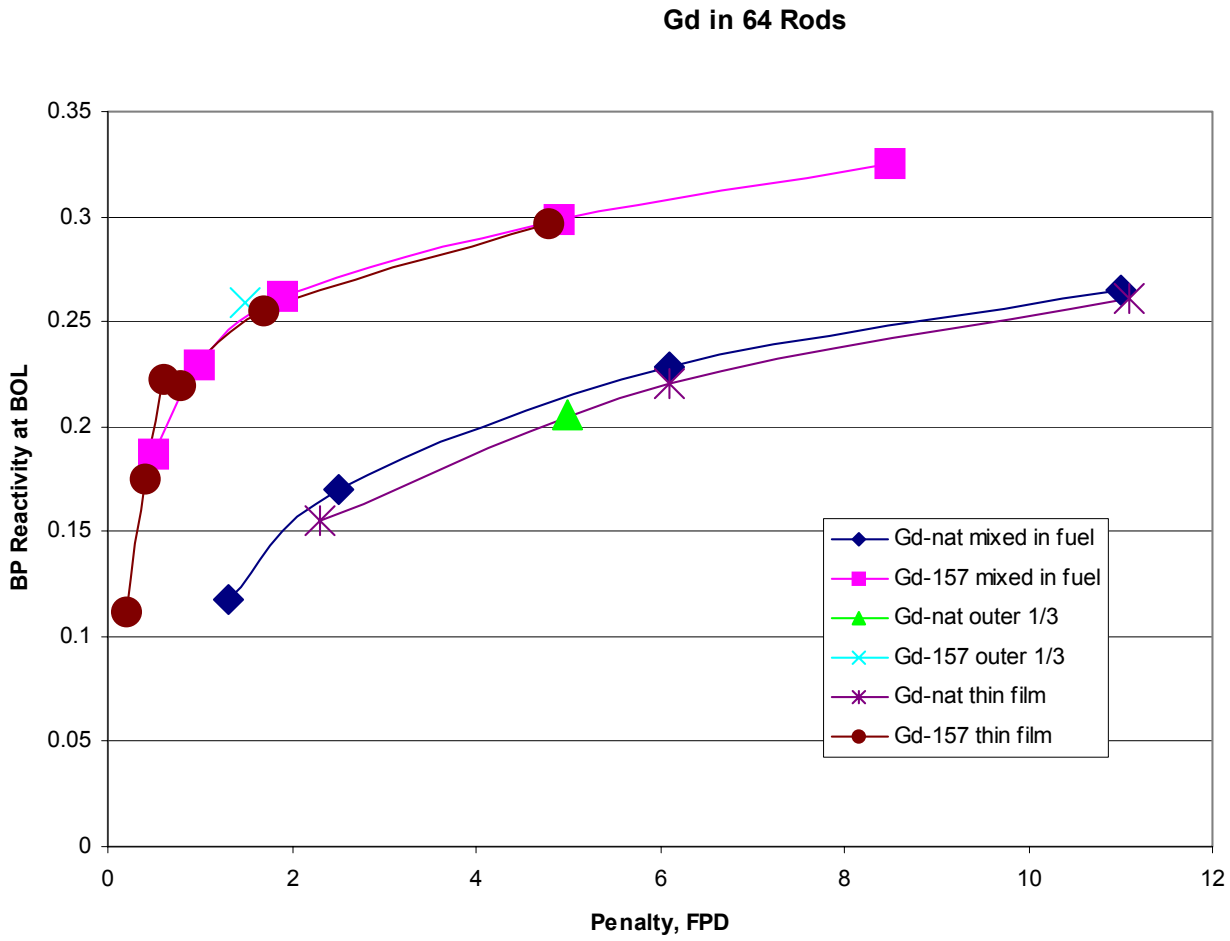

Figure 11 Burnable poison initial reactivity worth as a function of FPD penalty -- Gd in 64 IFBA rods

Neutronics Performance Results for Samarium

The use of samarium with natural isotopic abundances as a burnable poison has been previously discarded because of the large residual negative reactivity worth of the samarium burnable poison isotopes and their daughters at EOL of the fuel. The use of samarium enriched in ^{149}Sm greatly reduces this residual absorber burden.

In this section, we will investigate the potential benefits of using enriched samarium as a burnable absorber in PWRs. Four different configurations of the samarium burnable poison, similar to those of the case of Gd, were investigated. The results for each configuration are summarized in Tables 9-12.

In all the neutronics calculations presented in this section, a theoretical density of 7.43 g/cm^3 was used for Sm_2O_3, and 7.7 g/cm^3 for metallic samarium. For UO_2 a theoretical density of 10.97 g/cm^3 was used. The actual density fraction of the fuel pellets and of the burnable poison pellets was 95% of theoretical density.

The half-lives, natural isotopic abundances, and burnup chains related to the depletion and transmutation of samarium are given below. Note that the adjacent bands of isotopes such as the Gd isotopes (decay from Eu isotopes) and Nd isotopes (decay from Pm isotopes) are not shown. Also the isomeric states of certain isotopes are not shown. However, the generation of these daughters was taken into account in the BP depletion and decay calculations.

The ^{149}Sm stable isotope (13.8% natural isotopic abundance) exhibits a very large neutron capture cross section (thermal cross section of 40,150 barns and an RI of 3,400 barns). The ^{149}Sm (n,γ) ^{150}Sm reaction leads to ^{150}Sm, which is stable and has a thermal capture cross section of 104 barns. ^{144}Sm (3%) and ^{148}Sm (11%) have small capture cross sections (thermal values of 0.7 and 2.5 barns, respectively). ^{154}Sm (27%) has a capture cross section of approximately 10 barns at 0.0253 eV. The other stable isotopes, such as ^{147}Sm (15%) and ^{150}Sm (7%), have thermal capture cross sections of the order of 57 and 104 barns, respectively. The ^{150}Sm (n,γ) ^{151}Sm reaction leads to ^{151}Sm, which has a very large neutron capture cross section (thermal value of 15,200 barns and RI of 3,520 barns). ^{151}Sm decays to ^{151}Eu with a half-life of 93 years. Because of the long half-life, only very small amounts of ^{151}Eu will be generated. Note that ^{151}Eu exhibits a very large capture cross section. (thermal value of 9,200 barns and RI of 3,300 barns). Because of the long half-life of ^{151}Sm and the very large thermal capture cross section of ^{151}Sm, the preferential path will be the transmutation of ^{151}Sm into ^{152}Sm. The stable isotope ^{152}Sm (26.7%) has a large neutron capture cross section (thermal value of 206 barns and RI 2,970 barns). The ^{152}Sm (n,γ) ^{153}Sm reaction leads to ^{153}Sm which decays to ^{153}Eu with a half-life of 46.7 hours. Because of the relatively short half-life of ^{153}Sm, most of the generated ^{153}Sm will be converted into ^{153}Eu. ^{153}Eu is stable and exhibits a very large capture cross section. Transmutation to ^{154}Eu (8.6 year half-life) and ^{155}Eu (4.76 year half-life) will still result in an appreciable combined residual capture. Because of the presence of isotopes with small to medium capture cross sections in samarium with natural isotopic abundances, and because of the generation of ^{153}Eu, enriching samarium in ^{149}Sm should lead to a smaller residual neutron absorption of the BP.

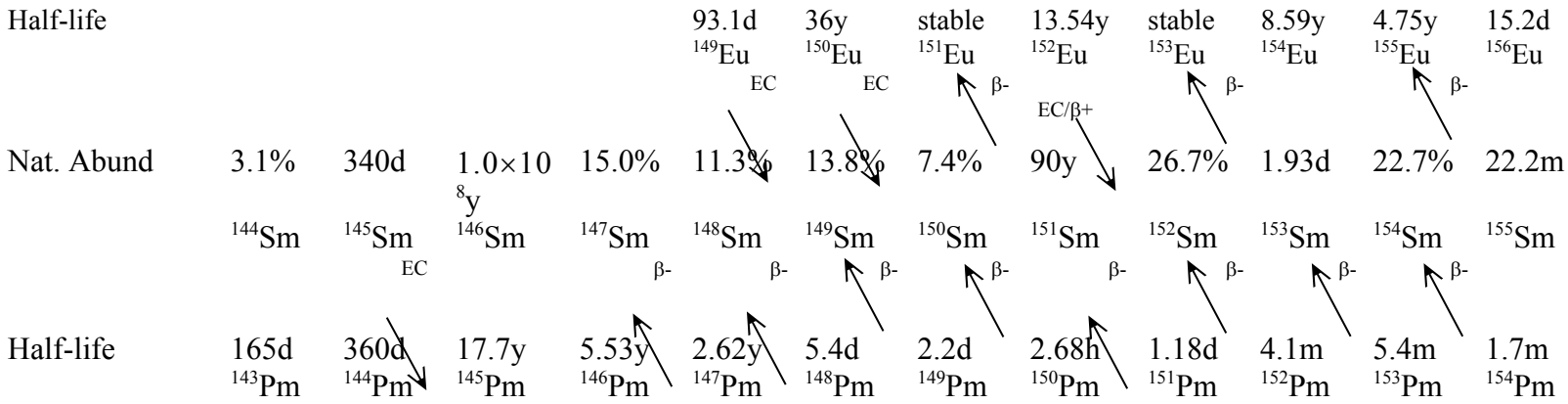
Half-life
93.1d
149Eu
36y
150Eu
stable
151Eu
13.54y
152Eu
stable
153Eu
8.59y
154Eu
4.75y
155Eu
15.2d
156Eu
EC
EC
β-
EC/β+
β-
β-
Nat. Abund
3.1%
340d
1.0×10
8y
15.0%
11.3%
13.8%
7.4%
90y
26.7%
1.93d
22.7%
22.2m
144Sm
145Sm
146Sm
147Sm
148Sm
149Sm
150Sm
151Sm
152Sm
153Sm
154Sm
155Sm
EC
β-
β-
β-
β-
β-
β-
β-
β-
Half-life
165d
360d
17.7y
5.53y
2.62y
5.4d
2.2d
2.68h
1.18d
4.1m
5.4m
1.7m
143Pm
144Pm
145Pm
146Pm
147Pm
148Pm
149Pm
150Pm
151Pm
152Pm
153Pm
154Pm

Table 9 displays the results of using Sm_2O_3, mixed homogeneously with the fuel pellets of a number of fuel rods, and Tables 10-12 summarize similar data for the other three configurations. Note that for the same initial reactivity worth of the BP, the residual negative reactivity worth of samarium enriched in ^{149}Sm is smaller than the residual worth of samarium with natural isotopic abundances. The relative contribution from the europium daughters is also smaller.

The reactivity worths of the BP isotopes, for a 4.0 wt % loading of Sm_2O_3 with natural isotopic abundances, homogeneously mixed inside the fuel pellets of 16 IFBA rods per fuel assembly, are shown in Figure 35. The initial reactivity worth of the BP is 0.112 and the residual reactivity ratio is 16.1%. For a 1.0 wt % homogeneous loading in 16 IFBA rods containing Sm_2O_3 fully enriched in ^{149}Sm, the results are shown in Figure 37. The initial reactivity worth of the BP is 0.114, and the residual reactivity ratio is 5.5%. While for these two cases the initial reactivity worth of the BP is the same, the use of samarium enriched in ^{149}Sm requires a loading that is four times smaller than a BP containing samarium with natural isotopic abundances. If the weight percentage loading of the BP is a limiting factor due to material considerations, then the use of ^{149}Sm will produce an added benefit, such as increased allowable amounts of BP in each of the IFBA rods. Longer burnout times with the same initial reactivity worth of the BP can then be achieved, which are needed for long fuel cycles.

In Table 9 the residual reactivity worths, due to the Pm daughters of the BP containing samarium enriched in ^{149}Sm, should essentially be zero, since only the decay of ^{145}Sm leads to ^{145}Pm. There are essentially no paths from the transmutation of ^{149}Sm to any of the Pm isotopes. However, the table shows residual reactivity worths of the order of 1.0×10^{-10}. This is because for each case, all the BP isotopes and their daughters (which are not present in the initial loading of the BP) have been added as traces to the BP with a number density of 1.0×10^{-15} instead of zero. This is to avoid problems at the BOC in the input to the MCNP4C code and to avoid computer exception errors (division by zero) when calculating spectrum-weighted cross sections in the TALLY code.

Comparison of the cases containing 64 IFBA rods with the cases containing 16 or 8 IFBA rods clearly show that, for a given initial reactivity worth, the burnout rates are greater for 64 IFBA rods than for 16 or 8 IFBA rods. This is clearly due to the self-shielding effect of the neutrons in the IFBA rods. Note that the residual BP reactivity worths are smaller for the 64 IFBA cases.

Figure 12 exhibits several interesting features. The reactivity worth of the burnable poison isotope ^{149}Sm decreases rapidly with depletion time, and reaches a nearly constant value at approximately 350 FPDs (approximately 13 GWD/MTU burnup). The reactivity worth of ^{148}Sm increases slightly with depletion time, due the production of ^{148}Sm through the ^{147}Sm (n,γ) ^{148}Sm reaction, and it reaches a nearly equilibrium value. Since the neutron capture cross section of ^{149}Sm is much greater than that of ^{148}Sm, the capture reaction rate (and thus the reactivity worth) of ^{149}Sm reaches a secular equilibrium with the capture reaction rate of ^{148}Sm. After most of the original ^{149}Sm nuclei have burned out, ^{149}Sm nuclei are produced through the ^{148}Sm (n,γ) ^{149}Sm reaction. Since the neutron capture cross section of ^{149}Sm is much larger than that of ^{148}Sm, these ^{149}Sm nuclei will burn away at a much higher rate than the ^{148}Sm nuclei, essentially immediately after they were created. This effect is similar to the secular equilibrium effect in the decay of a parent isotope that has a very long

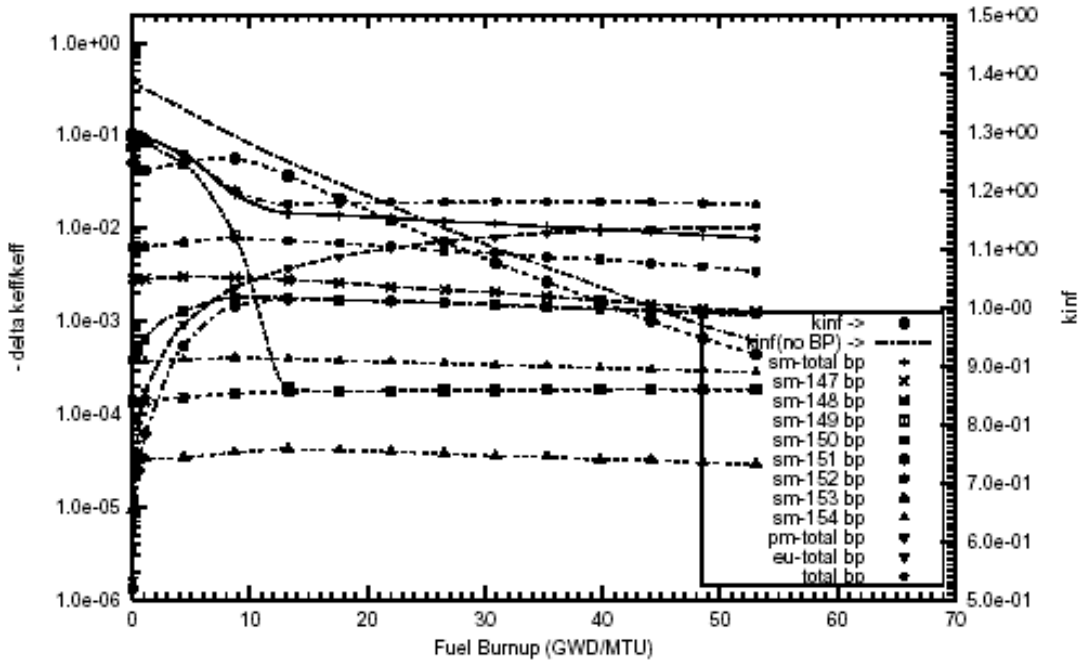

Figure 12 Negative reactivity of BP for Sm-nat and transmutation daughters as a function of fuel life for 17x17 fuel assemblies with 16 poison rods, 4.0wt% Sm_20_3 poison homogeneously mixed in the UO_2 pellets. Reactor power is 3400 MWth, 193 fuel assemblies, initial enrichment is 4.5wt%^{235}U.

half-life together with its daughter, which has a very short half-life. In the case of ^{148}Sm/^{149}Sm, we reach a secular equilibrium between a parent isotope that has a small neutron capture cross section (^{148}Sm), together with its daughter, which has a very large cross section (^{149}Sm).

Table 9. Sm Burnable Poison Integrally mixed with the UO2 Fuel Pellets of Selected Fuel Rods - Summary Results.

Initial BP Isotope	Initial Loading BP (wt%Sm2O3 in UO2)	Initial Fuel Enrich-ment (wt%U235)	Number Fuel Rods with BP (per Fuel Assembly)	BP Mass (per Fuel Assembly) (gram)	Initial BP Reactivity Worth for Reactor Core (-dkeff/keff)	Reactivity Ratio 120 FPD vs.BOL BP-tot per Sm(BOL)	Reactivity Ratio 1 FPY vs.BOL BP-tot per Sm(BOL)	Reactivity Ratios 4 FPY vs. BOL Sm-tot per Sm(BOL)	Pm-tot per Sm(BOL)	Eu-tot per Sm(BOL)	BP-tot per Sm(BOL)	BP Penalty at 4 FPY (FPD)	MVC at BOL dkeff per -10% water density change (STD)
Sm-nat	4.0	4.5	08	5.664+2	5.922-2	5.593-1 (52.1%)	1.587-1 (99.4%)	6.619-2	5.209-9	8.723-2	1.534-1	39.7	-1.64-3 (2.7-4)
Sm-nat	8.0	4.5	08	1.112+3	6.740-2	7.595-1 (31.3%)	3.344-1 (86.5%)	1.070-1	9.464-9	1.234-1	2.304-1	68.5	-2.96-3 (2.7-4)
Sm-nat	0.5	4.5	16	1.440+2	6.090-2	5.762-2 (98.7%)	5.941-2 (98.5%)	1.572-2	1.502-9	2.937-2	4.509-2	11.7	-1.21-3 (2.8-4)
Sm-nat	1.0	4.5	16	2.873+2	7.942-2	8.153-2 (98.5%)	8.057-2 (98.6%)	2.506-2	2.000-9	4.267-2	6.773-2	22.6	-9.70-4 (2.7-4)
Sm-nat	2.0	4.5	16	5.718+2	9.567-2	2.441-1 (84.5%)	1.156-1 (98.9%)	4.215-2	3.254-9	6.333-2	1.055-1	41.3	-2.19-3 (2.5-4)
Sm-nat	4.0	4.5	16	1.133+3	1.120-1	5.684-1 (51.5%)	1.635-1 (99.7%)	6.970-2	5.422-9	9.150-2	1.612-1	79.7	-2.45-3 (2.5-4)
Sm-nat	8.0	4.5	16	2.224+3	1.274-1	7.580-1 (21.7%)	3.359-1 (87.0%)	1.104-1	9.710-9	1.259-1	2.363-1	126.2	-3.41-3 (2.6-4)
Sm-nat	2.0	4.5	20	7.147+2	1.172-1	2.427-1 (84.8%)	1.168-1 (98.9%)	4.256-2	3.276-9	6.421-2	1.068-1	49.1	
Sm-nat	4.0	4.5	20	1.416+3	1.371-1	5.744-1 (50.4%)	1.686-1 (99.3%)	7.095-2	5.547-9	9.189-2	1.628-1	105.8	
Sm-nat	0.1	4.5	64	1.154+2	8.483-2	4.132-2 (98.4%)	3.918-2 (98.6%)	8.543-3	8.995-10	1.684-2	2.540-2	9.5	
Sm-nat	0.2	4.5	64	2.307+2	1.328-1	4.947-2 (98.2%)	4.847-2 (98.3%)	1.089-2	9.765-10	2.157-2	3.245-2	21.1	+8.6-4 (3.4-4)
Sm-nat	0.5	4.5	64	5.759+2	2.083-1	6.786-2 (98.3%)	6.865-2 (98.2%)	1.797-2	1.403-9	3.354-2	5.151-2	37.8	
Sm-nat	1.0	4.5	64	1.149+3	2.580-1	9.751-2 (98.3%)	9.811-2 (98.2%)	3.053-2	2.182-9	5.133-2	8.186-2	90.0	
Sm-149	1.0	4.5	08	1.434+2	6.039-2	6.964-1 (32.0%)	1.323-1 (91.5%)	3.569-2	4.825-10	1.637-2	5.205-2	13.1	-1.77-3 (2.6-4)
Sm-149	2.0	4.5	08	2.855+2	6.820-2	7.970-1 (22.1%)	4.109-1 (64.0%)	5.784-2	5.724-10	2.143-6	7.926-2	22.5	-2.72-3 (2.7-4)
Sm-149	4.0	4.5	08	5.657+2	7.587-2	8.408-1 (19.1%)	6.200-1 (45.6%)	9.300-2	8.316-10	2.366-2	1.667-1	35.5	
Sm-149	0.1	4.5	16	2.881+1	6.889-2	7.476-3(100.3%)	8.755-3(100.2%)	6.857-3	3.285-10	4.273-3	1.113-2	2.7	-9.7-4 (2.8-4)
Sm-149	0.2	4.5	16	5.759+1	8.404-2	5.113-2 (96.6%)	1.400-2(100.4%)	1.122-2	2.840-10	6.683-3	1.790-2	6.8	-8.4-4 (2.8-4)
Sm-149	0.5	4.5	16	1.437+2	1.013-1	4.746-1 (54.4%)	2.610-2(100.8%)	2.215-2	2.765-10	1.189-2	3.404-2	12.8	-1.63-3 (2.7-4)
Sm-149	1.0	4.5	16	2.869+2	1.136-1	7.022-1 (31.5%)	1.343-1 (91.6%)	3.745-2	3.200-10	1.732-2	5.477-2	23.4	-2.11-3 (2.5-4)
Sm-149	2.0	4.5	16	5.710+2	1.273-1	7.921-1 (22.7%)	4.238-1 (62.9%)	6.126-2	4.435-10	2.258-2	8.384-2	43.0	-3.63-3 (2.4-4)
Sm-149	4.0	4.5	16	1.131+3	1.413-1	8.408-1 (18.1%)	6.197-1 (43.3%)	9.686-2	7.464-10	2.471-2	1.216-1	65.9	-5.34-3 (2.6-4)
Sm-149	1.0	4.5	20	3.586+2	1.397-1	6.914-1 (32.7%)	1.140-1 (93.9%)	3.839-2	2.882-10	1.772-2	5.611-2	34.9	
Sm-149	2.0	4.5	20	7.138+2	1.537-1	8.006-1 (21.8%)	4.250-1 (63.0%)	6.368-2	4.289-10	2.326-2	8.694-2	56.1	
Sm-149	4.0	4.5	20	1.414+3	1.716-1	8.388-1 (18.4%)	6.220-1 (43.2%)	9.994-2	7.266-10	2.586-2	1.258-1	85.0	
Sm-149	8.0	4.5	20	2.777+3	1.905-1	8.663-1 (16.2%)	7.180-1 (34.2%)	1.527-1	1.447-9	2.188-2	1.746-1	225.1	
Sm-149	0.05	4.5	64	5.763+1	1.757-1	5.892-3(100.3%)	7.036-3(100.2%)	5.448-3	1.344-10	3.532-3	8.980-3	2.1	+1.91-3 (3.0-4)
Sm-149	0.1	4.5	64	1.152+2	2.261-1	9.340-3(100.5%)	1.108-2(100.3%)	8.467-3	1.155-10	5.415-3	1.388-2	15.7	+3.11-3 (2.7-4)
Sm-149	0.2	4.5	64	2.304+2	2.678-1	5.089-2 (97.1%)	1.784-2(100.5%)	1.411-2	1.160-10	8.668-3	2.278-2	24.7	

Table 10. Sm Burnable Poison Integrally mixed with the Outer One Third Part of the UO2 Fuel Pellets of Selected Fuel Rods - Summary Results.

Initial BP Isotope	Initial Loading BP (wt%Sm2O3 in UO2)	Initial Fuel Enrich-ment (wt%U235)	Number Fuel Rods with BP (per Fuel Assembly)	BP Mass (per Fuel Assembly) (gram)	Initial BP Reactivity Worth for Reactor Core (-dkeff/keff)	Reactivity Ratio 120 FPD vs.BOL BP-tot per Sm(BOL)	Reactivity Ratio 1 FPY vs.BOL BP-tot per Sm(BOL)	Reactivity Ratios 4 FPY vs. BOL Sm-tot per Sm(BOL)	Pm-tot per Sm(BOL)	Eu-tot per Sm(BOL)	BP-tot per Sm(BOL)	BP Penalty at 4 FPY (FPD)	MVC at BOL dkeff per -10% water density change (STD)
Sm-nat	4.0	4.5	08	1.888+2	4.621-2	9.087-2 (98.7%)	9.027-2 (98.7%)	2.973-2	2.525-9	4.896-2	7.869-2	14.5	
Sm-nat	8.0	4.5	08	3.707+2	5.454-2	2.966-1 (80.0%)	1.287-1 (99.1%)	4.921-2	3.960-9	7.171-2	1.209-1	25.4	
Sm-nat	12.0	4.5	08	5.460+2	5.924-2	5.388-1 (54.4%)	1.589-1 (99.3%)	6.551-2	5.106-9	8.739-2	1.529-1	36.7	
Sm-nat	1.0	4.5	16	9.575+1	5.094-2	5.187-2 (98.5%)	5.113-2 (98.5%)	1.248-2	1.345-9	2.395-2	3.643-2	7.8	-1.16-3 (2.8-4)
Sm-nat	2.0	4.5	16	1.906+2	7.014-2	6.519-2 (98.7%)	6.672-2 (98.5%)	1.857-2	1.613-9	3.397-2	5.254-2	15.4	-1.32-3 (2.7-4)
Sm-nat	4.0	4.5	16	3.776+2	8.731-2	9.762-2 (98.3%)	9.450-2 (98.7%)	3.145-2	2.435-9	5.066-2	8.211-2	29.3	-1.55-3 (2.804)
Sm-nat	8.0	4.5	16	7.414+2	1.040-1	2.928-1 (80.9%)	1.315-1 (99.3%)	5.176-2	3.927-9	7.365-2	1.254-1	59.2	-1.80-3 (2.8-4)
Sm-nat	2.0	4.5	18	2.144+2	7.848-2	6.687-2 (98.6%)	6.735-2 (98.5%)	1.903-2	1.575-9	3.412-2	5.315-2	15.2	
Sm-nat	4.0	4.5	18	4.248+2	9.754-2	9.737-2 (98.3%)	9.366-2 (98.7%)	3.108-2	2.365-9	5.060-2	8.168-2	29.3	
Sm-nat	0.1	4.5	64	3.846+1	3.535-2	3.640-2 (98.4%)	3.367-2 (98.7%)	6.900-3	1.125-9	1.371-1	2.060-2	2.8	
Sm-nat	0.2	4.5	64	7.689+1	6.372-2	3.927-2 (98.3%)	3.598-2 (98.7%)	7.603-3	9.150-10	1.515-2	2.276-2	6.8	
Sm-nat	0.5	4.5	64	1.920+2	1.229-1	4.714-2 (98.2%)	4.522-2 (98.4%)	1.010-2	9.319-10	1.998-2	3.008-2	15.3	
Sm-nat	1.0	4.5	64	3.830+2	1.780-1	5.854-2 (98.2%)	5.855-2 (98.2%)	1.406-2	1.156-9	2.727-2	4.133-2	31.6	
Sm-nat	2.0	4.5	64	7.624+2	2.328-1	7.894-2 (98.2%)	8.032-2 (98.1%)	2.212-2	1.672-9	4.020-2	6.232-2	63.1	
Sm-149	2.0	4.5	08	9.517+1	5.779-2	5.855-1 (43.2%)	3.167-2(101.0%)	2.681-2	4.526-10	1.445-2	4.126-2	9.9	
Sm-149	4.0	4.5	08	1.886+2	6.414-2	7.706-1 (24.5%)	5.845-2(100.5%)	4.318-2	4.902-10	2.023-6	6.340-2	17.2	
Sm-149	8.0	4.5	08	3.702+2	7.171-2	8.300-1 (18.8%)	5.531-1 (49.5%)	7.175-2	6.168-10	2.589-2	9.704-2	30.3	
Sm-149	12.0	4.5	08	5.453+2	7.638-2	8.333-1 (18.9%)	6.431-1 (40.5%)	9.143-2	7.555-10	2.626-2	1.177-1	38.6	
Sm-149	16.0	4.5	08	7.142+2	8.054-2	8.461-1 (17.8%)	6.820-1 (36.7%)	1.083-1	9.717-10	2.482-2	1.331-1	45.0	
Sm-149	0.2	4.5	16	1.920+1	5.845-2	6.172-3(100.3%)	7.545-3(100.2%)	5.748-3	3.830-10	3.732-3	9.479-3	2.4	-9.9-4 (2.9-4)
Sm-149	0.5	4.5	16	4.793+1	8.227-2	1.547-2(100.1%)	1.295-2(100.3%)	1.006-2	2.860-10	6.272-3	1.633-2	5.6	-1.05-3 (2.6-4)
Sm-149	1.0	4.5	16	9.562+1	9.582-2	1.695-1 (85.3%)	2.108-2(100.6%)	1.672-2	2.680-10	9.922-3	2.664-2	9.9	-1.63-3 (2.7-4)
Sm-149	2.0	4.5	16	1.903+2	1.085-1	6.005-1 (41.8%)	3.352-2(101.0%)	2.823-2	2.833-10	1.524-2	4.347-2	20.9	-1.75-3 (2.5-4)
Sm-149	1.0	4.5	18	1.076+2	1.065-1	1.717-1 (85.1%)	2.120-2(100.6%)	1.664-2	2.462-10	1.003-2	2.667-2	11.0	
Sm-149	2.0	4.5	18	2.141+2	1.205-1	5.998-1 (41.9%)	3.424-2(101.0%)	2.902-2	2.657-10	1.524-2	4.426-2	21.9	
Sm-149	0.05	4.5	64	1.921+1	9.585-2	4.136-3(100.2%)	4.921-3(100.1%)	3.551-3	2.330-10	2.451-3	6.003-3	2.2	
Sm-149	0.1	4.5	64	3.841+1	1.469-1	5.269-3(100.3%)	6.346-3(100.1%)	4.638-3	1.578-10	3.169-3	7.806-3	5.9	
Sm-149	0.25	4.5	64	7.679+1	2.006-1	7.661-3(100.4%)	9.076-3(100.2%)	6.686-3	1.229-10	4.480-3	1.117-2	7.8	

Table 11. Sm Burnable Poison in a Sm2O3 Coating between the UO2 Fuel Pellet and the Zr-4 Cladding of Selected Fuel Rods - Summary Results.

Initial BP Isotope	Thickness BP Layer (mills)	Initial Density Fraction BP Sm2O3	Initial Fuel Enrich-ment (wt%U235)	Number Fuel Rods with BP (per Fuel Assembly)	BP Mass (per Fuel Assembly) (gram)	Initial BP Reactivity Worth for Reactor Core (-dkeff/keff)	Reactivity Ratio 120 FPD vs.BOL	Reactivity Ratio 1 FPY vs.BOL	Reactivity Ratios 4 FPY vs. BOL				BP Penalty at 4 FPY (FPD)	MVC at BOL
							BP-tot per Sm(BOL)	BP-tot per Sm(BOL)	Sm-tot per Sm(BOL)	Pm-tot per Sm(BOL)	Eu-tot per Sm(BOL)	BP-tot per Sm(BOL)		dkeff per -10% water density change (STD)
Sm-nat	2.0	1.00	4.5	08	2.362+2	4.627-2	1.328-1 (96.1%)	1.082-1 (98.8%)	3.807-2	3.333-9	5.914-2	9.720-2	18.6	
Sm-nat	4.0	1.00	4.5	08	4.696+2	5.416-2	4.729-1 (62.1%)	1.593-1 (99.1%)	6.447-2	5.319-9	8.717-2	1.516-1	34.7	
Sm-nat	1.0	1.00	4.5	16	2.369+2	7.127-2	7.907-2 (98.7%)	8.158-2 (98.4%)	2.477-2	1.969-9	4.223-2	6.700-2	16.9	
Sm-nat	2.0	1.00	4.5	16	4.724+2	8.716-2	1.415-1 (95.7%)	1.145-1 (98.8%)	4.049-2	3.101-9	6.283-2	1.033-1	40.5	
Sm-nat	4.0	1.00	4.5	16	9.391+2	1.019-1	4.807-1 (61.7%)	1.669-1 (98.9%)	6.693-2	5.119-9	9.070-2	1.576-1	64.6	
Sm-nat	1.0	1.00	4.5	18	2.666+2	7.886-2	8.150-2 (98.6%)	8.309-2 (98.4%)	2.534-2	1.994-9	4.286-2	6.820-2	25.2	
Sm-nat	2.0	1.00	4.5	18	5.315+2	9.753-2	1.420-1 (95.6%)	1.166-1 (98.4%)	4.038-2	2.969-9	6.196-2	1.023-1	49.3	
Sm-nat	0.2	1.00	4.5	64	1.900+2	1.147-1	5.084-2 (98.2%)	4.970-2 (98.3%)	1.135-2	9.939-10	2.177-2	3.312-2	14.8	
Sm-nat	0.5	1.00	4.5	64	4.746+2	1.818-1	7.158-2 (97.9%)	7.145-2 (98.0%)	1.832-2	1.388-9	3.373-2	5.205-2	33.5	
Sm-nat	1.0	1.00	4.5	64	9.478+2	2.330-1	9.655-2 (98.2%)	9.927-2 (97.9%)	2.945-2	2.081-9	5.017-2	7.963-2	71.8	
Sm-nat	1.0	0.10	4.5	104	1.540+2	1.109-1	4.540-2 (98.2%)	4.390-2 (98.4%)	9.483-3	8.606-10	1.837-2	2.785-2	16.1	
Sm-nat	0.1	1.00	4.5	104	1.544+2	1.080-1	4.677-2 (98.1%)	4.516-2 (98.3%)	9.518-3	8.907-10	1.867-2	2.819-2	12.4	
Sm-149	0.5	1.00	4.5	08	5.925+1	5.296-2	3.023-1 (72.1%)	2.579-2(100.7%)	2.037-2	4.600-10	1.179-2	3.216-2	6.8	
Sm-149	1.0	1.00	4.5	08	1.183+2	5.960-2	6.777-1 (34.0%)	4.058-2(101.0%)	3.358-2	4.680-10	1.732-2	5.090-2	12.2	
Sm-149	2.0	1.00	4.5	08	2.359+2	6.646-2	7.850-1 (23.3%)	1.931-1 (87.5%)	5.410-2	5.258-10	2.325-2	7.735-2	19.2	
Sm-149	4.0	1.00	4.5	08	4.689+2	7.423-2	8.275-1 (19.4%)	6.223-1 (42.5%)	8.528-2	7.115-10	2.687-2	1.122-1	36.1	
Sm-149	8.0	1.00	4.5	08	9.263+2	8.355-2	8.588-1 (16.7%)	7.123-1 (34.0%)	1.293-1	1.151-9	2.327-2	1.526-1	46.7	
Sm-149	0.1	1.00	4.5	16	2.373+1	6.322-2	8.368-3(100.3%)	9.977-3(100.2%)	6.972-3	3.580-10	4.860-3	1.183-2	3.2	-9.2-4 (2.8-4)
Sm-149	0.2	1.00	4.5	16	4.744+1	8.072-2	1.772-2(100.0%)	1.490-2(100.3%)	1.084-2	2.940-10	7.179-3	1.802-2	6.4	-8.0-4 (2.7-4)
Sm-149	0.5	1.00	4.5	16	1.185+2	9.977-2	3.063-1 (71.7%)	2.691-2(100.6%)	2.075-2	2.738-10	1.235-2	3.310-2	13.5	-1.55-3 (2.6-4)
Sm-149	1.0	1.00	4.5	16	2.366+2	1.122-1	6.728-1 (34.6%)	4.258-2(101.1%)	3.491-2	3.027-10	1.815-2	5.306-2	22.1	-2.18-3 (2.6-4)
Sm-149	2.0	1.00	4.5	16	4.718+2	1.239-1	8.040-1 (21.4%)	1.896-1 (88.3%)	5.766-2	3.996-10	2.451-2	8.216-2	42.9	-3.02-3 (2.5-4)
Sm-149	4.0	1.00	4.5	16	9.379+2	1.371-1	8.448-1 (17.7%)	6.297-1 (42.1%)	9.190-2	6.206-10	2.857-2	1.205-1	72.0	-4.30-3 (2.5-4)
Sm-149	8.0	1.00	4.5	16	1.853+3	1.540-1	8.654-1 (16.0%)	7.149-1 (33.9%)	1.347-1	1.150-9	2.503-2	1.597-1	108.0	-5.44-3 (2.6-4)
Sm-149	1.0	1.00	4.5	18	2.662+2	1.236-1	6.887-1 (32.9%)	4.268-1 (60.6%)	3.568-2	2.885-10	1.879-2	5.446-2	32.1	
Sm-149	2.0	1.00	4.5	18	5.308+2	1.372-1	8.003-1 (21.8%)	1.949-1 (87.7%)	5.747-2	3.822-10	2.476-2	8.223-2	42.6	
Sm-149	4.0	1.00	4.5	18	1.055+3	1.525-1	8.370-1 (18.5%)	6.307-1 (42.0%)	9.204-2	6.055-10	2.857-2	1.206-1	75.9	
Sm-149	8.0	1.00	4.5	18	2.084+3	1.701-1	8.681-1 (15.8%)	7.170-1 (33.8%)	1.369-1	1.165-9	2.534-2	1.632-1	109.2	
Sm-149	0.5	0.10	4.5	64	4.740+1	1.584-1	7.238-3(100.3%)	8.492-3(100.2%)	5.817-3	1.506-10	4.275-3	1.009-2	7.2	
Sm-149	1.0	0.10	4.5	64	9.465+1	2.126-1	1.030-2(100.5%)	1.227-2(100.3%)	8.643-3	1.226-10	6.099-3	1.474-2	13.2	
Sm-149	0.1	1.00	4.5	64	9.491+1	2.119-1	1.034-2(100.4%)	1.222-2(100.2%)	8.511-3	1.223-10	5.933-3	1.445-2	11.9	
Sm-149	0.2	0.10	4.5	104	3.084+1	1.372-1	5.387-3(100.2%)	6.465-3(100.1%)	4.409-3	1.673-10	3.218-3	7.628-3	3.7	
Sm-149	0.5	0.10	4.5	104	7.702+1	2.236-1	8.253-3(100.3%)	9.808-3(100.2%)	6.762-3	1.129-10	4.875-3	1.164-2	13.4	

Table 12. Sm Burnable Poison Integrally mixed with the Zr-4 Cladding of Selected Fuel Rods - Summary Results.

Initial BP Isotope	Initial loading BP (wt%Sm in Zr-4)	Initial Fuel Enrich-ment (wt%U235)	Number Fuel Rods with BP (per Fuel Assembly)	BP Mass (per Fuel Assembly) (gram)	Initial BP Reactivity Worth for Reactor Core (-dkeff/keff)	Reactivity Ratio 120 FPD vs.BOL BP-tot per Sm(BOL)	Reactivity Ratio 1 FPY vs.BOL BP-tot per Sm(BOL)	Reactivity Ratios 4 FPY vs. BOL Sm-tot per Sm(BOL)	Pm-tot per Sm(BOL)	Eu-tot per Sm(BOL)	BP-tot per Sm(BOL)	BP Penalty at 4 FPY (FPD)	MVC at BOL dkeff per -10% water density change (STD)
Sm-nat	2.0	4.5	16	1.152+2	5.916-2	5.471-2 (98.4%)	5.564-2 (98.3%)	1.382-2	1.319-9	2.585-2	3.967-2	11.1	-1.24-3 (2.9-4)
Sm-nat	4.0	4.5	16	2.312+2	7.988-2	7.290-2 (98.5%)	7.465-2 (98.3%)	2.110-2	1.694-9	3.748-2	5.855-2	21.5	-1.17-3 (2.7-4)
Sm-nat	0.10	4.5	104	3.733+1	3.691-2	3.601-2 (98.4%)	3.364-2 (98.6%)	6.932-3	1.079-9	1.328-2	2.022-2	2.8	-4.8-4 (4.6-4)
Sm-nat	0.50	4.5	104	1.868+2	1.333-1	4.609-2 (98.2%)	4.408-2 (98.4%)	9.548-3	8.327-10	1.865-2	2.819-2	19.5	
Sm-nat	1.00	4.5	104	3.739+2	2.001-1	5.827-2 (97.9%)	5.622-2 (98.1%)	1.297-2	1.034-9	2.486-2	3.783-2	35.7	
Sm-nat	1.00	6.0	104	3.739+2	1.766-1	6.378-2 (97.3%)	6.258-2 (97.4%)	1.280-2	9.739-10	2.454-2	3.734-2	25.0	
Sm-149	0.1	4.5	16	5.743+0	3.036-2	4.826-3(100.2%)	5.497-3(100.1%)	3.775-3	7.187-10	2.792-3	6.567-3	0.8	-1.18-3 (3.0-4)
Sm-149	0.2	4.5	16	1.149+1	4.761-2	5.967-3(100.2%)	6.870-3(100.1%)	4.772-3	4.633-10	3.472-3	8.244-3	1.6	-8.8-4 (2.8-4)
Sm-149	0.5	4.5	16	2.874+1	7.359-2	9.351-3(100.4%)	1.093-2(100.2%)	7.548-3	3.115-10	5.424-3	1.297-2	3.9	-9.5-4 (2.8-4)
Sm-149	1.0	4.5	16	5.752+1	9.226-2	2.236-2 (99.8%)	1.658-2(100.4%)	1.212-2	2.635-10	8.093-3	2.021-2	7.4	-1.34-3 (2.7-4)
Sm-149	2.0	4.5	16	1.152+2	1.076-1	2.321-1 (79.4%)	2.595-2(100.6%)	1.975-2	2.540-10	1.244-2	3.218-2	14.8	-1.75-3 (2.6-4)
Sm-149	0.05	4.5	104	1.866+1	1.035-1	4.656-3(100.2%)	5.570-3(100.1%)	3.713-3	2.172-10	2.791-3	6.503-3	2.8	+3.8-4 (4.2-4)
Sm-149	0.10	4.5	104	3.733+1	1.645-1	5.843-3(100.2%)	6.929-3(100.1%)	4.574-3	1.422-10	3.472-3	8.046-3	6.4	+2.13-3 (3.8-4)
Sm-149	0.20	4.5	104	7.468+1	2.319-1	8.120-3(100.3%)	9.528-3(100.2%)	6.380-3	1.087-10	4.825-3	1.121-2	11.7	+3.16-3 (3.3-4)
Sm-149	0.10	6.0	104	3.733+1	1.396-1	5.969-3(100.3%)	7.464-3(100.2%)	4.919-3	6.054-11	4.103-3	9.022-3	9.3	
Sm-149	0.20	6.0	104	7.468+1	2.056-1	8.119-3(100.4%)	9.789-3(100.2%)	6.599-3	4.926-11	5.433-3	1.203-2	14.4	

The MVCs were calculated by decreasing the water coolant density by 10%. Note that for all the cases containing 8 and 16 IFBA rods, the MVCs remain negative. For the cases with 64 IFBA rods, the MVC becomes positive for the lattices containing identical standard 17 × 17 fuel assemblies with the same BP loadings. Calculations of the MVC were not performed for checkerboard loadings of selected fuel assemblies containing 64 IFBA rods.

Figure 13 displays the initial reactivity worths of the samarium-based BP as a function of the residual BP penalty in FPDs for several configurations containing 16 IFBA rods. The trend for the four different forms of BP are very similar. Note also the clear advantage of using samarium enriched in ^{149}Sm over samarium with natural isotopic abundances. Figure 14 displays the initial reactivity worths of the BP vs FPD penaltyfor fuel assembly configurations containing 64 IFBA rods.

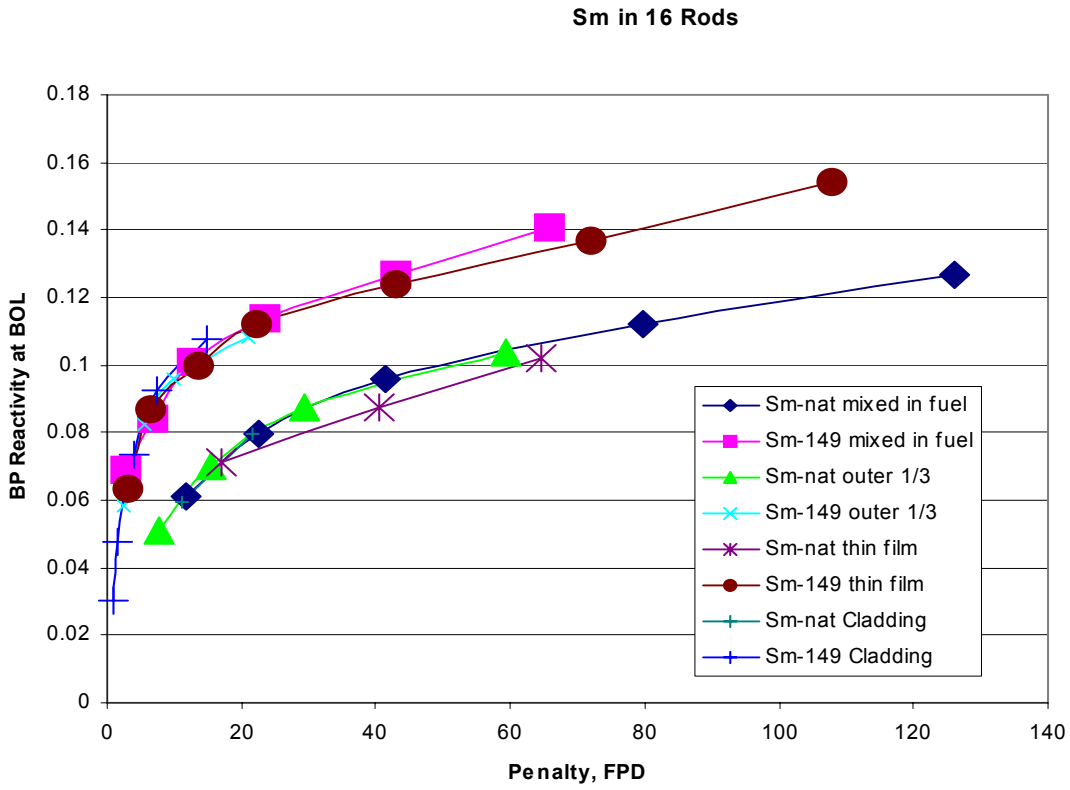

Figure 13 Burnable poison initial reactivity worth as a function of FPD penalty -- Sm in 16 IFBA rods

NEUTRONICS PERFORMANCE RESULTS FOR ERBIUM

Erbia (Er_2O_3) as a burnable poison has been used in designs of the modular high temperature reactors (MHTRs). More recently Er_2O_3 has also been used as burnable poisons in System-80 PWRs. In this section, we will investigate the potential benefits of using enriched erbium as a burnable absorber in PWRs. Four different types of burnable poison rods containing erbium, similar to those of the cases of Gd, were investigated.

In all the neutronics calculations presented in this section, a theoretical density of 8.64 g/cm^3 was used for Er_2O_3, and 9.00 g/cm^3 for metallic erbium. For UO_2, a theoretical density of 10.97 g/cm^3 was used. The actual density fraction of the fuel pellets and of the burnable poison pellets was 95% of theoretical density.

The half-lives, natural isotopic abundances, and burnup chains related to the depletion and transmutation of erbium are given below. Note that the adjacent bands of isotopes such as the Yb isotopes (decay from Tm isotopes) and Dy isotopes (decay from Ho isotopes) are not shown. Also the isomeric states of certain isotopes are not shown. However, the generation of these daughters was taken into account in the BP depletion and decay calculations.

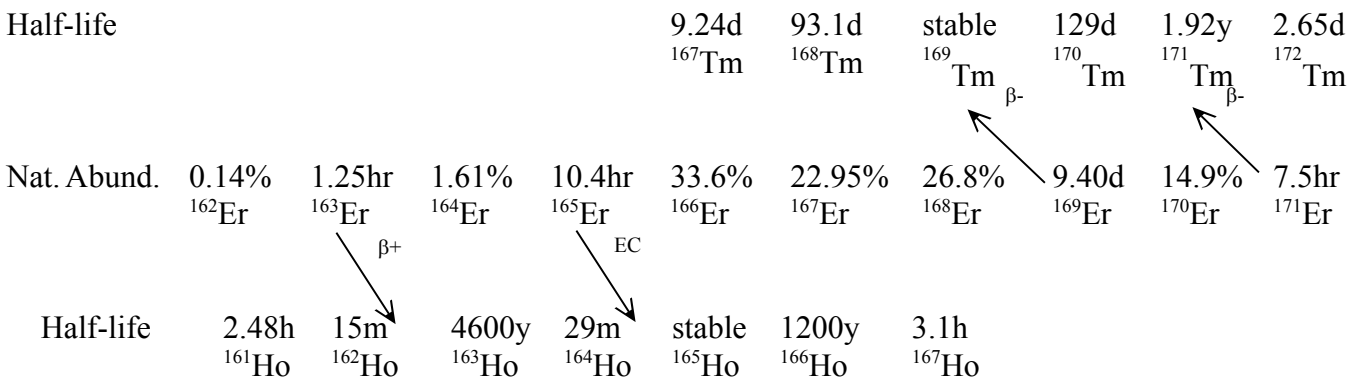
Half-life
9.24d
167Tm
93.1d
168Tm
stable
169Tm
β-
129d
170Tm
1.92y
171Tm
β-
2.65d
172Tm
Nat. Abund.
0.14%
162Er
1.25hr
163Er
β+
1.61%
164Er
10.4hr
165Er
EC
33.6%
166Er
22.95%
167Er
26.8%
168Er
9.40d
169Er
14.9%
170Er
7.5hr
171Er
Half-life
2.48h
161Ho
15m
162Ho
4600y
163Ho
29m
164Ho
stable
165Ho
1200y
166Ho
3.1h
167Ho

The erbium stable isotope ^{167}Er (22.9% natural isotopic abundance) exhibits a large neutron capture cross section (thermal cross section of 660 barns and a RI of 2,970 barns). The isotopes ^{162}Er (0.14% natural isotopic abundance), ^{164}Er (1.6%), ^{166}Er (33.4%), and ^{170}Er (14.9%) have smaller capture cross sections: ^{162}Er (thermal 19 barns, RI 480 barns), ^{164}Er (thermal 13 barns, RI 105 barns), ^{166}Er (thermal 19.6 barns, RI 96 barns), and ^{170}Er (thermal 5.8 barns, RI 45 barns). Because of the small cross sections, these isotopes are difficult to burn out and they will thus leave a residual negative reactivity burden at EOL of the BP. ^{168}Er (27.1% natural isotopic abundance) has a small neutron capture cross section (thermal 2.7 barns, RI 37 barns). The ^{167}Er (n,γ) ^{168}Er reaction, together with the use of erbium fully enriched in ^{167}Er, will thus mainly lead to ^{168}Er. The residual burden of the BP enriched in ^{167}Er should thus be small. The ^{168}Er (n,γ) ^{169}Er reaction leads to ^{169}Er, which decays into ^{169}Tm with a half-life of 9.4 days. The ^{169}Tm capture cross section is large (thermal 105 barns, RI 1,720 barns). In erbium with natural isotopic abundances, ^{168}Er has an isotopic abundance of 26.8%. Even though the capture cross section of ^{168}Er is small, the ^{168}Er (n,γ) ^{169}Er reaction will lead to ^{169}Tm. Also, ^{170}Er (14.9% natural isotopic abundance) has a small neutron capture cross section (thermal 5.8 barns, RI 45 barns), but the ^{170}Er (n,γ) ^{171}Er reaction will lead to ^{171}Er, which decays with a half-life of 7.5 hours to ^{171}Tm. The capture cross section of ^{171}Tm is large (thermal 160 barns, RI 118 barns). Note that the use of ^{167}Er will not create any of the holmium isotopes. The use of erbium with natural isotopic abundances will lead to ^{163}Ho and ^{165}Ho. These have large capture cross sections. However, since the natural isotopic abundances of ^{162}Er and ^{164}Er are small, they will only slightly contribute to the residual reactivity burden at EOL of the BP.

Table 13 displays the results of using Er_2O_3 mixed homogeneously with the fuel pellets of a number of fuel rods. Note that for the same initial reactivity worth of the BP, the residual negative reactivity worth of erbium fully enriched in ^{167}Er is smaller than for erbium with natural isotopic abundances. The relative contribution from the thulium daughters is also smaller.

The reactivity worths of the BP isotopes, for a 4.0 wt % loading of Er_2O_3 with natural isotopic abundances, homogeneously mixed inside the fuel pellets of 64 IFBA rods per fuel assembly, are shown in Figure 15. The initial reactivity worth of the BP is 0.141 and the residual reactivity ratio is 9.0%. For a 1.0 wt % homogeneous loading in 64 IFBA rods of Er_2O_3 fully enriched in ^{167}Er, the results are shown in Figure 16. The initial reactivity worth of the BP is 0.140 and the residual reactivity ratio is 1.6%. The use of erbium enriched in ^{167}Er, instead of with natural isotopic abundances, will thus lead to a substantial reduction of the residual reactivity burden at EOL of the fuel. Note that the trends of the fuel assembly lattice k_{inf}'s are fairly flat for almost 2 years of reactor operation. Figure 16 also displays a secular equilibrium between the ^{166}Er and ^{167}Er neutron capture reaction rates. However, since the cross section of ^{167}Er is smaller than in the case of gadolinium or samarium, the secular equilibrium happens much later (approximately 4 years).

In Tables 13 through 16 the residual reactivity worths, due to the Ho daughters of the BP containing erbium enriched in ^{167}Er, should essentially be zero, since only the decay of ^{163}Er and ^{165}Er leads to ^{163}Ho and ^{165}Ho, respectively. There are essentially no paths from the transmutation of ^{167}Er to any of the Ho isotopes. However, the tables show residual reactivity worths of the order of 1.0×10^{-10}. This is because for each case, all the BP isotopes and their daughters (which are not present in the initial loading of the BP) have been added as traces to the BP with a number density of 1.0×10^{-15}

instead of zero. This is to avoid problems at the BOC in the input to the MCNP4C code and to avoid computer exception errors (division by zero) when calculating spectrum-weighted cross sections. The MVCs were calculated by decreasing the water coolant density by 10% (see Tables 13–16). Note that for all the cases containing 8, 16, and 64 IFBA rods, the MVCs remain negative. This is in contrast to the use of 64 IFBA rods containing gadolinium or samarium as the BP.

Figure17 displays the initial reactivity worths of the erbium based BP as a function the residual BP penalty in FPDs for several configurations containing 16 IFBA rods. Figure 18 displays the initial reactivity worths of the BP vs FPD penalty for fuel assembly configurations containing 64 IFBA rods. The trends for the four different forms of BPs are very similar. Note also the clear advantage of using enriched erbium (enriched in ^{167}Er) over erbium with natural isotopic abundances.

Table 13. Er Burnable Poison Integrally mixed with the UO2 Fuel Pellets of Selected Fuel Rods - Summary Results.

Initial BP Isotope	Initial Loading BP (wt%Er2O3 in UO2)	Initial Fuel Enrich-ment (wt%U235)	Number Fuel Rods with BP (per Fuel Assembly)	BP Mass (per Fuel Assembly) (gram)	Initial BP Reactivity Worth for Reactor Core (-dkeff/keff)	Reactivity Ratio 120 FPD vs.BOL BP-tot per Er(BOL)	Reactivity Ratio 1 FPY vs.BOL BP-tot per Er(BOL)	Reactivity Ratios 4 FPY vs. BOL Er-tot per Er(BOL)	Ho-tot per Er(BOL)	Tm-tot per Er(BOL)	BP-tot per Er(BOL)	BP Penalty at 4 FPY (FPD)	MVC at BOL dkeff per -10% water density change (STD)
Er-nat	4.0	4.5	08	5.790+2	1.935-2	7.306-1 (29.3%)	4.084-1 (64.3%)	6.718-2	8.335-4	1.197-2	7.999-2	5.8	
Er-nat	2.0	4.5	16	5.822+2	2.307-2	6.748-1 (35.0%)	3.302-1 (72.1%)	5.918-2	7.543-4	1.093-2	7.087-2	6.9	
Er-nat	4.0	4.5	16	1.158+3	3.783-2	7.326-1 (29.2%)	4.162-1 (63.7%)	6.908-2	8.997-4	1.320-2	8.318-2	12.6	-3.48-3 (2.9-4)
Er-nat	8.0	4.5	16	2.292+3	5.913-2	7.851-1 (24.0%)	5.092-1 (54.8%)	8.579-2	1.113-3	1.658-2	1.035-1	25.0	-3.62-3 (2.704)
Er-nat	12.0	4.5	16	3.402+3	7.449-2	8.109-1 (21.5%)	5.681-1 (49.2%)	1.021-1	1.256-3	1.894-2	1.223-1	37.4	-4.69-3 (2.9-4)
Er-nat	4.0	4.5	20	1.448+3	4.644-2	7.370-1 (28.8%)	4.150-1 (63.9%)	7.043-2	9.236-11	1.375-2	8.511-2	16.1	
Er-nat	8.0	4.5	20	2.865+3	7.270-2	7.833-1 (24.2%)	5.173-1 (53.9%)	8.687-2	1.121-3	1.690-2	1.049-1	89.1	
Er-nat	1.0	4.5	64	1.167+3	5.084-2	6.360-1 (38.9%)	2.804-1 (77.0%)	5.373-2	7.147-4	1.087-2	6.531-2	16.8	-3.62-3 (3.6-4)
Er-nat	2.0	4.5	64	2.329+3	8.678-2	6.955-1 (33.0%)	3.391-1 (71.6%)	6.349-2	8.184-4	1.225-2	7.656-2	25.4	-6.05-3 (3.8-4)
Er-nat	4.0	4.5	64	4.632+3	1.405-1	7.461-1 (27.9%)	4.214-1 (63.6%)	7.452-2	9.870-4	1.495-2	9.045-2	46.9	-7.12-3 (3.4-4)
Er-167	4.0	4.5	08	5.789+2	4.407-2	8.015-1 (20.6%)	5.764-1 (44.1%)	2.884-2	4.242-10	9.533-3	3.837-2	6.6	
Er-167	1.0	4.5	16	2.918+2	3.833-2	7.090-1 (29.5%)	3.712-1 (63.8%)	8.091-3	4.900-10	6.400-3	1.449-2	2.4	
Er-167	2.0	4.5	16	5.820+2	5.879-2	7.659-1 (23.9%)	4.731-1 (53.8%)	1.269-2	3.195-10	7.614-3	2.031-2	4.7	-3.75-3 (2.9-4)
Er-167	4.0	4.5	16	1.158+3	8.457-2	8.100-1 (19.8%)	5.819-1 (43.5%)	2.820-2	2.216-10	1.021-2	3.841-2	14.1	-4.25-3 (2.8-4)
Er-167	8.0	4.5	16	2.291+3	1.154-1	8.450-1 (17.4%)	6.563-1 (38.7%)	9.928-2	1.603-10	1.178-2	1.111-1	83.8	-5.21-3 (2.7-4)
Er-167	4.0	4.5	20	1.447+3	1.042-1	8.050-1 (20.3%)	5.765-1 (44.1%)	2.885-2	1.796-10	1.027-2	3.912-2	17.6	
Er-167	0.2	4.5	64	2.339+2	4.314-2	6.055-1 (39.9%)	2.226-1 (78.5%)	5.564-3	4.375-10	4.497-3	1.006-2	1.6	-3.65-3 (4.0-4)
Er-167	0.5	4.5	64	5.844+2	8.770-2	6.770-1 (32.7%)	2.932-1 (71.6%)	6.725-3	2.160-10	5.555-3	1.228-2	5.3	-5.78-3 (3.7-4)
Er-167	1.0	4.5	64	1.167+3	1.396-1	7.265-1 (27.8%)	3.824-1 (62.8%)	9.275-3	1.357-10	6.832-3	1.611-2	9.8	-6.85-3 (3.5-4)

Table 14. Er Burnable Poison Integrally mixed with the Outer One Third Part of the UO2 Fuel Pellets of Selected Fuel Rods - Summary Results.

Initial BP Isotope	Initial Loading BP (wt%Er2O3 in UO2)	Initial Fuel Enrich-ment (wt%U235)	Number Fuel Rods with BP (per Fuel Assembly)	BP Mass (per Fuel Assembly) (gram)	Initial BP Reactivity Worth for Reactor Core (-dkeff/keff)	Reactivity Ratio 120 FPD vs.BOL BP-tot per Er(BOL)	Reactivity Ratio 1 FPY vs.BOL BP-tot per Er(BOL)	Reactivity Ratios 4 FPY vs. BOL Er-tot per Er(BOL)	Ho-tot per Er(BOL)	Tm-tot per Er(BOL)	BP-tot per Er(BOL)	BP Penalty at 4 FPY (FPD)	MVC at BOL dkeff per -10% water density change (STD)
Er-nat	4.0	4.5	08	1.930+2	8.453-3	6.502-1 (37.4%)	2.918-1 (75.8%)	5.374-2	7.025-4	1.134-2	6.579-2	2.3	
Er-nat	8.0	4.5	08	3.820+2	1.452-2	7.103-1 (31.3%)	3.463-1 (70.6%)	6.066-2	7.935-4	1.208-2	7.353-2	4.3	
Er-nat	12.0	4.5	08	5.669+2	1.928-2	7.304-1 (29.4%)	3.953-1 (65.9%)	6.717-2	9.435-4	1.373-2	8.184-2	6.4	
Er-nat	16.0	4.5	08	7.481+2	2.335-2	7.477-1 (27.7%)	4.466-1 (60.6%)	7.213-2	9.403-4	1.435-2	8.742-2	8.8	
Er-nat	1.0	4.5	16	9.729+1	4.866-3	5.902-1 (43.5%)	2.392-1 (80.8%)	4.800-2	6.317-4	9.620-3	5.825-2	1.2	-1.99-3 (4.2-4)
Er-nat	2.0	4.5	16	1.941+2	9.138-3	6.219-1 (40.3%)	2.604-1 (78.8%)	4.948-2	6.780-4	1.089-2	6.106-2	2.4	-2.36-3 (3/1-4)
Er-nat	4.0	4.5	16	3.860+2	1.674-2	6.489-1 (37.6%)	2.902-1 (76.1%)	5.533-2	7.162-4	1.089-2	6.693-2	5.2	-2.38-3 (3.2-4)
Er-nat	8.0	4.5	16	7.639+2	2.850-2	7.057-1 (31.9%)	3.520-1 (70.2%)	6.300-2	8.158-4	1.263-2	7.644-2	9.2	-3.10-3 (3.1-40
Er-nat	1.0	4.5	18	1.095+2	5.465-3	5.868-1 (44.0%)	2.391-1 (80.9%)	4.920-2	6.251-4	1.004-2	5.986-2	1.7	
Er-nat	4.0	4.5	18	4.343+2	1.862-2	6.589-1 (36.5%)	2.955-1 (75.4%)	5.473-2	7.213-4	1.041-2	6.586-2	4.2	
Er-nat	0.5	4.5	64	1.948+2	1.013-2	5.742-1 (45.1%)	2.244-1 (82.2%)	4.665-2	6.141-4	9.325-3	5.659-2	2.8	-1.99-3 (4.2-4)
Er-nat	1.0	4.5	64	3.891+2	1.937-2	5.965-1 (42.9%)	2.403-1 (80.7%)	4.881-2	6.267-4	9.505-3	5.894-2	4.0	-2.79-3 (3.9-4)
Er-nat	2.0	4.5	64	7.762+2	3.631-2	6.147-1 (41.1%)	2.592-1 (79.0%)	5.166-2	6.686-4	1.015-2	6.248-2	9.3	-3.39-3 (4.0-4)
Er-nat	4.0	4.5	64	1.544+3	6.464-2	6.578-1 (36.8%)	2.969-1 (75.6%)	5.741-2	7.652-4	1.152-2	6.970-2	16.6	-3.69-3 (3.8-4)
Er-nat	8.0	4.5	64	3.056+3	1.074-1	7.135-1 (31.2%)	3.639-1 (69.2%)	6.705-2	8.853-4	1.322-2	8.116-2	33.5	-5.88-3 (3.9-4)
Er-167	4.0	4.5	08	1.930+2	2.349-2	7.418-1 (26.1%)	4.071-1 (60.0%)	9.387-3	7.984-10	2.101-3	1.149-2	1.0	
Er-167	8.0	4.5	08	3.819+2	3.593-2	7.901-1 (21.5%)	5.032-1 (50.9%)	1.523-2	5.224-10	8.377-3	2.361-2	3.6	
Er-167	12.0	4.5	08	5.668+2	4.410-2	8.109-1 (19.6%)	5.717-1 (44.4%)	2.521-2	4.269-10	9.614-3	3.482-2	6.6	
Er-167	0.2	4.5	16	1.949+1	4.119-3	5.543-1 (45.0%)	1.834-1 (82.4%)	4.914-3	4.560-9	4.069-3	9.984-3	0.15	-1.75-3 (3/2-4)
Er-167	0.5	4.5	16	4.870+1	9.593-3	5.931-1 (41.1%)	2.038-1 (80.4%)	5.358-3	1.920-9	4.171-3	9.529-3	0.4	-2.21-3 (2.9-4)
Er-167	1.0	4.5	16	9.726+1	1.707-2	6.453-1 (35.9%)	2.442-1 (76.4%)	5.940-3	1.100-9	4.800-3	1.074-2	0.75	-2.45-3 (3.0-4)
Er-167	2.0	4.5	16	1.940+2	2.916-2	6.873-1 (31.7%)	3.098-1 (69.9%)	7.152-3	6.420-10	5.641-3	1.279-2	1.5	-3.14-3 (3/1-4)
Er-167	4.0	4.5	16	3.859+2	4.655-2	7.365-1 (26.8%)	4.064-1 (60.3%)	9.780-3	4.035-10	6.468-3	1.625-2	3.35	-3.00-3 (2.9-4)
Er-167	4.0	4.5	18	4.342+2	5.224-2	7.416-1 (26.3%)	4.080-1 (60.2%)	1.035-2	3.587-10	6.921-3	1.727-2	3.8	
Er-167	0.5	4.5	64	1.948+2	3.775-2	5.946-1 (40.9%)	2.081-1 (80.0%)	5.230-3	5.000-10	4.548-3	9.778-3	1.55	-3.70-3 (4.1-4)
Er-167	1.0	4.5	64	3.891+2	6.657-2	6.362-1 (36.8%)	2.460-1 (76.2%)	6.106-3	2.816-10	4.965-3	1.107-2	2.8	-4.92-3 (3.9-4)
Er-167	2.0	4.5	64	7.760+2	1.097-1	6.916-1 (31.3%)	3.160-1 (69.4%)	7.601-3	1.708-10	6.137-3	1.374-2	5.6	-6.23-3 (3.6-4)
Er-167	4.0	4.5	64	1.544+3	1.676-1	7.516-1 (25.3%)	4.181-1 (59.3%)	1.009-2	1.119-10	7.772-3	1.786-2	12.9	-7.18-3 (3.3-4)

Table 15. Er Burnable Poison in a Er2O3 Coating between the UO2 Fuel Pellet and the Zr-4 Cladding of Selected Fuel Rods - Summary Results.

Initial BP Isotope	Thickness BP Layer (mills)	Initial Density Fraction BP Er2O3	Initial Fuel Enrich-ment (wt%U235)	Number Fuel Rods with BP (per Fuel Assembly)	BP Mass (per Fuel Assembly) (gram)	Initial BP Reactivity Worth for Reactor Core (-dkeff/keff)	Reactivity Ratio 120 FPD vs.BOL BP-tot per Er(BOL)	Reactivity Ratio 1 FPY vs.BOL BP-tot per Er(BOL)	Reactivity Ratios 4 FPY vs. BOL at 4 FPY Er-tot per Er(BOL)	Ho-tot per Er(BOL)	Tm-tot per Er(BOL)	BP-tot per Er(BOL)	BP Penalty (FPD)	MVC at BOL dkeff per -10% water density change (STD)
Er-nat	2.0	1.00	4.5	16	5.571+2	2.165-2	6.955-1 (32.9%)	3.323-1 (72.1%)	6.073-2	7.838-4	1.171-2	7.323-2	6.5	
Er-nat	4.0	1.00	4.5	16	1.107+3	3.621-2	7.491-1 (27.5%)	4.162-1 (64.0%)	7.246-2	9.264-4	1.444-2	8.783-2	13.5	
Er-nat	8.0	1.00	4.5	16	2.187+3	5.639-2	8.106-1 (21.2%)	5.190-1 (53.9%)	8.943-2	1.157-3	1.769-2	1.083-1	26.0	
Er-nat	2.0	1.00	4.5	18	6.267+2	2.421-2	6.941-1 (33.1%)	3.400-1 (71.4%)	6.183-2	7.933-4	1.255-2	7.517-2	6.3	
Er-nat	4.0	1.00	4.5	18	1.246+3	4.019-2	7.614-1 (26.1%)	4.200-1 (63.5%)	7.127-2	9.418-4	1.397-2	8.618-2	14.0	
Er-nat	1.0	1.00	4.5	64	1.118+3	4.850-2	6.491-1 (37.6%)	2.852-1 (76.6%)	5.582-2	7.213-4	1.082-2	6.736-2	10.5	
Er-nat	2.0	1.00	4.5	64	2.228+3	8.316-2	7.026-1 (32.3%)	3.454-1 (71.0%)	6.438-2	8.377-4	1.291-2	7.813-2	28.0	
Er-nat	4.0	1.00	4.5	64	4.429+3	1.330-1	7.680-1 (25.6%)	4.292-1 (62.9%)	7.640-2	1.039-3	1.552-2	9.295-2	51.9	
Er-nat	1.0	1.00	4.5	104	1.816+3	7.517-2	6.638-1 (36.2%)	2.952-1 (75.9%)	5.888-2	7.851-4	1.185-2	7.151-2	28.0	
Er-167	1.0	1.00	4.5	16	2.793+2	3.701-2	7.218-1 (28.2%)	3.658-1 (64.4%)	8.352-3	5.075-10	6.276-3	1.463-2	2.3	
Er-167	2.0	1.00	4.5	16	5.569+2	5.738-2	7.664-1 (23.8%)	4.727-1 (53.8%)	1.203-2	3.268-10	8.148-3	2.018-2	4.5	
Er-167	4.0	1.00	4.5	16	1.107+3	8.322-2	8.114-1 (19.5%)	5.810-1 (43.4%)	2.508-2	2.248-10	9.953-3	3.503-2	13.5	
Er-167	1.0	1.00	4.5	18	3.142+2	4.148-2	7.168-1 (28.8%)	3.678-1 (64.2%)	8.574-3	4.514-10	6.312-3	1.489-2	2.4	
Er-167	2.0	1.00	4.5	18	6.265+2	6.370-2	7.733-1 (23.1%)	4.776-1 (53.3%)	1.216-2	2.953-10	8.322-3	2.048-2	6.6	
Er-167	4.0	1.00	4.5	18	1.245+2	9.300-2	8.081-1 (19.9%)	5.717-1 (44.3%)	2.386-2	2.015-10	1.016-2	3.402-2	13.9	
Er-167	0.2	1.00	4.5	64	2.240+2	4.141-2	6.177-1 (38.6%)	2.239-1 (78.4%)	5.705-3	4.543-10	4.889-3	1.059-2	2.2	
Er-167	0.5	1.00	4.5	64	5.595+2	8.540-2	6.716-1 (33.3%)	2.930-1 (71.6%)	6.828-3	2.197-10	5.690-3	1.252-2	4.2	
Er-167	1.0	1.00	4.5	64	1.117+3	1.368-1	7.221-1 (28.3%)	3.781-1 (63.2%)	9.237-3	1.378-10	6.936-3	1.617-2	13.6	
Er-167	0.2	1.00	4.5	104	3.640+2	6.548-2	6.175-1 (38.7%)	2.410-1 (76.7%)	5.542-3	2.864-10	5.006-3	1.055-2	2.6	
Er-167	0.5	1.00	4.5	104	9.091+2	1.301-1	6.853-1 (31.9%)	3.037-1 (70.6%)	7.244-3	1.452-10	6.130-3	1.337-2	12.1	

Table 16. Er Burnable Poison Integrally mixed with the Zr-4 Cladding of Selected Fuel Rods - Summary Results.

Initial BP Isotope	Initial BP loading (wt%Er in Zr-4)	Initial Fuel Enrich-ment (wt%U235)	Number Fuel Rods with BP (per Fuel Assembly)	BP Mass (per Fuel Assembly) (gram)	Initial BP Reactivity Worth for Reactor Core (-dkeff/keff)	Reactivity Ratio 120 FPD vs.BOL BP-tot per Er(BOL)	Reactivity Ratio 1 FPY vs.BOL BP-tot per Er(BOL)	Reactivity Ratios 4 FPY vs. BOL Er-tot per Er(BOL)	Ho-tot per Er(BOL)	Tm-tot per Er(BOL)	BP Penalty at 4 FPY BP-tot per Er(BOL)	MVC at BOL (FPD)	dkeff per -10% water density change (STD)
Er-nat	1.0	4.5	104	3.743+2	1.972-2	5.776-1 (44.8%)	2.228-1 (82.5%)	4.721-2	7.964-4	9.551-3	5.755-2	4.2	
Er-nat	4.0	4.5	104	1.510+3	6.943-2	6.274-1 (39.9%)	2.618-1 (79.0%)	5.347-2	8.850-4	1.059-2	6.494-2	22.7	
Er-167	0.5	4.5	104	1.869+2	3.857-2	5.740-1 (43.0%)	1.878-1 (82.0%)	5.033-3	4.910-10	4.269-3	9.302-3	1.5	
Er-167	1.0	4.5	104	3.743+2	7.054-2	6.040-1 (40.0%)	2.120-1 (79.6%)	5.479-3	2.702-10	4.849-3	1.033-2	3.2	
Er-167	2.0	4.5	104	7.507+2	1.204-1	6.487-1 (35.6%)	2.623-1 (74.7%)	6.387-3	1.574-10	5.553-3	1.194-2	6.3	
Er-167	2.0	6.0	104	7.507+2	1.132-1	6.990-1 (30.5%)	3.351-1 (67.4%)	6.567-3	1.970-10	6.148-3	1.272-2	6.9	

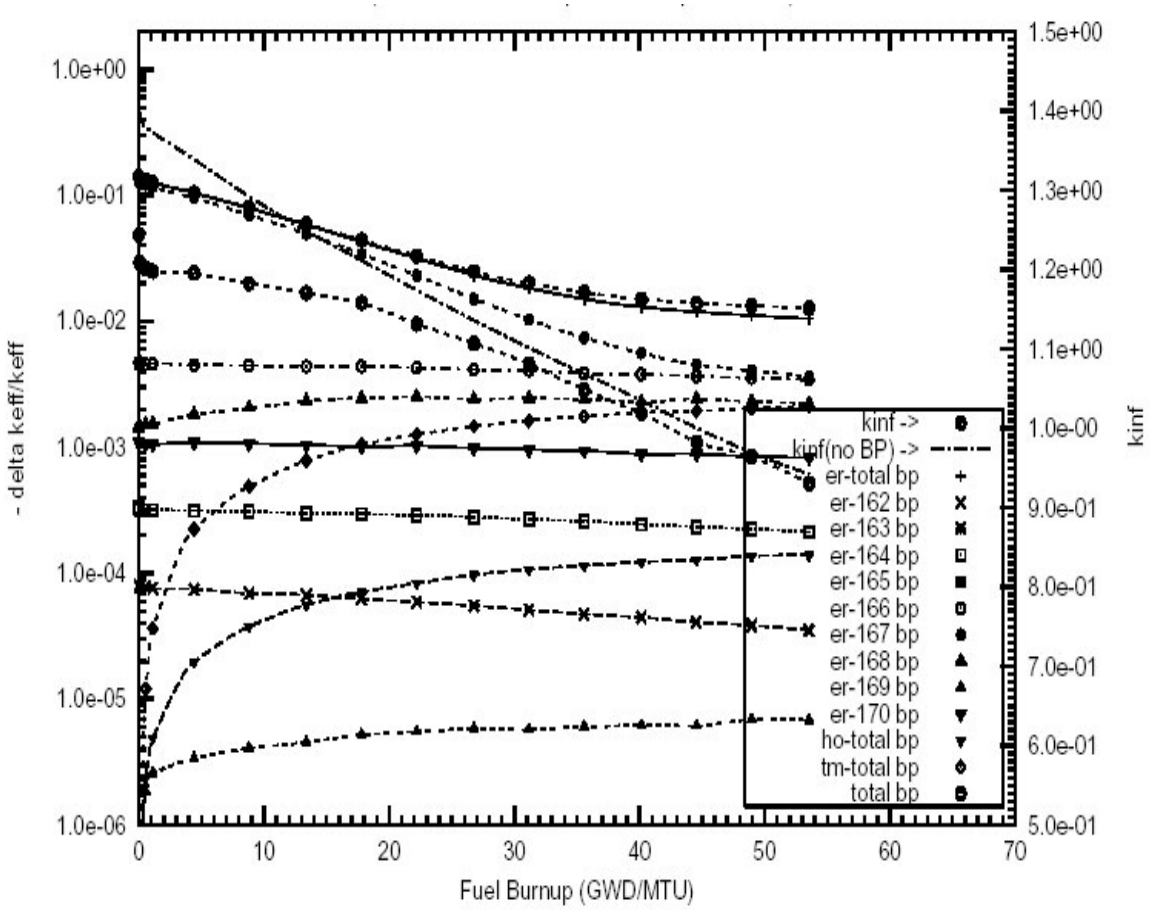

Figure 15 Negative reactivity of BP for Er-167 and transmutation daughters as a function of fuel life for 17x17 fuel assemblies with 64 poison rods, 4.0wt% Er_20_3 poison homogeneously mixed in the UO_2 pellets. Reactor power is 3400 MWth, 193 fuel assemblies, initial enrichment is 4.5wt%^{235}U.

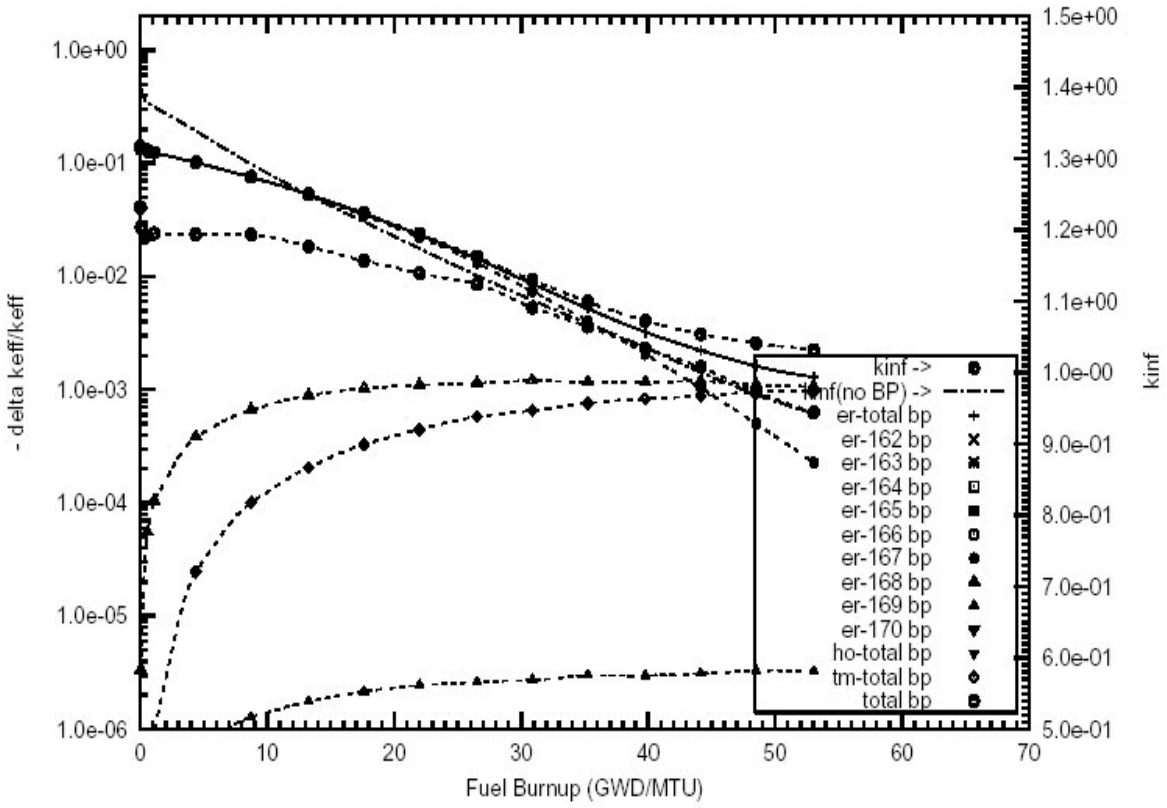

Figure 16 Negative reactivity of BP for Er-167 and transmutation daughters as a function of fuel life for 17x17 fuel assemblies with 64 poison rods, 1.0wt% Er_20_3 poison homogeneously mixed in the UO_2 pellets. Reactor power is 3400 MWth, 193 fuel assemblies, initial enrichment is 4.5wt%^{235}U.

Figure 17 displays the initial reactivity worths of the erbium based BP as a function the residual BP penalty in FPDs for several configurations containing 16 IFBA rods. Figure 18 displays the initial reactivity worths of the BP vs FPD penalty for fuel assembly configurations containing 64 IFBA rods. The trends for the four different forms of BPs are very similar. Note also the clear advantage of using enriched erbium (enriched in ^{167}Er) over erbium with natural isotopic abundances.

NEUTRONICS PERFORMANCE RESULTS FOR DYSPROSIUM

In the proposed use of the CANDU reactor for burning ex-weapons plutonium as MOX, depleted uranium is used as the matrix material throughout the fuel bundle (ref 1). In the central fuel rod and in the next ring of fuel rods, dysprosium burnable poison is mixed with the depleted uranium of those fuel rods not containing plutonium. This increases the amount of plutonium required to achieve a given burnup (and thus increases the Pu disposition rate), reduces the local peak power after refueling, and reduces the local positive MVC in the middle of the fuel bundle (and thus the dysprosium makes the overall bundle MVC more negative). In this case the residual reactivity worth should remain high throughout the life of the fuel.

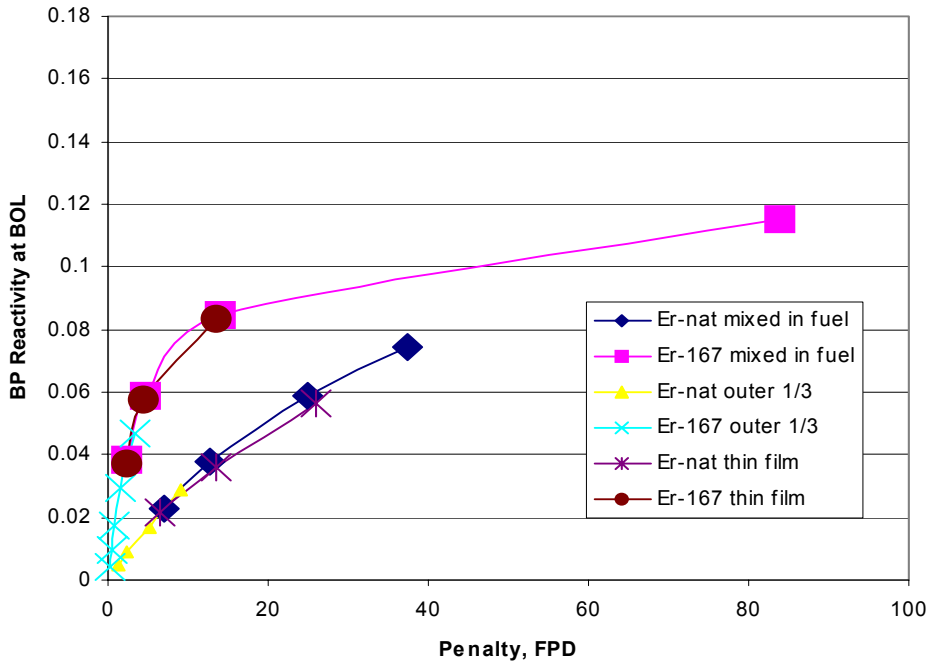

Figure 17 Burnable poison initiao reactivity worth as a function of FPD penalty--Er in 16 IFBA rods

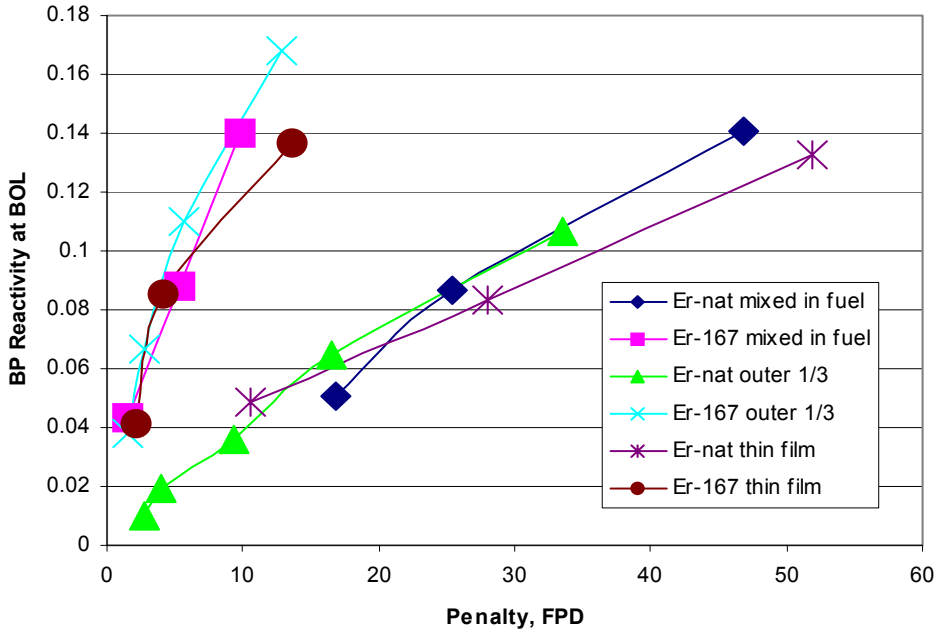

Figure 18 Burnable poison initial reactivity worth as a function of FPD penalty --Er in 64 IFBA rods

In this section, we will show that the use of enriched dysprosium (fully enriched in ^{164}Dy) will improve the performance of dysprosium-based BPs in PWRs. The residual reactivity worth ratio for BPs containing dysprosium with natural isotopic abundances is high, between 30 and 40%, depending on the dysprosium initial loading and the number of IFBA rods per fuel assembly. The use of dysprosium fully enriched in ^{164}Dy reduces the residual reactivity worth ratio of the BPs to between 8 and 18%.

The same four configurations as used for the previously studied elements will be used for dysprosium In all the neutronics calculations presented in this section, a theoretical density of 7.81 g/cm^3 was used for Dy_2O_3, and 8.56 g/cm^3 for metallic dysprosium. For UO_2 a theoretical density of 10.97 g/cm^3 was used. The actual density fraction of the fuel pellets and of the burnable poison pellets was 95% of theoretical density.

The half-lives, natural isotopic abundances and burnup chains related to the depletion and transmutation of dysprosium are given below. Note that the adjacent bands of isotopes such as the Er isotopes (decay from Ho isotopes) are not shown. Also, the isomeric states of certain isotopes are not shown. However, the generation of these daughters was taken into account in the BP depletion and decay calculations.

Half-life								29m ^{164}Ho	stable ^{165}Ho	26.8h ^{166}Ho
									β-	
Nat. Abund.	0.06% ^{156}Dy	8.1h ^{157}Dy	0.10% ^{158}Dy	144.4d ^{159}Dy	2.34% ^{160}Dy	18.9% ^{161}Dy	25.5% ^{162}Dy	24.9% ^{163}Dy	28.2% ^{164}Dy	2.33h ^{165}Dy
		EC		EC						
Half-life	5.3d ^{155}Tb	5.3d ^{156}Tb	110y ^{157}Tb	180y ^{158}Tb	stable ^{159}Tb	72.3d ^{160}Tb	6.91d ^{161}Tb	7.6m ^{162}Tb		

The capture cross sections for Dy and its transmutants are shown in ref. 11. The generation of Tb isotopes is essentially zero, since the natural isotopic abundances of ^{156}Dy (0.06%) and ^{158}Dy (0.1%) are very small.

The stable isotopes ^{156}Dy (0.06% natural isotopic abundance, thermal cross section 33 barns, RI 884 barns), ^{158}Dy (0.1%, thermal 43 barns, RI 120 barns), ^{160}Dy (2.3%, thermal 56 barns, RI 1,160 barns), ^{162}Dy (25.5%, thermal 194 barns, RI 2,755 barns) and ^{163}Dy (24.9%, thermal 124 barns, RI 1,470 barns) exhibit medium-sized capture cross sections, while ^{161}Dy (18.9%, thermal 600 barns, RI 1,200 barns) and ^{164}Dy (28.1%, thermal 2,650 barns, RI 340 barns) have large capture cross sections. Since the majority of the stable dysprosium isotopes (^{160}Dy through ^{164}Dy) are adjacent to each other (in the chart of the nuclides), and since they have medium to large capture cross sections, the residual reactivity ratio of BPs containing dysprosium with natural isotopic abundances will be high. Also, the ^{164}Dy (n,γ) ^{165}Dy reaction leads to ^{165}Dy, which decays to ^{165}Ho with a half-life of 2.33 hours. The thermal capture cross section of ^{165}Ho is approximately 65 barns,

and the RI is 670 barns. Dysprosium with natural isotopic abundances is thus attractive if the burnout of the BP has to be minimized (such as for use in the Pu-burner CANDU). Since the thermal capture cross section of ^{164}Dy is much larger than that for ^{165}Ho, enriching dysprosium in ^{164}Dy will thus reduce the residual reactivity ratio of the BP.

The neutronics calculations for Dy are summarized in Tables 17-20 for the four configurations of the burnable poison. Table 17 displays the results of using Dy_2O_3, mixed homogeneously with the fuel pellets of a number of fuel rods. For the same initial reactivity worth of the BP, the residual negative reactivity worth ratio of dysprosium, fully enriched in ^{164}Dy, is more than two times smaller than the residual worth of dysprosium with natural isotopic abundances. The relative contribution to the residual reactivity ratio from ^{165}Ho is higher for BP containing enriched ^{164}Dy.

The reactivity worths of the BP isotopes, for a 4.0 wt % loading of Dy_2O_3 with natural isotopic abundances, homogeneously mixed in the fuel pellets of 16 IFBA rods per fuel assembly, are shown in Figure 19. The initial reactivity worth of the BP is 6.08×10^{-2} and the residual reactivity ratio is 38.5%. The residual reactivity worth of the Tb daughters is essentially zero, since the natural isotopic abundances of ^{156}Dy and ^{158}Dy are very small, 0.06% and 0.10%, respectively.

For a 4.0 wt % homogeneous loading of Dy_2O_3 (fully enriched in ^{164}Dy) in 16 IFBA rods, the results of the reactivity worths are shown in Figure 20. The initial reactivity worth of the BP is 6.75×10^{-2} and the residual reactivity ratio is 18.0%. The total loading of ^{164}Dy per fuel assembly is 1,150 grams of ^{164}Dy. Most of the residual reactivity burden of the enriched dysprosium BP comes from the buildup of ^{165}Ho. Figure 20 also displays the masses of the burnable poison isotopes. The use of dysprosium as a BP, enriched in ^{164}Dy instead of with natural isotopic abundances, thus leads to a reduction of the residual reactivity burden at EOL of the fuel. For cases of a greater number of IFBA rods, the results show that the shape of the fuel assembly lattice k_{inf}'s is flatter. The BP burnout rate is also slower, which might be useful in applications requiring longer fuel cycles.

Table 17. Dy Burnable Poison Integrally mixed with the UO2 Fuel Pellets of Selected Fuel Rods - Summary Results.

Initial BP Isotope	Initial BP Loading (wt%Dy2O3 in UO2)	Initial Fuel Enrich-ment (wt%U235)	Number Fuel Rods with BP (per Fuel Assembly)	BP Mass (per Fuel Assembly) (gram)	Initial BP Reactivity Worth for Reactor Core (-dkeff/keff)	Reactivity Ratio 120 FPD vs.BOL BP-tot per Dy(BOL)	Reactivity Ratio 1 FPY vs.BOL BP-tot per Dy(BOL)	Reactivity Ratios 4 FPY vs.BOL Dy-tot per Dy(BOL)	Tb-tot per Dy(BOL)	Ho-tot per Dy(BOL)	BP Penalty at 4 FPY BP-tot per Dy(BOL)	(FPD)	MVC at BOL dkeff per -10% water density change (STD)
Dy-nat	4.0	4.5	08	5.730+2	3.179-2	8.326-1 (26.9%)	6.955-1 (49.0%)	3.032-1	1.146-10	7.541-2	3.786-1	56.2	-2.28-3 (2.8-4)
Dy-nat	2.0	4.5	16	5.776+2	3.691-2	8.430-1 (24.5%)	6.980-1 (47.2%)	2.823-1	9.840-11	7.715-2	3.594-1	61.8	-2.24-3 (2.9-4)
Dy-nat	4.0	4.5	16	1.146+3	6.082-2	8.484-1 (24.7%)	7.100-1 (47.2%)	3.108-1	5.880-11	7.425-2	3.850-1	106.4	-3.94-3 (2.8-4)
Dy-nat	8.0	4.5	16	2.256+3	9.182-2	8.661-1 (23.3%)	7.378-1 (45.7%)	3.548-1	3.790-11	7.112-2	4.259-1	180.6	-5.01-3 (2.6-4)
Dy-nat	4.0	4.5	20	1.433+3	7.509-2	8.484-1 (24.6%)	7.093-1 (47.2%)	3.102-1	4.704-11	7.318-2	3.834-1	135.0	
Dy-nat	0.5	4.5	64	5.811+2	4.550-2	8.253-1 (25.2%)	6.660-1 (48.2%)	2.301-1	7.970-11	7.758-2	3.077-1	92.3	-2.29-3 (3.5-4)
Dy-nat	1.0	4.5	64	1.159+3	8.118-2	8.347-1 (24.8%)	6.815-1 (47.8%)	2.544-1	4.383-11	7.960-2	3.340-1	135.0	-3.58-3 (3.6-4)
Dy-nat	2.0	4.5	64	2.310+3	1.363-1	8.429-1 (24.6%)	6.937-1 (43.8%)	2.830-1	2.500-11	7.776-2	3.608-1	200.0	-4.26-3 (3.4-4)
Dy-161	none												
Dy-164	4.0	4.5	08	5.745+2	3.547-2	8.386-1 (19.5%)	6.636-1 (40.7%)	5.895-2	1.036-10	1.134-1	1.729-1	29.6	-1.98-3 (2.8-4)
Dy-164	1.0	4.5	16	2.907+2	2.934-2	7.606-1 (26.5%)	5.062-1 (54.6%)	1.448-2	1.260-10	8.047-2	9.495-2	11.1	-1.56-3 (3.0-4)
Dy-164	2.0	4.5	16	5.791+2	4.745-2	7.995-1 (22.8%)	5.780-1 (47.9%)	2.522-2	7.750-11	9.327-2	1.185-1	20.9	-1.35-3 (2.9-4)
Dy-164	4.0	4.5	16	1.149+3	6.747-2	8.453-1 (18.9%)	6.785-1 (39.2%)	6.308-2	5.390-11	1.173-1	1.804-1	55.1	-2.06-3 (2.7-4)
Dy-164	4.0	4.5	20	1.436+3	8.347-2	8.385-1 (19.7%)	6.640-1 (41.0%)	6.357-2	4.339-11	1.174-1	1.810-1	82.8	
Dy-164	0.5	4.5	64	5.826+2	6.520-2	7.282-1 (29.6%)	4.584-1 (59.0%)	9.654-3	5.620-11	7.221-2	8.187-2	25.2	-1.07-3 (3.4-4)
Dy-164	1.0	4.5	64	1.163+3	1.085-1	7.633-1 (26.3%)	5.100-1 (54.5%)	1.473-2	3.365-11	8.636-2	1.011-1	56.4	

Table 18. Dy Burnable Poison Integrally mixed with the Outer One Third Part of the UO2 Fuel Pellets of Selected Fuel Rods - Summary Results.

Initial BP Isotope	Initial Loading BP (wt%Dy2O3 in UO2)	Initial Fuel Enrich-ment (wt%U235)	Number Fuel Rods with BP (per Fuel Assembly)	BP Mass (per Fuel Assembly) (gram)	Initial BP Reactivity Worth for Reactor Core (-dkeff/keff)	Reactivity Ratio 120 FPD vs.BOL BP-tot per Dy(BOL)	Reactivity Ratio 1 FPY vs.BOL BP-tot per Dy(BOL)	Reactivity Ratios 4 FPY vs.BOL Dy-tot per Dy(BOL)	Reactivity Ratios 4 FPY vs.BOL Tb-tot per Dy(BOL)	Reactivity Ratios 4 FPY vs.BOL Ho-tot per Dy(BOL)	BP Penalty at 4 FPY BP-tot per Dy(BOL)	BP Penalty at 4 FPY (FPD)	MVC at BOL dkeff per -10% water density change (STD)
Dy-nat	4.0	4.5	08	1.910+2	1.382-2	8.302-1 (25.4%)	6.829-1 (47.4%)	2.535-1	2.659-10	7.749-2	3.310-1	17.2	
Dy-nat	8.0	4.5	08	3.760+2	2.372-2	8.403-1 (24.9%)	6.911-1 (48.2%)	2.840-1	1.547-10	7.485-2	3.588-1	37.3	
Dy-nat	1.0	4.5	64	3.866+2	3.299-2	8.134-1 (26.2%)	6.517-1 (48.8%)	2.107-1	1.109-10	7.607-2	2.867-1	49.7	
Dy-161	4.0	4.5	08	1.911+2	1.279-2	9.010-1 (19.5%)	7.745-1 (44.4%)	4.577-1	2.865-10	3.498-2	4.926-1	24.5	
Dy-164	4.0	4.5	08	1.915+2	1.884-2	7.691-1 (25.5%)	5.256-1 (52.3%)	1.383-2	1.963-10	7.987-2	9.370-2	8.3	
Dy-164	8.0	4.5	08	3.770+2	2.910-2	8.237-1 (20.2%)	6.068-1 (45.1%)	2.814-2	1.266-10	9.923-2	1.274-1	14.4	
Dy-164	12.0	4.5	08	5.568+2	3.541-2	8.535-1 (17.5%)	6.691-1 (39.5%)	4.941-2	1.040-10	1.128-1	1.623-1	27.7	
Dy-164	1.0	4.5	64	3.876+2	4.839-2	7.088-1 (31.4%)	4.274-1 (61.8%)	6.785-3	7.623-11	6.657-2	7.335-2	17.0	

Table 19. Dy Burnable Poison in a Dy2O3 Coating between the UO2 Fuel Pellet and the Zr-4 Cladding of Selected Fuel Rods - Summary Results.

Initial BP Isotope	Thickness BP Layer (mills)	Initial Density Fraction BP Dy2O3	Initial Fuel Enrich-ment (wt%U235)	Number Fuel Rods with BP (per Fuel Assembly)	BP Mass (per Fuel Assembly) (gram)	Initial BP Reactivity Worth for Reactor Core (-dkeff/keff)	Reactivity Ratio 120 FPD vs.BOL BP-tot per Dy(BOL)	Reactivity Ratio 1 FPY vs.BOL BP-tot per Dy(BOL)	Reactivity Ratios 4 FPY vs.BOL Dy-tot per Dy(BOL)	Tb-tot per Dy(BOL)	Ho-tot per Dy(BOL)	BP Penalty at 4 FPY BP-tot per Dy(BOL)	(FPD)	MVC at BOL dkeff per -10% water density change (STD)
Dy-nat	2.0	1.00	4.5	18	5.636+2	3.770-2	8.450-1 (23.8%)	6.756-1 (49.8%)	2.727-1	9.651-11	7.584-2	3.485-1	60.0	
Dy-nat	1.0	1.00	4.5	64	1.005+3	7.397-2	8.295-1 (25.0%)	6.736-1 (47.8%)	2.409-1	4.804-11	7.590-2	3.168-1	107.4	
Dy-161	1.0	1.00	4.5	64	1.005+3	6.892-2	8.925-1 (21.1%)	7.664-1 (45.9%)	4.535-1	5.102-11	3.747-2	4.910-1	138.4	
Dy-164	4.0	1.00	4.5	08	4.992+2	3.329-2	8.382-1 (19.1%)	6.594-1 (40.2%)	4.417-2	1.105-10	1.084-1	1.525-1	21.8	
Dy-164	8.0	1.00	4.5	08	9.861+2	4.513-2	8.752-1 (17.0%)	7.455-1 (34.8%)	1.331-1	8.082-11	1.345-1	2.676-1	61.2	
Dy-164	2.0	1.00	4.5	18	5.651+2	4.824-2	7.977-1 (22.8%)	5.620-1 (49.3%)	1.970-2	7.629-11	9.094-2	1.106-1	25.2	
Dy-164	4.0	1.00	4.5	18	1.123+2	7.114-2	8.378-1 (19.3%)	6.587-1 (40.7%)	4.774-2	5.121-11	1.127-1	1.605-1	52.8	
Dy-164	0.5	1.00	4.5	64	5.046+2	5.947-2	7.261-1 (29.7%)	4.470-1 (59.9%)	7.059-3	6.170-11	6.982-2	7.688-2	16.5	
Dy-164	1.0	1.00	4.5	64	1.008+3	9.868-2	7.634-1 (26.1%)	5.035-1 (54.7%)	1.088-2	3.716-11	8.165-2	9.254-2	46.0	
Dy-164	2.0	1.00	4.5	64	2.009+3	1.523-1	7.990-1 (22.9%)	5.758-1 (48.4%)	2.115-2	2.371-11	1.018-1	1.229-1	112.2	
Dy-164	0.5	1.00	4.5	104	8.199+2	8.981-2	7.392-1 (28.5%)	4.617-1 (58.7%)	8.151-3	4.091-11	7.534-2	8.349-2	30.5	

Table 20. Dy Burnable Poison Integrally mixed with the Zr-4 Cladding of Selected Fuel Rods - Summary Results.

Initial BP Isotope	Initial loading BP (wt%Dy in Zr-4)	Initial Fuel Enrich-ment (wt%U235)	Number Fuel Rods with BP (per Fuel Assembly)	BP Mass (per Fuel Assembly) (gram)	Initial BP Reactivity Worth for Reactor Core (-dkeff/keff)	Reactivity Ratio 120 FPD vs.BOL BP-tot per Dy(BOL)	Reactivity Ratio 1 FPY vs.BOL BP-tot per Dy(BOL)	Reactivity Ratios 4 FPY vs.BOL Dy-tot per Dy(BOL)	Tb-tot per Dy(BOL)	Ho-tot per Dy(BOL)	BP-tot per Dy(BOL)	BP Penalty at 4 FPY (FPD)	MVC at BOL dkeff per -10% water density change (STD)
Dy-nat	4.0	4.5	104	3.041+3	1.856-1	8.365-1 (25.2%)	6.820-1 (49.0%)	2.718-1	7.610-10	7.956-2	3.513-1	342.0	
Dy-161	None												
Dy-164	2.0	4.5	64	4.616+2	5.805-2	7.129-1 (30.9%)	4.245-1 (62.0%)	5.631-3	9.595-11	6.587-2	7.150-2	19.0	
Dy-164	2.0	4.5	104	7.501+2	8.907-2	7.209-1 (30.2%)	4.367-1 (61.0%)	6.415-3	7.935-11	6.962-2	7.604-2	28.3	
Dy-164	2.0	6.0	104	7.501+2	7.492-2	7.838-1 (23.5%)	5.390-1 (50.1%)	6.642-3	9.823-11	7.362-2	8.026-2	19.6	

In Tables 17 through 20 the residual reactivity worths, due to the Tb daughters of the BP containing dysprosium enriched in ^{164}Dy, should be zero, since there are essentially no paths from the transmutation of ^{164}Dy to any of the Tb isotopes. However, the tables show residual reactivity worths of the order of 1.0×10^{-11}. This is because for each case, all the BP isotopes and their daughters (which are not present in the initial loading of the BP) have been added as traces to the BP with a number density of 1.0×10^{-15} instead of zero. This is to avoid problems at the BOC in the input to the MCNP4C code and to avoid computer exception errors (division by zero) when calculating spectrum-weighted cross sections.

The MVCs were calculated by decreasing the water coolant density by 10%. Note that for all the cases containing 8, 16, and 64 IFBA rods, the MVCs remain negative.

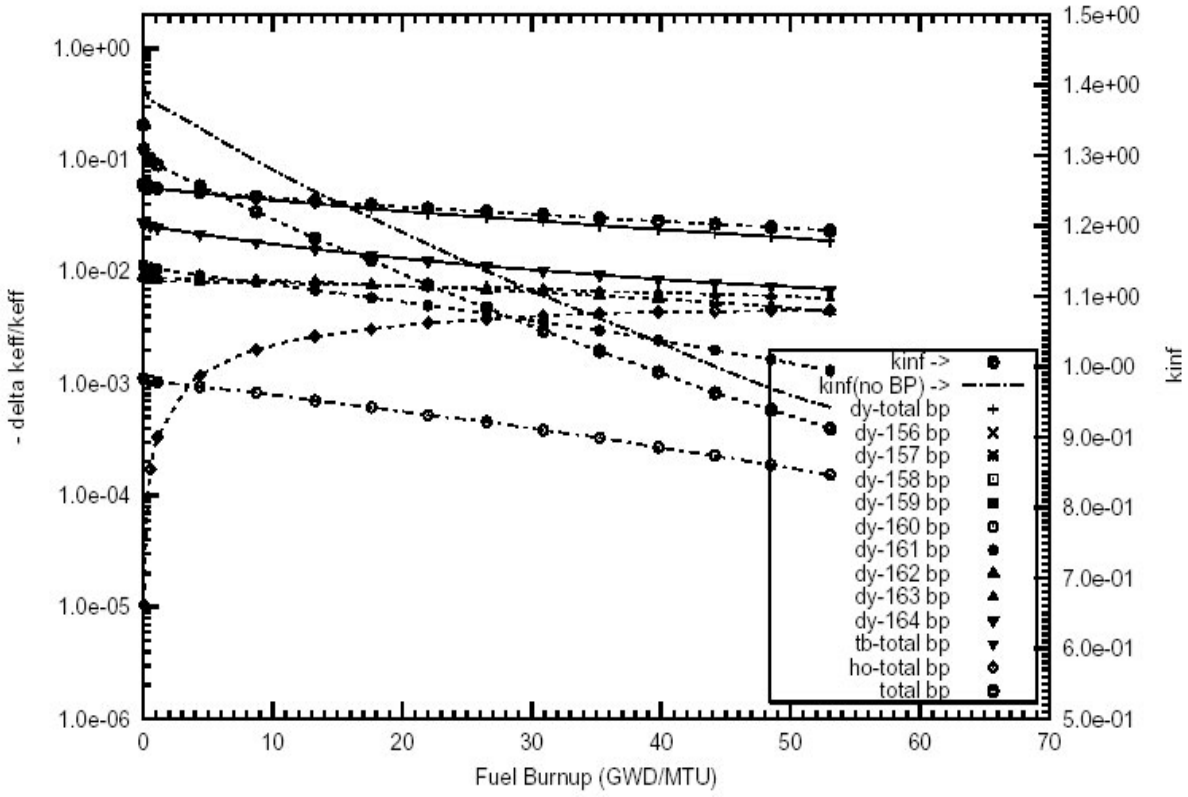

Figure 19 Negative reactivity of BP for Dy-nat and transmutation daughters as a function of fuel life for 17x17 fuel assemblies with 16 poison rods, 4.0 wt% Dy_20_3 poison homogeneously mixed in the UO_2 pellets. Reactor power is 3400 MWth, 193 fuel assemblies, initial enrichment is 4.5wt%^{235}U.

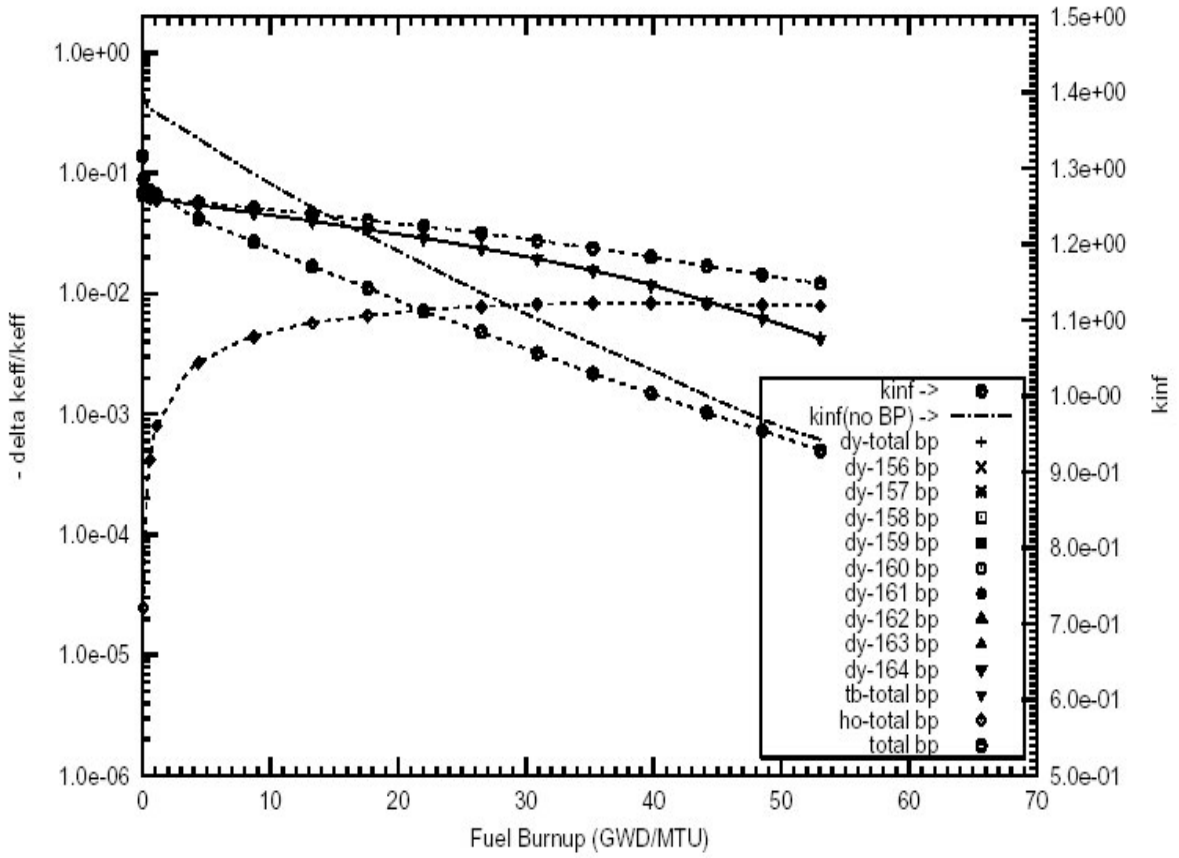

Figure 20 Negative reactivity of BP for Dy-164 and transmutation daughters as a function of fuel life for 17x17 fuel assemblies with 16 poison rods, 4.0 wt% Er_20_3 poison homogeneously mixed in the UO_2 pellets. Reactor power is 3400 MWth, 193 fuel assemblies, initial enrichment is 4.5wt%^{235}U.

Figure 20 displays the initial reactivity worths of the BP containing dysprosium as a function of the residual BP penalty in FPDs for several configurations containing 64 IFBA rods. The trends for the different forms of the BPs are very similar. Note also the advantage of using dysprosium enriched in ^{164}Dy over dysprosium with natural isotopic abundances.

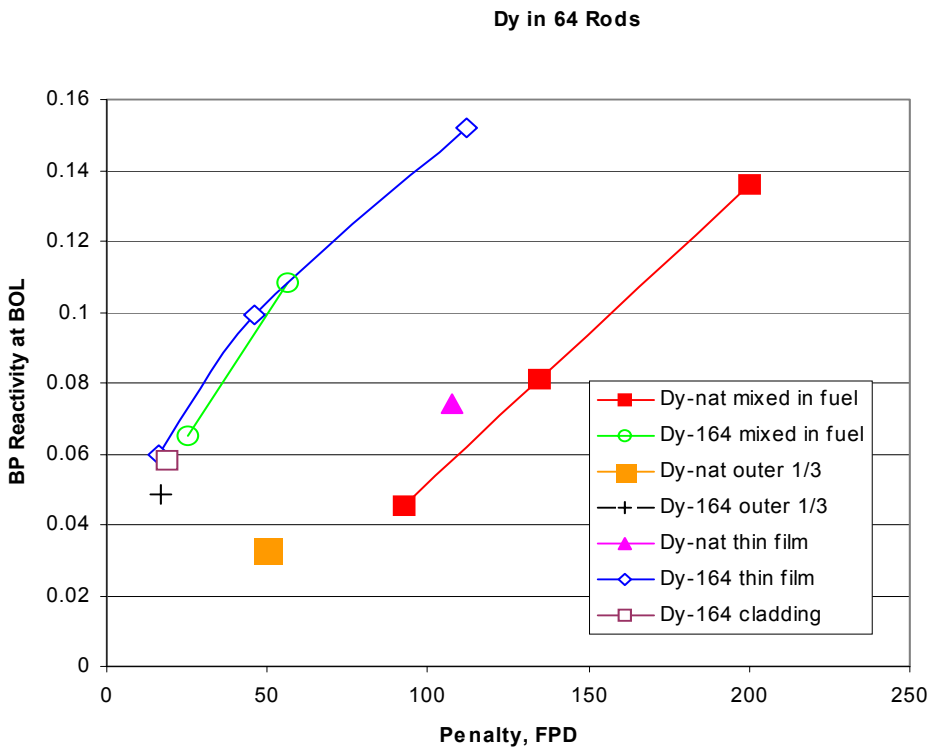

Figure 21 Burnable poison initial reactivity worth as a function of FPD penalty--Dy in 64 IFBA rods

NEUTRONICS PERFORMANCE RESULTS FOR EUROPIUM

The stable isotopes of europium, ^{151}Eu (47.8% natural isotopic abundance) and ^{153}Eu (52.2%), exhibit very large thermal neutron capture cross sections. The radioactive isotopes ^{152}Eu, ^{154}Eu, and ^{155}Eu, produced by neutron capture, have multi-year half-lives and exhibit large neutron capture cross sections. Because of these characteristics, europium with natural isotopic abundances will not burn out easily. It is thus an ideal control rod material and has been used in research reactors [e.g., the High Flux Isotope Reactor (HFIR)]. In this section, we will investigate whether europium, enriched in ^{151}Eu, could be used as a burnable poison in PWRs.

The half-lives, natural isotopic abundances, and burnup chains related to the depletion and transmutation of europium are given below. The isomeric states of certain isotopes are not shown. However, the generation of these daughters was taken into account in the BP depletion and decay calculations.

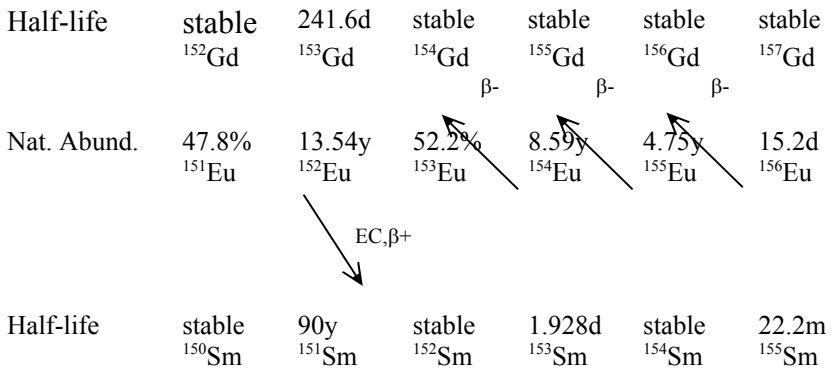

The neutron capture cross sections for the europium isotopes are graphed in ref. 11. The europium stable isotope ^{151}Eu (47.8% natural isotopic abundance) exhibits a thermal capture cross section of 9,200 barns and a RI of 3,300 barns. The ^{151}Eu (n,γ) ^{152}Eu reaction leads to ^{152}Eu, which has a half-life of 13.54 years, a thermal neutron capture cross section of 12,800 barns, and a RI of 1,580 barns. The other stable europium isotope, ^{153}Eu (52.2% natural isotopic abundance) has a thermal neutron capture cross section of 310 barns and a RI of 1,420 barns. The ^{153}Eu (n,γ) ^{154}Eu reaction leads to ^{154}Eu, which has a half-life of 8.6 years, a thermal neutron capture cross section of 1,340 barns, and a RI of 800 barns. Because of the long half-life of ^{154}Eu, the principal transmutation route for ^{154}Eu will be via the ^{154}Eu (n,γ) ^{155}Eu reaction, leading to ^{155}Eu, which has a half-life of 4.75 years, a capture cross section of 3,950 barns, and a RI of 23,200 barns. Again, because of the long half-life of ^{155}Eu, the principal transmutation route for ^{155}Eu will be via the ^{155}Eu (n,γ) ^{156}Eu reaction, leading to ^{156}Eu, which decays to ^{156}Gd with a half-life of 15.2 days. ^{156}Gd has a capture cross section of 1.5 barns and a RI of 104 barns. The use of ^{151}Eu in a BP will lead by transmutation to ^{152}Eu, which has a higher thermal neutron capture cross section than ^{151}Eu. Transmutation of ^{152}Eu leads to ^{153}Eu, which has a much smaller thermal cross section than either ^{151}Eu or ^{152}Eu. The sequence of ^{151}Eu and ^{152}Eu, exhibits a pair of very high thermal cross sections, followed by ^{153}Eu with a much smaller cross section. This will lead to a decrease of the burnout rate of the BP, together with a reduction

of the residual reactivity fraction of the BP. The use of ^{153}Eu as a BP will lead to ^{154}Eu, which has a higher thermal neutron capture cross section than ^{153}Eu. Further transmutation leads to ^{155}Eu, which has an even higher thermal cross section than ^{154}Eu. Transmutation to ^{156}Eu will lead to a 15.2-day decay of ^{156}Eu to ^{156}Gd, which has a very small thermal cross section. Since the thermal cross section of ^{153}Eu is smaller than that of ^{151}Eu, a larger amount of ^{153}Eu is needed than of ^{151}Eu in order to achieve a desired initial reactivity worth of the BP. In addition, the sequence ^{153}Eu-^{154}Eu-^{155}Eu exhibits an increasing thermal neutron capture cross section. This will thus give rise to a much higher residual reactivity fraction than the use of a BP fully enriched in ^{151}Eu. Enriching europium in the ^{151}Eu isotope should thus reduce the residual negative reactivity fraction of the BP, together with decreasing the burnout rate of the BP.

In all the neutronics calculations presented in this section, a theoretical density of 7.42 g/cm^3 was used for europia (Eu_2O_3), and 5.22 g/cm^3 was used for metallic europium. For UO_2, a theoretical density of 10.97 g/cm^3 was used. The actual density fraction of the fuel pellets and of the burnable poison pellets was 95% of theoretical density.

As with the other candidate elements, four different configurations of the burnable poison were investigated. The results of each calculation run are given in Tables 21-24 for each configuration.

The reactivity worths of the BP isotopes, for a 2.0 wt % loading of europium with natural isotopic abundances, alloyed with the Zircaloy cladding of 64 fuel rods per fuel assembly, are shown in Figure 22. The initial reactivity worth of the BP is 0.124, and the residual reactivity ratio was 11.4%. The total initial mass of natural europium was 457 grams per fuel assembly containing BPs.

For a 1.0 wt % homogeneous loading of europium, fully enriched in ^{151}Eu, alloyed in the Zircaloy cladding of 64 fuel rods, the reactivity worths of the BP isotopes are shown in Figure 23. The initial reactivity worth of the BP was 0.118 and the residual reactivity ratio was 6.8%. The total initial mass of ^{151}Eu was 229 grams per fuel assembly. Figure 58 also shows that the reactivity worths of the BP transmutation daughters ^{152}Eu to ^{155}Eu initially increase with depletion time, then reach a maximum, followed by a decrease of the reactivity worth. The time at which the reactivity worth reaches its maximum increases with the isotope transmutation sequence chain from ^{152}Eu to ^{155}Eu.

The use of europium enriched in ^{151}Eu, instead of with natural isotopic abundances, will thus lead to a reduction of the residual reactivity burden at EOL of the fuel.

The MVCs were calculated by decreasing the water coolant density by 10%. The results are shown in Tables 21 through 24. For all the cases containing 64 and 104 IFBA rods, the MVCs remain negative.

Table 21. Eu Burnable Poison Integrally mixed with the UO2 Fuel Pellets of Selected Fuel Rods - Summary Results.

Initial BP Isotope	Initial Loading BP (wt%Eu2O3 in UO2)	Initial Fuel Enrich-ment (wt%U235)	Number Fuel Rods with BP (per Fuel Assembly)	BP Mass (per Fuel Assembly) (gram)	Initial BP Reactivity Worth for Reactor Core (-dkeff/keff)	Reactivity Ratio 120 FPD vs.BOL BP-tot per Eu(BOL)	Reactivity Ratio 1 FPY vs.BOL BP-tot per Eu(BOL)	Reactivity Ratios 4 FPY vs.BOL Eu-tot per Eu(BOL)	Sm-tot per Eu(BOL)	Gd-tot per Eu(BOL)	BP-tot per Eu(BOL)	BP Penalty at 4 FPY (FPD)	MVC at BOL dkeff per -10% water density change (STD)
Eu-nat	4.0	4.5	08	5.672+2	6.511-2	8.535-1 (20.9%)	6.346-1 (52.0%)	2.697-1	3.160-3	2.471-2	2.976-1	90.7	
Eu-151	4.0	4.5	08	5.667+2	7.374-2	8.892-1 (15.5%)	7.239-1 (38.6%)	2.591-1	7.568-3	1.825-2	2.849-1	96.7	
Eu-153	4.0	4.5	08	5.677+2	2.429-2	1.067+0(-25.9%)	1.184+0(-70.8%)	6.710-1	1.280-6	6.992-2	7.409-1	89.1	

Table 22. Eu Burnable Poison Integrally mixed with the Outer One Third Part of the UO2 Fuel Pellets of Selected Fuel Rods - Summary Results.

Initial BP Isotope	Initial Loading BP (wt%Eu2O3 in UO2)	Initial Fuel Enrich-ment (wt%U235)	Number Fuel Rods with BP (per Fuel Assembly)	BP Mass (per Fuel Assembly) (gram)	Initial BP Reactivity Worth for Reactor Core (-dkeff/keff)	Reactivity Ratio 120 FPD vs.BOL BP-tot per Eu(BOL)	Reactivity Ratio 1 FPY vs.BOL BP-tot per Eu(BOL)	Reactivity Ratios 4 FPY vs.BOL Eu-tot per Eu(BOL)	Sm-tot per Eu(BOL)	Gd-tot per Eu(BOL)	BP-tot per Eu(BOL)	BP Penalty at 4 FPY (FPD)	MVC at BOL dkeff per -10% water density change (STD)
Eu-nat	8.0	4.5	08	3.712+2	5.444-2	8.035-1 (25.9%)	5.314-1 (61.7%)	2.168-1	1.955-3	2.168-2	2.404-1	56.0	
Eu-151	4.0	4.5	08	1.889+2	4.937-2	7.760-1 (26.3%)	4.310-1 (66.9%)	1.335-1	2.248-3	1.337-2	1.491-1	35.9	
Eu-153	8.0	4.5	08	3.715+2	1.776-2	1.079+0(-23.2%)	1.203+0(-59.7%)	5.914-1	1.035-6	6.866-2	6.601-1	52.7	

Table 23. Eu Burnable Poison in a Eu2O3 Coating between the UO2 Fuel Pellet and the Zr-4 Cladding of Selected Fuel Rods - Summary Results.

Initial BP Isotope	Thickness BP Layer (mils)	Initial Density Fraction BP Eu2O3	Initial Fuel Enrich-ment (wt%U235)	Number Fuel Rods with BP (per Fuel Assembly)	BP Mass (per Fuel Assembly) (gram)	Initial BP Reactivity Worth for Reactor Core (-dkeff/keff)	Reactivity Ratio 120 FPD vs.BOL BP-tot per Eu(BOL)	Reactivity Ratio 1 FPY vs.BOL BP-tot per Eu(BOL)	Reactivity Ratios 4 FPY vs.BOL Eu-tot per Eu(BOL)	Sm-tot per Eu(BOL)	Gd-tot per Eu(BOL)	BP-tot per Gd(BOL)	BP Penalty at 4 FPY (FPD)	MVC at BOL dkeff per -10% water density change (STD)
Eu-nat	1.0	1.00	4.5	64	9.479+2	1.875-1	6.657-1 (40.0%)	3.893-1 (73.0%)	1.430-1	7.670-4	1.942-2	1.632-1	205.0	
Eu-151	0.2	1.00	4.5	64	1.899+2	9.787-2	4.793-1 (56.0%)	1.856-1 (87.5%)	6.072-2	5.562-4	8.404-3	6.968-2	44.2	
Eu-151	0.5	1.00	4.5	64	4.742+2	1.754-1	6.093-1 (43.4%)	2.594-1 (82.2%)	8.704-2	9.068-4	1.105-2	9.900-2	100.1	
Eu-151	0.2	1.00	4.5	104	3.085+2	1.444-1	5.118-1 (52.8%)	1.986-1 (86.7%)	6.631-2	5.991-4	8.960-3	7.587-2	33.1	
Eu-153	0.2	1.00	4.5	64	1.902+2	1.200-2	1.100+0(-17.8%)	1.243+0(-43.2%)	3.681-1	7.796-7	6.982-2	4.380-1	22.9	

Table 24. Eu Burnable Poison Integrally mixed with the Zr-4 Cladding of Selected Fuel Rods - Summary Results.

Initial BP Isotope	Initial loading BP (wt%Eu in Zr-4)	Initial Fuel Enrich-ment (wt%U235)	Number Fuel Rods with BP (per Fuel Assembly)	BP Mass (per Fuel Assembly) (gram)	Initial BP Reactivity Worth for Reactor Core (-dkeff/keff)	Reactivity Ratio 120 FPD vs.BOL BP-tot per Eu(BOL)	Reactivity Ratio 1 FPY vs.BOL BP-tot per Eu(BOL)	Reactivity Ratios 4 FPY vs.BOL Eu-tot per Eu(BOL)	Sm-tot per Eu(BOL)	Gd-tot per Eu(BOL)	BP-tot per Eu(BOL)	BP Penalty at 4 FPY (FPD)	MVC at BOL dkeff per -10% water density change (STD)
Eu-nat	1.00	4.5	64	2.292+2	7.437-2	4.747-1 (58.1%)	2.668-1 (81.0%)	8.100-2	3.542-4	1.366-2	9.502-2	28.8	-3.06-3 (3.8-4)
Eu-nat	2.00	4.5	64	4.572+2	1.244-1	5.508-1 (50.7%)	3.114-1 (77.7%)	9.783-2	4.489-4	1.572-2	1.140-1	64.5	-4.26-3 (3.4-4)
Eu-nat	0.50	4.5	104	1.864+2	6.418-2	4.508-1 (60.3%)	2.558-1 (81.7%)	7.517-2	3.358-4	1.308-2	8.858-2	22.1	-2.91-3 (4.4-4)
Eu-nat	1.00	4.5	104	3.724+2	1.132-1	4.954-1 (56.1%)	2.825-1 (79.8%)	8.642-2	3.797-4	1.443-2	1.012-1	49.4	-3.64-3 (4.3-4)
Eu-151	0.50	4.5	64	1.147+2	7.083-2	7.077-1 (31.0%)	1.551-1 (89.6%)	4.908-2	4.019-4	7.316-3	5.680-2	17.2	-2.62-3 (3.7-4)
Eu-151	1.00	4.5	64	2.292+2	1.183-1	4.757-1 (56.3%)	1.855-1 (87.4%)	5.954-2	4.958-4	8.450-3	6.848-2	38.6	-3.65-3 (3.4-4)
Eu-151	0.20	4.5	104	7.461+1	5.026-2	3.707-1 (66.4%)	1.415-1 (90.5%)	4.468-2	3.492-4	6.747-3	5.178-2	9.5	-2.30-3 (4.4-4)
Eu-151	0.50	4.5	104	1.864+2	1.077-1	4.247-1 (61.3%)	1.646-1 (88.9%)	5.255-2	4.282-4	7.719-3	6.070-2	24.9	-3.11-3 (4.1-4)
Eu-151	0.50	6.0	104	1.864+2	9.635-2	4.958-1 (53.5%)	1.988-1 (85.0%)	4.796-2	3.216-4	8.959-3	5.724-2	21.2	
Eu-151	1.00	6.0	104	3.724+2	1.587-1	5.780-1 (45.4%)	2.411-1 (81.7%)	5.918-2	4.067-4	1.091-2	7.050-2	58.1	

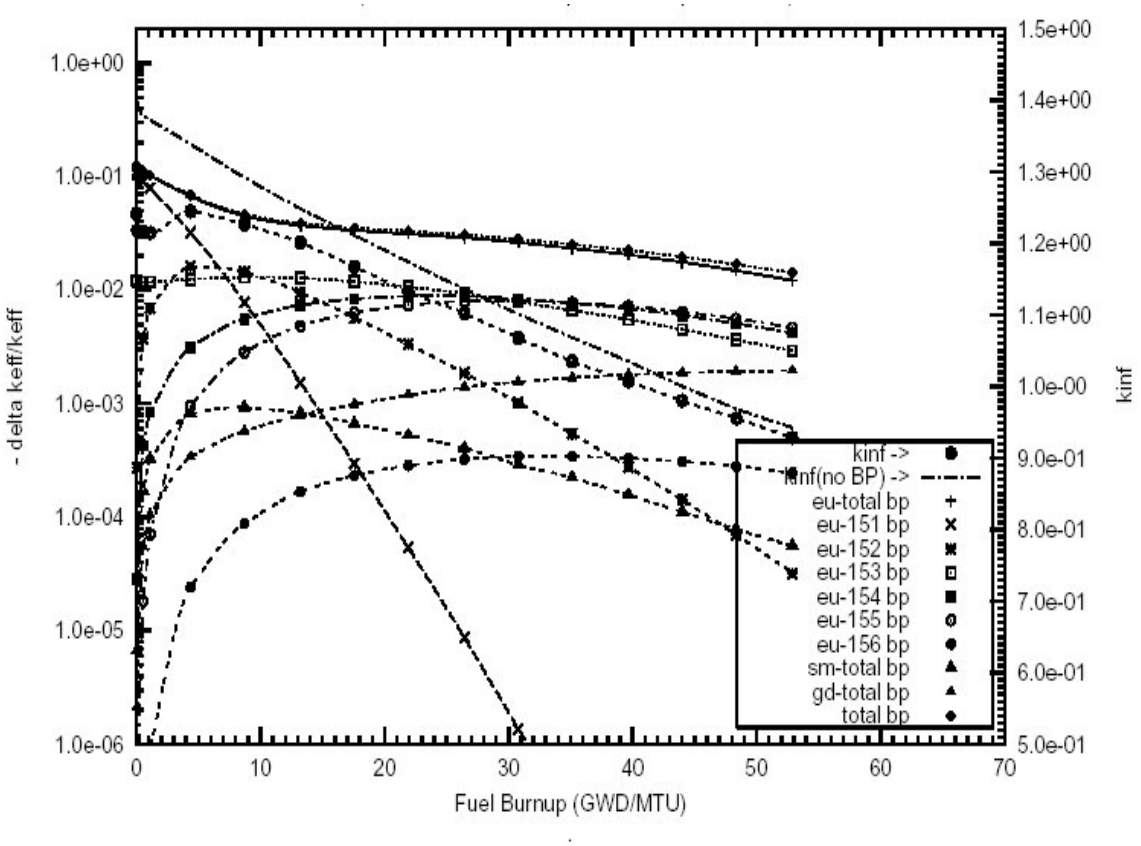

Figure 22 Negative reactivity of BP for Eu-nat and transmutation daughters as a function of fuel life for 17x17 fuel assemblies with 64 poison rods, 2.0wt% Eu_20_3 poison homogeneously mixed in the UO_2 pellets. Reactor power is 3400 MWth, 193 fuel assemblies, initial enrichment is 4.5wt%^{235}U.

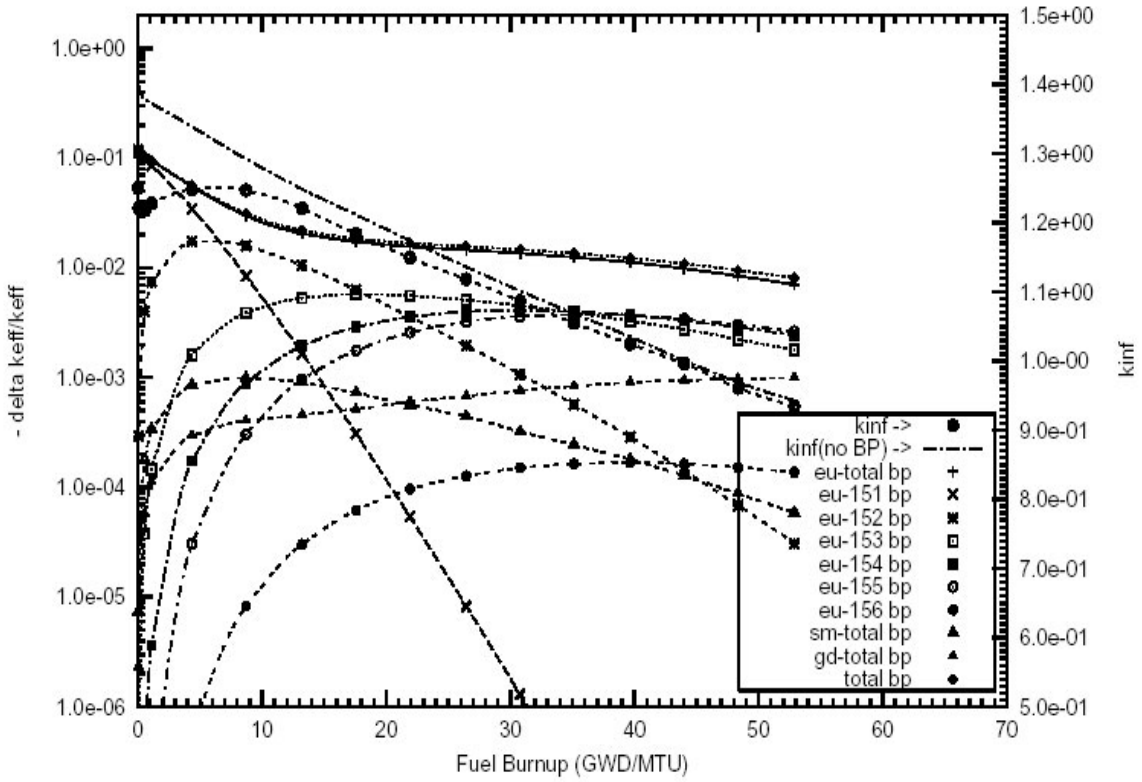

Figure 23 Negative reactivity of BP for Eu-151 and transmutation daughters as a function of fuel life for 17x17 fuel assemblies with 64 poison rods, 1.0wt% Eu_20_3 poison homogeneously mixed in the UO_2 pellets. Reactor power is 3400 MWth, 193 fuel assemblies, initial enrichment is 4.5wt%^{235}U.

NEUTRONICS PERFORMANCE RESULTS FOR HAFNIUM

The half-lives, natural isotopic abundances, and burnup chains related to the depletion and transmutation of hafnium are given below. The isomeric states of certain isotopes are not shown. However, the generation of these daughters was taken into account in the BP depletion and decay calculations.

Half-life							Stable	114.4d
							^{181}Ta	^{182}Ta
							↖ β- ↗	
Nat. Abund.	0.162 %	70.0d	5.21%	18.61 %	27.30 %	13.63 %	35.10 %	42.4d
	^{174}Hf	^{175}Hf ↘ EC	^{176}Hf	^{177}Hf	^{178}Hf	^{179}Hf	^{180}Hf	^{181}Hf
Half-life			stable	stable	160.7d	28.5m	4.6h	5.7m
			^{175}Lu	^{176}Lu	^{177}Lu	^{178}Lu	^{179}Lu	^{180}Lu

The stable hafnium isotopes are ^{174}Hf (0.16% natural isotopic abundance, thermal capture cross section 560 barns, RI 436 barns), ^{176}Hf (5.2%, 23 barns, RI 880 barns), ^{177}Hf (18,6%, 373 barns, RI 7,173 barns), ^{178}Hf (27.1%, 84 barns, RI 1,950 barns), ^{179}Hf (13.7%, 41 barns, RI 630 barns), and ^{180}Hf (35.2%, 13 barns, RI 35 barns). Transmutation reactions of the hafnium isotopes through the (n,γ) reaction lead to other hafnium isotopes with relatively high capture cross sections. The ^{180}Hf (n,γ) ^{181}Hf reaction leads to ^{181}Hf, which decays to ^{181}Ta with a half-life of 42.4 days. ^{181}Ta has a thermal cross section of 20 barns and a RI of 660 barns. The relatively high capture cross sections of the transmutant hafnium isotopes will lead to a substantial residual negative reactivity worth ratio of the BP. However, the ^{177}Hf (n,γ) ^{178}Hf reaction leads to ^{178}Hf, which has a lower capture cross section than that of ^{177}Hf. Further transmutation to ^{179}Hf and ^{180}Hf will lead to progressively smaller thermal neutron capture cross sections. Enriching hafnium in ^{177}Hf should thus lead to a lower residual reactivity burden than that of hafnium with natural isotopic abundances.

In all the neutronics calculations presented in this section, a theoretical density of 9.69 g/cm^3 was used for hafnia (HfO_2), and 13.11 g/cm^3 for metallic hafnium. For UO_2 a theoretical density of 10.97 g/cm^3 was used. The actual density fraction of the fuel pellets and of the burnable poison pellets was 95% of theoretical density.

In this section, we will investigate the potential benefits of using enriched hafnium as a burnable absorber. Four different configurations of the hafnium burnable poison, similar to those of the other candidate elements. The results, given in Tables 25 through 28, show that a reduction of the residual reactivity ratio by a factor of two can be achieved by enriching hafnium in ^{177}Hf.

The reactivity worths of the BP isotopes for a 0.001 inch (0.025 mm) coating of the fuel pellets with HfO_2 (fully enriched in ^{177}Hf) inside 64 IFBA rods are shown in Figure 24. The initial reactivity worth of the BP is 0.112, and the residual reactivity ratio is approximately 8.8%. The total initial mass of ^{177}Hf was 1,212 grams per fuel assembly containing BPs.

The use of hafnium enriched in ^{177}Hf instead of with natural isotopic abundances will thus lead to a reduction of the residual reactivity burden at EOL of the fuel. However, the savings is small. The MVCs were calculated by decreasing the water coolant density by 10%. Note that for the cases containing 64 and 104 IFBA rods, the MVCs remain negative.

Table 25. Hf Burnable Poison Integrally mixed with the UO2 Fuel Pellets of Selected Fuel Rods - Summary Results.

Initial BP Isotope	Initial Loading BP (wt%HfO2 in UO2)	Initial Fuel Enrich-ment (wt%U235)	Number Fuel Rods with BP (per Fuel Assembly)	BP Mass (per Fuel Assembly) (gram)	Initial Reactivity BP Worth for Reactor Core (-dkeff/keff)	Reactivity Ratio 120 FPD vs.BOL BP-tot per Hf(BOL)	Reactivity Ratio 1 FPY vs.BOL BP-tot per Hf(BOL)	Reactivity Ratios 4 FPY vs.BOL Hf-tot per Hf(BOL)	Lu-tot per Hf(BOL)	Ta-tot per Hf(BOL)	BP-tot per Hf(BOL)	BP Penalty at 4 FPY (FPD)	MVC at BOL dkeff per -10% water density change (STD)
Hf-nat	4.0	4.5	08	5.645+2	1.428-2	8.129-1 (23.3%)	5.430-1 (56.9%)	1.792-1	5.653-4	1.685-2	1.966-1	11.9	
Hf-174	4.0	4.5	08	5.645+2	1.673-2	8.655-1 (37.8%)	7.845-1 (60.6%)	3.630-1	2.811-1	9.888-6	6.441-1	44.0	
Hf-177	4.0	4.5	08	5.637+2	3.408-2	8.477-1 (17.5%)	6.501-1 (40.1%)	1.281-1	1.641-9	2.016-4	1.283-1	20.7	

Table 26. Hf Burnable Poison Integrally mixed with the Outer One Third Part of the UO2 Fuel Pellets of Selected Fuel Rods - Summary Results.

Initial BP Isotope	Initial Loading BP (wt%HfO2 in UO2)	Initial Fuel Enrich-ment (wt%U235)	Number Fuel Rods with BP (per Fuel Assembly)	BP Mass (per Fuel Assembly) (gram)	Initial Reactivity BP Worth for Reactor Core (-dkeff/keff)	Reactivity Ratio 120 FPD vs.BOL BP-tot per Hf(BOL)	Reactivity Ratio 1 FPY vs.BOL BP-tot per Hf(BOL)	Reactivity Ratios 4 FPY vs.BOL Hf-tot per Hf(BOL)	Lu-tot per Hf(BOL)	Ta-tot per Hf(BOL)	BP-tot per Hf(BOL)	BP Penalty at 4 FPY (FPD)	MVC at BOL dkeff per -10% water density change (STD)
Hf-nat	8.0	4.5	08	3.743+2	1.111-2	7.757-1 (27.6%)	4.782-1 (64.2%)	1.718-1	2.041-5	1.482-2	1.866-1	8.9	
Hf-177	8.0	4.5	08	3.738+2	2.666-2	8.347-1 (18.4%)	5.985-1 (44.8%)	1.031-1	1.386-9	2.424-4	1.034-1	12.3	
Hf-177	12.0	4.5	08	5.578+2	3.468-2	8.317-1 (19.2%)	6.384-1 (41.3%)	1.238-1	1.622-9	2.083-4	1.240-1	19.1	

Table 27. Hf Burnable Poison in a HfO2 Coating between the UO2 Fuel Pellet and the Zr-4 Cladding of Selected Fuel Rods - Summary Results.

Initial BP Isotope	Thickness BP Layer (mills)	Initial Density Fraction BP HfO2	Initial Fuel Enrich-ment (wt%U235)	Number Fuel Rods with BP (per Fuel Assembly)	BP Mass (per Fuel Assembly) (gram)	Initial BP Reactivity Worth for Reactor Core (-dkeff/keff)	Reactivity Ratio 120 FPD vs.BOL BP-tot per Hf(BOL)	Reactivity Ratio 1 FPY vs. BOL BP-tot per Hf(BOL)	Reactivity Ratios 4 FPY vs.BOL Hf-tot per Hf(BOL)	Lu-tot per Hf(BOL)	Ta-tot per Hf(BOL)	BP-tot per Hf(BOL)	BP Penalty at 4 FPY (FPD)	MVC at BOL dkeff per -10% water density change (STD)
Hf-nat	4.00	1.00	4.5	16	1.203+3	3.040-2	7.978-1 (25.2%)	5.436-1 (56.9%)	1.799-1	5.704-4	1.726-2	1.977-1	23.7	
Hf-nat	8.00	1.00	4.5	16	2.376+3	4.770-2	8.266-1 (22.2%)	6.138-1 (49.5%)	2.007-1	7.051-4	1.869-2	2.201-1	40.9	
Hf-nat	4.00	1.00	4.5	18	1.353+3	3.382-2	8.012-1 (24.8%)	5.494-1 (56.3%)	1.829-1	5.765-4	1.632-2	1.998-1	30.1	
Hf-nat	2.00	1.00	4.5	64	2.420+3	7.213-2	7.683-1 (28.6%)	4.895-1 (63.0%)	1.744-1	4.869-4	1.518-2	1.900-1	49.3	
Hf-nat	1.00	1.00	4.5	104	1.973+3	6.875-2	7.380-1 (32.2%)	4.375-1 (69.2%)	1.174-1	4.197-4	1.380-2	1.876-1	62.5	
Hf-nat	2.00	1.00	4.5	104	3.933+3	1.114-1	7.743-1 (28.0%)	4.971-1 (62.5%)	1.789-1	4.991-4	1.562-2	1.950-1	66.4	
Hf-177	2.00	1.00	4.5	16	6.043+2	4.584-2	8.305-1 (18.8%)	5.880-1 (45.8%)	9.563-2	1.102-9	2.678-4	9.590-2	19.7	
Hf-177	4.00	1.00	4.5	16	1.201+3	6.945-2	8.503-1 (17.3%)	6.561-1 (39.7%)	1.338-1	1.454-9	2.229-4	1.340-1	44.3	
Hf-177	4.00	1.00	4.5	18	1.351+3	7.788-2	8.446-1 (18.0%)	6.479-1 (40.7%)	1.341-1	1.421-9	2.175-4	1.343-1	46.7	
Hf-177	0.50	1.00	4.5	64	6.071+2	7.139-2	7.730-1 (24.7%)	4.443-1 (60.6%)	8.219-2	5.524-10	3.552-4	8.254-2	27.3	
Hf-177	1.00	1.00	4.5	64	1.212+3	1.118-1	7.979-1 (22.2%)	5.249-1 (52.1%)	8.827-2	6.920-10	3.260-4	8.860-2	41.7	
Hf-177	0.20	1.00	4.5	104	3.950+2	5.815-2	7.189-1 (30.1%)	3.633-1 (69.0%)	7.628-2	4.836-10	3.846-4	7.666-2	20.4	
Hf-177	0.50	1.00	4.5	104	9.865+2	1.109-1	7.630-1 (25.9%)	4.620-1 (58.8%)	8.397-2	5.155-10	3.629-4	8.433-2	65.0	

Table 28. Hf Burnable Poison Integrally mixed with the Zr-4 Cladding of Selected Fuel Rods - Summary Results.

Initial BP Isotope	Initial loading BP (wt%Hf in Zr-4)	Initial Fuel Enrich-ment (wt%U235)	Number Fuel Rods with BP (per Fuel Assembly)	BP Mass (per Fuel Assembly) (gram)	Initial BP Reactivity Worth for Reactor Core (-dkeff/keff)	Reactivity Ratio 120 FPD vs.BOL BP-tot per Hf(BOL)	Reactivity Ratio 1 FPY vs.BOL BP-tot per Hf(BOL)	Reactivity Ratios 4 FPY vs.BOL Hf-tot per Hf(BOL)	Lu-tot per Hf(BOL)	Ta-tot per Hf(BOL)	BP-tot per Hf(BOL)	BP Penalty at 4 FPY (FPD)	MVC at BOL dkeff per -10% water density change (STD)
Hf-nat	1.0	4.5	64	2.308+2	1.153-2	6.598-1 (40.6%)	3.698-1 (75.1%)	1.501-1	2.665-4	1.089-2	1.613-1	6.7	
Hf-nat	1.0	4.5	104	3.751+2	1.836-2	6.692-1 (39.5%)	3.698-1 (75.3%)	1.520-1	2.708-4	1.107-2	1.633-1	11.6	-2.36-3 (5.3-4)
Hf-nat	4.0	4.5	104	1.524+3	5.890-2	7.263-1 (33.6%)	4.146-1 (71.8%)	1.712-1	3.334-4	1.308-2	1.846-1	44.2	-5.34-3 (4.7-4)
Hf-177	1.0	4.5	64	2.308+2	3.798-2	6.898-1 (33.5%)	3.266-1 (72.7%)	7.314-2	5.437-10	3.990-4	7.354-2	12.1	
Hf-177	0.5	4.5	104	1.871+2	3.465-2	6.505-1 (37.5%)	2.861-1 (76.6%)	6.733-2	5.495-10	4.050-4	6.774-2	11.0	-4.22-3 (4.8-4)
Hf-177	1.0	4.5	104	3.751+2	5.936-2	7.009-1 (32.4%)	3.400-1 (71.4%)	7.491-2	4.234-10	3.987-4	7.531-2	18.9	-5.51-3 (4.9-4)
Hf-177	2.0	4.5	104	7.541+2	9.848-2	7.431-1 (28.0%)	4.017-1 (65.1%)	8.109-2	3.971-10	3.934-4	8.148-2	26.4	-6.99-3 (4.4-4)

NEUTRONICS PERFORMANCE RESULTS FOR OTHER ELEMENTS

During this project, we investigated the potential of enriching other elements for use as burnable poisons. We have discarded them, however, mostly for economic reasons, with the exception of lutetium, which, although costly, was considered worth evaluation.

The use of lutetium as a burnable poison was investigated. The lutetium stable isotopes are ^{175}Lu and ^{176}Lu, with natural isotopic abundances of 97.4% and 2.6%, respectively. ^{175}Lu has a thermal neutron capture cross section of 30 barns and a RI of 610 barns. The (n,γ) reaction on ^{176}Lu leads to ^{177}Lu and ^{177m1}Lu. The ^{176}Lu (n,γ) ^{177}Lu reaction has a thermal neutron capture cross section of 2,090 barns and a RI of 1,090 barns. ^{177}Lu decays to ^{177}Hf with a half-life of 6.71 days. Another branch in the (n,γ) reaction on ^{176}Lu leads to ^{177m1}Lu with a thermal capture cross section of 7.0 barns. ^{177m1}Lu decays to ^{177}Hf with a half-life of 160.7 days. The ^{177}Hf (n,γ) ^{178}Hf reaction leads to ^{178}Hf with a thermal neutron capture cross section of 373 barns and a RI of 7,173 barns. The ^{178}Hf (n,γ) ^{179}Hf reaction leads to ^{179}Hf with a thermal capture cross section of 84 barns and a RI of 1,950 barns. The sequence ^{176}Lu **6** ^{177}Lu **6** ^{177}Hf **6** ^{178}Hf **6** ^{179}Hf will lead via neutron transmutations and decay to nuclides with smaller and smaller thermal neutron capture cross sections. The ^{175}Lu (n,γ) ^{176}Lu reaction will thus transmute ^{175}Lu, which has a small thermal cross section, into ^{176}Lu, which has a much larger capture cross section. In order to achieve a desired initial reactivity worth of the BP, the use of natural lutetium will require a much larger amount of lutetium than lutetium fully enriched in ^{176}Lu. The transmutation from ^{175}Lu into the ^{176}Lu **6** ^{177}Lu **6** ^{177}Hf **6** ^{178}Hf **6** ^{179}Hf sequence will thus lead to a substantially greater residual reactivity fraction of the BP . Enriching lutetium in ^{176}Lu will thus reduce substantially the residual reactivity worth ratio of the BP.

A summary of the results for lutetium is shown in Table 29. The table shows that the decrease of the residual reactivity ratio of lutetium fully enriched in ^{176}Lu is substantial when compared with the use of lutetium with natural isotopic abundances. Plots for the reactivity worths and the masses of the BP isotopes and their daughters are displayed in Ref. 11.

The reactivity worths of the BP isotopes, for a 0.5-mil thick coating with Lu_2O_3 (fully enriched in ^{176}Lu) of the fuel pellets in 64 IFBA rods, are shown in Figure 25. The initial reactivity worth of the BP was 0.171, and the residual reactivity ratio is approximately 3.8%. The total mass of ^{176}Lu per fuel assembly was 614 grams.

Note that the shapes of the fuel assembly lattice k_{inf}'s for this case is fairly flat. However, the natural isotopic abundance of ^{176}Lu is only 2.6%. Enriching lutetium in ^{176}Lu will probably be expensive.

Other elements and isotopes, such as Nd and ^{143}Nd and Os and ^{184}Os, were also investigated. We have discarded them because of the very low natural abundance or the very small reduction in the residual reactivity worth ratios of the BP.

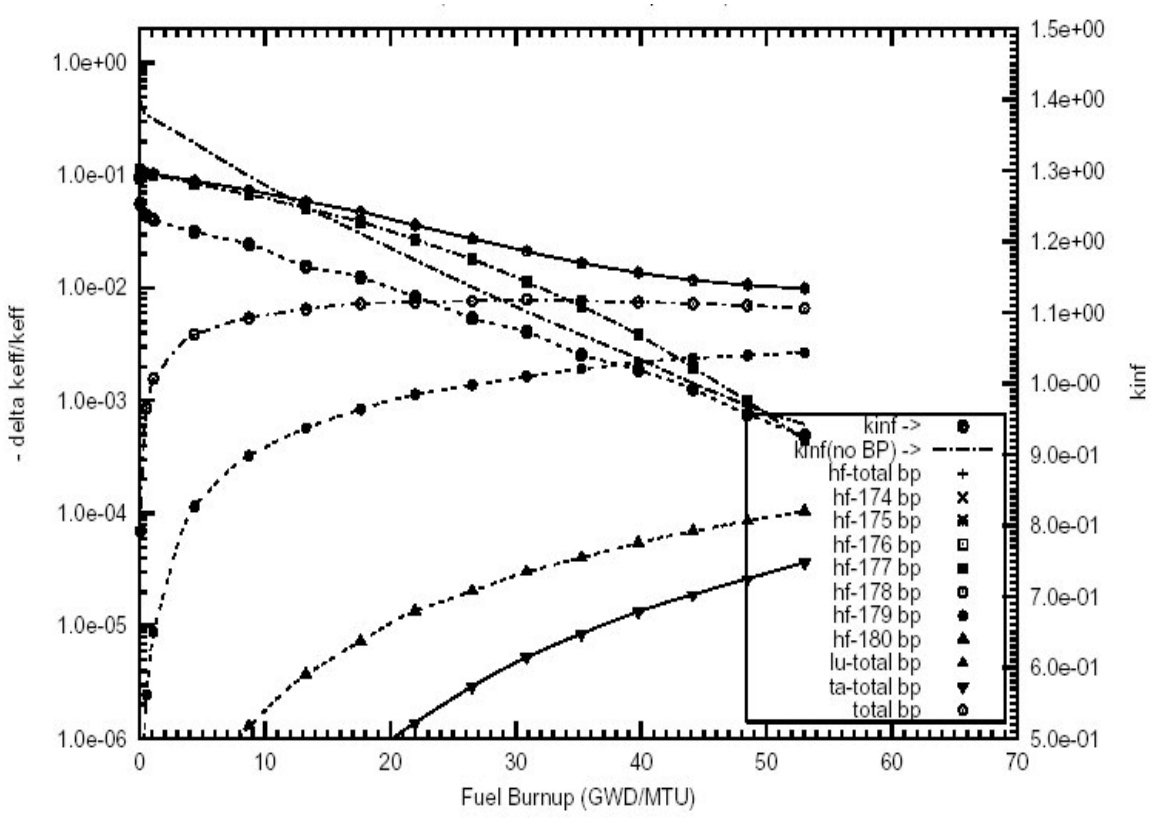

Figure 24 Negative reactivity of BP for Hf-177 and transmutation daughters as a function of fuel life for 17x17 fuel assemblies with 64 poison rods, 1.0 mil thick $Hf0_2$ poison coating on the outer radial surface of the UO_2 pellets. Reactor power is 3400 MWth, 193 fuel assemblies, initial enrichment is 4.5wt%^{235}U.

Table 29. Lu Burnable Poison in a Lu2O3 coating between the UO2 Fuel Pellet and the Zr-4 Cladding of Selected Fuel Rods - Summary Results.

Initial BP Isotope	Thickness BP Layer (mills)	Initial Density Fraction BP Lu2O3	Initial Fuel Enrich-ment (wt%U235)	Number Fuel Rods with BP (per Fuel Assembly)	BP Mass (per Fuel Assembly) (gram)	Initial BP Reactivity Worth for Reactor Core (-dkeff/keff)	Reactivity Ratio 120 FPD vs.BOL BP-tot per Lu(BOL)	Reactivity Ratio 1 FPY vs.BOL BP-tot per Lu(BOL)	Reactivity Ratios 4 FPY vs.BOL Lu-tot per Lu(BOL)	Yb-tot per Lu(BOL)	Hf-tot per Lu(BOL)	BP-tot per Lu(BOL)	BP Penalty at 4 FPY (FPD)	MVC at BOL dkeff per -10% water density change (STD)
Lu-nat	4.0	1.00	4.5	64	4.856+3	1.256-1	6.754-1 (55.9%)	5.884-1 (71.0%)	2.439-1	2.263-10	1.755-1	4.194-1	203.0	
Lu-nat	1.0	1.00	4.5	104	1.991+3	5.931-2	7.427-1 (48.8%)	6.607-1 (64.3%)	2.458-1	4.933-10	2.266-1	4.724-1	109.0	
Lu-176	0.5	1.00	4.5	64	6.139+2	1.709-1	6.269-1 (38.7%)	2.798-1 (74.6%)	1.311-5	1.797-10	3.477-2	3.479-2	19.1	
Lu-176	1.0	1.00	4.5	64	1.226+3	2.409-1	6.943-1 (32.0%)	3.838-1 (64.4%)	2.457-5	1.283-10	4.327-2	4.330-2	47.6	
Lu-176	0.2	1.00	4.5	104	3.994+2	1.398-1	5.492-1 (46.6%)	2.192-1 (80.7%)	8.901-6	2.213-10	3.248-2	3.249-2	21.5	

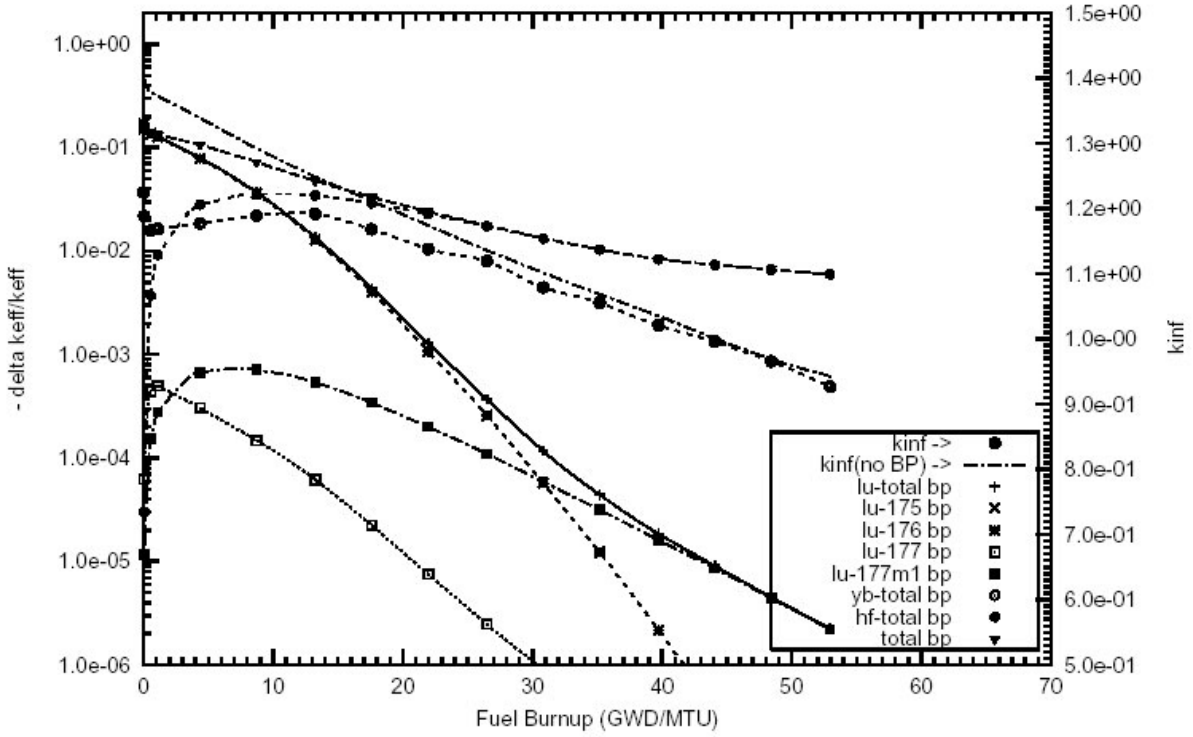

Figure 25 Negative reactivity of BP for Lu-176 and transmutation daughters as a function of fuel life for 17x17 fuel assemblies with 64 poison rods, 0.5 mil thick Lu_20_3 poison coating on the outer radial surface of the UO_2 pellets. Reactor power is 3400 MWth, 193 fuel assemblies, initial enrichment is 4.5wt%^{235}U.

DISCUSSION OF THE RESULTS OF THE CALCULATIONS

The primary objective of the calculations was to evaluate separated isotopes of candidate burnable poisons. This was achieved with pleasing results. In addition, much was learned about configurations of burnable poisons. This is especially evident in the suggestion and analysis of incorporating metallic burnable poisons in the cladding. It is also noteworthy that the fuel life used was 4 years with a limited number of cases explored with 6% enrichment to achieve a 5-year fuel life.

Tables 30 through 48 show a summary of input parameters and results for the four different configurations of the natural elements and separated isotopes of ^{157}Gd, ^{149}Sm, ^{167}Er, ^{164}Dy, ^{177}Hf, and ^{151}Eu. A measure of the isotope separation benefit is the ratio of the residual negative reactivity worth at EOL to that at BOL for a separated isotope divided by a similar ratio for the naturally occurring element. From these tables it can be observed that the residual reactivity worth ratio changes slightly with BP loading and that it is dependent on the number of IFBA rods and on the nature of the BP isotopes. The ratio decreases when the poison is spread over more IFBA rods. When the number of fuel pins containing BP increases, the BP is spread thinner, and this reduces the rod self-shielding.

Another important parameter that must be considered in selecting a burnable poison is the reactivity worth burnout rate of the BP (including the BP daughters). The rate of burnup is considered by displaying the ratio of the negative reactivity worth of the BP at three different burnup time intervals of interest (e.g., 120 days, 1 year, and 4 years) to the reactivity worth of the BP at BOL. The ratio depends on the BP loading, the number of IFBA rods per fuel assembly, the BP loading type, and the BP element or isotopes.

Table 30. The effect of isotope separation for the case of burnable poison in the form of gadolinium oxide homogeneously mixed with the fuel.

Isotope	Number IFBA	%loading	-dk_Bol	dk_EOL dk_EOL/dk_BOL|Isot ------ dk_BOL	------ dk_EOL/dk_BOL|Nat	BP Mass (g/assembly)	% of BP Worth Burned After Specified Time 120 d	1 yr	4 yrs
Gd-nat	08	3.60	5.74-2	2.25-2	0.202	515	32	82	98
Gd-157	08	1.00	5.74-2	4.53-3		144	30	86	100
Gd-nat	08	4.00	5.84-2	2.40-2	0.212	570	30	79	98
Gd-157	08	1.13	5.84-2	5.08-3		163	27	80	100
Gd-nat	08	6.15	6.31-2	3.12-2	0.243	865	23	64	97
Gd-157	08	2.00	6.31-2	7.60-3		288	20	59	100
Gd-nat	08	8.00	6.63-2	3.68-2	0.255	1118	21	52	96
Gd-nat	08	8.00	6.63-2	3.68-2	0.255	1118	21	52	96
Gd-157	08	2.86	6.63-2	9.41-3		409	17	47	99
Gd-nat	16	0.50	6.85-2	5.81-3	0.150	145	94	100	100
Gd-157	16	0.10	6.85-2	8.68-4		29	100	100	100
Gd-nat	16	0.67	8.17-2	9.31-3	0.155	281	76	99	99
Gd-157	16	0.20	8.17-2	1.44-3		58	100	100	100
Gd-nat	16	1.00	8.24-2	9.50-3	0.154	289	75	99	99
Gd-157	16	0.21	8.24-2	1.47-3		60	92	100	100
Gd-nat	16	2.00	9.73-2	1.53-2	0.137	575	48	97	98
Gd-157	16	0.48	9.73-2	2.08-3		140	66	100	100
Gd-nat	16	2.06	9.80-2	1.56-2	0.138	592	47	97	98
Gd-157	16	0.50	9.80-2	2.15-4		145	65	100	100
Gd-nat	16	2.27	0.100	1.68-2	0.150	652	44	95	98
Gd-157	16	0.57	0.100	2.52-3		164	58	99	100
Gd-nat	16	3.43	1.08-1	2.25-2	0.225	980	33	84	98
Gd-157	16	1.00	1.08-1	5.06-3		289	29	85	99
Gd-nat	16	4.00	1.10-1	2.51-2	0.237	1140	29	79	98
Gd-157	16	1.22	1.10-1	5.94-3		352	25	78	99
Gd-nat	16	5.83	1.18-1	3.19-2	0.257	1646	23	66	97
Gd-157	16	2.00	1.18-1	8.19-3		575	19	58	99
Gd-nat	16	8.00	1.25-1	3.88-2	0.271	2237	20	52	99
Gd-157	16	3.05	1.25-1	1.05-2		871	16	45	99
Gd-nat	64	0.27	1.87-1	4.50-3	0.145	310	98	99	100
Gd-157	64	0.05	1.87-1	6.52-4		58	100	100	100

Table 31. The effect of isotope separation for the case of burnable poison in the form of samarium oxide homogeneously mixed with the fuel.

Isotope	Number IFBA	%loading	-dk_Bol	dk_EOL / dk_BOL	dk_EOL/dk_BOL|Isot / dk_EOL/dk_BOL|Nat	BP Mass (g/assembly)	% of BP Worth Burned After Specified Time 120 d	1 yr	4 yrs
Sm-nat	08	4.57	6.04-2	1.64-1	0.317	644	41	82	84
Sm-149	08	1.00	6.04-2	5.21-2		144	30	87	95
Sm-nat	08	8.00	6.74-2	2.30-1	0.320	1112	24	67	77
Sm-149	08	1.85	6.74-2	7.36-2		264	21	61	93
Sm-nat	16	0.65	6.89-2	5.23-1	0.213	186	95	93	95
Sm-149	16	0.10	6.89-2	1.11-2		29	99	99	99
Sm-nat	16	1.00	7.94-2	6.77-1	0.224	287	92	92	93
Sm-149	16	0.16	7.94-2	1.52-2		45	99	99	99
Sm-nat	16	1.22	8.40-2	7.67-2	0.233	350	89	91	92
Sm-149	16	0.20	8.40-2	1.79-2		58	95	99	99
Sm-nat	16	2.00	9.57-2	1.06-1	0.260	572	76	88	89
Sm-149	16	0.38	9.57-2	2.74-2		109	66	98	97
Sm-nat	16	2.38	1.0-1	1.18-1	0.274	680	68	87	88
Sm-149	16	0.47	1.0-1	3.24-2		135	55	97	97
Sm-nat	16	2.52	1.013-1	1.22-1	0.278	718	65	87	88
Sm-149	16	0.50	1.013-1	3.40-2		144	53	97	97
Sm-nat	16	4.00	1.12-1	1.61-1	0.321	1133	43	84	84
Sm-149	16	0.92	1.12-1	5.17-2		265	32	89	95
Sm-nat	16	4.28	1.14-1	1.68-1	0.326	1212	41	83	83
Sm-149	16	1.00	1.14-1	5.48-2		287	30	87	95
Sm-nat	16	7.97	1.27-1	2.36-1	0.356	2215	24	67	76
Sm-149	16	2.00	1.27-1	8.38-2		571	21	58	92
Sm-nat	16	8.00	1.27-1	2.36-1	0.356	2224	24	66	76
Sm-149	16	2.01	1.27-1	8.41-2		574	21	57	92

Table 32. The effect of isotope separation for the case of burnable poison in the form of erbium oxide homogeneously mixed with the fuel.

Isotope	Number IFBA	%loading	-dk_Bol	dk_EOL / dk_BOL	dk_EOL/dk_BOL|Isot / dk_EOL/dk_BOL|Nat	BP Mass (g/assembly)	% of BP Worth Burned After Specified Time 120 d	1 yr	4 yrs
Er-nat	16	4.08	3.83-2	8.36-2	0.173	1181	27	58	92
Er-167	16	1.00	3.83-2	1.45-2		292	29	63	99
Er-nat	16	7.93	5.88-2	1.03-1	0.197	2271	22	49	90
Er-167	16	2.00	5.88-2	2.03-2		582	23	53	98
Er-nat	16	8.00	5.91-2	1.04-1	0.198	2292	21	49	90
Er-167	16	2.02	5.91-2	2.04-2		588	23	53	98
Er-nat	16	12.00	7.45-2	1.22-1	0.240	3402	19	43	88
Er-167	16	3.10	7.45-2	2.93-2		901	21	46	97
Er-nat	64	1.00	5.08-2	6.53-2	0.159	1167	36	72	93
Er-167	64	0.24	5.08-2	1.04-2		284	38	77	99
Er-nat	64	2.00	8.68-2	7.66-2	0.160	2329	30	66	92
Er-167	64	0.49	8.68-2	1.22-2		576	32	71	99
Er-nat	64	2.03	8.77-2	7.68-2	0.160	2364	30	66	92
Er-167	64	0.50	8.77-2	1.23-2		584	32	71	99
Er-nat	64	2.44	0.100	8.03-2	0.163	2843	29	64	92
Er-167	64	0.61	0.100	1.31-2		707	31	69	99
Er-nat	64	3.96	1.40-1	9.02-2	0.179	4589	25	58	91
Er-167	64	1.00	1.40-1	1.61-2		1167	27	62	98

Table 33. The effect of isotope separation for the case of burnable poison in the form of dysprosium oxide homogeneously mixed with the fuel.

Isotope	Number IFBA	%loading	-dk_Bol	dk_EOL / dk_BOL	dk_EOL/dk_BOL|Isot / dk_EOL/dk_BOL|Nat	BP Mass (g/assembly)	% of BP Worth Burned After Specified Time 120 d	1 yr	4 yrs
Dy-nat	16	2.00	3.69-2	3.59-1	0.281	578	16	30	64
Dy-164	16	1.32	3.69-2	1.01-1		384	22	47	90
Dy-nat	16	2.75	4.75-2	3.70-1	0.320	793	16	30	63
Dy-164	16	2.00	4.75-2	1.19-1		579	20	42	88
Dy-nat	16	4.00	6.08-2	3.85-1	0.405	1146	15	29	62
Dy-164	16	3.24	6.08-2	1.56-1		932	17	36	84
Dy-nat	16	4.74	6.75-2	3.93-1	0.459	1353	15	29	61
Dy-164	16	4.00	6.75-2	1.80-1		1149	15	32	82
Dy-nat	64	0.76	6.52-2	3.23-1	0.253	880	17	32	68
Dy-164	64	0.50	6.52-2	8.19-2		583	27	54	92
Dy-nat	64	1.00	8.12-2	3.34-1	0.266	1159	17	32	67
Dy-164	64	0.68	8.12-2	8.90-2		797	26	52	91
Dy-nat	64	1.32	0.100	3.45-1	0.282	1523	16	31	66
Dy-164	64	0.90	0.100	9.73-2		1049	24	50	90
Dy-nat	64	1.47	1.09-2	3.49-1	0.290	1697	16	31	65
Dy-164	64	1.00	1.09-2	1.01-1		1163	24	49	90

Table 34. The effect of isotope separation for the case of burnable poison in the form of gadolinium oxide homogeneously mixed into the outer one-third volume of fuel pellets.

Isotope	Number IFBA	%loading	-dk_Bol	dk_EOL / dk_BOL	dk_EOL/dk_BOL|Isot / dk_EOL/dk_BOL|Nat	BP Mass (g/assembly)	% of BP Worth Burned After Specified Time 120 d	1 yr	4 yrs
Gd-nat	08	12.00	5.90-2	2.29-2	0.249	549	29	89	98
Gd-157	08	4.00	6.08-2	5.70-3		190	23	98	99
Gd-nat	16	2.00	7.58-2	6.83-3	0.151	192	90	99	99
Gd-157	16	0.39	7.58-2	1.03-3		38	99	100	100
Gd-nat	16	2.41	8.02-2	7.95-3	0.153	231	84	99	99
Gd-157	16	0.50	8.02-2	1.22-3		48	99	100	100
Gd-nat	16	4.00	8.96-2	1.13-2	0.161	380	68	98	99
Gd-157	16	0.88	8.96-2	1.83-3		84	85	100	100
Gd-nat	16	4.56	9.20-2	1.25-2	0.164	432	63	98	99
Gd-157	16	1.00	9.20-2	2.04-3		96	80	100	100
Gd-nat	16	6.96	1.00-1	1.67-2	0.185	652	45	97	98
Gd-157	16	1.63	1.00-1	3.08-3		156	49	100	100
Gd-nat	16	8.00	1.028-1	1.84-2	0.194	746	39	97	98
Gd-157	16	1.94	1.028-1	3.56-2		186	39	100	100
Gd-nat	16	8.20	1.033-1	1.87-2	0.195	763	38	96	98
Gd-157	16	2.00	1.033-1	3.65-3		192	38	100	100
Gd-nat	16	12.00	1.11-1	2.38-2	0.222	1098	28	89	98
Gd-157	16	3.43	1.11-1	5.28-3		326	24	98	99

Table 35. The effect of isotope separation for the case of burnable poison in the form of samarium oxide homogeneously mixed into the outer one-third volume of fuel pellets.

Isotope	Number IFBA	%loading	-dk_Bol	dk_EOL / dk_BOL	dk_EOL/dk_BOL|Isot / dk_EOL/dk_BOL|Nat	BP Mass (g/assembly)	% of BP Worth Burned After Specified Time 120 d	1 yr	4 yrs
Sm-nat	08	10.58	5.78-2	1.42-1	0.290	484	55	85	86
Sm-149	08	2.00	5.78-2	4.13-2		95	41	97	96
Sm-nat	08	12.00	5.92-2	1.53-1	0.299	546	46	84	85
Sm-149	08	2.34	5.92-2	4.57-2		112	36	95	96
Sm-nat	16	1.26	5.85-2	4.07-2	0.233	121	94	94	96
Sm-149	16	0.20	5.85-2	9.48-3		19	99	99	99
Sm-nat	16	2.00	7.01-2	5.25-2	0.219	191	93	93	95
Sm-149	16	0.28	7.01-2	1.15-2		27	99	99	99
Sm-nat	16	3.26	8.23-2	7.19-2	0.227	309	92	92	93
Sm-149	16	0.50	8.23-2	1.63-2		48	99	99	99
Sm-nat	16	4.00	8.73-2	8.21-2	0.236	378	90	91	92
Sm-149	16	0.64	8.73-2	1.93-2		61	95	98	98
Sm-nat	16	5.74	9.58-2	1.02-1	0.260	537	83	89	90
Sm-149	16	1.00	9.58-2	2.66-2		96	83	98	98
Sm-nat	16	6.84	1.00-1	1.14-1	0.276	636	77	88	89
Sm-149	16	1.26	1.00-1	3.13-2		120	73	98	97
Sm-nat	16	8.00	1.04-1	1.25-1	0.292	741	71	87	87
Sm-149	16	1.58	1.04-1	3.66-2		150	59	97	97
Sm-nat	64	0.35	9.59-2	2.64-2	0.227	135	96	96	97
Sm-149	64	0.05	9.59-2	6.00-3		19	99	99	100
Sm-nat	64	0.37	0.100	2.69-2	0.226	143	96	96	97
Sm-149	64	0.05	0.100	6.10-3		20	100	100	100
Sm-nat	64	0.50	1.23-1	3.00-2	0.226	192	95	95	97
Sm-149	64	0.065	1.23-1	6.78-3		27	100	100	100
Sm-nat	64	1.00	1.78-1	4.13-2	0.232	383	94	94	96
Sm-149	64	0.18	1.78-1	9.58-3		58	99	99	99
Sm-nat	64	1.34	2.00-1	4.85-2	0.230	511	93	93	95
Sm-149	64	0.25	2.00-1	1.12-2		77	99	99	99

Table 36. The effect of isotope separation for the case of burnable poison in the form of erbium oxide homogeneously mixed onto the outer one-third volume of fuel pellets.

Isotope	Number IFBA	%loading	-dk_Bol	dk_EOL / dk_BOL	dk_EOL/dk_BOL|Isot / dk_EOL/dk_BOL|Nat	BP Mass (g/assembly)	% of BP Worth Burned After Specified Time 120 d	1 yr	4 yrs
Er-nat	16	1.00	4.87-3	5.83-2	0.169	97	41	76	94
Er-167	16	0.24	4.87-3	9.83-3		23	44	81	99
Er-nat	16	2.00	9.14-3	6.11-2	0.155	194	38	74	94
Er-167	16	0.47	9.14-3	9.47-3		46	41	80	99
Er-nat	16	2.11	9.60-3	6.14-2	0.155	205	38	74	94
Er-167	16	0.50	9.60-3	9.53-3		49	41	80	99
Er-nat	16	4.00	1.67-2	6.69-2	0.160	386	35	71	93
Er-167	16	0.98	1.67-2	1.07-2		95	36	76	99
Er-nat	16	4.09	4.71-2	6.72-2	0.160	395	35	71	94
Er-167	16	1.00	4.71-2	1.07-2		97	35	76	99
Er-nat	16	8.00	2.85-2	7.64-2	0.166	764	29	65	92
Er-167	16	1.94	2.85-2	1.27-2		188	31	69	99
Er-nat	64	2.09	3.78-2	6.28-2	0.156	811	38	74	94
Er-167	64	0.50	3.78-2	9.78-3		195	41	79	99
Er-nat	64	4.00	6.46-2	6.97-2	0.157	1544	34	70	94
Er-167	64	0.96	6.46-2	1.10-2		375	37	76	99
Er-nat	64	4.15	6.66-2	7.02-2	0.158	1602	34	70	93
Er-167	64	1.00	6.66-2	1.11-2		389	36	75	99
Er-nat	64	7.23	1.00-1	7.91-2	0.166	2768	30	65	92
Er-167	64	1.75	1.00-1	1.31-2		678	32	70	99
Er-nat	64	8.00	1.07-1	8.12-2	0.167	3056	29	64	92
Er-167	64	1.94	1.07-1	1.36-2		752	31	69	99

Table 37. The effect of isotope separation for the case of burnable poison in the form of dysprosium oxide homogeneously mixed into the outer one-third volume of fuel pellets.

Isotope	Number IFBA	%loading	-dk_Bol	dk_EOL / dk_BOL	dk_EOL/dk_BOL|Isot / dk_EOL/dk_BOL|Nat	BP Mass (g/assembly)	% of BP Worth Burned After Specified Time 120 d	1 yr	4 yrs
Dy-nat	08	6.03	1.88-2	3.45-1	0.272	285	16	31	65
Dy-164	08	4.00	1.88-2	9.37-2		192	23	47	91
Dy-nat	08	8.00	2.37-2	3.59-1	0.298	376	16	31	64
Dy-164	08	5.59	2.37-2	1.07-1		266	20	44	89
Dy-nat	64	1.00	3.29-2	2.87-1	0.256	387	19	35	71
Dy-164	64	1.00	4.84-2	7.34-2		387	29	57	93

Table 38. The effect of isotope separation for the case of burnable poison in the form of gadolinium oxide deposited in a thin coating on the lateral surface of the fuel pellets.

Isotope	Number IFBA	Coating Thickness (0.001 in)	Relative Density	-dk_Bol	dk_EOL / dk_BOL	dk_EOL/dk_BOL|Isot / dk_EOL/dk_BOL|Nat	BP Mass (g/asbl)	% of BP Worth Burned After Specified Time 120 d	1 yr	4 yrs
Gd-nat	16	2.18	1.00	9.54-2	1.45-2	0.176	516	55	98	99
Gd-157	16	0.50	1.00	9.54-2	2.54-3		119	65	100	100
Gd-nat	16	2.76	1.00	1.00-1	1.69-2	0.184	652	45	97	98
Gd-157	16	0.650	1.00	1.00-1	3.12-3		155	47	98	100
Gd-nat	16	3.76	1.00	1.06-1	2.07-2	0.203	885	34	94	98
Gd-157	16	1.00	1.00	1.06-1	4.20-3		238	31	99	100
Gd-nat	16	4.00	1.00	1.08-1	2.16-2	0.207	942	32	93	98
Gd-157	16	1.10	1.00	1.08-1	4.47-3		260	28	98	100
Gd-nat	16	6.31	1.00	1.17-1	2.88-2	0.239	1473	23	77	97
Gd-157	16	2.00	1.00	1.17-1	6.87-3		474	20	79	99
Gd-nat	64	0.20	1.00	1.55-1	3.49-3	0.137	191	99	100	100
Gd-157	64	0.36	0.10	1.55-1	4.80-4		35	100	100	100
Gd-nat	64	0.24	1.00	1.75-1	3.96-3	0.145	227	82	99	100
Gd-157	64	0.50	0.10	1.75-1	5.72-4		48	100	100	100
Gd-nat	104	0.50	0.10	1.05-1	2.13-3	0.189	74	100	100	100
Gd-157	104	0.20	0.10	1.64-1	4.02-4		31	100	100	100

Table 39. The effect of isotope separation for the case of burnable poison in the form of samarium oxide deposited in a thin coating on the lateral surface of the fuel pellets.

Isotope	Number IFBA	Coating Thickness (0.001 in)	Relative Density	-dk_Bol	dk_EOL / dk_BOL	dk_EOL/dk_BOL|Isot / dk_EOL/dk_BOL|Nat	BP Mass (g/asbl)	% of BP Worth Burned After Specified Time 120 d	1 yr	4 yrs
Sm-nat	08	3.70	1.00	5.30-2	1.43-1	0.224	434	58	85	86
Sm-149	08	0.50	1.00	5.30-2	3.22-2		59	70	97	97
Sm-nat	08	4.00	1.00	5.42-2	1.52-1	0.231	470	53	84	85
Sm-149	08	0.56	1.00	5.42-2	3.50-2		66	61	98	97
Sm-nat	16	1.00	1.00	7.13-2	6.70-2	0.207	237	92	92	93
Sm-149	16	0.13	1.00	7.13-2	1.39-2		30	99	99	99
Sm-nat	16	1.46	1.00	8.07-2	8.59-2	0.210	345	92	92	91
Sm-149	16	0.20	1.00	8.07-2	1.80-2		47	98	98	98
Sm-nat	16	2.00	1.00	8.72-2	1.03-1	0.212	472	86	89	90
Sm-149	16	0.27	1.00	8.72-2	2.19-2		65	91	98	98
Sm-nat	16	3.64	1.00	9.98-2	1.48-1	0.223	856	59	84	85
Sm-149	16	0.50	1.00	9.98-2	3.31-2		119	69	97	97
Sm-nat	16	3.68	1.00	1.00-1	1.49-1	0.223	865	58	84	85
Sm-149	16	0.50	1.00	1.00-1	3.33-2		120	69	97	97
Sm-nat	16	4.00	1.00	1.02-1	1.58-1	0.226	939	52	83	84
Sm-149	16	0.55	1.00	1.02-1	3.55-2		131	64	97	97
Sm-nat	64	0.36	1.00	1.58-1	4.35-2	0.232	337	94	94	96
Sm-149	64	0.50	0.10	1.58-1	1.01-2		47	99	99	99
Sm-nat	64	0.50	1.00	1.82-1	5.21-2	0.232	475	93	93	95
Sm-149	64	0.50	0.10	1.82-1	1.21-2		47	99	99	99

Table 40. The effect of isotope separation for the case of burnable poison in the form of erbium oxide deposited in a thin coating on the lateral surface of the fuel pellets.

Isotope	Number IFBA	Coating Thickness (0.001 in)	Relative Density	-dk_Bol	dk_EOL / dk_BOL	dk_EOL/dk_BOL|Isot / dk_EOL/dk_BOL|Nat	BP Mass (g/asbl)	% of BP Worth Burned After Specified Time 120 d	1 yr	4 yrs
Er-nat	16	4.14	1.00	3.70-2	8.96-2	0.165	1144	25	58	91
Er-149	16	2.00	1.00	3.70-2	1.46-2		279	28	63	99
Er-nat	16	8.00	1.00	5.64-2	1.08-1	0.183	2187	19	48	89
Er-149	16	1.94	1.00	5.64-2	1.98-2		540	24	53	98
Er-nat	64	1.00	1.00	4.85-2	6.74-2	0.161	1118	35	71	93
Er-149	64	0.24	1.00	4.85-2	1.08-2		269	37	77	99
Er-nat	64	2.00	1.00	8.32-2	7.81-2	0.159	2228	30	65	92
Er-149	64	0.48	1.00	8.32-2	1.24-2		539	33	71	99
Er-nat	64	2.08	1.00	8.54-2	7.88-2	0.159	2314	29	65	92
Er-149	64	0.50	1.00	8.54-2	1.25-2		560	33	71	99
Er-nat	64	2.61	1.00	1.00-1	8.32-2	0.161	2904	27	63	92
Er-167	64	0.63	1.00	1.00-1	1.34-2		701	31	68	99
Er-nat	64	4.00	1.00	1.33-1	9.30-2	0.171	4429	23	57	91
Er-149	64	0.96	1.00	1.33-1	1.59-2		1070	28	68	98
Er-nat	104	1.00	1.00	7.52-2	7.15-2	0.153	1816	34	70	93
Er-149	104	0.24	1.00	7.52-2	1.10-2		446	37	75	99

Table 41. The effect of isotope separation for the case of burnable poison in the form of dysprosium oxide deposited in a thin coating on the lateral surface of the fuel pellets.

Isotope	Number IFBA	Coating Thickness (0.001 in)	Relative Density	-dk_Bol	dk_EOL / dk_BOL	dk_EOL/dk_BOL|Isot / dk_EOL/dk_BOL|Nat	BP Mass (g/asbl)	% of BP Worth Burned After Specified Time 120 d	1 yr	4 yrs
Dy-nat	64	1.00	1.00	7.40-2	3.17-1	0.259	1005	17	33	68
Dy-164	64	0.66	1.00	7.40-2	8.19-2		664	26	53	92
Dy-nat	64	1.00	1.00	7.40-2	3.17-1	0.292	1005	17	33	68
Dy-164	64	1.00	1.00	9.87-2	9.25-2		1008	24	50	91

Table 42. The effect of isotope separation for the case of burnable poison in the form of hafnium oxide deposited in a thin coating on the lateral surface of the fuel pellets.

Isotope	Number IFBA	Coating Thickness (0.001 in)	Relative Density	-dk_Bol	dk_EOL / dk_BOL	dk_EOL/dk_BOL|Isot / dk_EOL/dk_BOL|Nat	BP Mass (g/asbl)	% of BP Worth Burned After Specified Time 120 d	1 yr	4 yrs
Hf-nat	16	7.57	1.00	4.58-2	2.18-1	0.441	2250	18	39	78
Hf-177	16	2.00	1.00	4.58-2	9.59-2		604	17	41	90
Hf-nat	16	8.00	1.00	4.77-2	2.20-1	0.449	2376	17	39	78
Hf-177	16	2.16	1.00	4.77-2	9.89-2		651	17	41	90
Hf-nat	64	2.00	1.00	7.21-2	1.90-1	0.435	2420	23	51	81
Hf-177	64	0.51	1.00	7.21-2	8.27-2		618	23	55	92
Hf-nat	64	2.00	1.00	7.21-2	1.90-1	0.466	2420	23	51	81
Hf-177	64	1.00	1.00	1.12-1	8.86-2		1212	20	48	91
Hf-nat	104	1.00	1.00	6.88-2	1.88-1	0.417	1973	26	56	81
Hf-177	104	0.26	1.00	6.88-2	7.82-2		514	27	62	92
Hf-nat	104	1.73	1.00	1.00-1	1.93-1	0.429	3409	24	52	81
Hf-177	104	0.44	1.00	1.00-1	8.27-2		864	25	56	92
Hf-nat	104	2.00	1.00	1.11-1	1.95-1	0.433	3910	23	50	81
Hf-177	104	0.50	1.00	1.11-1	8.43-2		987	24	54	92

Table 43. The effect of isotope separation for the case of burnable poison in the form of gadolinium alloyed in the Zircaloy cladding.

Isotope	Number IFBA	%loading	-dk_Bol	dk_EOL / dk_BOL	dk_EOL/dk_BOL|Isot / dk_EOL/dk_BOL|Nat	BP Mass (g/assembly)	% of BP Worth Burned After Specified Time 120 d	1 yr	4 yrs
Gd-nat	16	1.03	5.27-2	3.28-3	0.139	59	99	100	100
Gd-157	16	0.20	5.27-2	4.55-4		11	100	100	100
Gd-nat	16	2.00	6.92-2	4.83-3	0.142	115	97	99	100
Gd-157	16	0.40	6.92-2	6.85-4		23	100	100	100
Gd-nat	16	4.00	8.61-2	7.39-3	0.156	231	88	99	99
Gd-157	16	0.85	8.61-2	1.16-3		49	100	100	100
Gd-nat	16	4.67	8.96-2	8.22-3	0.159	271	84	99	99
Gd-157	16	1.00	8.96-2	1.31-3		58	99	100	100
Gd-nat	16	7.66	1.00-1	1.21-2	0.166	446	65	98	99
Gd-157	16	1.76	1.00-1	2.00-3		101	80	100	100
Gd-nat	16	8.00	1.01-1	1.25-2	0.167	467	63	98	99
Gd-157	16	1.85	1.01-1	2.10-3		107	77	100	100

Table 44. The effect of isotope separation for the case of burnable poison in the form of samarium alloyed in the Zircaloy cladding.

Isotope	Number IFBA	%loading	-dk_Bol	dk_EOL / dk_BOL	dk_EOL/dk_BOL|Isot / dk_EOL/dk_BOL|Nat	BP Mass (g/assembly)	% of BP Worth Burned After Specified Time 120 d	1 yr	4 yrs
Sm-nat	16	2.00	5.92-2	3.97-2	0.253	115	95	95	96
Sm-149	16	0.31	5.92-2	1.00-2		18	99	99	99
Sm-nat	16	3.39	7.36-2	5.28-2	0.246	196	93	93	95
Sm-149	16	0.50	7.36-2	1.30-2		29	99	99	99
Sm-nat	16	4.00	8.00-2	5.86-2	0.252	231	93	93	94
Sm-149	16	0.62	8.00-2	1.48-2		35	99	99	99

Table 45. The effect of isotope separation for the case of burnable poison in the form of erbium alloyed in the Zircaloy cladding.

Isotope	Number IFBA	%loading	-dk_Bol	dk_EOL / dk_BOL	dk_EOL/dk_BOL|Isot / dk_EOL/dk_BOL|Nat	BP Mass (g/assembly)	% of BP Worth Burned After Specified Time 120 d	1 yr	4 yrs
Er-nat	104	2.14	3.86-2	6.04-2	0.154	805	40	76	94
Er-167	104	0.50	3.86-2	9.30-3		187	43	81	99
Er-nat	104	4.00	6.94-2	6.49-2	0.159	1510	31	74	94
Er-167	104	0.98	6.94-2	1.03-2		367	40	79	99

Table 46. The effect of isotope separation for the case of burnable poison in the form of europium alloyed in the Zircaloy cladding.

Isotope	Number IFBA	%loading	-dk_Bol	dk_EOL / dk_BOL	dk_EOL/dk_BOL|Isot / dk_EOL/dk_BOL|Nat	BP Mass (g/assembly)	% of BP Worth Burned After Specified Time 120 d	1 yr	4 yrs
Eu-nat	64	1.00	7.44-2	9.50-2	0.607	229	53	73	91
Eu-151	64	0.54	7.44-2	5.77-2		123	31	84	94
Eu-nat	64	1.51	1.00-1	1.05-1	0.611	346	49	71	90
Eu-151	64	0.81	1.00-1	6.40-2		185	43	83	94
Eu-nat	64	1.88	1.18-1	1.12-1	0.613	429	46	69	89
Eu-151	64	1.00	1.18-1	6.85-2		229	52	81	93
Eu-nat	104	0.50	6.42-2	8.86-2	0.610	186	55	74	91
Eu-151	104	0.27	6.42-2	5.39-2		102	62	85	95
Eu-nat	104	0.87	1.00-1	9.78-2	0.608	322	52	72	90
Eu-151	104	0.46	1.00-1	5.95-2		171	58	84	94
Eu-nat	104	0.94	1.08-1	9.98-2	0.608	352	51	72	90
Eu-151	104	0.50	1.08-1	6.07-2		186	58	84	94

Table 47. The effect of isotope separation for the case of burnable poison in the form of hafnium alloyed in the Zircaloy cladding.

Isotope	Number IFBA	%loading	-dk_Bol	dk_EOL dk_BOL	dk_EOL/dk_BOL|Isot dk_EOL/dk_BOL|Nat	BP Mass (g/assembly)	% of BP Worth Burned After Specified Time 120 d	1 yr	4 yrs
Hf-nat	104	2.21	3.47-2	1.72-1	0.394	837	31	61	83
Hf-177	104	0.50	3.47-2	6.77-2		187	35	71	93
Hf-nat	104	4.00	5.89-2	1.85-1	0.407	1524	27	59	82
Hf-177	104	0.99	5.89-2	7.52-2		371	30	66	92

Table 48. The effect of isotope separation for the case of burnable poison in the form of osmium alloyed in the Zircaloy cladding.

Isotope	Number IFBA	%loading	-dk_Bol	dk_EOL dk_BOL	dk_EOL/dk_BOL|Isot dk_EOL/dk_BOL|Nat	BP Mass (g/assembly)	% of BP Worth Burned After Specified Time 120 d	1 yr	4 yrs
Os-nat	264	15.00	8.96-2	5.43-1	0.109	19620	11	17	46
Os-184	264	0.35	8.96-2	5.92-2		378	47	77	94
Os-nat	264	17.50	1.00-1	5.44-1	0.111	22291	10	17	46
Os-184	264	0.40	1.00-1	6.02-2		432	46	77	94
Os-nat	264	17.67	1.01-1	5.45-1	0.111	22474	10	17	46
Os-184	264	0.40	1.01-1	6.03-2		436	46	77	94
Os-nat	264	20.00	1.12-1	5.46-1	0.112	25340	10	17	45
Os-184	264	0.45	1.12-1	6.13-2		494	46	77	94
Os-nat	264	25.00	1.39-1	5.48-1	0.117	33050	11	18	45
Os-184	264	0.60	1.39-1	6.41-2		651	45	76	94

The results have been further arranged in a set of four summary tables, one for each configuration. Tables 49 through 52 show input parameters and results from a representative number of runs to compare natural elements with separated isotopes. As much as possible, the initial negative reactivity has been held near 10% in these tables. Since the long run time for each case prohibited many iterations for fine tuning, there is sometimes a greater variation from 10% than desired; however, the effect of this variation has been minimized by taking appropriate ratios.

The calculations for the first phase of the project have assumed that the isotopes have been separated completely. In reality, the enrichment achievable depends upon the particular isotope, its abundance, and the number of passes in the enrichment process. The enrichment levels actualy achieved are presented in the section on isotope separation.

Table 49. The effect of isotope separation for the case of burnable poison in the form of oxide homogeneously mixed with the fuel.

Isotope	Number IFBA	%loading	-dk_Bol	dk_EOL / dk_BOL	dk_EOL/dk_BOL|Isot / dk_EOL/dk_BOL|Nat	BP Mass (g/assembly)	% of BP Worth Burned After Specified Time 120 d	1 yr	4 yrs
Gd-nat	16	2.27	0.100	1.68-2	0.15	652	44	95	98
Gd-157	16	0.57	0.100	2.52-3		164	58	99	100
Sm-nat	16	2.38	0.100	1.18-1	0.27	680	68	87	88
Sm-149	16	0.47	0.100	3.24-2		135	55	97	97
Er-nat	16	12.00	7.45-2	1.22-1	0.24	3402	19	43	88
Er-167	16	3.10	7.45-2	2.93-2		901	21	46	97
Er-nat	64	2.44	0.100	8.03-2	0.16	2843	29	64	92
Er-167	64	0.60	0.100	1.31-2		707	31	69	99
Dy-nat	16	4.74	6.75-2	3.93-1	0.46	1353	15	29	61
Dy-164	16	4.00	6.75-2	1.80-1		1149	15	32	82
Dy-nat	64	1.32	0.100	3.45-1	0.28	1523	16	31	66
Dy-164	64	0.90	0.100	9.73-2		1049	24	50	90
Eu-nat	08	4.00	6.51-2	2.98-1	0.96	567	15	37	70
Eu-151	08	4.00	7.37-2	2.85-1		567	11	28	72
Hf-nat	08	4.00	1.43-2	1.97-1	0.65	565	19	46	80
Hf-177	08	4.00	3.41-2	1.28-1		564	15	35	87
Lu-nat	08	4.00	1.54-2	4.39-1	0.25	585	29	39	56
Lu-176	08	4.00	6.26-2	1.08-1		585	18	32	89
Yb-nat	08	4.00	3.01-3	5.56-1	0.25	583	14	26	44
Yb-169	08	4.00	4.80-2	1.42-1		581	11	30	86

Table 50. The effect of isotope separation for the case of burnable poison in the form of oxide homogeneously mixed into the outer one-third volume of fuel pellets.

Isotope	Number IFBA	%loading	-dk_Bol	dk_EOL / dk_BOL	dk_EOL/dk_BOL|Isot / dk_EOL/dk_BOL|Nat	BP Mass (g/assembly)	% of BP Worth Burned After Specified Time 120 d	1 yr	4 yrs
Gd-nat	16	6.96	0.100	1.67-2	0.18	652	45	98	98
Gd-157	16	1.63	0.100	3.08-3		156	49	100	100
Sm-nat	16	6.84	0.100	1.14-1	0.28	636	77	88	89
Sm-149	16	1.26	0.100	3.13-2		120	73	97	97
Sm-nat	64	3.73-1	0.100	2.69-2	0.23	143	96	96	97
Sm-149	64	5.06-2	0.100	6.10-3		20	100	100	100
Er-nat	64	7.23	0.100	7.91-2	0.17	2768	30	65	92
Er-167	64	1.75	0.100	1.31-2		678	32	70	99
Dy-nat	64	1.00	3.30-2	2.87-1	0.26	287	19	35	71
Dy-164	64	1.00	4.84-2	7.34-2		388	29	57	92
Eu-nat	08	8.00	5.44-2	2.40-1	0.62	371	20	42	76
Eu-151	08	4.00	4.94-2	1.49-1		189	22	57	85
Hf-nat	08	8.00	1.11-2	1.87-1	0.55	374	22	52	82
Hf-177	08	8.00	2.67-2	1.03-1		374	17	40	90
Yb-nat	08	16.00	3.82-3	5.75-1	0.15	760	14	23	43
Yb-168	08	4.00	2.74-2	8.59-2		194	14	45	91

Table 51. The effect of isotope separation for the case of burnable poison in the form of oxide deposited in a thin coating on the lateral surface of the fuel pellets.

Isotope	Number IFBA	Coating Thickness (0.001 in)	-dk_Bol	dk_EOL / dk_BOL	dk_EOL/dk_BOL|Isot / dk_EOL/dk_BOL|Nat	BP Mass (g/asbl)	% of BP Worth Burned After Specified Time 120 d	1 yr	4 yrs
Gd-nat	16	2.76	0.100	1.69-2	0.18	652	45	97	98
Gd-157	16	0.65	0.100	3.12-3		155	47	98	100
Sm-nat	16	3.68	0.100	1.49-1	0.22	865	58	84	85
Sm-149	16	0.51	0.100	3.33-2		120	69	97	97
Er-nat	16	8.0	5.64-2	1.08-1	0.18	2187	19	48	89
Er-167	16	1.94	5.64-2	1.98-2		540	24	53	98
Er-nat	64	2.61	0.100	8.32-2	0.16	2904	27	63	92
Er-167	64	0.63	0.100	1.34-2		701	31	68	99
Dy-nat	64	1.00	7.40-2	3.17-1	0.26	1005	17	33	68
Dy-164	64	0.66	7.40-2	8.19-2		664	26	53	92
Eu-nat	64	1.00	1.88-1	1.63-1	0.61	948	33	61	84
Eu-151	64	0.50	1.75-1	5.90-2		474	39	74	90
Hf-nat	16	8.00	4.77-2	2.20-1	0.45	2376	17	39	78
Hf-177	16	2.16	4.77-2	9.89-2		651	17	41	90
Hf-nat	64	2.00	7.21-2	1.90-1	0.43	2420	23	51	81
Hf-177	64	0.51	7.21-2	8.27-2		618	23	55	92
Hf-nat	104	1.73	0.100	1.93-1	0.43	3409	24	52	81
Hf-177	104	0.44	0.100	8.27-2		864	25	56	92

Table 52. The effect of isotope separation for the case of burnable poison in the form of a metal alloyed in the Zircaloy cladding.

Isotope	Number IFBA	%loading	-dk_Bol	dk_EOL / dk_BOL	dk_EOL/dk_BOL|Isot / dk_EOL/dk_BOL|Nat	BP Mass (g/assembly)	% of BP Worth Burned After Specified Time 120 d	1 yr	4 yrs
Gd-nat	16	7.66	0.100	1.20-2	0.17	446	65	98	99
Gd-157	16	1.76	0.100	2.00-3		101	80	100	100
Sm-nat	16	4.00	8.00-2	5.86-2	0.25	231	93	93	94
Sm-149	16	0.62	8.00-2	1.48-2		35	99	99	99
Er-nat	104	4.00	6.94-2	6.49-2	0.16	1510	31	74	94
Er-167	104	1.00	7.05-2	1.03-2		37	40	79	99
Dy-nat	104	8.00	1.86-1	3.51-1	0.22	3041	16	32	65
Dy-164	104	2.00	8.91-2	7.60-2		750	28	56	92
Eu-nat	64	1.51	0.100	1.05-1	0.61	346	49	71	90
Eu-151	64	0.81	0.100	6.40-2		185	43	83	94
Eu-nat	104	0.87	0.100	9.78-2	0.61	322	52	72	90
Eu-151	104	0.46	0.100	5.95-2		171	58	84	94
Hf-nat	104	4.00	5.89-1	1.85-1	0.41	1524	27	59	82
Hf-177	104	1.00	5.89-1	7.52-2		371	30	66	92
Os-nat	264	17.50	0.100	5.44-1	0.11	22290	10	17	46
Os-184	264	0.40	0.100	6.02-2		432	46	77	94

RESIDUAL REACTIVITY

Detailed results of the residual reactivity worth of the BPs are displayed in Tables 30 through 48. The results are further summarized by graphing the data in Tables 49 through 52 in several forms. The first plot is shown in Figure 26, where the residual reactivity ratio, the ratio of negative reactivity due to the burnable poison at EOL to the negative reactivity due to the burnable poison at BOL, dk_{EOL}/dk_{BOL}, is plotted for each of the four configurations of each of six isotopes. Two observations may be made from Figure 26. The first is that the residual reactivity ratios are best for ^{157}Gd and worsen in the order of ^{167}Er, ^{149}Sm, ^{164}Dy, ^{177}Hf, and ^{151}Eu. The second observation is that, for the same initial reactivity worth of the BP, the ratio decreases when the poison is spread over more IFBA rods. When the number of fuel pins containing BP increases, the BP is spread thinner and is placed in a higher thermal flux position, and this reduces self-shielding.

Another observation that may be made directly from Tables 49 through 52 is that the loading of separated isotopes to achieve the same negative reactivity at BOL is much smaller than for naturally occurring elements. This is also an intuitive result and is often not a great benefit. However, in cases where the amount of material added is limited, there is a definite benefit. This is particularly true in advanced reactors, where it is desired to extend the fuel cycle. Thus more fuel may be added in a limited core volume. In the case of coatings, time of deposition, impediment of heat transfer, and cracking of thick coatings due to thermal expansion all limit the thickness of the coatings. In the case of BP in the cladding, high concentrations of rare earths might alter the structure of the cladding or cause degradation by segregation at grain boundaries in the metal. As will be discussed later, at

concentrations appropriate for burnable poisons, the zircaloy-4 is not embrittled. In all these cases, there is a decided benefit of isotope separation.

A measure of the isotope separation benefit is the ratio of the residual negative reactivity at EOL to that at BOL for a separated isotope divided by a similar ratio for the naturally occurring element. This compound ratio is shown in Tables 49 through 52 and is plotted in Figure 27. Here it is seen that the benefit ratio, defined above, varies with configuration and isotope in the range of 0.15 to 0.96, which shows a reactivity ratio benefit of nearly an order of magnitude for ^{157}Gd, ^{149}Sm, and ^{167}Er to almost no benefit for ^{151}Eu homogeneously mixed with the fuel in eight IFBAs per fuel assembly. As expected, the ratio improves when the self-shielding is minimized by the configuration. Exceptions exist in the figure, largely because of differences in initial reactivity due to running a limited number of cases.

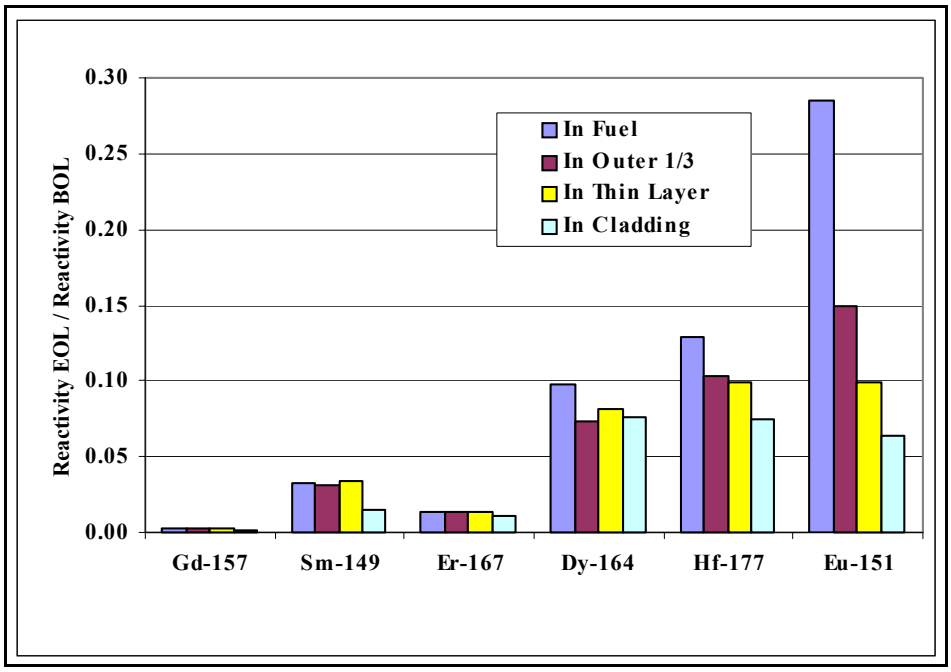

Figure 26. Ratio of negative reactivity due to burnable poison (BP) at the end of fuel life to that at the beginning of fuel life for various configurations of the BP.

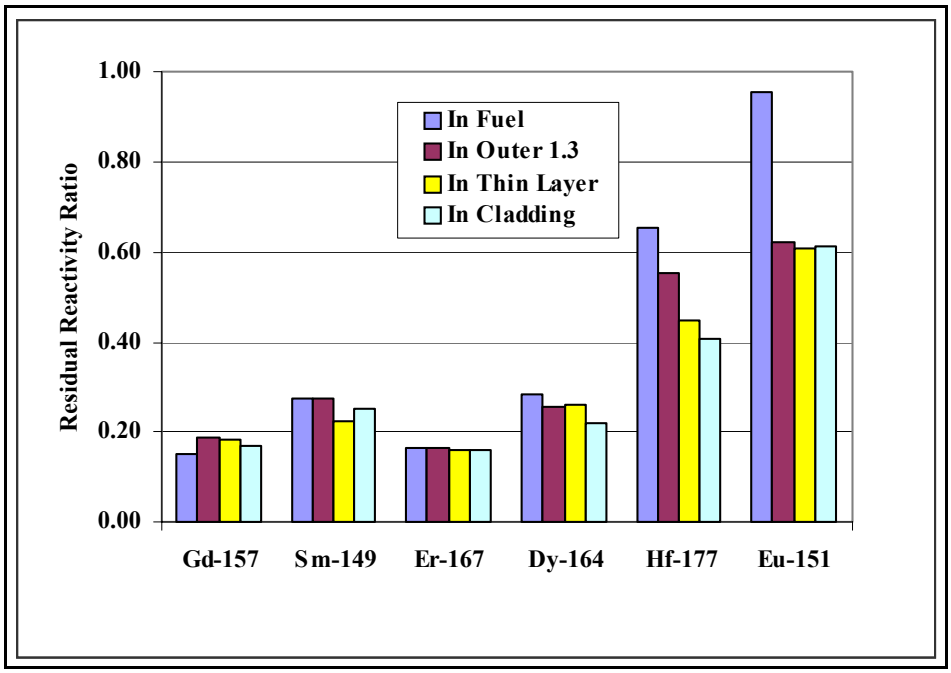

Figure 27. Isotope separation benefit shown by the compound ratio of negative reactivity due to the burnable poison (BP) at end of life to that at beginning of life for a single isotope to a similar ratio for the corresponding natural element.

TIME DEPENDENCE

Residual reactivity is not the only parameter that must be considered in selecting a burnable poison. Another important consideration is the time dependence of burnup. The residual reactivity ratio can be minimized by choosing very high absorbers, but if the BP burns too fast, it will be useless. The rate of burnup is considered by displaying the ratio of the negative reactivity worth of the BP at each of three time intervals of interest to the reactivity worth of the BP at BOL. The times chosen were 120 days, 1 year, and 4 years.

The results are tabulated as a percentage of BOL reactivity worth in Tables 49 through 52 and are plotted in Figures 28 through 35. From Figure 28, showing the time dependence of burnup of burnable poisons mixed in the fuel, it can be seen that, except for Gd and Sm, which burn rather rapidly, the time dependence is uniform, but the burnup is incomplete with the exception of Gd, Sm, and Er. From Figure 29, for separated isotopes, it can be seen that the ^{157}Gd as well as ^{149}Sm burn too rapidly. However, at the end of 4 years, the burnup is greater than 90% for ^{157}Gd, ^{149}Sm, ^{167}Er, and ^{164}Dy, and almost 90% for ^{177}Hf.

For the case of mixing the BP in the outer one-third of the fuel, Figures 30 and 31 show that both natural Gd and ^{157}Gd as well as ^{149}Sm burn too rapidly. However, ^{167}Er and ^{164}Dy now become uniformly burning poisons with over 90% burnup at the end of 4 years. Figures 32 and 33 illustrate

the case of a coating on the fuel pellets. Here it is apparent that Gd and Sm burn too fast to be useful. However, ^{167}Er with 96% burnup at the end of 4 years becomes very promising, and ^{164}Dy, ^{177}Hf, and ^{151}Eu all become candidates. For the case of BP in the cladding, separation of isotopes becomes more advantageous. As shown in Figures 34 and 35, the burnup at 4 years is improved for most candidate isotopes. For ^{157}Gd and ^{149}Sm, the burnup rates are clearly too high, but natural Eu, ^{167}Er, ^{164}Dy, ^{177}Hf, ^{151}Eu, and ^{184}Os all become good candidates on the basis of burnup. However, cost and availability are also major factors and will almost certainly eliminate Os and possibly Eu.

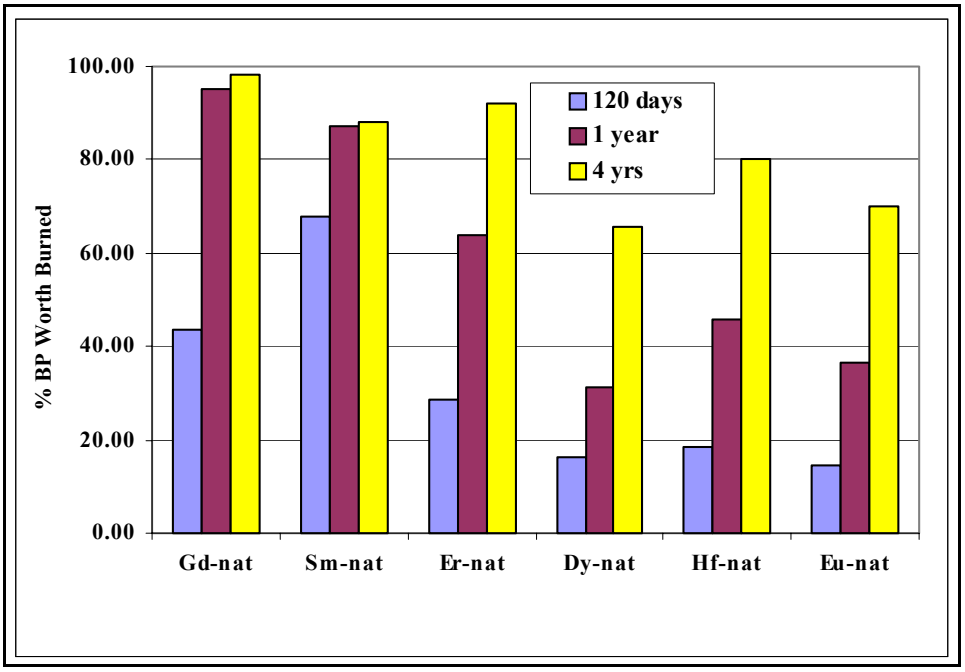

Figure 28. Burn rate for naturally occurring element burnable poisons homogeneously mixed in the fuel as oxides shown as a percentage of the initial negative reactivity remaining at a given time.

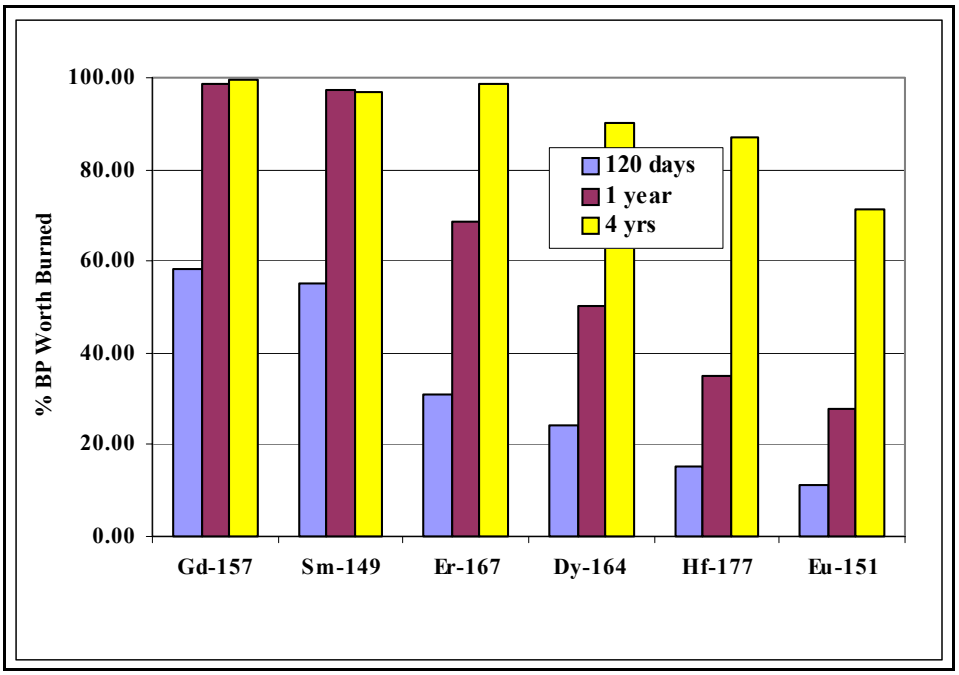

Figure 29. Burn rate for single burnable poisons homogeneously mixed in the fuel as oxides shown as a percentage of the initial negative reactivity remaining at a given time.

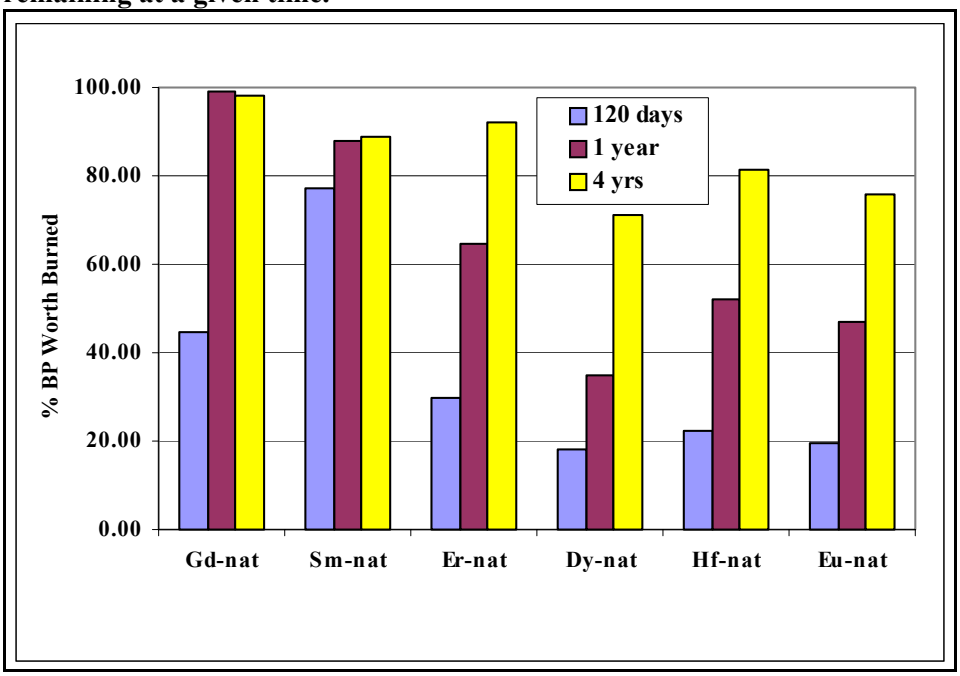

Figure 30. Burn rate for naturally occurring element burnable poisons homogeneously mixed into the outer one-third of the fuel pellets shown as a percentage of the initial negative reactivity remaining at a given time.

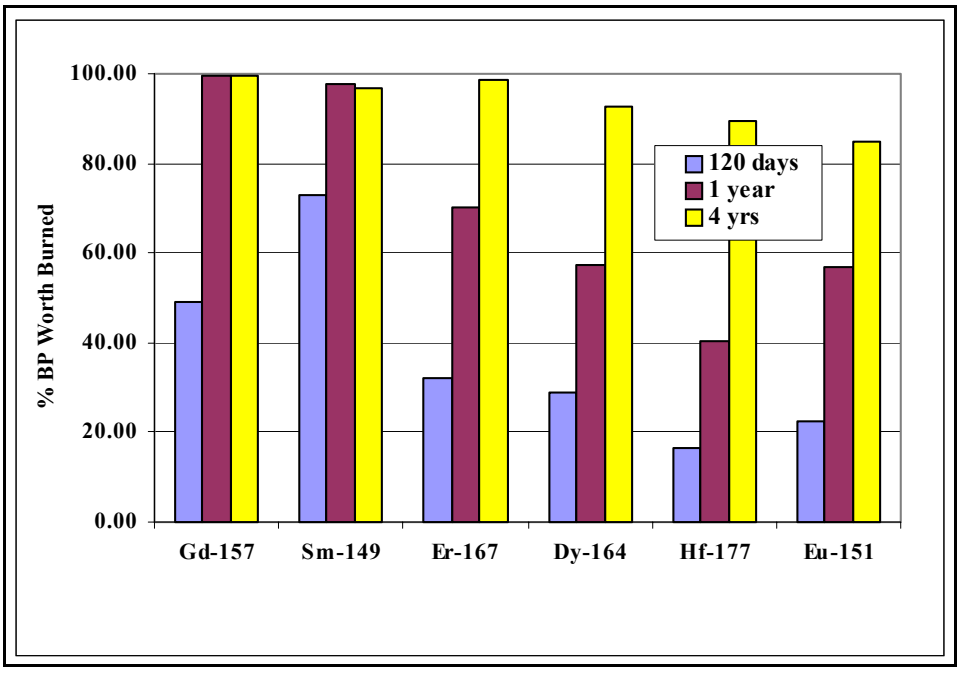

Figure 31. Burn rate for single burnable poisons homogeneously mixed into the outer one-third of the fuel pellets shown as a percentage of the initial negative reactivity remaining at a given time.

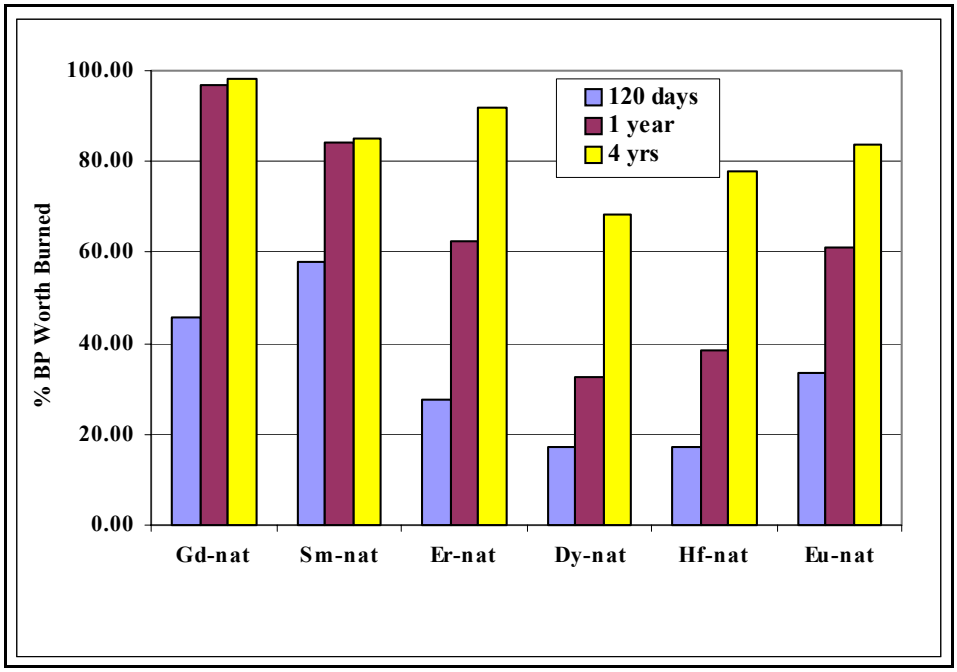

Figure 32. Burn rate for naturally occurring element burnable poisons coated on the outer surface of the fuel pellets as oxides, shown as a percentage of the initial negative reactivity remaining at a given time.

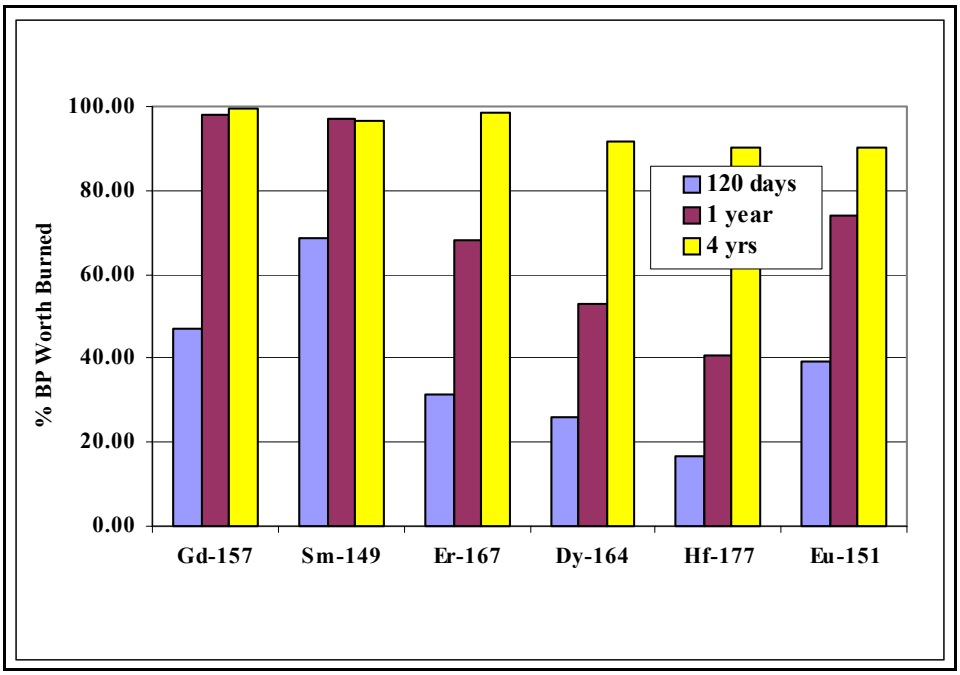

Figure 33. Burn rate for single burnable poisons coated on the outer surface of the fuel pellets as oxides, shown as a percentage of the initial negative reactivity remaining at a given time.

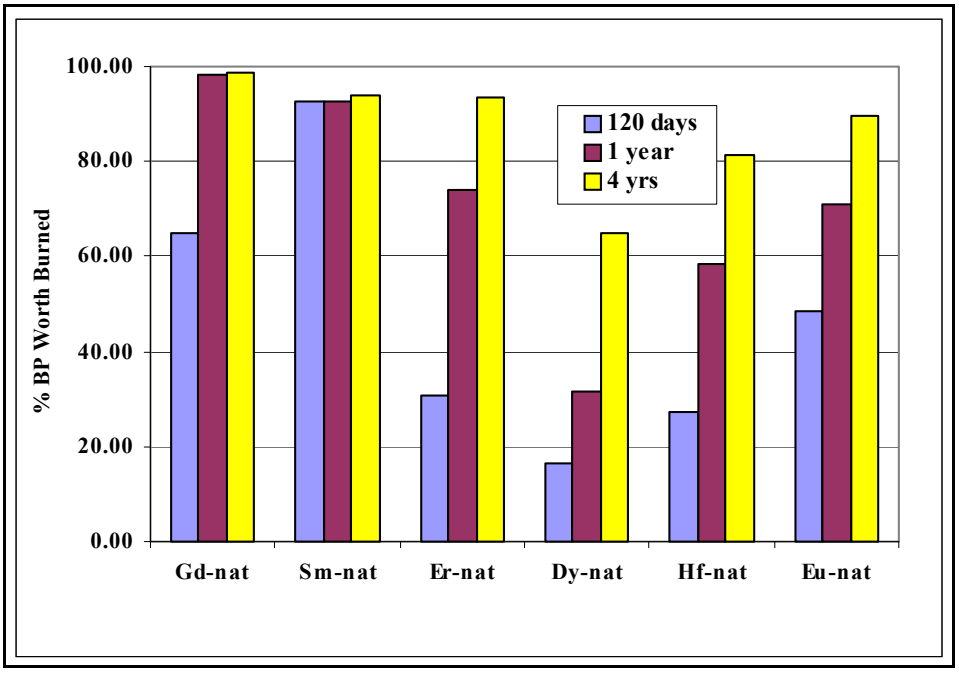

Figure 34. Burn rate for naturally occurring element burnable poisons in the form of a metal alloyed in the Zircaloy cladding, shown as a percentage of the initial negative reactivity remaining at a given time.

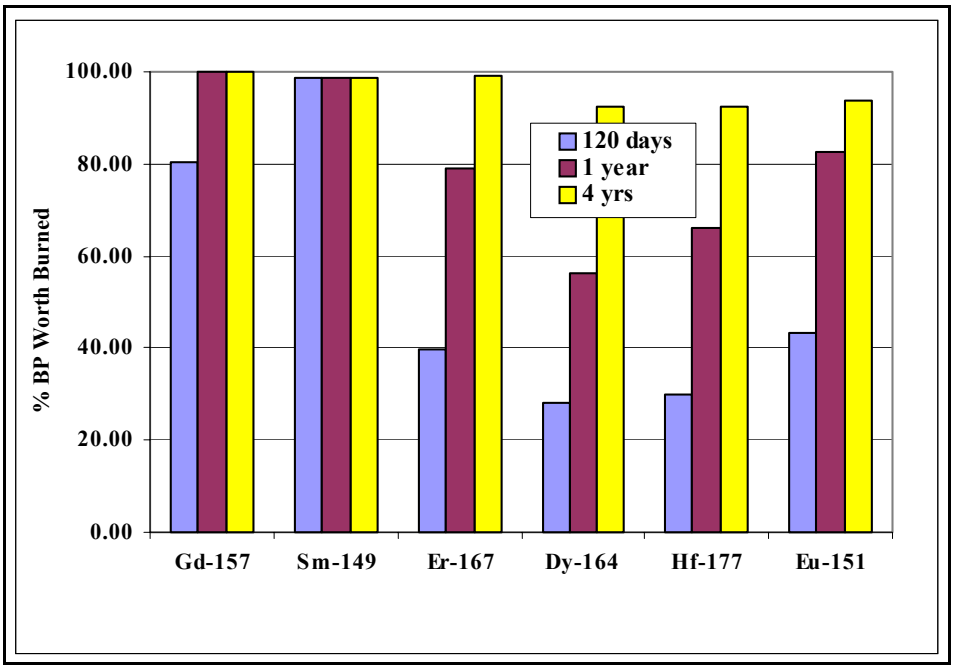

Figure 35. Burn rate for single burnable poisons in the form of a metal alloyed in the Zircaloy cladding, shown as a percentage of the initial negative reactivity remaining at a given time.

RESIDUAL REACTIVITY PENALTY

A useful method to evaluate the isotope separation advantage is to plot the initial negative reactivity as a function of the number of days lost due to residual BP at the end of 4 years, which we shall call the residual absorber penalty (RAP). These parameters are plotted both for the naturally occurring elements and separated isotopes. The difference in the RAP in FPDs between the natural element and the single isotope is the bonus for using separated isotopes. The initial negative reactivity as a function of the RAP (all configurations of the BP), has been previously plotted in Figures 10, 13, and 17 for the case of 16 rods and in Figures 11, 14, 18, and 21 for the case of 64 rods. Table 53 summarizes the results. The RAP for the naturally occurring element is given for the cases of 16 and 64 fuel rods as well as the savings achieved by using the specified separated isotope. It can be seen that using ^{157}Gd in 16 rods results in a savings of 6.3 FPD, leaving only one day RAP. The isotope ^{167}Er results in a savings of 32 days for 16 fuel rods, but a RAP of 33 days remains. On the basis of RAP alone, Gd is the most beneficial isotope, but there are other considerations, as discussed previously. In order to achieve a uniform burnout over several years, lower absorbing isotopes must be used, either alone or in conjunction with Gd. However, in all cases, separation of isotopes results in a significant savings, considering that the revenue from a 1000-MW plant is about $1 million per day.

Table 53. Savings in full-power days achieved by the use of single isotopes over the same naturally occurring elements for 10% initial negative reactivity

Isotope	RAP (natural) 16 rods	Savings 16 rods	RAP (natural) 64 rods	Savings 64 rods
^{157}Gd	7	6.3	1	1
^{149}Sm	50	41	10	10
^{167}Er	65	32	30	28
^{164}Dy	200	64	160	110
^{177}Hf	~100	20		
^{151}Eu			45	30

An interesting phenomenon is that the curves are similar for each configuration of the BP. The initial reactivity is strongly dependent upon where the BP is placed, but for a given initial negative reactivity, the penalty at 4 years is the same. This is not the case when the number of fuel rods containing BP is changed. When Sm is distributed in 64 fuel rods, the new set of curves shown in Figure 14 is obtained. The savings from isotope separation is nonetheless apparent.

The values given in Table 53 are theoretical. The actual values are smaller and will be discussed in the section on isotope separation.

METHOD OF ISOTOPE SEPARATION

Theragenics Corporation has recomissioned the Plasma Separation Process system originally developed for DOE by TRW and has successfully separated isotopes of molybdenum to a fairly high enrichment factor. Following this initial shakedown using molybdenum, the plant was ready to attempt gadolinium. Unfortunately due to the higher mass of gadolinium, the close spacing (1 AMU) of isotopes adjacent to ^{157}Gd, and the low thermal conductivity of gadolinum, the ^{157}Gd enrichment job has been quite difficult relative to molybdenum and other isotopes previously separated by TRW. Nevertheless, an output assay of 32% (enrichment factor $\beta 1=2.2$) for ^{157}Gd was demonstrated with a throughput of 5.9 kg/year effective production rate. Modeling results performed by Theragenics and similar modeling by TRW were more optimistic, predicting up to 50% output assay at a throughput greater than 15 kg/yr. With experience and improvement in the techniques, it is anticipated that enriching ^{157}Gd and similar isotopes can be improved significantly in the future.

Figure 36 The plasma separation device at the Theragenics plant showing the vacuum chamber, associated pumps, and auxiliary equipment.

Figure 36 shows the PSP facility at Theragenics. Figure 37 describes the basic operating principle of the PSP. The PSP appears to have unique capabilities for handling rare earth elements among the available isotope separation technologies available today. PSP can handle elements in metal form without the need for a stable gas phase required by gas centrifuges and has a relatively high throughput compared to calutrons. Rare earth elements are apparently difficult to convert into gaseous phases for gas centrifuge or gaseous diffusion separation methods. Previous attempts by groups using laser separation processes have reportedly been unsuccessful at handling gadolinium and other rare earths due to a lack of mass dependent photoionization spectral lines.

PSP OPERATING PRINCIPLES

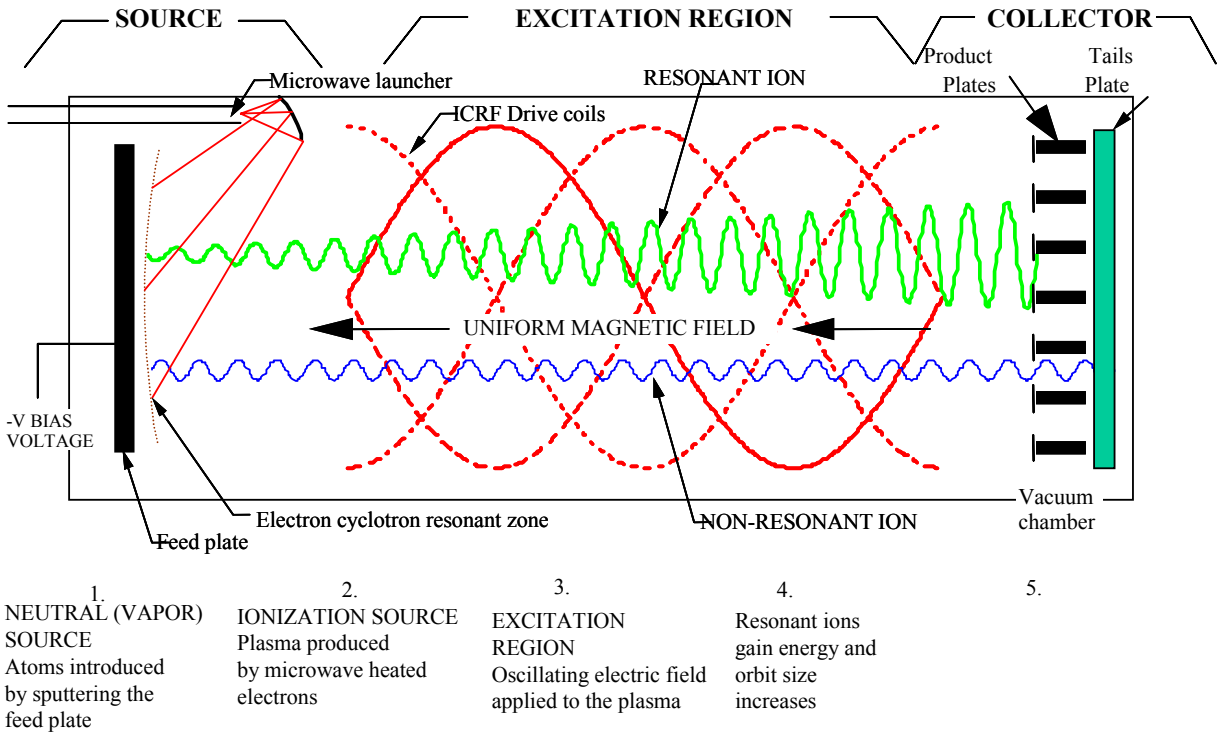

Figure 37 Schematic diagram of the plasma separation process to demonstrate operating principles.

TARGET FABRICATION

Three targets were fabricated for the PSP separation of the following elements: gadolinium, dysprosium, and erbium. The gadolinium target was the first to be made. Pieces of gadolinium metal were melted in a tantalum crucible and cast into an ingot approximately 5 inches in diameter by 8 inches long (12.7 cm diameter x 20 cm long) by Ames Laboratory. Since rare earth metals are pyrophoric, it was decided not to use conventional machining in order to avoid the danger of igniting chips. Electro-discharge machining was used to slice the ingot into plates 3.18 mm thick to form a mosaic structure 23 x 24 inches (58.4 x 70.0 cm). The seams were then welded to form a single plate.

The welding was done in a argon atmosphere using tungsten inert gas welding with the electrode negative using a 2.4 mm thoriated tungsten electrode. Scrap plates were cut to make filler wire for the welding process. The welded plate is shown in Figure 38. Cracking is visible in Figure 39, but each individual platelet is held in place by at least two and most often four sides, resulting in a plate with structural integrity.

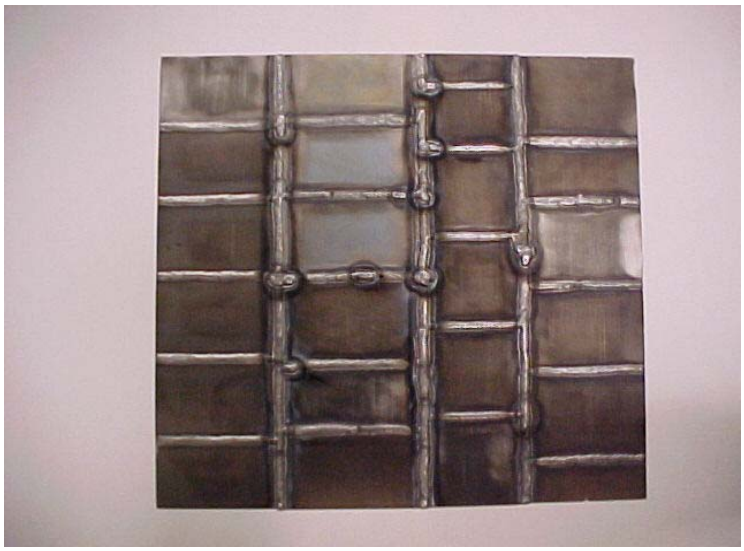

Figure 38 Gadolinium plate fabricated by welding together 3.18 mm thick slabs. The weld bead facing the plasma does not harm the process. The back side, which attaches to the cooling coils is very flat.

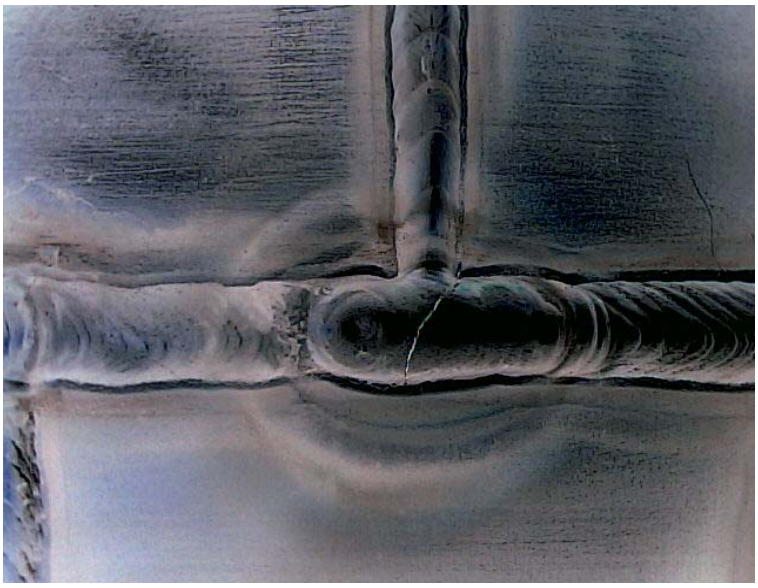

Figure 39 Welded gadolinium plate showing weld cracking.

The dysprosium target was also made from a cast ingot and again sliced into 3.18 mm thick plates to form a plate 58.4 x 70 cm. However, considering the difficulty in welding gadolinium, another approach was tried. The platelets were beveled at the edges in order to block line-of-sight passage of ions through the target. The platelets were then soldered individually to form a single target plate. The advantage is apparent, but achieving a flat target plate with good adheasion to the backing plate proved difficult. The soldering was performed by pre-tinning surfaces and clamping the assembly in a specially designed press which was heated by propane burners. The soldered Dy plate assembly is shown in Figure 40 (which was taken after completing the dysprosium campaign as can be confirmed by the visible burn-through regions). To ensure adequate cooling, voids in the solder must be minimized to limit the path length between the heat flux on the plasma facing side and the cooling water. Dysprosium has a rather low thermal conductivity of 10.8 W/m-°K. As with the Gd target, an IR camera system was used to check the integrity of the solder layer by alternately passing hot and cold water through the cooling lines.

A number of "hot spots" were located using the IR camera upon initial inspection. Several occurred near corners in the plates which were slightly warped away from the backing plate. These were patched where possible by heating with a torch and feeding in additional solder and then reheating the entire assembly in the press. After several attempts an adequate cooling uniformity was achieved based on IR camera measurements. The Dy source plate assembly was installed on the PSP and operated for a short period of time at a low source current. Several trouble spots quickly became apparent including some of the smaller

Dy tiles around the edge which became slightly detached. These sections were removed and recoated with copper and resoldered. Silver paint filler was added to a few other spots.

Eventually, adequate cooling was achieved across the entire plate with the exception of a few hot spots around the edge. Operation of the PSP was possible; however, there were frequent source arcs throughout the entire Dy campaign. Solder that leaked between the tiles is believed to be one cause of the frequent arcing. This solder gradually disintegrated over the course of the run. There was an edge tile that became slightly detached during the campaign and sharp corners and gaps around the loose section may have also contributed to the arcing.

Figure 40 Dysprosium target assembly after completion of the production campaign. Note the absence of weld bead and some edge separation of the tiles.

The dysprosium target plate was operated a total of ~ 630 amp-hours at a typical current of 15 amps (approximately 42 hours run time). Upon removal, there were several burn through spots in the plate where the copper backing plate was visible.

The erbium target was fabricated from rolled plate, having located a source of rolled rare earth plates. Although a plate the size of the target could not be obtained, four quarter size plates were purchased. Considering the difficulties with the soldered tiles of the Dy plate, it was decided to again attempt welding the plates. An inert gas welding glove box with a high capacity purification system was procured and dedicated to welding rare earth plates. A dedicated facility was necessary because what appeared to be an oxide of gadolinium was deposited over surfaces inside the welding glove box during the Gd target fabrication, necessitating an extensive cleaning operation, perhaps with

Figure 41 Inert gas welding glove box

some residual gadolinium contamination. The new rare earth welding glove box is shown in Figure 41. It is capable of moisture and oxygen levels below 1 ppm.

The erbium plates were welded using the method of tungsten inert gas welding with a 2.4 mm thoriated tungsten electrode made negative with respect to the erbium plate. A maximum of 200 amperes was used with a voltage of about 12 volts. Single pass welds were made using filler metal made from scrap erbium plate. Although the impurity levels in the box quickly rose to over 20 ppm, they decreased to below 5 ppm as welding progressed. It was found that the weld cracked when the torch was removed in the middle of a plate. The cracks were then rewelded and the torch not removed until the edge of the plate was reached. This resulted in a plate with no cracks visible to the naked eye. The weld bead on the back surface was removed by grinding and the plate prepared for the next stage. The plate was then thermal sprayed with copper in preparation for soldering.

Since this plate was a single full-size unit, it was possible to directly attach heat exchanger cooling lines without the need for a copper backing plate. The weld beads on the plasma side were ground flat to facilitate water line attachment. To ensure that adequate cooling existed in the gaps between the water lines, additional copper was plasma sprayed on the erbium plate to a thickness of ~ 0.1". The additional copper backing application caused the plate to warp slightly but not enough to affect installation or operation on the PSP. The soldering was performed by applying a layer of paste solder and clamping the assembly in a specially designed press which is heated by propane burners. The soldered erbium plate assembly is shown in figure 42. To protect the exposed water line ends, two copper shields were soldered to them since the width of the erbium plate was not quite their full width. Sharp corners at the edge of the erbium plate were smoothed down to reduce the likelihood of arcing.

An infrared camera survey of the erbium plate assembly indicated that the waterline attachment was very good with no significant non-uniformity in the cooling. There is non-uniformity in the infrared surface emissivity of the rough, slightly oxidized metal surface which makes interpretation of the IR camera image more difficult. Observation of the uniformity of the change in apparent temperature as the cooling (or heating) water is turned on is the most meaningful technique.

Figure 42 Erbium target assembly after attaching the coolant lines.

The erbium plate was installed on the PSP and operated for about 1 hour and then inspected. There was no sign of hot spots. The erbium plate was operated a total of ~ 330 amp-hours at a typical current of 10-12 amps (approximately 30 hours run time). Upon removal, there were no burn through spots in the plate where the copper backing plate was visible. There are clear indications of cracks in the erbium plates at various locations and also variations in the grain structure in some regions which were produced during the manufacturing process. The welds show no sign of failure. A triangular patch apparently replaced by the manufacutrer (visible in figure 42) became more pronounced since its grain structure does not match that of the surrouding area. This plate operated very smoothly with very little source arcing as experienced with the multi-tile dysprosium plate.

During exposure to the plasma, the target must be actively cooled to prevent melting. The source plate must be attached to a water cooling heat exchanger. During typical PSP operation, the heat flux on the source plate is 60 W/cm^2. Many metals have no difficulty handling this heat flux provided cooling lines are attached with soft solder and any voids in the solder interface are 3-4 cm diameter or less. Due to the low thermal conductivity of gadolinium and other rare earth metals, the acceptable void diameter is much less- probably 1 cm diameter depending upon the thickness.

Copper was plasma sprayed onto the back of the target plates by commercial suppliers to simplify soldering. The single plate unit can have the waterlines directly attached whereas the multiple section plates, such as the Dy plates, need a thin copper backing plate for support. A single plate assembly with waterlines attached directly has been found to be the most reliable. However, gaps between water lines are a concern just like voids in the solder. Warpage in a thin single plate makes reliable attachment more difficult. The multiple plate units must be attached to an intermediate backing plate to provide support, which requires two solder joints to be reliable. However the copper backing plate does a better job spreading out the heat flux.

To qualify the source plate and cooling line assembly for installation in the PSP, two techniques have been used. An ultrasonic probing technique was studied and found to be quite sensitive for locating voids in the solder. However, the ultrasonic probe requires good contact with the source plate and must be manually scanned across the entire plate. Interpreting the signals is somewhat difficult, especially with the complicated shape of the cooling lines on the backside of the plate. An infrared camera technique was found to provide fairly meaningful two-dimensional images of the cooling uniformity and therefore can indicate locations of voids in the solder when used with changing water temperature. The IR camera method has the potential for viewing the entire source plate simultaneously and can provide quick feedback. Unfortunately, the surface emissivity of the source plate material strongly affects the apparent surface temperature. Variations in surface roughness and the presence of surface oxide or soldering flux residue make interpretation of the images difficult. An image processing method that subtracts off the baseline temperature and shows only changes in temperature as cold or warm water is flowed through the cooling lines drastically simplifies interpretation.

A number of attempts were made before successfully attaching a gadolinium source plate that could handle the heat flux without overheating and melting at any location. The Gd plate, formed from several smaller 1/8" thick plates welded together was placed in the soldering fixture, using small aluminum filler plates to compensate for a slight curvature resulting from the welding and thermal spray processes. It was then soldered directly to the water lines. This plate, as with a preliminary test plate, did not last very long, apparently due to the water lines detaching in a few places. This was believed to be due to the difficulty in getting a good fit between the water lines and the warped plate. The melting damage to the target plate is shown in Figure 43. Later a rigid clamping fixture was utilized which solved this difficulty. Another attempt was with two 6.4 mm half plates which were soldered to a backing plate. The IR camera system was

Figure 43 Gadolinium target showing damage caused by melting. The hole is approximately 4cm across.

available to test this assembly before it was used, and several hot spots were located. A filling method using silver paint was used to patch the known voids through small holes drilled between water lines from the backside. This plate was run in the PSP a short while, and evidence for hot spots was still visible but much smaller than in previous attempts. A few more attempts and improved soldering were made before finally getting an acceptable solder job combined with a few patches to fill in smaller voids. The use of lead/tin solder proved to be much better at minimizing the void areas than the previously used lead-free solder, which was used because of its lower vapor pressure and thus better vacuum compatibility. A typical infrared scan is shown in Figure 44.

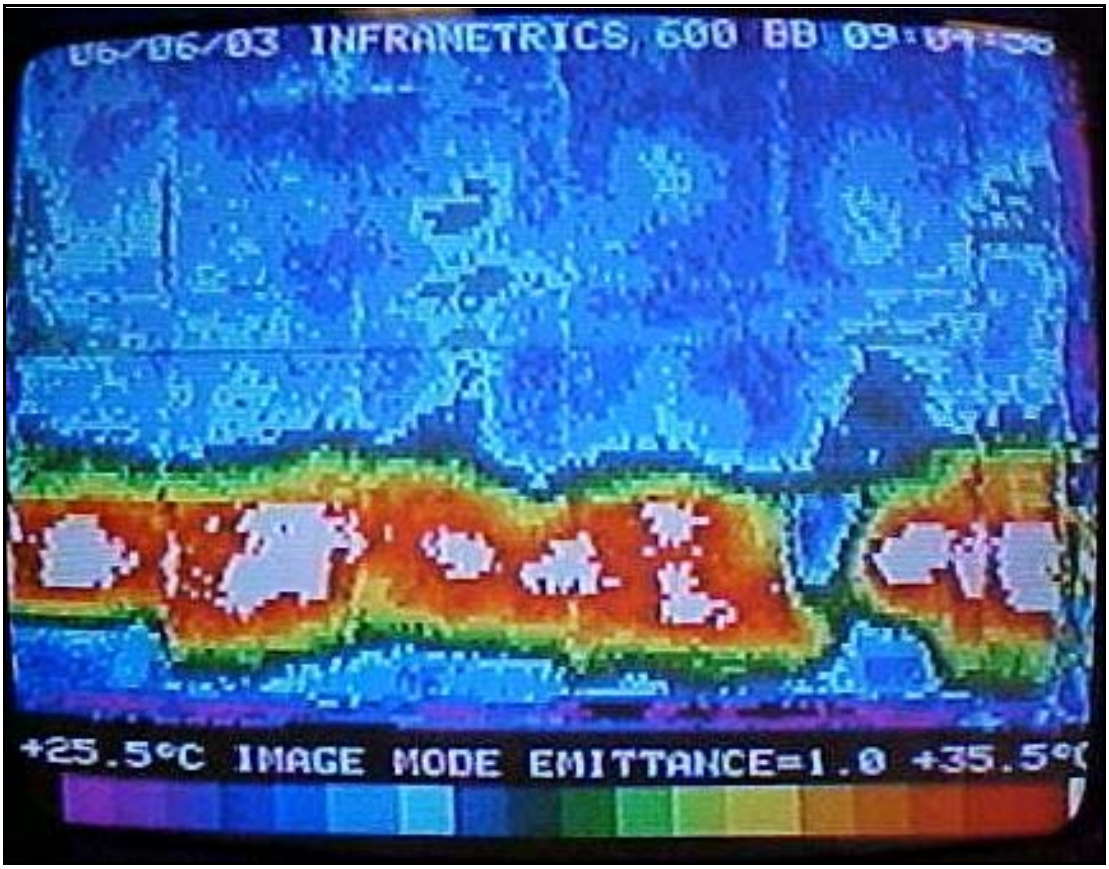

Figure 44 A typical infrared image of the erbium plate with hot water flowing in one sector of the cooling lines. A cold spot is visible toward the left, indicating a void in the solder in that region.

MODELING OF PLASMA SEPARATION

Modeling enrichment capabilities of the PSP facility at Theragenics (1.8 T magnetic field) and a future 6 T magnetic field device have been performed and are summarized in this section. The models which have been developed have been fairly accurate at predicting output assay and throughput for some isotopes, especially those of lower mass and with greater mass separation. For the purpose of illustration, ^{157}Gd will be used as an example. The modeling process begins by analyzing the ion cyclotron excitation process of the uniform low-temperature plasma incident from the source end. Electromagnetic waves generated by the antenna structure are analyzed inside the plasma using a numerical technique. A set of test particles of each isotope is then launched and tracked along the plasma and its net energy gain evaluated at the collector entrance. Usually a scan of the ion perpendicular temperature vs. magnetic field is plotted for each isotope, as shown in Figures 45 and 46 for two cases of plasma density corresponding to very low source current and to a medium source current. An exact relationship between source current and plasma density requires more complicated modeling or actual measurements. The important features visible in Figures 45 and 46 are the ratios of the ^{157}Gd ion temperature to that of its neighbors. This ratio directly translates to the product assay recovered in the collector. The low-density conditions in Figure 45 show fairly sharp resonance lines and a ^{157}Gd to ^{158}Gd (or ^{156}Gd) ratio >10:1. The peak height can be adjusted somewhat arbitrarily by changing the RF drive level applied. As the density increases, the rate of collisions between particles in the plasma increases, which spoils the resonance and rapidly decreases the temperature ratio (Figure 46 shows ~ 4:1). This depicts the fundamental trade-off between high enrichment and high throughput in the PSP device and

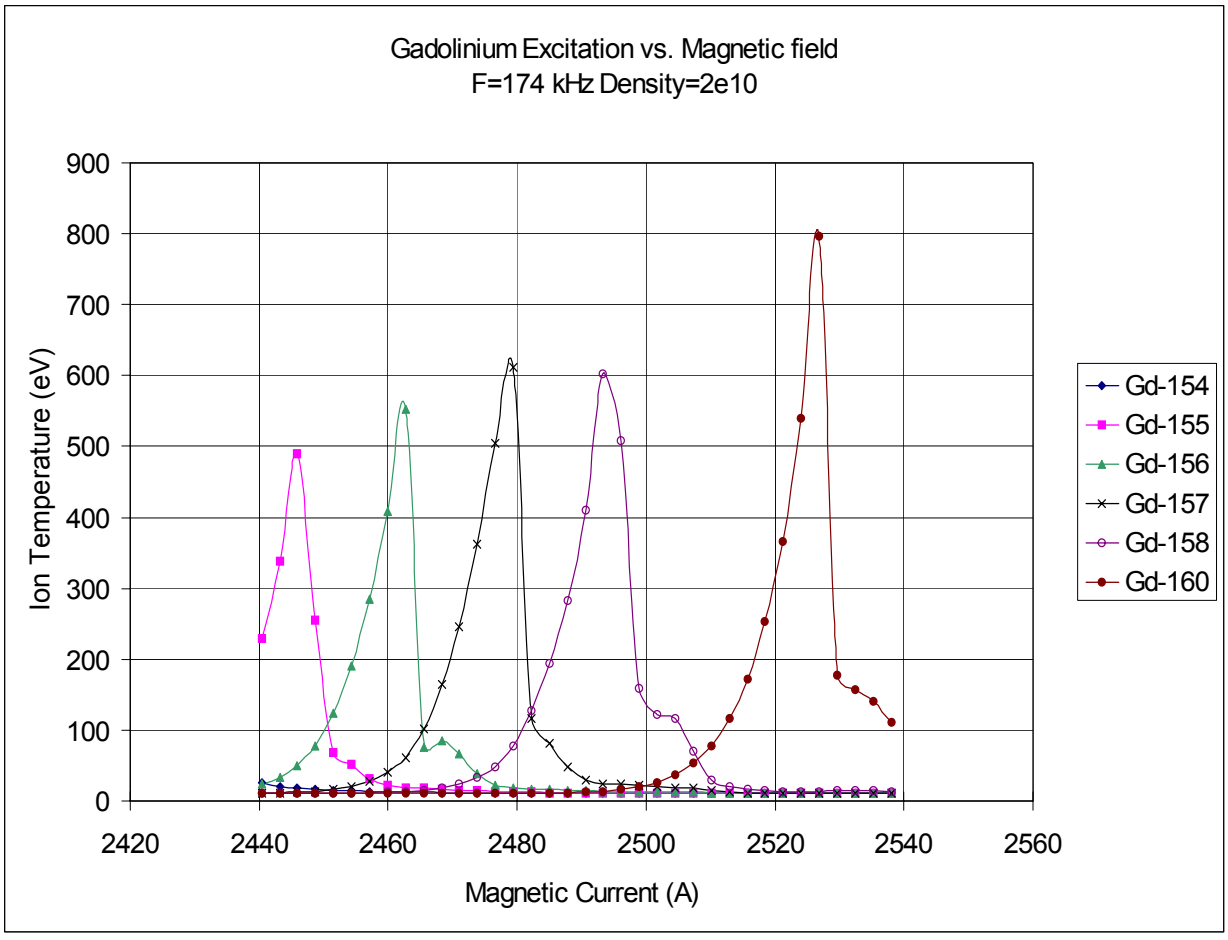

Figure 45 Predicted gadolinium ion excitation at low density

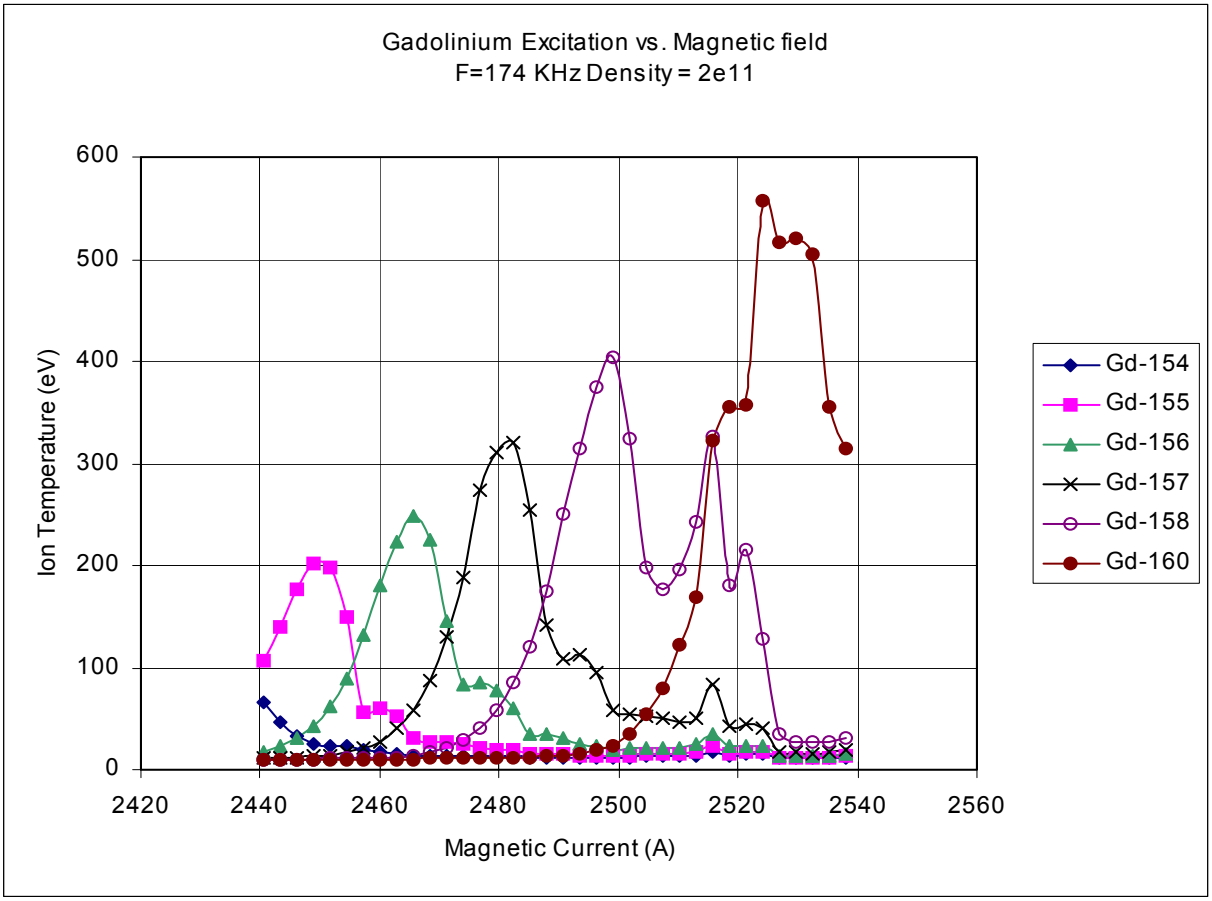

Figure 46 Predicted gadolinium ion excitation at medium density

is also the situation for most other isotope separation technologies.

Other factors which can be varied to optimize either throughput or product assay are the collector bias and fence width. Details of the collector structure are depicted in Figure 47. The highest assay product is on the leading edge of the collector blades in the shadow region behind the fences. Material further back on the collectors has lower assay due to depletion of the higher energy particles and more sputtering of low enriched material from the fence edges and tails plate regions. There are several other factors affecting the actual throughput and assay levels obtained. Many are accounted for in the models. The dominant effect is driven by the plasma ion collision process which has several contributors. One is the "hard body" collision with a cross section that is highly dependent on the particular isotope and plasma temperature. Exact parameters for this effect for a particular isotope have not been incorporated in the model. In the case of small mass separation, these approximated factors are more likely to reduce the accuracy of the modeling. Actual diagnostic collector analysis of the performance is necessary for making the final determination of the process performance. The diagnostic collector (called HDC) used is a small version that can easily be inserted through a vacuum lock and retrieved without breaking the PSP vacuum. The full production collector requires an up-to-air event to change out a collector. The HDC has approximately 1/15 of the useful area of the full production collector. During HDC operation, the remaining material that

misses the HDC is deposited on a tails plate. Numerous diagnostic collector runs were performed to optimize the ^{157}Gd assay. Modeling had predicted that an assay of 50% for ^{157}Gd might be possible on the 1.8 T PSP facility. It was determined that if a low density were used and a wide collector fence width with 150 V collector bias, it would be possible to approach this assay on the leading edge of the collector blades. An assay of 48% was achieved for one case, which is shown in Figure 48. The consequence of having to operate at reduced source current, use wide collector fences and operate at high bias voltages to achieve the reasonably high assay has resulted in relatively lower product throughput than is possible for other isotopes of lower mass and wider mass separation.

The material collected on the graphite blades is essentially a thin metallic film that must be processed to convert it into a useful form. Two techniques have been used for harvesting

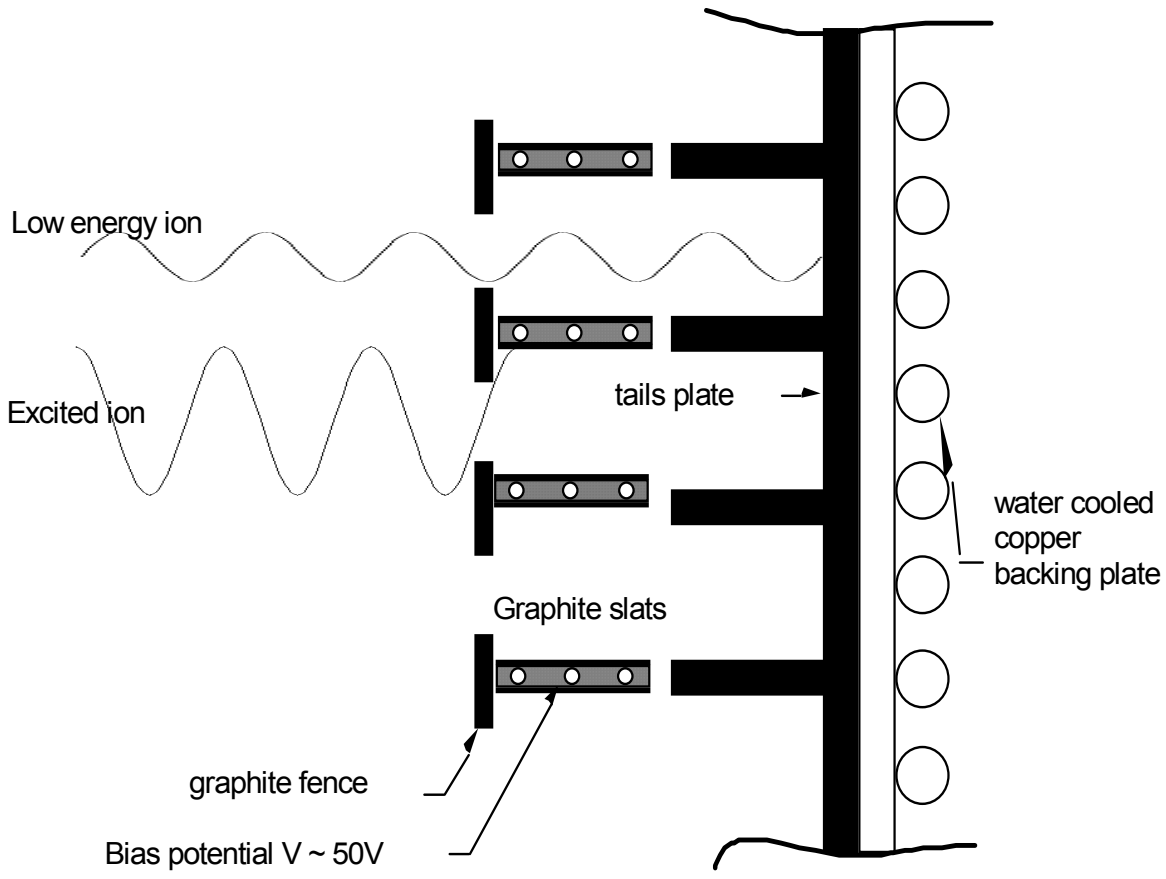

Figure 47 Schematic diagram of the cross section through a PSP collector

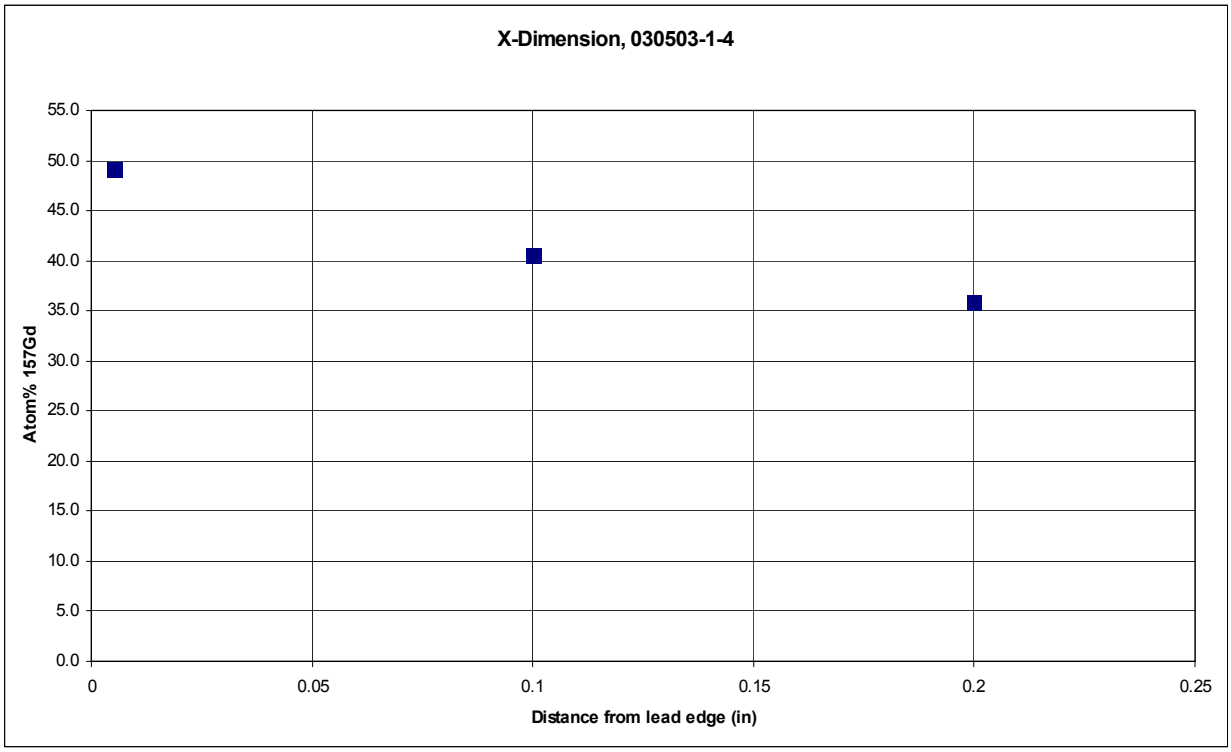

Figure 48 Point assay of ^{157}Gd as a function of distance from the leading edge of the collector.

gadolinium: acid dissolution and calcining in an oxidizing furnace. Both have similar collection efficiency and, depending upon the element, both have advantages. To produce sufficient product material, a greater portion of the collector must be harvested than the leading edge. A trade-off must be made between throughput or high assay in deciding where to section the collector blades. The processed material for a production run corresponding to the point data in Figure 48 is assayed in Figure 49. This material is from the first 0.5-cm of the collector blades (called U material) and corresponds to the region that all 3 data points of Figure 48 are taken from. A reduction in assay from the leading edge to essentially the location of the lowest value of the point data was observed. During a production campaign, approximately 26-33 hours of plasma time were required to collect 0.75 gram of 36% assay ^{157}Gd with the HDC, which translates to ~ 12 grams using the production collector or 0.3 g/h production rate. Harvesting other regions on the collector can result in a greater throughput. The second half-cm on the blades (referred to as "V" material) indicated a lower ^{157}Gd assay (typically 28%) and contained about 49% more ^{157}Gd than the U material alone, as summarized in Table 54 below. It should also be noted that the ^{155}Gd is ~ 5-8% of the output material assay, so the effectiveness of the output material as a burnable poison is slightly greater. Other portions of the collector blades have significant quantities of ^{157}Gd at slightly lower enrichment levels. These batch categories have traditionally been called X, Y and Z. The X and Y material are recovered from the edge regions of the collector blades and further back from the leading edge on the central blades. The enrichment factor for these batches is typically half that of the U+V category and the production rate total is typically comparable to the U+V rate.

Table 54 Production values for ^{157}Gd

Run #	"U" mass (metal)	"V" mass (metal)	Run time	(amp-hours)	Gd-157 U
H031003-1	0.754 g	0.504 g	26 hours	400 A-H	34.8%
H031703-1	0.767 g	0.529 g	33 hours	495 A-H	34.5%

- The ratio between U and V mass collected appears to be ~ 1.49 If U+V are combined, the resulting assay will be proportional
- The production rate using the production collector would be typically 0.4 g/hour U or 0.68 g/hour U+V
- Typical isotopic distribution comparison

		Gd-152	154	155	156	157	158	160
H031003-1	U	0.03	0.49	5.84	26.4	34.8	29.2	4.26
H031003-2	V	0.06	0.82	8.41	28.1	28.8	29.9	4.79

ESTIMATED COST FOR COMMERCIAL PRODUCTION OF ^{157}Gd

Pricing for production of enriched ^{157}Gd is highly dependent on the throughput and enrichment level required. Using the weighted average throughput of the processing of 1.3g per hour, throughput, based on total available hours in one year, is approximately 11.2kg of 28% assay ^{157}Gd. If only higher assay material (up to 36% ^{157}Gd) is desired, then the annual throughput would be less and cost per gram proportionally higher.

The following table presents the estimated pricing per gram, based on varying levels of utilization, and includes estimated cost of natural gadolinium source plates:

	Based on total product (2)		Based on isotope (3)	
Utilization (1)	Pricing range per gram	Annual capacity (kg)	Pricing range per gram	Annual capacity (kg)
100%	$600-$1,000	11.0-11.4	$2,100-$3,500	3.1-3.2
75%	$800-$1,300	8.1- 8.5	$2,800-$4,600	2.3-2.4
50%	$1,200-$2,000	5.2- 5.6	$4,300-$7,100	1.5-1.6

This cost estimate is intended for scientific feasibility studies only. An actual price depends upon many factors which are functions of time.

(1) Actual production hours divided by total available hours. 24 hours per day considered total available hours. 100% utilization is theoretical maximum (24 hours per day, 7 days per week, 365 days).

(2) Gadolinium enriched to 28% of ^{157}Gd. (i.e. 28% of total product is ^{157}Gd).

(3) ^{157}Gd only. This is a function of enrichment multiplied by the total product.

SEPARATION OF DYSPROSIUM-164

The separation of ^{157}Gd was used as an illustration of the PSP process. For the other isotopes, the results and peculiarities will be discussed. Based on a ^{164}Dy production run, it has been determined that an annual production rate of 2.2 - 4 kg/year at an assay of 61-67% can be achieved on the existing PSP facility at Theragenics™. The production rate and output assay depend on system availability and blending of lower and higher assay collected material. The price range for enriching ^{164}Dy is in the range of $1000-$3200/gram depending on availability and assay. On a future 6 Tesla

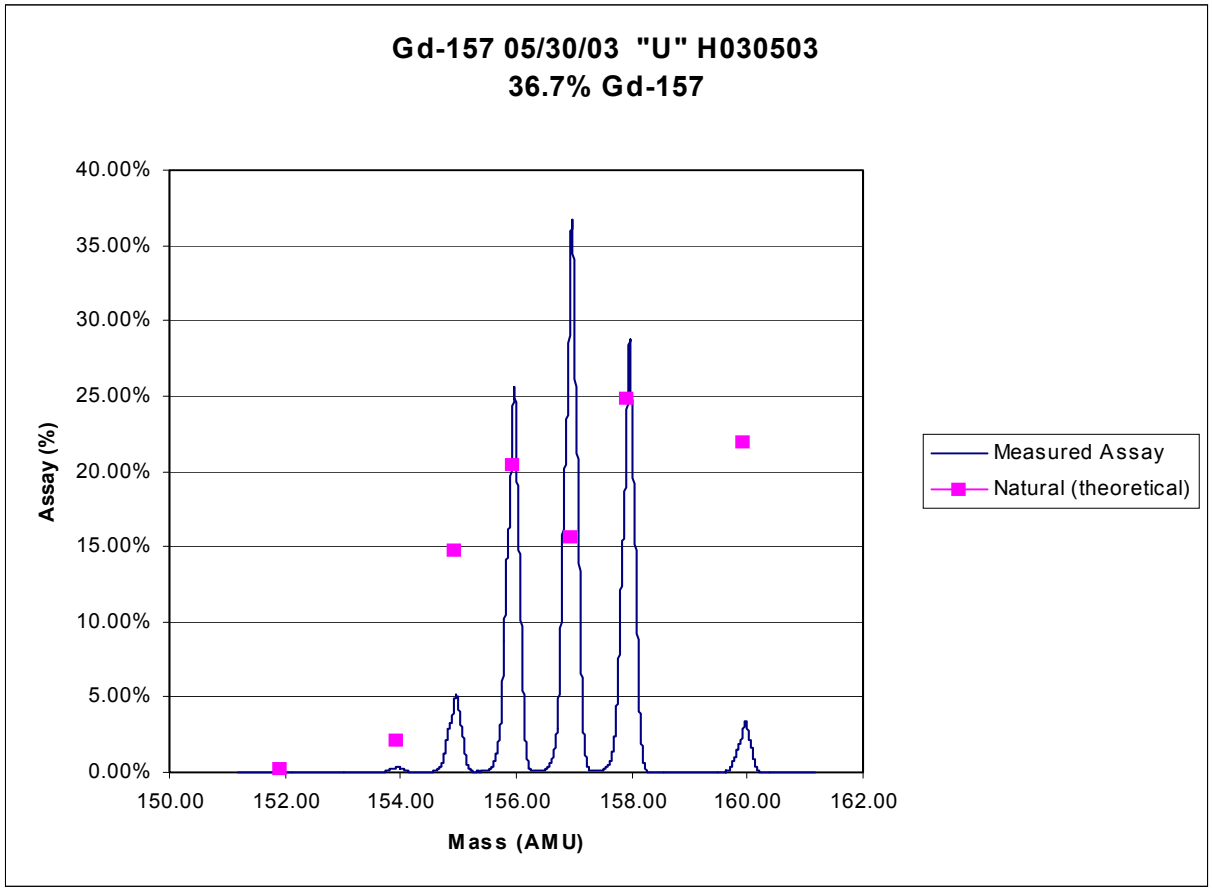

Figure 49 Plot of relative concentration of the isotopes of an enrichment sample from a ^{157}Gd run.

PSP device, an annual ^{164}Dy production rate of 125 kg/yr at an assay of 90% is likely to be feasible and the processing cost per gram would be significantly lower.

Several diagnostic collector runs of ~ 1 hour each were performed to optimize conditions for best ^{164}Dy enrichment. The magnetic field, RF drive level, neutral source current and other parameters were varied based on REA diagnostic signals and mass spectrometer analysis of the product. The best assay achieved is ~ 74% Dy-164 for 0.25 cm of the leading edge of the collector blade. The mass spectrometer analysis for this sample is shown in figure 50.

A production collector run was performed. The run lasted 20 hours at an average source current of ~ 14 A (280 A-H). The collector blades were harvested in the Theragenics™ chemistry lab and analyzed with the Theragenics™ ICP-MS mass spectrometer system. A few of the collector blades insulation shorted during the run so their bias voltage dropped to zero at that point. Batches were separated out to account for the various conditions.

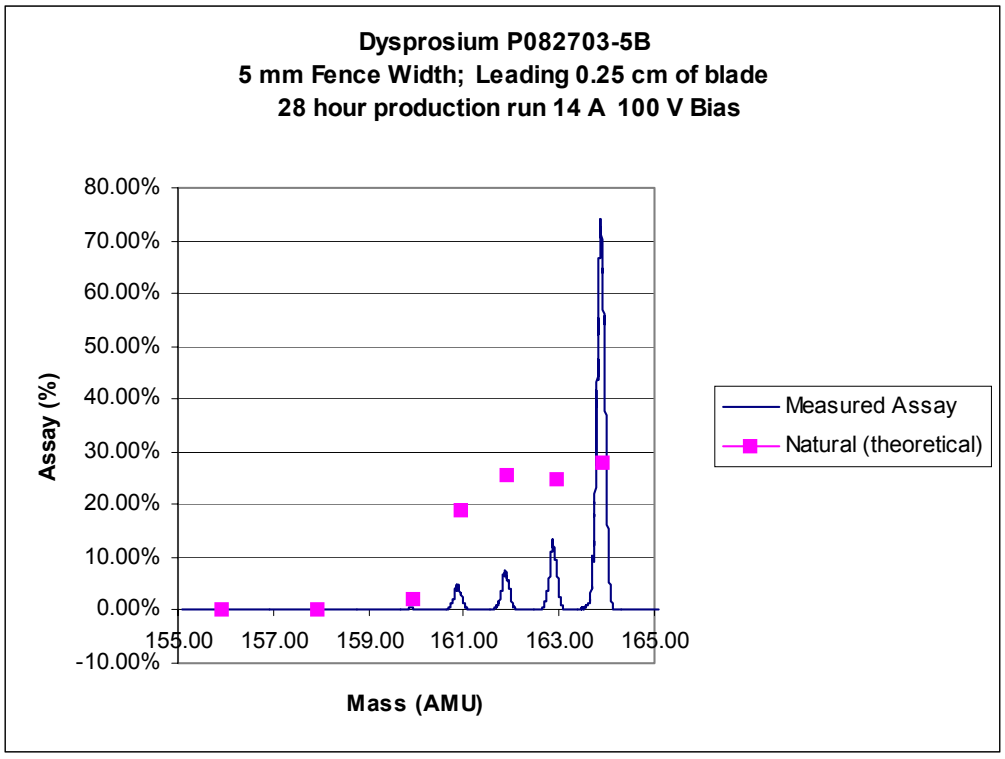

Figure 50 Relative concentrations of isotopes for a production run to separate ^{164}Dy

Production run data for ^{164}Dy:

Run conditions:
14 A Neutral source current
20 hours of operation (280 A-H)
100 V bias for 90% of the run
● Note: a few blades bias shorted toward the end of the run. They are the blades processed (data below). The un-shorted blade had ~ 2% higher assay.

● Note: only 6 blades out of 10 were processed in the main batch. The full production rate is 10/6 times higher for 20 hours.

Batches processed:

U1 6 blades (of 10); Leading 0.5 cm 2.62 g recovered
Assay = 67.1% ^{164}Dy
Other isotopes: 16.58% ^{163}Dy, 9.4% ^{162}Dy, 5.7% ^{161}Dy, 0.8% ^{160}Dy

V1 6 blades (of 10); Second 0.5 cm 2.38 g recovered
Assay = 64.1% ^{164}Dy

Y 4 blades, outer positions, first 1 cm leading edge 3.27 g recovered
Assay = 61.7 % ^{164}Dy

X 10 blades top and bottom 8 cm 1 cm leading edge 4.35 g recovered
Assay = 61.2% ^{164}Dy

Therefore, depending on the assay level desired, we get the following rates for annual production assuming 55% availability .

U 67.1% assay 0.210 g/hour 1011 g/year
V 64.1% assay 0.199 g/hour 958 g/year
X 61.2% assay 0.217 g/hour 1045 g/year
Y 61.7% assay 0.163 g/hour 785 g/year

If we combine them all, we get about 3.8 kg/year at an assay of ~ 63%

ESTIMATED COST FOR COMMERCIAL PRODUCTION OF ^{164}Dy

Pricing for production of enriched ^{164}Dy is highly dependent on the throughput and enrichment level required. Using the weighted average throughput of the processing of 0.8g per hour, the throughput based on total available hours in one year is approximately 6.75kg of 63% assay ^{164}Dy. The following table presents the estimated pricing per gram, based on varying levels of utilization and includes the estimated cost of natural dysprosium source plates:

	Based on total product (2)		Based on isotope (3)	
Utilization (1)	Pricing range per gram	Annual capacity (kg)	Pricing range per gram	Annual capacity (kg)
100%	$1,000-$1,600	6.5-7.0	$1,600-$2,500	4.1-4.4
75%	$1,200-$2,200	4.7-5.2	$1,900-$3,500	3.0-3.3
50%	$1,900-$3,300	3.0-3.5	$3,000-$5,200	1.9-2.2

As with ^{157}Gd, this is a cost estimate for scientific research, not a price quotation.

(1) Actual production hours divided by total available hours. 24 hours per day considered total available hours. 100% utilization is theoretical maximum (24 hours per day, 7 days per week, 365 days).

(2) Dysprosium enriched to 63% of ^{164}Dy. (i.e. – 63% of total product is ^{164}Dy).

(3) ^{164}Dy only. This is a function of enrichment multiplied by total product.

SEPARATION OF ERBIUM-167

Several diagnostic collector runs of ~ 1 hour each were performed to optimize conditions for best ^{167}Er enrichment and the results analyzed on a mass spectrometer. The magnetic field, RF drive level, neutral source current and other parameters were varied based on diagnostic signals and mass spectrometer analysis of the product. The best assay achieved is ~ 37.5% ^{167}Er for 0.25 cm of the leading edge of the HDC collector blade for this study. A lower source current (10A) than used during dysprosium operation was needed to give an acceptable ^{167}Er assay due to the difficulty of this isotope. The same conditions were used for a 19 hour production run where a slightly better assay was obtained. This is likely to be due to the slightly wider fence used for the production run.

A production collector run was performed which lasted 19 hours at an average source current of ~ 10 A (190 A-H). The collector blades were harvested in the Theragenics™ chemistry lab and analyzed with the Theragenics™ ICP-MS mass spectrometer system. Figure 51 shows the isotope distribution

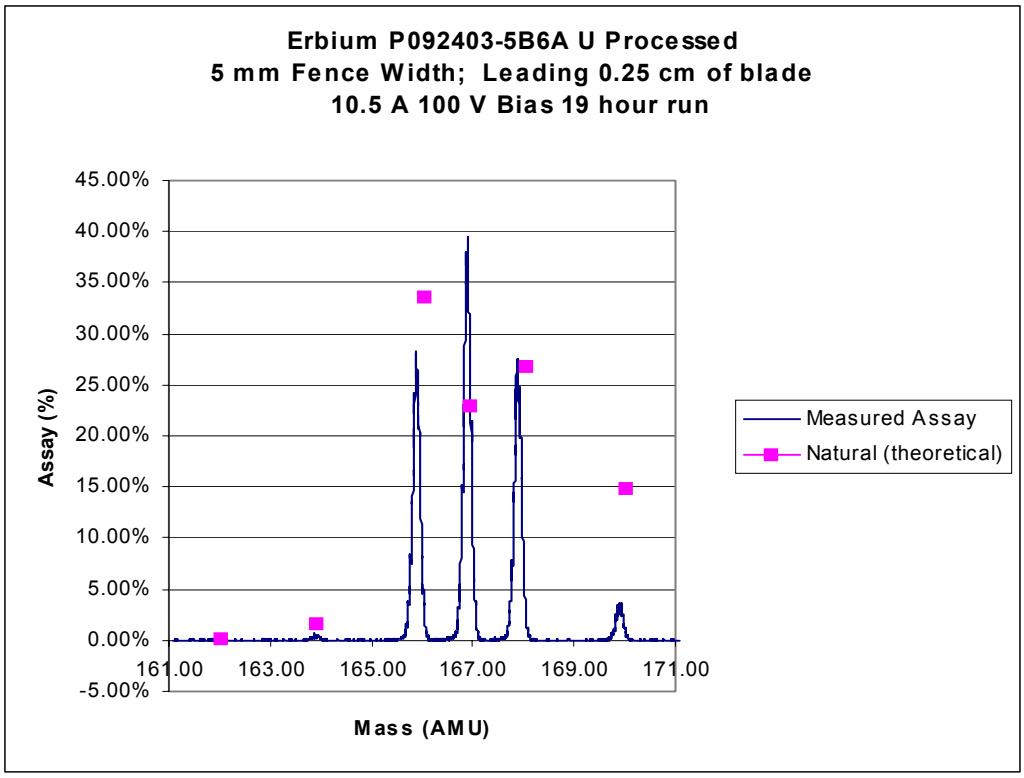

Figure 51 Isotope distribution achieved in a 19 hour production run to separate ^{167}Er.

achieved. A few of the collector blade's insulation shorted during the run so their bias voltage dropped to zero at that point. A view of the collector plates following the run is shown in Figure 52. Batches were separated out to account for the various conditions.

Production run data for Er-167

Run conditions:
10.5 A Neutral source current
~19 hours of operation (190 A-H)
100 V bias for 100% of the run

These batches were processed using acid dissolution of the metal film off the collector blades then filtered and dried:

U: 1.9 out of 10 blades; Leading 0.5 cm; 1.193 g recovered. Assay = 39.4 % ^{167}Er
Other isotopes: 0.06% ^{167}Er, 27.3% ^{166}Er, 26.8% ^{168}Er, 2.58% ^{170}Er

V: 1.9 out of 10 blades; Second 0.5 cm; 1.017 g recovered. Assay = 33.7% ^{167}Er

Y and X portions of the blades can be scaled from U &V results based on ratios from earlier more extensive processing operations since the plasma cross section is identical.

Figure 52 Production collector following a production run showing the outline of the plasma and erbium metal films becoming detached from the tails plate and fences.

Therefore, depending on the assay level desired, we get the following rates for annual production assuming 55% continuous availability .

U 39.4% assay 0.330 g/hour 1591 g/year (Yearly rates based on 55% availability)
V 33.7% assay 0.278 g/hour 1348 g/year
X 31% assay 0.315 g/hour 1530 g/year (**scaled based on Dy ratio)
Y 31% assay 0.247 g/hour 1192 g/year (**scaled based on Dy ratio)

If we combine them all, we get about 5.66 kg/year at an assay of ~ 33% and 55% run time availability.

ESTIMATED COST FOR COMMERCIAL PRODUCTION OF ^{167}Er

Pricing for production of enriched ^{167}Er is highly dependent on the throughput and enrichment level required. By combining all grades of recovered product, a production rate 1.17 g per hour at an assay level of ~33% is available. Equivalent throughput based on total available hours in one year is approximately 10.2 kg of ~33% assay product. The following table presents the estimated pricing per gram, based on varying levels of run-time utilization, and includes estimated cost of natural erbium source plates.

Utilization (1)	Based on total product (2) Pricing range per gram	Annual capacity	Based on isotope (3) Pricing range per gram	Annual capacity
100%	$600 - $1100	9.8-10.2 kg	$1800 - $3400	3.2-3.4 kg
75%	$800 - $1500	7.4-7.8 kg	$2400 - $4600	2.4-2.6 kg
55%	$1200 - $2200	4.8-5.2 kg	$3600 - $6700	1.5-1.7 kg

This cost estimate is only for scientific purposes. It is not meant to be a price.

(1) Actual production hours divided by total available hours. 24 hours per day considered total available hours. 100% utilization is theoretical maximum (24 hours per day, 7 days per week, 365 days).

(2) Erbium enriched to 33% of ^{167}Er. (i.e. – 33% of total product is ^{167}Er).

(3) ^{167}Er only. This is a function of enrichment multiplied by total product.

For comparison purposes, the parameters for the erbium runs are presented in Table 55 with the corresponding parameters for gadolinium and dysprosium.

Table 55 Comparison of burnable poison isotope separation on the Theragenics™ PSP

	2 Tesla PSP Unit		
	Gd-157	Dy-164	Er-167
Source current (A)	15.00	14.00	10.00
Particle mass number	157	164	167
Particle mass (g)	2.61E-22	2.72E-22	2.77E-22
Isotope natural abundance	16.30%	28.20%	22.95%
Calculated assay %	36.00%	67.50%	37.50%
Collector cut	0.03	0.04	0.04
Overall cut	0.02	0.02	0.02
Collector flux (g/hour)	0.72	0.86	0.92
Isotope flux (g/hour)	0.2581	0.5804	0.3436
Run time fraction	0.6	0.6	0.6
Isotope flux (g/year)	1356	3051	1806
Product flux (g/year)	3768	4519	4815
Feed mass (Kg/yr)	693	676	492

DISCUSSION OF RESULTS OF ISOTOPE SEPARATION

The experimental values achieved in the PSP isotope separation are given in Table 56. The enrichment values, although lower than expected for ^{157}Gd and ^{167}Er, are reasonable for a single pass

process. The production rates are disappointing. With the present PSP device, such a throughput, leading to an associated cost of approximately $1,000 per gram is not viable for present day commercial reactors.

Table 56 Comparison of experimental and calculated values of enrichment and production rates of PSP separated isotopes. Production rates are based on 24 hours/day, 365 days/year.

Isotope	Natural Abundance (%)	Theoretical Enrichment (%)		Experimental Enrichment (%)	Theoretical Production Rate (kg/year)		Experimental Production Rate (kg/year)
		2 Tesla	6 Tesla	2 Tesla	2 Tesla	6 Tesla	2 Tesla
^{157}Gd	15.65	45.8	72	32	51	87	5.9
^{164}Dy	28.2	63.1	90	63	96	130	6.9
^{167}Er	22.9	55.5	79	33	79	120	10.2

However, ^{164}Dy has favorable qualities. Of course, the higher the enrichment, the lower the percentage of undesirable isotopes, but it is the distribution of the undesirable isotopes that determines the performance of the burnable poison. Calculations have determined the residual negative reactivity due to each isotope remaining and produced. A reasonable prediction of performance of the actual material can be computed by considering the reactions that lead to the production of each isotope. Then the ratio of the actual concentration of each isotope to the natural concentration is multiplied by the negative reactivity of the isotope generated. The sum of each of these negative reactivities is then used to linearly interpolate a value for the RAP. The values calculated in this manner appear in Table 57. It is evident that ^{157}Gd and certainly ^{167}Er will not serve as economical burnable absorbers for commercial reactors. ^{164}Dy, with its uniform burn rate over a period of four years, is a strong potential candidate for use in a generation IV reactor with an extended fuel cycle. This is particularly true if a PSP device with a 6T magnet is used, which is predicted to result in a 2-3 times higher production rate as well as an enrichment value 30% higher or a production rate 50% higher and a corresponding enrichment value nearly twice as high.

Table 57 Residual absorber penalty in days resulting from the candidate burnable poisons in 16 rods.

Isotope	RAP Natural Element	RAP (100% Separated) (Days)	RAP (Experimental) (Days)	Savings (Experimental) (Days)
^{157}Gd	7	0.7	6.5	0.5
^{164}Dy	200	136	163	37
^{167}Er	65	33	66	0

MATERIALS ISSUES WITH BURNABLE POISONS

GADOLINIUM OXIDE IN FUEL

The third phase of this project is to investigate the product form of the fuel and burnable poison, or as has been discovered during phase one, to explore the possibility of incorporating the burnable poison into the cladding. The addition of gadolinium oxide to uranium oxide is not a new concept. In fact, the addition of gadolinia to UO_2 nuclear fuels to depress early life power levels and homogenize core power distributions has been accepted in commercial power reactors for many years. For this reason, a literature search was conducted to determine the issues involved with incorporating Gd_2O_3 into the fuel and to what extent the problems have already been solved.

EFFECTS OF Gd_2O_3 in UO_2

Experience with Gd_2O_3 as a burnable poison dates back to the 1960's. ASEA-ATOM began testing fuel rods containing gadolinia in 1971 and a full-scale demonstration was conducted during 1976-1977 (ref 18). By 1982, 3223 fuel assemblies containing 2 to 6 wt% gadolinia had been utilized to 90% of the design burnup without any fuel failure. Destructive examination of fourteen of the rods showed that dimensional changes, fission gas release and fuel structure was within the range of standard fuel rods.

Kansai Electric also uses fuel containing gadolinia in commercial reactors. Eight fuel assemblies with 6 wt% Gd_2O_3 in UO_2 were tested beginning in 1984. The measured physics parameters during the startup operation agreed with predicted values. Destructive post irradiation examination indicated that the fission gas release was less in the gadolinia doped fuel than in the UO_2 rods irradiated concurrently (ref 19).

Advanced Nuclear Fuels Corporation introduced gadolinia bearing nuclear fuel in the late 1970's. By 1988, 45,000 fuel rods containing 1 to 10 wt % gadolinina had been irradiated in 29 reactors: 11 pressurized water reactors and 18 boiling water reactors. Hot cell examinations indicated that the mechanical behavior of the gadolinia bearing rods was fully satisfactory (ref 20).

UO_2 forms a single phase cubic fluorite type solid solution with Gd_2O_3 up to 20-30 wt % at temperatures above 1300 K (ref 21). The addition of gadolinia to UO_2 modifies the material properties of the fuel. During calcination and sintering of a homogeneous mixture, the Gd atoms can replace the U atom in the crystal structure. Since Gd has a lower atomic weight, the density of the solid solution decreases as the gadolinia concentration increases. However, this effect is somewhat offset since the lattice parameter of $(U,Gd)O_2$ solid solutions decreases with increasing Gd_2O_3 content (ref 22). The final density depends on the sintering temperature, the sintering atmosphere, and on the characteristics of the UO_2 powder used to prepare the fuel. In a hydrogen atmosphere, UO_2 containing up to 6 wt % Gd_2O_3 shows a reduced sinterability compared to UO_2 (ref 23). As the oxygen potential in the sintering atmosphere increases, the sintered density of UO_2-2% Gd_2O_3 pellets increases, but that of UO_2-10% Gd_2O_3 pellets decreases. The grain size of UO_2-Gd_2O_3 fuel also increases with increased oxygen potential, and a short range Gd distribution becomes homogeneous (ref 24).

The thermal and physical properties of $(U,Gd)O_2$ fuel were measured to serve as a benchmark to existing UO_2 data in support of U.S. reactor designs. For reactor design purposes, the thermal conductivity is the only property among the thermal expansion, the specific heat, and the solidus temperature, that significantly changes from those of UO_2 (ref 25). The melting temperature of UO_2 and UO_2-2wt% Gd_2O_3 fuel irradiated in a commercial LWR has been measured (ref 26). There is no decrease in the melting temperature with irradiation to a burnup of about 30GWd/t, and Gd_2O_3 addition below 2 wt% has little, if any, influence on the melting temperature. The melting behavior for irradiated UO_2 containing higher concentrations of Gd_2O_3 has not been reported. The melting point of Gd_2O_3 doped UO_2 should be sufficiently high so as not to impact reactor safety during normal operations.

Limited data exist in the literature on the thermal expansion coefficient (CTE) for $(U,Gd)O_2$. Additions of Gd_2O_3 up to about 12 wt% have little effect on the CTE for temperatures below 1233 K (ref 27). At temperatures exceeding about 1300 K the CTE for unirradiated solid solutions becomes larger with increasing Gd_2O_3 content. At 1973 K the CTE values for 5, 8, and 10 wt % Gd_2O_3 are 2.7, 5.4 and 6.2 % larger than for UO_2 (ref 28). CTE values as a function of fuel burnup have not been reported in the open literature.

The thermal conductivity of UO_2 is reduced when gadolinia is added to form a solid solution. The reduction is most pronounced at lower temperatures and is about a factor of two at room temperature but only about 20% at 1400 K. Irradiation also reduces the thermal conductivity of UO_2 and UO_2-10 wt% Gd_2O_3 due to the formation of point defects. The reduction in the thermal conductivity is less at higher irradiation temperatures and is small in samples that are irradiated at temperatures exceeding 1273 K (ref 29). The relative reduction in the thermal conductivity of gadolinia doped fuel during irradiation is smaller than that of UO_2 (ref 30). Furthermore, the difference in relative thermal conductivities between UO_2 and $(U,Gd)O_2$ become insignificant with increasing burnup (ref 31). This suggests that the effects of soluble fission products and irradiation induced defects are more significant than those of the added Gd.

This reduction in fuel thermal conductivity can cause gadolinia doped fuel to reach higher

temperatures during irradiation than UO_2 operating at the same power. As a consequence, fission gas release from the gadolinia-doped fuel is predicted to be higher. The fission gas diffusion coefficient in $(U,Gd)O_2$ under irradiation is independent of temperature below 1073 K, but increases with temperature above this value. In contrast to UO_2, the diffusion coefficient is independent of O potential in UO_2-8 wt% Gd_2O_3 and less sensitive than UO_2 to the O potential in 4 wt% Gd_2O_3. The oxygen/metal (O/M) stoichiometry in the $(U,Gd)O_2$ also affects the diffusion coefficient. It is independent of the O/M ratio in the hypostoichiometric region, but increases sharply with increasing O/M ratio in the hyperstoichometric region (ref 32).

Heat capacity measurements have been performed on unirradiated and irradiated $(U,Gd)O_2$ fuel. Measurements of the heat capacities of undoped UO_2 pellets agree well, but measurements of the gadolinia doped material show considerable scatter. The heat capacity of unirradiated 6 wt% Gd_2O_3 doped UO_2 containing fission products that simulate a burnup of 30 GWd/t is the same as that of UO_2 up to about 800 K. Above this temperature the heat capacity of the Gd_2O_3 containing material is somewhat lower than that of UO_2 (ref 33).

The behavior of $(U,Gd)O_2$ during fuel irradiation in boiling water reactors has been successfully modeled and incorporated into the ABB Atom fuel performance code STAV-6 (ref 34). The model considers burnable absorber rods with 6 and 9 wt% Gd and accounts for both nuclear burnup and the thermal-mechanical properties of the Gd bearing fuel. The fission gas release behavior uses an empirical model that assumes that the release rate is lowered by an increase in oxygen vacancies caused by doping with the trivalent Gd^{+3}. Out-of-pile results seem to show that the diffusion coefficients decrease with increasing gadolinia content; which contrasts with the in-pile results presented above.

In conclusion, gadolinia-doped UO_2 neutron absorber material is a proven concept to extend the lifetime and to shape the power distribution in commercial reactors. Experimental data concerning the effects of adding the gadolinia on the fuel performance have been measured and are sufficient to use in performance modeling and prediction codes for normal operating conditions. In fact, in the U.S., the American Society for Testing and Materials (ASTM) has issued a standard specification for finished sintered gadolinium oxide-uranium dioxide pellets for use in light-water reactors (ref 35). The use of Gd_20_3 enriched to about 32% in ^{157}Gd, the amount achieved by the 2 T PSP device, will decrease the required concentration of Gd_20_3 in the fuel by about a factor of two. This will reduce the effects of the Gd in the fuel even further.

It is clear that more research has been conducted on gadolinium-containing fuel than could be conducted in this investigation. As a result, the study turned to the rather new idea of incorporating metallic burnable poison elements into the fuel cladding.

INVESTIGATION OF ZIRCONIUM AND ITS ALLOYS DOPED WITH RARE EARTHS

There are two primary concerns with doping an alloy with an element of different properties and structure. The first is that impurity elements frequently have low solubility in the solvent metal and

tend to precipitate or segregate at grain boundaries. In the first case, a second phase is formed which can sometimes strengthen the host material, especially with respect to high temperature creep deformation. However, perhaps more commonly, it can embrittle the host material, enhancing intergranular fracture. In the second case, the foreign element might diffuse to a lower energy site while remaining in solid solution. Such segregation can still embrittle a material since it coats grain boundaries where it forms a weaker metallic bond with the host element than the atoms of the host form with themselves. The second concern is degradation of corrosion resistance of the host alloy. This is an even more subtle effect since it depends on many factors such as diffusion of protective oxide-forming elements to the surface or the formation of a second phase which depletes the surface region of the protective oxide-forming element. In other cases, a dopant can change the thermodynamic stability of a gettering element which perhaps protects the host alloy from hydrogen or other gas embrittlement. The area of corrosion is left for a follow-on project.

Embrittlement was first approached by a scoping experiment using pure zirconium. Pure Zr was doped with levels of Gd, Dy, and Er found to be relevant to their use as a burnable poison, in particular, concentrations of the separated isotopes which result in an initial addition of negative reactivity of approximately 0.1. The concentrations selected were: 0.5% Gd, 0.5% Sm, 2% Dy, and 2% Er. It was attempted to prepare all of these alloys and conduct bend tests to scope ductility behavior.

An immediate difficulty was encountered with samarium as can be seen in Table 58.

Table 58 Melting and boiling points of metals used in the study of rare earth-doped zirconium

Element	Melting Point (EC)	Boiling Point (EC)
Zr	1852	4409
Gd	1314	3264
Sm	1072	1778
Dy	1411	2561
Er	1529	2862

The boiling point of samarium is lower than the melting point of zirconium. The alloys were melted with an inert gas arc melter and cast into a copper mold. An attempt to directly melt the Sm alloy would result in the metal being vapor deposited on the chamber walls. Instead, it was considered that zircaloys contain approximately 1.5% tin. Since tin boils at 2602 EC, it could be used to form an alloy with samarium, then the Sm-Sn alloy could be melted with Zr to form the desired alloy with the expectedly innocuous addition of tin. Such an alloy was melted, but it was found that the high vapor pressure of the Sm caused it to be removed from the final alloy nonetheless. Because of its difficulty in alloying and its high reactivity in air, making handling difficult, samarium was excluded from further investigation.

The remaining alloys were melted, and a strip approximately 0.76 mm in thickness was cut from the ingot and bent around a 6.4 mm mandrel 180E. In all cases, the alloys were bent without cracking. In one case, there was a pre-existing crack which did not propagate further during the bending. The alloys are pictured in Figure 53.

A more realistic and quantitative series of tests was run by melting alloys of Zircaloy-4 doped with Gd, Dy, and Er. This series of alloys was arc melted in an inert atmosphere then rolled to a thickness of approximately 1 mm in five steps with intermediate anneals. For the first three stages, the alloys were rolled to 35% reduction of area then annealed in a vacuum of approximately 10^{-4} Pa at 815EC. In last stage, the annealing temperature was increased to 850EC and the rolling taken to 50% reduction of area. Following the final rolling, the material was annealed again at 850EC for 30 minutes. This processing was done with only the anticipated edge cracking. This operation, therefore, demonstrated adequate ductility in the rare earth-doped Zircaloy-4.

Optical metallography was done to detect any large changes in microstructure or precipitate morphology upon addition of the rare earth dopants. Although expected precipitates were observed on grain boundaries and on what appeared to be former grain boundaries, no new precipitates were observable. The 30 minute anneals appear to have resulted in little grain growth, although some grain boundary migration is anticipated. The structures of the four alloys appear in Figures 54-57.

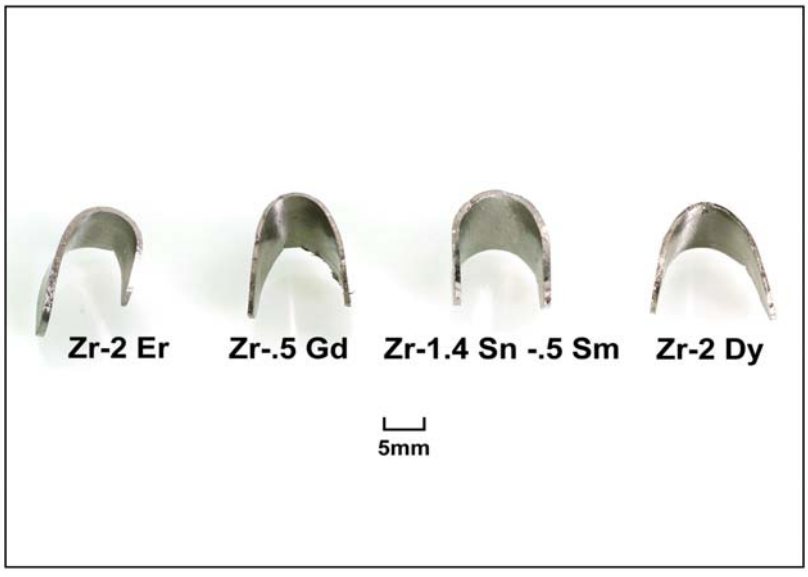

Figure 53 Alloys of zirconium and rare earths in concentrations typical of burnable poison alloys showing high ductility in a bend test around a 6.3 mm mandrel. The Sm alloy was later found to contain only trace amounts of Sm.

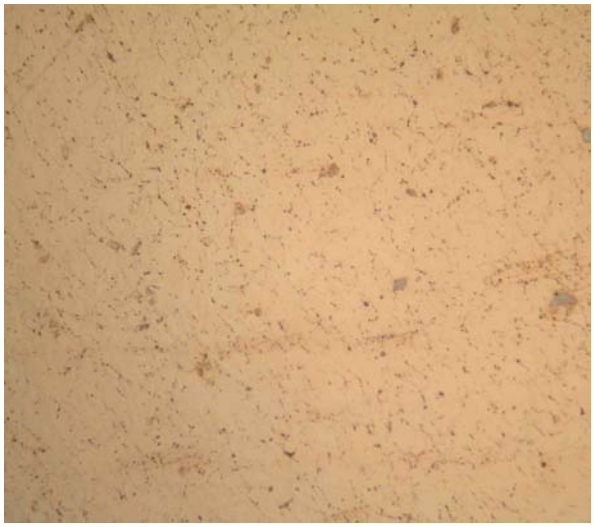

Figure 54 Zircaloy-4 following rolling

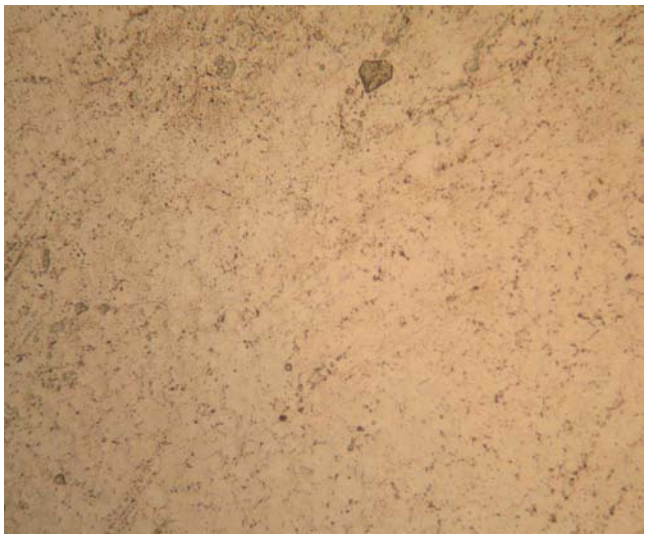

Figure 55 Zircaloy-4 doped with 0.5% Gd

Figure 56 Zircaloy-4 doped with 2% Dy

Figure 57 Zircaloy-4 doped with 2% Er

CONCLUSIONS

The isotopes ^{157}Gd, ^{149}Sm, ^{167}Er, ^{164}Dy, and ^{177}Hf were identified as potential candidates based on nuclear performance. All of them result in a significant increment in performance in terms of reduced residual negative reactivity. In all cases of separated isotopes, less of the burnable poison will have to be used, resulting in a higher allowable fuel loading in cases where core volume is limited. As can be concluded from the time dependence of burnout, each of these isotopes has a potential for use in leveling the power distribution in an extended life core. The configuration as well as the particular isotope can be used to adjust the time dependence of the burnout.

In the practical demonstration of isotope separation by the plasma separation process, the enrichments were below expected values for gadolinium and erbium, but at the calculated value for dysprosium. The remaining undesirable isotopes caused the savings in fuel life to be favorable in the case of dysprosium, of small advantage for gadolinium, and erbium. The production rate of the separated isotopes was also less favorable resulting in a cost of $600 to $1600 per gram. This could be far more favorable if a future PSP plant used a higher field magnet. A possibility that should not be ignored.

In summary:

1. ^{157}Gd, ^{149}Sm, ^{167}Er, ^{164}Dy, and ^{177}Hf have been identified as candidates for advanced burnable poisons.

2. ^{164}Dy was demonstrated to be the most easily separated by the PSP and at the attained 63% enrichment is calculated to result in a savings of 37 days at the end of a 4 year fuel cycle in a PWR.

3. An understanding of burnable poison behavior in various configurations in a PWR has been acquired and can be applied to the design of an advanced reactor with an extended fuel cycle.

4. The method of incorporation of metallic burnable poisons into the fuel cladding has been suggested. Preliminary experiments and calculations have shown this to be a viable alternative to blending rare earth oxides with fuel.

5. The cost of producing separated isotopes is on the order of $600 to $1600 per gram using the present PSP facility. A device with a 6 Tesla magnet is predicted to reduce the price on the order of $60 to $160 per gram. This, along with improved techniques of operation, could make the process cost effective in the future.

DIRECTIONS FOR FUTURE RESEARCH

This project was intended to be a scoping study to test the feasibility of using isotopically enriched burnable poisons. Several opportunities have been revealed for further development.

1. The behavior of burnable poisons has been investigated using a state-of-the-art system of computer codes. These codes can now be used to aid in the design of an advance reactor with an

extended-life fuel cycle. The behavior of the partially-enriched isotopes produced by PSP should now be calculated using these codes.

2. The method of incorporating the burnable poison into the fuel cladding is an innovative idea. Further work must be done on the effect of the rare earths on corrosion properties, and further development should be done to test the commercial feasibility and cost effectiveness of this process.

3. The PSP is still in its infancy as an isotope separation method. Further fine tuning might increase both the enrichment and the production rates. There is probably much to be gained using the present system even without increasing the field strength of the magnet.

4. Other methods of isotope separation might be explored. For example, gas centrifuge and laser isotope separation. Different methods of separation might be used for different isotopes.

REFERENCES

1. P. G. Boczar, "CANDU Fuel-Cycle Vision," presented at IAEA Technical Committee Meeting on "Fuel Cycle Options for LWRs and HWRs, Victoria, B.C., April 28–May 1, 1998.
2. P. Blanpain, D. Haas, and F. Motte, "High Rated and High Burnup Gadolinia Fuel Irradiated in the BR3 17 × 17 PWR," *Proc. Symposium on Improvements in Water Reactor Fuel Technology and Utilization*, Vienna, IAEA, 1987, p. 305.
3. A. Radkowsky, *Naval Reactors Physics Handbook*, Vol.1, U.S. Atomic Energy Commission, Washington, D.C., 1964.
4. IAEA, *Design and Performance of WWER Fuel*, Technical Reports Series No.379, Vienna, International Atomic Energy Agency, 1996, p. 44.
5. F. J. Rahn, A. G. Adamantiades, J. E. Kenton, and C. Braun, *A Guide to Nuclear Power Technology: A Resource for Decision Making*, New York, John Wiley & Sons, 1984, 436–38.
6. R. G. Cochran and N. Tsoulfanidis, *The Nuclear Fuel Cycle: Analysis and Management* American Nuclear Society, La Grange Park, Ill., 1990, p. 84.
7. C. Collette, G.Francillon, F. Abadia, and A. Darraud, "Operating Experience of the Fragema Gadolinia Bearing Fuel Assembly," *Proc. Symposium on Improvements in Water Reactor Fuel Technology and Utilization*, Vienna, IAEA, 1987, p. 255.
8. L. Goldstein and A. A. Strasser, "A Comparison of Gadolinia and Boron for Burnable Poison Applications in Pressurized Water Reactors," *Nucl .Tech*. **60** 352 (1983).
9. C. M. Hove and S. W. Spetz, "Improvement of Gadolinia Fuel Cycle Economics by Isotopic Enrichment of ^{157}Gd," *Trans. Am. Nucl. Soc*. **50**, 102 (1985).
10. Private communication, W. S. Aaron, Oak Ridge National Laboratory, November, 1998.
11. J.-P.A. Renier and M. L. Grossbeck, *Development of Improved Burnable Poisons for Commercial Nuclear Power Reactors*, ORNL-TM-2001/238, Oak Ridge National Laboratory, 2001.
12. A. G. Croff, *ORIGEN2.1—A Revised and updated Version of the Oak Ridge Isotope Generation and Depletion Code*, ORNL-5621, July 1980.

13. E. A. Villarino, R. J. Stammler, A. A. Ferri, and J. J. Casal, *Nucl Sci. Eng*. **112**, 16 (1992).
14. *HELIOS—General Two-Dimensional Neutron and Gamma Transport with Depletion Code*, Studvik-Scandpower, Inc.
15. R. E. MacFarlane and D. W. Muir, *The NJOY Nuclear Data Processing System*, LA-12740-M, 1994.
16. J. F. Briesmeister, ed., *MCNP—A General Monte Carlo N-Particle Transport Code 4C*, LA-13709-M, April 2000.
17. J. P. Renier and C. W. Alexander, *An Advanced Version of the Oak Ridge Isotope Generation and Depletion Code with Fission Product Yield for 34 Actinides*, ORNL-TM, 2001
18. A. Helmersson, et. al., Trans. Am. Nucl. Soc., 43, 162-163 (1982).
19. M. Yokote,., et. al, Trans. Am. Nucl. Soc., 57, 33-34 (1988).
20. F. B. Skogen, Trans. Am. Nucl. Soc., 57, 36, (1988).
21. R. J. Beals, J. Am. Ceram. Soc., 48, 272 (1965)
22. T. Ohmichi, et. al., J. of Nuclear Materials, 102, 40-46 (1981).
23. J.-H. Baek, Han'guk Chaelyo Hakhoechi, 5, 364-70 (1995).
24. Kun Woo Song, et. al., J. of the Korean Nuclear Society, 30, 128-139 (1998).
25. L. W. Newman, et. al., DOE/ET/34212-43 report (1984).
26. S. Yamanouchi, et. al., J. of Nuclear Science and Technology, 25, 528-533 (1988).
27. T. Wada, Proc. Int. Conf. Of Nuclear Fuel Performance, London, 1973 , British Nuclear Energy Soc., p 63.
28. K. Une, J. of Nuclear Science and Technology, 23, 1020-1022 (1986).
29. K. Minato et. al., J. of Nuclear Materials, 288, 57-65 (2001).
30. J. Nakamura, 24th NSRR Technical Review Meeting, 13-14 Nov. 2000, Tokyo, Japan
31. M. Amaya, et. al., J. of Nuclear Materials, 300, 57-64 (2002).
32. M. Hirai, J. of Nuclear Materials, 226, 238-251 (1995).
33. M. Amaya, J. of Nuclear Materials, 294, 1-7 (2001).
34. A. R.Massih, J. of Nuclear Materials, 188, 323-330 (1992).
35. "Standard Specification for Sintered Gadolinium Oxide-Uranium Dioxide Pellets," ASTM C 922-00, American Society for Testing and Materials, West Conshohocken, PA

INTERNAL DISTRIBUTION

1. H. L. Dodds
2. M. L. Grossbeck
3. L. F. Miller
4. L. W. Townsend
5. B. R. Upadhyaya

EXTERNAL DISTRIBUTION

6. Denise Berry, U.S. Department of Energy, Oakland Operations Office, 1301 Clay Street, Oakland, CA 94612

7. Rebecca Richardson, U.S. Department of Energy, Oakland Operations 1301 Clay Street, Oakland CA 94612

8. Madeline A. Feltus, NE-20, U.S Department of Energy, Office of Nuclear Energy, Science & Technology, 19901 Germantown Road, Germantown, MD 20874

9. Charles Thompson, NE-20, U.S Department of Energy, Office of Nuclear Energy, Science & Technology, 19901 Germantown Road, Germantown, MD 20874

10. Prof. Michael J. Driscoll, Massachusetts Institute of Technology, Department of Nuclear Engineering, 138 Albany Street Bldg. NW 13-259, Cambridge, MA 02139

11. Michael Natelson, Bettis Atomic Power Laboratory, P.O. Box 79 West Mifflin, PA 15122

12. Claude Degueldre, Paul Sherrer Institute, CH-5232 Villigen PSI, Switzerland

13. Alberto L. Casadei, European Fuel Group, Santiago Rusinol, 12, 28040 Madrid, Spain

14. Dick Kovan, Nuclear News UK Editorial Office, 8 Park Close, Strood Green, Betchworth, Surrey RH3 7 JB, England

15. S. D. Harkness, Bettis Atomic Power Laboratory, P.O. Box 79, West Mifflin, PA 15122

16. W. Ollinger, Bettis Atomic Power Laboratory, P.O. Box 79, West Mifflin, PA 15122

17. Gordon E. Michaels, Oak Ridge National Laboratory, P.O. Box 2008, Oak Ridge, TN 37831-6162

18. Bojan Petrovic, Westinghouse Electric Co., 1344 Beulah Road, Pittsburgh, PA 15235-5081

19. James E. Rushton, Oak Ridge National Laboratory, P.O. Box 2008, Oak Ridge, TN 37831-6243